Numerical modelling of Macquarie Harbour

by

Colin Terry, B.E. (Hons)

Submitted in fulfilment of the

requirements for the degree of

Doctor of Philosophy

University of Tasmania

31 March 1999

Declaration

I declare that this thesis contains no material which has been accepted for a degree or diploma by the University of Tasmania or any other institution, except by way of background information and duly acknowledged in this thesis, and to the best of my knowledge and belief no material previously published or written by another person except where due acknowledgment is made in the text of this thesis.

Colin T. Terry.

(Colin T. Terry)

Authority of access

This thesis may be made available from loan and limited copying in accordance with the *Australian Copyright Act 1968.*

Colin T. Terry.

(Colin T. Terry)

Abstract

This thesis is about the creation of a numerical model and its application to Macquarie Harbour (Tasmania, Australia). With the aim being to better understand the harbour and aid the management of its environment and industry. A numerical model was developed through the combination of an original two-dimensional laterally averaged river model and an existing three-dimensional ocean model. The existing three-dimensional model used is the Princeton Oceanographic Model (POM) by Blumberg and Mellor (1987), which is used for modelling the harbour. The author's river model is used for the two main rivers flowing into Macquarie Harbour, and part of the ocean surrounding the harbour.

The river model is based on non-Boussinesq primitive equations, which include the density terms neglected in the commonly used Boussinesq approximation. These density terms are important where there are large salinity stratifications, which occur in the rivers flowing into Macquarie Harbour. The primitive equations for the model are derived in a rectangular Cartesian co-ordinate system and then transformed to a σ co-ordinate system. The σ co-ordinate system transformation, also used by POM, non-dimensionalises depth - resulting in a more accurate and efficient method for handling a varying bathymetry.

The river model is solved with a finite difference implicit scheme, which is numerically centred in space and time. As the models' bathymetries vary from 1 to 90m, to get the required resolution in the deeper sections with the σ co-ordinates, the resulting vertical spacing in the shallow sections is small. Hence, the finite difference equations are solved vertically, which avoids a restrictive Courant, Friedrichs and Lewy (CFL) time restraint with the explicit finite difference operators.

The model successfully predicts the general circulation and pollution distribution in the harbour, agreeing to within 36% of peak velocities measured using a broad-band acoustic doppler current profiler (Koehnken, 1996). It also gives a reasonable representation of the salinity profile in the Gordon River compared to measurements taken by the Hydro-Electric Corporation (HEC), during the Lower Gordon River Scientific Survey (HEC, 1979). With an average depth of 25m, the harbour is sensitive to wind stresses and the large inflow from the Gordon River. In the northern harbour, the polluted King River water is mixed by the tide and action of the Gordon River water.

With no previously published numerical models of Macquarie Harbour, the model from this thesis has and will continue to be a useful management tool for the environmental instrumentalities and industry.

Acknowledgments

A PhD project is not undertaken lightly or alone. There are individuals and organisations whom I would like to acknowledge and give thanks. Firstly thanks to my supervisor Sergio Montes, for his enthusiasm and editing, and to the Department of Civil/Mechanical Engineering for the use of its technical staff. I acknowledge the assistance of an Australian Postgraduate Award scholarship from the Australian Government for 3.5 years and a Higher Education Contribution exception scholarship for 5 years.

Thanks to Peter Craig from CSIRO for introducing me to POM, George Mellor for allowing me to use POM, and Duncan Galloway for discussions about POM.

For vital information about Macquarie Harbour, foremost I thank Lois Koehnken from DELM for her discussions about the harbour, and allowing me use of BB-ADCP data and other reports on the harbour. Thanks also to the HEC Survey Dept for the data from their bathymetric survey of the northern harbour and King River; and Bob Grundy from the Hobart Port Corporation for bathymetry of Macquarie Harbour around mouth of Gordon River.

Thankyou to family and friends who were always supportive. A special thankyou to those who helped directly in the project, notably: Bruce Terry, Tom Terry, Tina Terry, Jason Roberts, and Damien Holloway.

Lastly, but most importantly, thankyou to my best friend Philippa Terry, who after a courtship of feeling second fiddle to my thesis still married me – this work is dedicated to you.

Contents

List of Figures

List of tables

Nomenclature

The following symbols are used in the thesis:

Symbol	Description	Units
A_f	horizontal diffusion value (generic version of A_H and A_M) element in tri-diagonal matrix used to solve for variable f	m^2/s
A_H	horizontal diffusivity for scalar diffusion	m^2/s
A_M	horizontal kinematic viscosity for velocity diffusion	m^2/s
B	river width	m
B_f	element in tri-diagonal matrix used to solve for variable f	
C	concentration of conservative pollutant	kg/m^3
$C_{f,i}$	coefficient of f^{n+1} at grid i in equation to solve for f^{n+1}	
C_f	element in tri-diagonal matrix used to solve for variable f	
c	phase speed	m/s
D	total water depth ($H+\eta$)	m
f	Coriolis parameter	s^{-1}
$f_{i,k}^n$	variable at grid (i,k) and time n	
g	gravitational acceleration (9.806)	m/s^2
H	water depth (down from mean water level)	m
H_s	significant wave height	m
$ISPLIT$	number of external steps done for every internal step	
IM	maximum i value	
i	horizontal grid index with x	
JM	maximum i value	
j	horizontal grid index with y	
K_1	lunisolar diurnal tide	
K_f	vertical diffusion value (generic version of K_H and K_M), and known values in equation to solve for f^{n+1}	m^2/s
K_H	vertical diffusivity for scalar diffusion	m^2/s
K_M	vertical eddy viscosity for velocity diffusion	m^2/s
KB	maximum number of vertical levels (where $\sigma = -1$)	

Symbol	Description	Units
KW	wind stress coefficient (POM variable)	
k	von-Karman constant (0.40), and vertical grid index with σ	
M_2	principal lunar semi-diurnal tide	
m	mass of control volume	kg
n	Manning's n, and current (known) time step	$m^{-1/3}s$
n-1	previous (known) time step	
n+1	next (unknown) time step	
O_1	principal lunar diurnal tide	
p	pressure	Pa
Q	volumetric flow rate	m^3/s
Q_{tide}	tide amplitude as a volumetric flow rate	m^3/s
R	hydraulic radius	m
R_i	Richardson number $= g\frac{\partial \rho}{\partial z^*}\Big/\rho\left(\frac{\partial u}{\partial z^*}\right)^2 = Dg\frac{\partial \rho}{\partial \sigma}\Big/\rho\left(\frac{\partial u}{\partial \sigma}\right)^2$	1
S	salinity	‰
S_2	principal solar semi-diurnal tide	
T	temperature	°C
t^*	time in Cartesian co-ordinates	s
t	time in sigma co-ordinates	s
t_f	radiation condition boundary condition time scale	s
u	horizontal velocity in x direction	m/s
v	horizontal velocity in y direction	m/s
w	vertical velocity in z direction	m/s
x^*	horizontal direction downstream for 2D river model, or east for 3D harbour model	m
x	x^* in sigma co-ordinates = x^*	m
y^*	horizontal direction across for 2D river model, or north for 3D harbour mode	m
y	y^* in sigma co-ordinates = y^*	m

Symbol	Description	Units
$Z0B$	bottom roughness length (POM variable)	m
z^*	vertical direction – positive up	m
α_t	temporal smoothing coefficient	1
α_x	spatial smoothing coefficient	1
Δt	time step	s
Δx	horizontal grid size	m
η	surface elevation (up from mean water level)	m
θ	generic term for S, T, or C, and temporal weight coefficient for implicit scheme (typically $0.5 < \theta \leq 1$)	
κ_f	empirical value used in function f	
λ	friction coefficient for momentum equation	1
η_{tide}	tide amplitude	m
ρ	density	kg/m
σ	z^* in sigma co-ordinates $= \frac{z-\eta}{H+\eta}$	1
τ_{ij}	shear stress, where i is the direction of the stress and j is the direction normal to the plane in which the stress acts	N/m^2
ϕ_H	vertical diffusivity amplification factor for unstable stratification	
ϕ_M	vertical eddy viscosity amplification factor for unstable stratification	
Ω	angular velocity of the earth	rad/s
ω	velocity perpendicular to σ level	m/s
ω_{tide}	angular frequency of tide	rad/s
‰	practical salinity units (psu) in parts per thousand by mass	1

Abbreviations

The following abbreviations are used in the thesis:

Abbreviation	Description
ADI	alternating direction implicit
AMG	Australian Map Grid
BB-ADCP	broad-band acoustic doppler current profiler
CFL	Courant, Friedrichs and Lewy
CFMI	Computational Fluid Mechanics International
CMT	Copper Mines of Tasmania
COAG	Council of Australian Government
CPU	central processing unit
CSIRO	Commonwealth Scientific and Industrial Research Organisation
DELM	Department of Environment and Land Management [now DPIWE]
DHB	Dead Horse Bluff [in Macquarie Harbour]
DPIF	Department of Primary Industries and Fisheries [now DPIWE]
DPIWE	Department of Primary Industries, Water and Environment
D/S	down stream
E. coli	*Escherichia coli*
Gb	gigabyte
GIS	geographical information system
GPS	global positioning system
HEC	Hydro Electric Corporation [was Hydro Electric Commission]
KP	King Point [in Macquarie Harbour]
LHS	left hand side
Mb	megabyte
MHz	megahertz
MDR	mean diurnal spring tide range
MLRRDP	Mt. Lyell Remediation, Research and Demonstration Program
MSR	mean semi-diurnal spring tide range

Abbreviation	Description
NSWC	Naval Surface Warfare Centre
NE	northeast [direction wind comes from]
NNW	north-northwest [direction wind comes from]
NW	northwest [direction wind comes from]
OSS	Office of the Supervising Scientist [Australian Federal Office]
POM	Princeton Oceanographic Model
PC	personal computer
psu	practical salinity units
RAM	random access memory
RHS	right hand side
SE	southeast [direction wind comes from]
SSE	south-southeast [direction wind comes from]
SSW	south-southwest [direction wind comes from]
SW	south west [direction wind comes from]
SGI	Silicon Graphics Indigo [computer]
Tcl	Tool command language
UNESCO	United Nations Educational, Scientific, and Cultural Organisation
U/S	up stream
W	west [direction wind comes from]
1D	one dimensional
2D	two dimensional
2DDAM	two dimensional depth averaged model
2DLAM	two dimensional laterally averaged model .
3D	three dimensional

Chapter One
Background

1.1 Introduction

This thesis is about the numerical modelling of estuaries. It describes the creation and application of a finite-difference numerical model to unsteady free-surface flow. This model was developed through the combination of an original two-dimensional laterally averaged river model and an existing three-dimensional ocean and estuary model. The existing three-dimensional model used is the Princeton Oceanographic Model (POM) by Blumberg and Mellor (1987). The aim of this numerical modelling is to predict the general circulation and water quality in the estuary of Macquarie Harbour, located in the Australian island state of Tasmania (Figure 1.1).

Estuaries, such as Macquarie Harbour, are important to society as sources of food, locations for trade, and routes for transport. They are also important as natural ecosystems because of their great species diversity. Therefore, the demands of society need to be managed in order to establish a sustainable, long-term relationship between society and nature.

Numerical modelling of water flow, also called computational hydraulics, is about predicting the movement and properties of water in space and time. These predictions use mathematical equations based on fundamental principles of mechanics, which describe how important physical quantities relate to each other. Numerical modelling is a powerful tool for environmental management, with applications in water quality and monitoring programs, as well as playing an important role in predicting the impact of development on an estuary.

The numerical model of the Macquarie Harbour system consists of a three-dimensional model of the main harbour and two-dimensional laterally averaged models for the Gordon River, the King River, and the sea. The Gordon River and King River, the two main rivers flowing into the harbour, have been modelled upstream from the harbour for 40km and 10km respectively. The sea model represents a 20km reach of water from the harbour, consisting

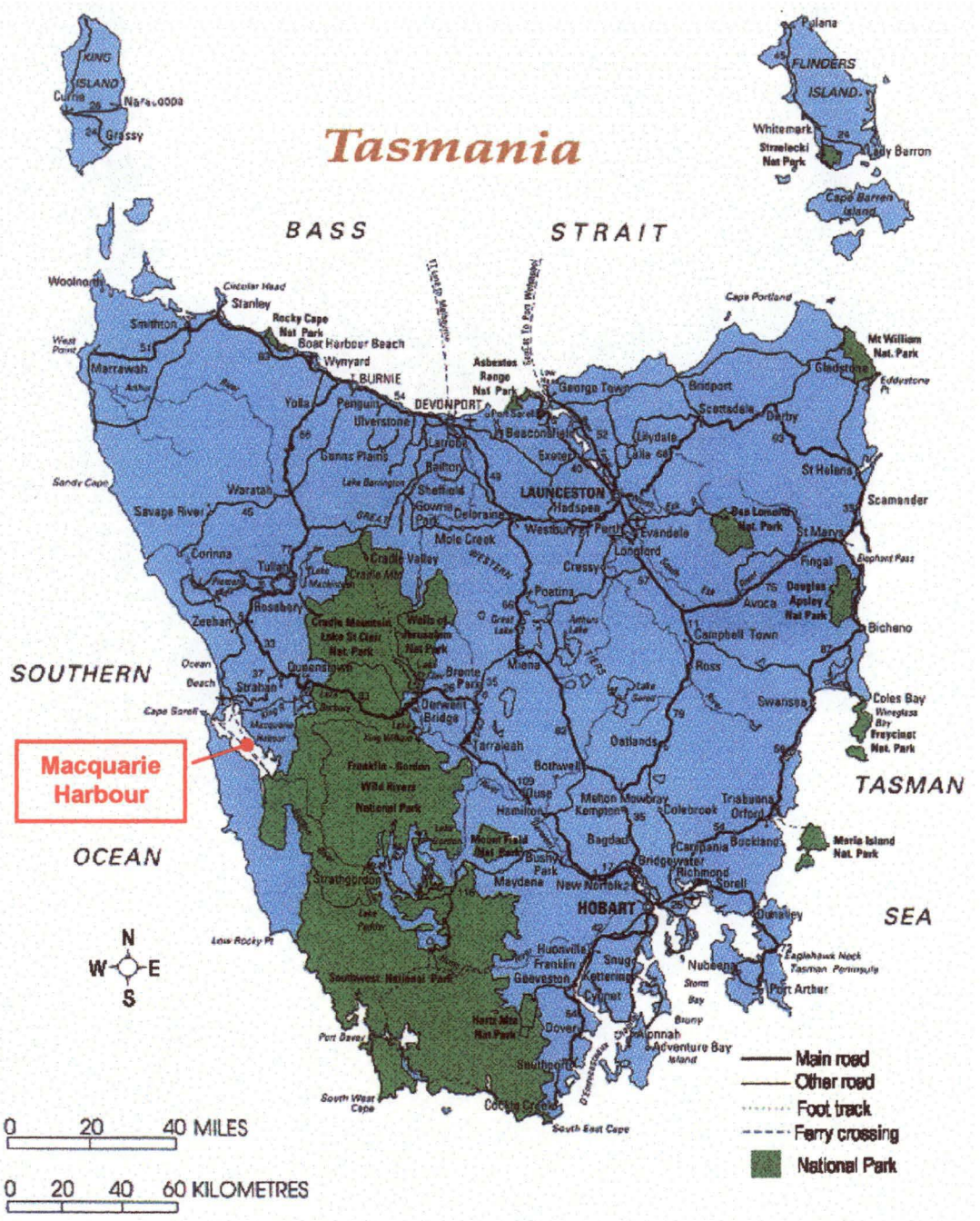

Figure 1.1 Location of Macquarie Harbour in western Tasmania

of a 3km restricted passage to open water, then continuing for 17km in a west-north-west direction into the Southern Ocean.

Numerical modelling of estuaries is a new area of research for the Department of Civil/Mechanical Engineering at the University of Tasmania, initiated with this project. As a new area of research, an existing three-dimensional model was used for part of the modelling, and other researchers had to be relied on for field data.

This chapter describes the previous studies on Macquarie Harbour and Chapter Two provides the background on the numerical modelling of estuaries. Chapter Three develops the analytical equations behind the river model, which are then solved with an implicit finite difference scheme described in Chapter Four. Chapter Five describes the application of the model to Macquarie Harbour and the output is given in Chapter Six and Seven to explain the hydraulic behavior of both the harbour and rivers respectively. Chapters Six and Seven also contain verification of the model against sparse field data. Finally, Chapter Eight discusses the model and its success in modelling Macquarie Harbour, including scope for future work and how the model has been used to manage aquaculture in the harbour.

1.2 Harbour surroundings and history

Macquarie Harbour is a hydraulically complex estuary located on the west coast of Tasmania. A state government Department of Environment and Land Management (DELM) map (Figure 1.2) gives an overview of the harbour and surroundings, with references to more detailed views. The west coast of Tasmania is the first major land mass encountered after Africa, resulting in strong westerly winds (the "Roaring Forties") and an annual rainfall of over four metres. Surrounding Macquarie Harbour the land is predominantly rugged wilderness, with the township of Strahan (population $\approx$ 600) at the north of the harbour being the only population centre in the area. This combination of remoteness and extreme weather conditions makes fieldwork in the area difficult and expensive.

The human history of Macquarie Harbour extends back tens of thousands of years to the first aboriginal inhabitants. The last two hundred years saw the settling of Europeans in Australia, with Tasmania used as penal settlements for convicts. Macquarie Harbour has a strong convict history with Sarah Island in the south of the harbour used as a prison for the worst felons, before the Port Arthur penal settlement in the South East of the state was completed. Sarah Island is now a popular destination for the harbour cruises that operate out of Strahan.

Tourism is Tasmania's main growth industry, relying on the state's clean green image, natural beauty, and interesting convict history. The spectacular beauty of the Tasmanian wilderness is evident with a cruise up the majestic Gordon River. With temperate rainforest down to the river and stunning gorges, it is clear why most of the land in South West Tasmania is listed as a World Heritage area.

Macquarie Harbour is a large estuary by Australian standards (Cresswell, Edwards, and Barker, 1989), with an area of approximately 280km^2, roughly 30km by 9km (Figure 1.3). It has an average depth of 25m and a maximum of 55m. The harbour has one narrow passage

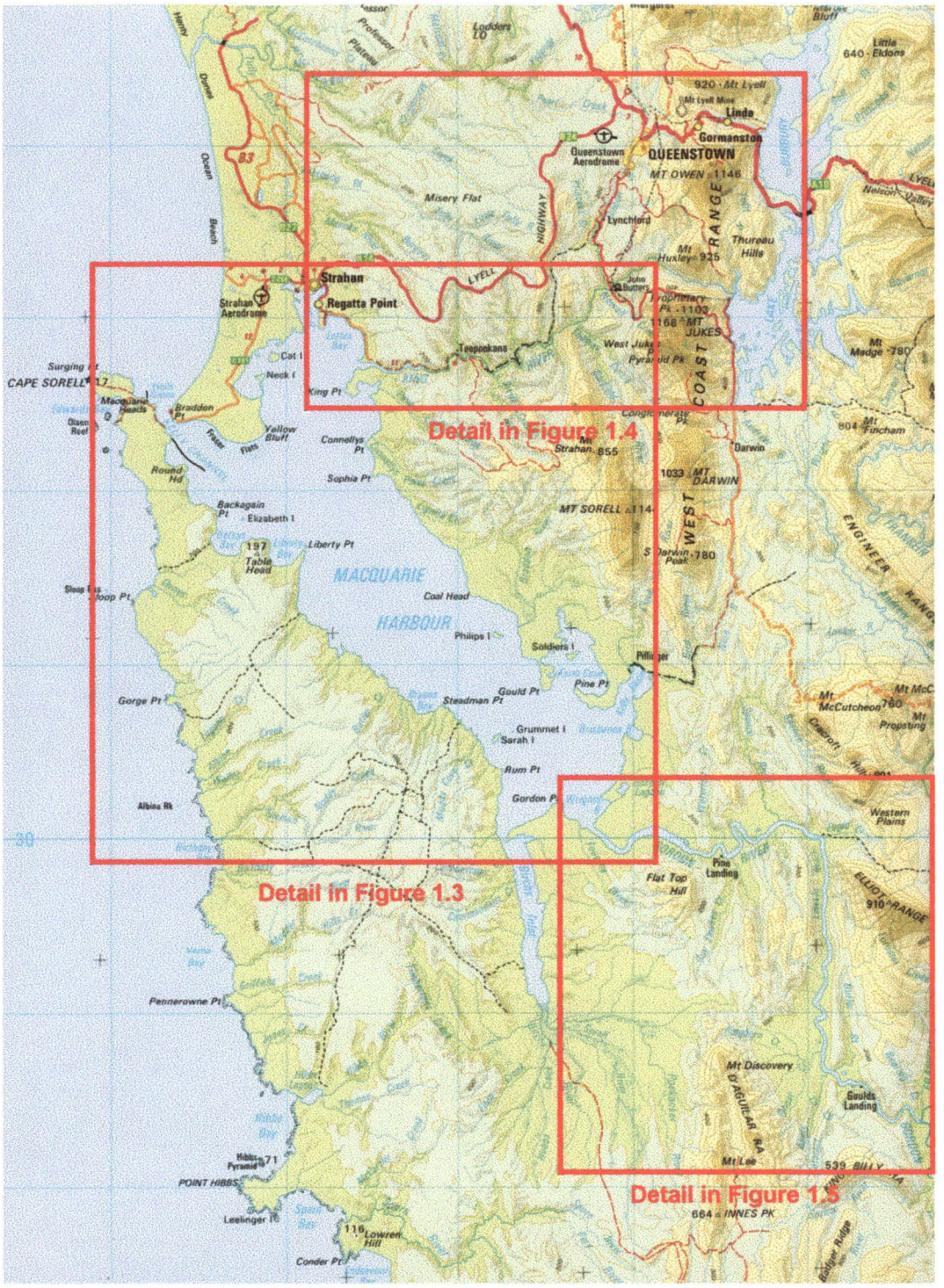

Figure 1.2 Macquarie Harbour and detail locations, with light blue grid on this and detailed maps at 10km intervals (DELM, 1994)

to the sea through Hells Gates in its north west corner. The main rivers feeding the estuary are the King River and the Gordon River. Both these rivers have been dammed upstream for hydro-electric power generation by the Hydro Electric Corporation (HEC).

Until recently, Strahan was predominantly a fishing town but now has an increasing income from tourism. The primary activities around Strahan are fishing, forestry, mining, and

Figure 1.3 Macquarie Harbour detail (DELM, 1994)

tourism. Several fish farms are scattered around the harbour, with more planned (Koehnken, 1998).

Mining has been the primary industry for most centres on the west coast of Tasmania. Tailings and dissolved heavy metals from the Mt. Lyell copper mine near Queenstown (population ≈ 3000) were discharged into the Queen River, which flows into the King River. The Mt. Lyell Mining and Railway Company stopped discharging tailings into the Queen River in December 1994 after 80 years of mining, and a 2.5km^2 tailings delta at the mouth of the King River still remains as a visible reminder of these mining operations. Without the buffering effect of the tailings from the mine, dissolved metal concentrations in the harbour increased immediately after the mine closure (Koehnken, 1996). Mining at Mt. Lyell resumed in 1995 with a new company, Copper Mines of Tasmania (CMT), under stringent environmental legislation.

1.3 King River and Gordon River

With a catchment of 809km^2, the King River flows into the north east corner of Macquarie Harbour (Figure 1.4). It has a flow rate varying from 1 – 300m^3/s, with a typical value of 70 m^3/s (Koehnken, 1996). The river is joined 20km upstream of the harbour after leaving the John Butters Power Station by the Queen River. The Queen River has a much smaller catchment than the King River at 78km^2, but is important because it continues to be heavily polluted - even without the dumping of mine tailings, due to acid mine drainage.

The Gordon River flows clean and cool from the Gordon Power Station 50km from the harbour. The Gordon River has a catchment of 5702km^2, with flow rates of 5 – 3000m^3/s, typically 300m^3/s (Koehnken, 1996). Downstream from the Gordon Power Station (with flow rate 0 - 173m^3/s), the Gordon River is joined by the Denison River, the Olga River and then the Franklin River, as illustrated in Figure 1.5. After the Franklin River joins the Gordon River, the Gordon River deepens and widens until reaching Macquarie Harbour. In this thesis 40km of the Gordon River upstream from the harbour has been modelled. This reach has many deep holes, with the bathymetry ranging from 5 - 25m. At the mouth of the river, there is a mobile sand bar at a depth of 3m.

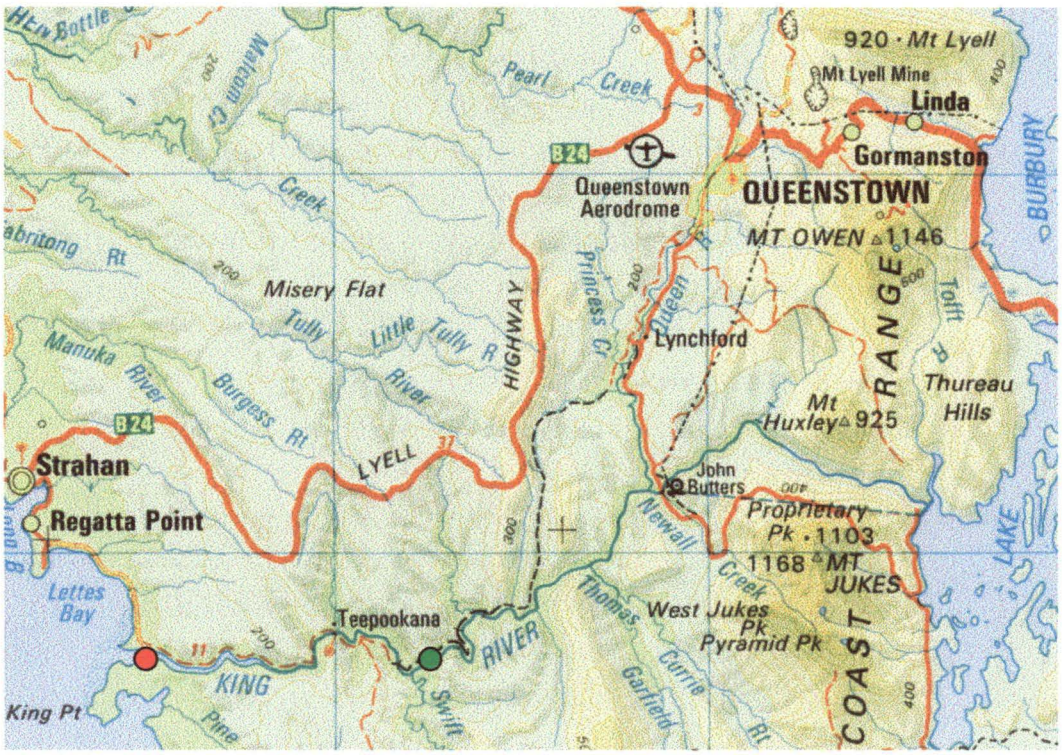

Figure 1.4 King River and surroundings, with upstream (●) and downstream (●) ends of 10km river model (DELM, 1994)

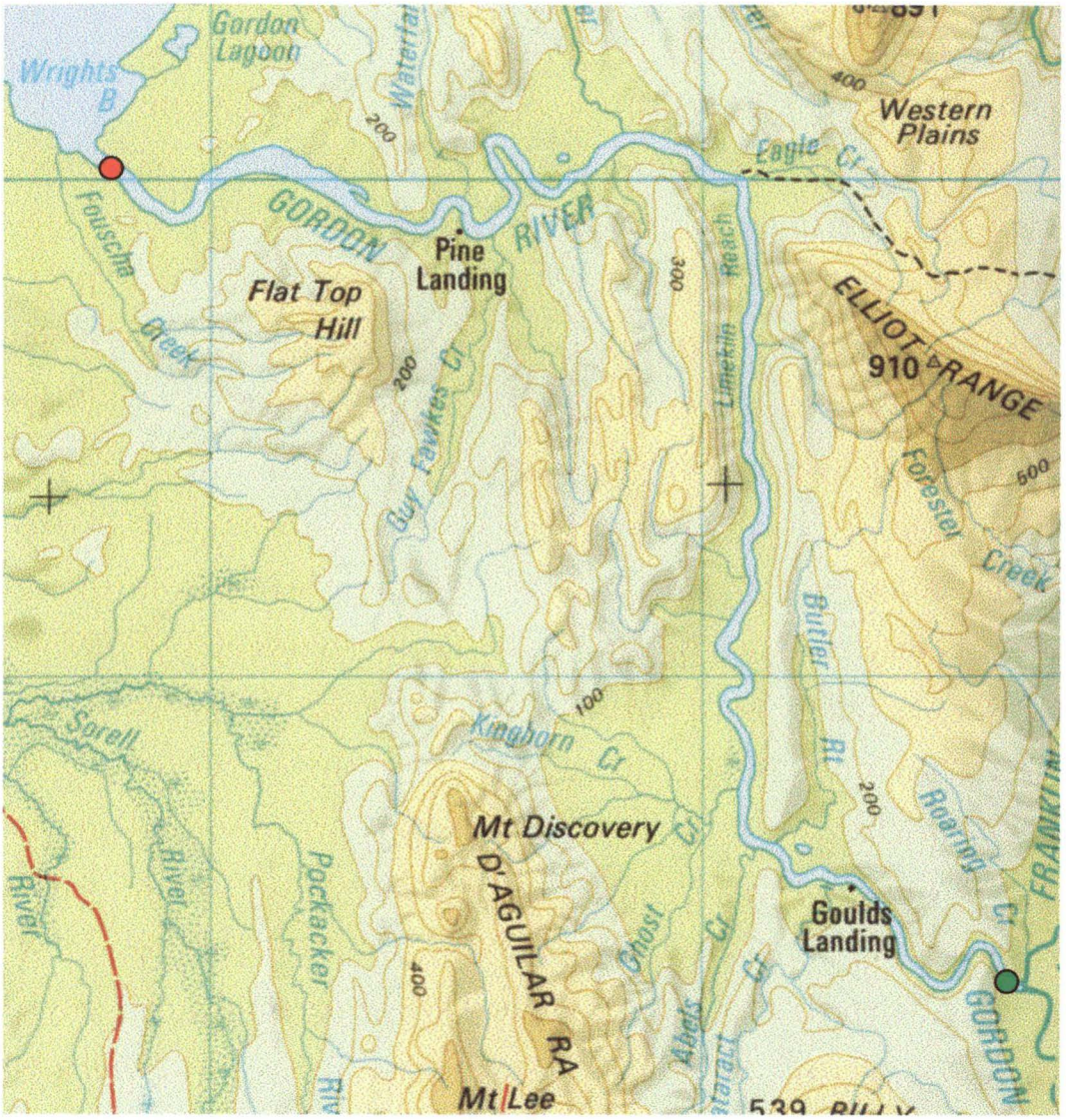

Figure 1.5 Gordon River and surroundings, with upstream (●) and downstream (●) ends of 40km river model (DELM, 1994)

1.4 Southern Ocean

Entering Macquarie Harbour through Hells Gates, the waters of the Southern Ocean have a salinity ranging from 32 - 35‰ and a temperature of 12 - 15°C. In calmer weather the water column entering the harbour is typically brackish for the surface 2-3m, with a salinity of 30‰ for the lower water column. When there are strong westerly winds the entire water column can be saline (Koehnken, 1996).

The tides in Macquarie Harbour are almost unpredictable and strongly influenced by meteorological forces and land drainage (Bell, 1899). Bell (1899) observed a 1.52m increase to tide levels during strong north-westerly winds, and an increase of 1.37m after a rainfall of 63.5mm in 24h. More recently, Easton (1970) classified the tide adjacent to the harbour as

mixed (Table 1.1). For south-west Tasmania, Matthews (1978) summarised the tide as having small diurnal to semi-diurnal ratios and a minor semi-diurnal solar component, classifying it as micro-tidal with a tidal range less than 1.2m.

From HEC tide gauges, Koehnken (1996) describes the tides as being diurnal with an occasional semi-diurnal component. Also evident is the effect of weather systems passing Macquarie Harbour, which can have a larger effect than the diurnal and semi-diurnal components. Typically the tide inside the harbour has a range of 0.12 – 0.22m, with meteorological conditions producing tides up to 0.70m (Koehnken, 1996).

Trailing walls have been used inside and outside the harbour to keep open a marked shipping lane. The restricted passage to the harbour provides shelter from the open ocean, with a tidal range of 0.76m at the entrance resulting in a tidal range of 0.30m at Strahan inside the harbour (Bell, 1899). As well as tidal changes, a 1965 Florida Coastal Engineering Laboratory Report (extract in Waterman and Matthews, 1979a) found the significant wave height was reduced as well. During a flood tide, 600m north west of the outside breakwater, the significant wave height $H_s = 1.98$m, while at the same time inside the passage to the sea $H_s = 0.762$m. The 1965 Florida Coastal Engineering Laboratory Report also detailed velocities near Hells Gates during the tidal cycle (Table 1.2).

Mean semi-diurnal spring tide range $MSR = 2 (M_2 + S_2)$	0.415m
Mean diurnal spring tide range $MDR = 2 (O_1 + K_1)$	0.652m
Tidal range $R_6 = MSR + MDR$	1.067m
Tidal type $R_3 = MSR / MDR$	1.57 (mixed)

Table 1.1 Tidal components for Cape Sorell, just outside Macquarie Harbour, M_2 = principal lunar semi-diurnal, S_2 = principal solar semi-diurnal, K_1 = lunisolar diurnal, O_1 = principal lunar diurnal (Matthews, 1978)

Tide	Normal peak velocity (m/s)	Maximum observed velocity (m/s)
Ebb tide	1.52 – 2.13	4.57
Flood tide	1.07 – 1.52	3.05

Table 1.2 Peak velocities near Hells Gates, (Waterman and Matthews, 1979a)

1.5 Hydraulic structure of the harbour

Previous studies of Macquarie Harbour have been undertaken to better understand and manage the harbour. Currently this need to manage the harbour has become more important with the increased used of the harbour for aquaculture and tourism. The environmental requirements of these industries conflicts with the water being polluted. This conflict in the past has resulted in the killing of fish from a fish farm near Yellow Bluff, in the north of the harbour, by a plume of polluted water originating from the King River (DELM, 1990).

Waterman and Matthews (1979a) reviewed published and unpublished studies on Macquarie Harbour as part of the *South West Tasmania Resources Survey* by National Parks and Wildlife Service, now part of the Department of Environment and Land Management (DELM). After the initial review, the harbour was studied to work out its currents, tide, temperature and salinity (Waterman and Matthews, 1979b). At a similar time, the HEC investigated the hydraulics of the Gordon River when they were considering damming its main tributary, the Franklin River (HEC, 1979). This survey described the general hydraulics of the river, including salinity profiles. Due to public outcry and protest in 1983, the Franklin Dam did not proceed. The area has since become part of the Franklin-Gordon Wild Rivers National Park (Figure 1.1).

Cresswell, Edwards, and Barker (1989) of the Commonwealth, Scientific, and Industrial Research Organisation (CSIRO) Division of Oceanography completed a survey in 1985 looking at the seasonal variability of water quality within Macquarie Harbour. This survey found the structure of the estuary to be similar to that found by Waterman and Matthews (1979b). These surveys indicate there are three layers in the estuary: a surface layer that is effected by the inflowing rivers with a seasonal temperature variation; a slowly changing mid-level layer; and in the deeper parts of the harbour there is a marine layer fed by tides flooding over the shallows from Hells Gates. This structure varies both daily and seasonally. Another CSIRO study of the harbour chemistry found the same three layers: a 0 - 10 m layer with a salinity range of 10 – 30‰ and temperature > 16°C; a middle layer with salinity 30 – 31.5‰ and temperature < 15°C; and a deep layer of marine water with salinity > 31.5‰ and temperature > 15°C (Carpenter *et al.*, 1991).

With the impending closure of the Mt. Lyell mine in 1994, a co-operative project was established to study Macquarie Harbour and the King River (Koehnken, 1996). This involved DELM, the Hydro Electric Commission (now the Hydro Electric Corporation), The Mt. Lyell Mining and Railway Co. Ltd, Inland Fisheries Commission, Department of Primary Industry and Fisheries - Sea Fisheries Division, and the Department of Community and Health Services. During pre and post Mt. Lyell Mining and Railway Co. mine operations, this study looked at estuarine structure and water quality through the

measurement of currents, tide, salinity, temperature, dissolved oxygen, sediment and dissolved metals. The velocity profiles found in a three day survey in the northern third of the harbour, using a RD Instruments 1200 kHz Broad-band acoustic doppler current profiler (BB-ADCP), provided a snapshot of the complex currents in the harbour (Koehnken, 1996).

Generally, the relatively clean water from the Gordon River flows north up the western side of the harbour. At mid depths south of the mouth of the King River, there is a mixing of the polluted King River water, Gordon River water, and seawater. This mixed water then flows south along the eastern harbour. Koehnken (1996) gave measurements from a July 1993 study that describe the water column, recorded mid-way along the eastern side of the harbour (Figure 1.6). These measurements are typical of the harbour's water column.

In 1996 the *Mt. Lyell Remediation, Research and Demonstration Program* (MLRRDP) was established with a $2 million grant from both the State and Federal governments in a joint program between DELM, the Federal Office of the Supervising Scientist (OSS), and the Environmental Research Institute of the Supervising Scientist (ERISS). The MLRRDP consisted of 17 projects that investigated the impact of mining at Mt. Lyell on its surroundings, including Macquarie Harbour, and to explore remedies for the damage. Part of a project looking at the behavior of copper in the sediments and waters of Macquarie Harbour, found that in general the water column contained at least two distinct bodies of water: a brackish layer (4 – 10‰) with an abrupt change to water approaching seawater salinity (25 – 35‰) (Teasdale *et al.*, 1996). At times, four layers were observed with considerable daily variation.

To illustrate the complexity of the harbour circulation Figure 1.7 illustrates BB-ADCP output on a vertical section between Yellow Bluff and Sophia Pt, while Figure 1.8 shows a vertical section between Dead Horse Bluff and King Pt on two successive days (Lawson and Treloar, 1994). The three sections are given at the same point in the tidal cycle, when the tide is turning from ebb to flood. The difference in velocities between Figure 1.8.a and Figure 1.8.b is attributed to changes in wind conditions. When these velocities were recorded the daily wind conditions at Granville Harbour (45km north of Strahan) varied by 2m/s and 10°C. The harbour is clearly sensitive to wind stresses and has large changes in velocity through the water column due to the wind.

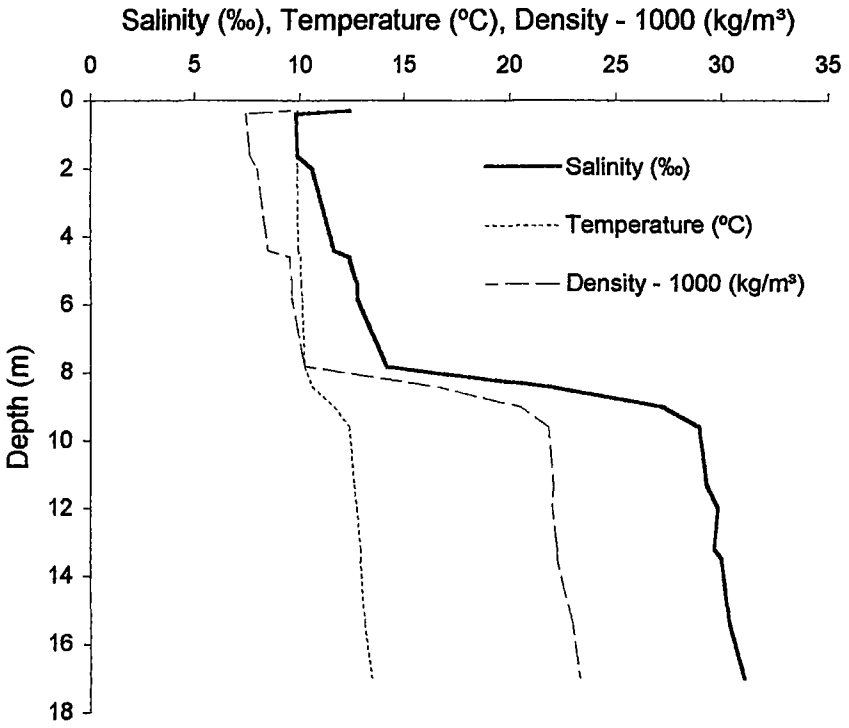

Figure 1.6 Typical salinity, temperature, and density variation in harbour off Sophia Pt in July 1993 (Koehnken, 1996)

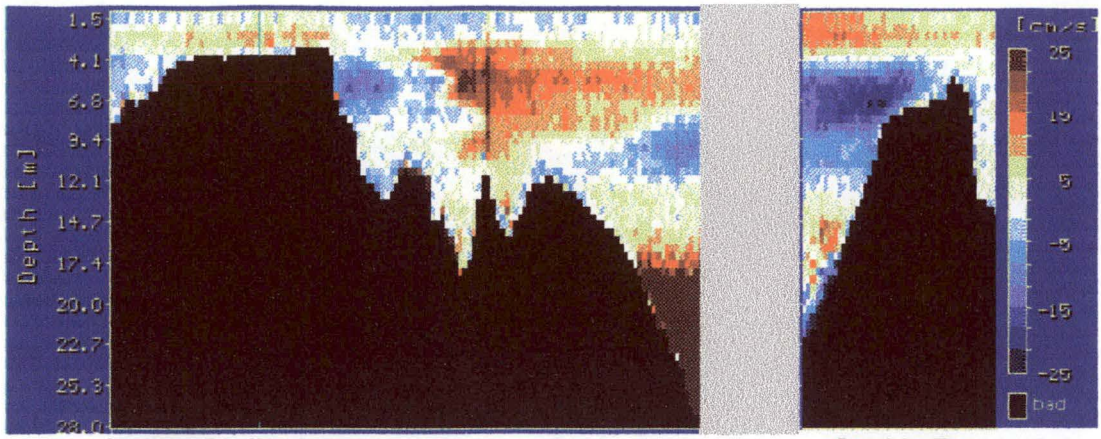

Figure 1.7 Horizontal velocity (north component) section compiled from BB-ADCP data between Yellow Bluff and Sophia Pt on 29 September 1993, grey area was not covered by the BB-ADCP (Lawson and Treloar, 1994)

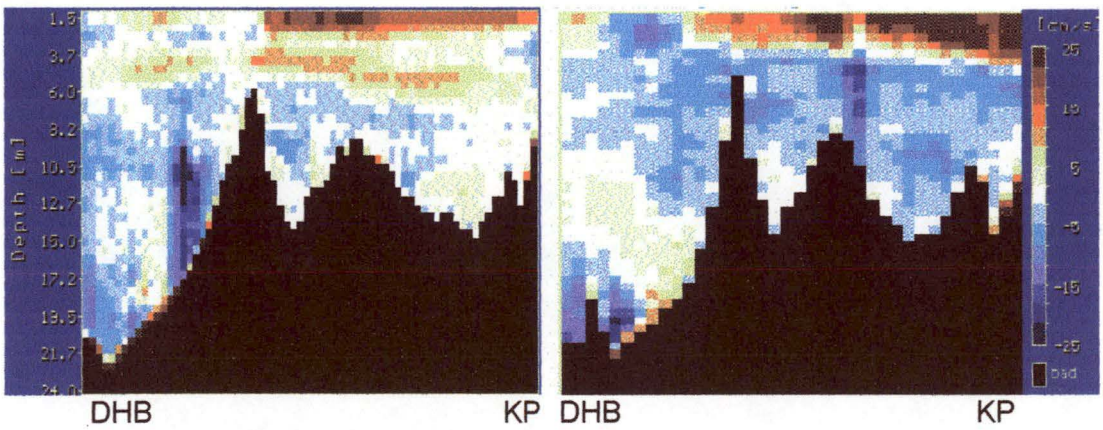

(a) 9:11am, 30 September 1993 (b) 9:50am, 1 October 1993

Figure 1.8 Horizontal velocity (north component) section between Dead Horse Bluff (DHB) and King Pt (KP) across the mouth of the King River, from BB-ADCP data on 30 September 1993 and 1 October 1993, with measurements taken at the same point in the tidal cycle on both days (Lawson and Treloar, 1994)

Chapter Two
Numerical modelling

2.1 Introduction

Numerical modelling is a tool for solving engineering problems. In the case of Macquarie Harbour the problem ranges from calculating general circulation to determining whether the pollutant distribution will effect a specific fish farm. There are many methods for numerically solving equations that describe fluid flow, and solution techniques are dependent on the particular physical situation and problem to be solved (Roache, 1976; Fletcher, 1988; Hirsch, 1988). Physically, estuaries combine aspects of river, coastal, and oceanic systems. An estuary is usually shallow like many rivers and lakes, and like oceans they contain density driven currents and are subject to the Coriolis force.

2.2 Direction of numerical modelling

Numerical modelling is constantly being refined with the aim of solving more sophisticated problems, more accurately, and for less time and money. The level of sophistication required for solving a problem will vary between estuaries due to their individual nature and their specific problems. "Sophistication" in this context means the level of realism and complexity of physical phenomena that are represented in the model. The level of sophistication that is solvable is limited by the modeller's skill, data availability, and computing power. With the progressive increase in computer processing speed and memory, there have been corresponding improvements in the accuracy of estuary models.

There appears to be as many solving schemes for estuary models as there are problems. This is because numerical modelling is a creative process, based on individual's interpretation and experience. While numerical modelling is a creative process, it relies on appropriate tools and could not start until the advent of computers in the 1950s, as numerical modelling with hand calculations is not practical for anything but simple cases. Since its inception,

numerical modelling has evolved dramatically. Four decades ago one-dimensional models were at the cutting edge of numerical modelling. Now there are three-dimensional models with second moment turbulence closures predicting recirculation, boundary layers, and pollution dispersion.

With numerical modelling becoming a more refined tool, there has been an increasing emphasis in the last two decades on using it in preference to physical modelling for studying water quality (Falconer, 1991). As well as solving problems better, numerical modelling is becoming available to a wider community of people due to low cost powerful computers and more user-friendly software. As the new community of users, often not specialists in numerical modelling, start to push the limits of their new tools, there will be problems when the limits are crossed without the user realising.

While numerical modelling is more appealing than physical modelling, because of better scalability, perceived cost, transportability, and adaptability, this appeal can cause problems with the misuse of the models through the placement of unrealistic expectations on them and their output. Like physical modelling, numerical modelling has its limitations and while the output of a model can look authoritative, it is only as good the assumptions made in the model. These limitations include using steady state bed friction assumptions for unsteady flow, uncertainty of diffusion and dispersion coefficients, limited chemical and biological models, simplifications used to make a numerical model, and inaccurate boundary conditions (Falconer, 1991). When users understand the limitations of a model, they will have realistic expectations of what it can do.

Even with the increased emphasis on numerical modelling there will always be a place for physical modelling and field data (Jirka, 1989), because numerical models need accurate data so they can be calibrated and verified. With the increasing ability of satellite and sonar technology, field measurements have become more accurate and accessible to make numerical modelling more accurate.

2.3 Model equations

A numerical model is based on analytical equations that relate the important fluid properties to each other and to a spatial and temporal co-ordinate system. In the study of an estuary, these quantities include water velocity, depth, temperature, salinity, pollutant concentration, density, eddy viscosity and eddy diffusivity.

The equations used as a basis for a model will depend on the problem and the method of solution. Due to the rectangular plan shape of Macquarie Harbour and its large density variations, three-dimensional equations are needed to fully study the hydraulics. As the

rivers are very slender in plan (that is, long compared to their width) and have complex vertical density variations, two-dimensional laterally averaged equations are needed. It would be possible to represent the system with simpler equations, such as horizontal two-dimensional equations for the harbour and one or zero-dimensional equations for the rivers, although these would not describe the system satisfactorily. Initially, zero-dimension equations were used, albeit unsuccessfully, to describe the river boundary conditions on the harbour. Three-dimensional river equations could provide more information, but not commensurate with the effort required.

As Macquarie Harbour is a shallow tidal estuary, exposed to strong winds and having varying river inflows, time dependent equations are required. Steady state equations would not be able to predict flood events that are responsible for river flushing and pollution plumes, and the flood tides that are the source of marine water in the deep basins of the harbour (Cresswell, Edwards, and Barker, 1989). Hence, the model is to be based on unsteady two and three-dimensional equations.

2.3.1 Co-ordinate system

Conservation equations are usually derived around an Eulerian co-ordinate system that is fixed with respect to the water flow. Alternatively, a Lagranian co-ordinate system can be used, which moves with the water flow like a tracer. Eulerian systems are favored as their fixed grid makes coding and visualisation easier to implement. In the horizontal plane, Eulerian co-ordinates are in general orthogonal curvilinear or as a special case they can be rectangular (Wang, 1992). Curvilinear co-ordinates are more computationally efficient, as co-ordinates that hug curved land boundaries waste fewer grids than a rectangular grid.

The river model in this thesis uses a fixed horizontal right hand co-ordinate system. The z^* direction is positive vertically upward, the x^* direction is positive along the river's main axis, and the y^* direction is positive in the lateral direction. The asterisk symbolises that the co-ordinate has not been transformed to σ co-ordinates. A σ co-ordinate is a scaled vertical co-ordinate that varies between 0 at the free surface and -1 at the bottom, and a σ transformation changes the dimensional vertical co-ordinates to σ co-ordinates. To be consistent with POM, a σ transformation is used on the river model's vertical co-ordinates to non-dimensionalise depth. Horizontally POM uses an orthogonal curvilinear horizontal co-ordinate system, although in this thesis a constant horizontal grid size is used throughout the solution space.

The z^* co-ordinates are often transformed to a σ co-ordinate system in estuary and ocean modelling. The σ co-ordinates can be time independent, $\sigma = z^*/H$, and used with a rigid

lid approximation (Gerdes, 1993), or time dependent, $\sigma = (z^* - H)/(H + \eta)$, as used in POM (Blumberg and Mellor, 1987). A σ transformation allows for greater vertical resolution in the shallow regions compared to a z^* co-ordinate system. It also handles the top and bottom boundaries more accurately, because the σ co-ordinates are the same as the top and bottom surfaces of the solution space. The greater vertical resolution, while more accurate, means there is a need to use a smaller time step based on the Courant, Friedrichs and Lewy (CFL) limit. As with curvilinear horizontal co-ordinates, when there is a varying bathymetry, the σ co-ordinates do not waste computational grids compared to a z^* co-ordinate system.

The σ co-ordinate system has the disadvantage of truncation errors in the horizontal pressure terms and an increased diapycnal diffusion (Gerdes, 1993). The truncation errors are caused by the extra term due to the σ transformation of the horizontal pressure derivative. The horizontal pressure gradient used in the river model is transformed to the σ co-ordinate system giving

$$\frac{\partial p}{\partial x^*} = \frac{\partial p}{\partial x} + \frac{\partial p}{\partial \sigma}\frac{\partial \sigma}{\partial x} \tag{2.1}$$

The $\frac{\partial p}{\partial \sigma}\frac{\partial \sigma}{\partial x}$ term from (2.1) creates the truncation errors. Erroneous diapycnal diffusion is due to diffusion in the numerical scheme, where the vertical co-ordinate surface is not aligned with the isopycnal surfaces. This will occur with both z^* co-ordinates and σ co-ordinates, but with large bottom slopes it is expected to occur more with the σ co-ordinate system (Gerdes, 1993). Blumberg and Mellor (1987) simplified their σ transformed diffusion terms to reduce errors for large bottom slopes.

2.3.2 Conservation equations

A three-dimensional model contains conservation equations for vector and scalar quantities in one temporal direction and the three spatial directions. The vector quantity is momentum, and the scalar quantities are water mass, salinity, temperature, pollution concentration, and turbulence energy. One and two-dimensional equations are derived by integrating the three-dimensional equations. Simplifications to the complete set of equations are required to make a solution practical. The simplifications are based on the problem being solved.

In estuaries, where the horizontal length scale of motion is several orders of magnitude larger than the vertical dimension, the vertical momentum equation reduces to a hydrostatic pressure variation (Koutitas, 1988).

Typically the Boussinesq approximation is applied to the conservation equations, which allows density variations to be neglected except in the gravity terms (Kundu, 1990). POM uses Boussinesq equations, although there was a version of POM that used non-Boussinesq equations to check the Boussinesq approximation (Mellor and Ezer, 1995). It was found that the Boussinesq approximation caused a 1cm variation in ocean surface elevation and reversed the vertically averaged flow, due to thermal expansion in the global model because of seasonal temperature variation. Mellor and Ezer (1995) suggested a correction to the Boussinesq equations that was spatially independent and time dependent.

2.3.3 Turbulence closure

Estuarine flow, as with most flows encountered in engineering, is turbulent. The random or turbulent nature of a fluid is probably the least understood aspect of fluid motion. In a viscous fluid such as water, diffusion will reduce the spatial gradients of vector and scalar quantities. Fick's Law for mass diffusion empirically represents the diffusion phenomena, which states that a quantity diffuses from high to low concentration. Fourier's Law for heat transport is similar to Fick's Law, whereby heat flows from high to low temperature. With both Fick's and Fourier's Law, the flow rate is $\mathbf{q} = -k\nabla C$, where k is a constant of proportionality and ∇C is the concentration gradient. In the case of mass flow C is the salt or pollutant concentration, in heat flow C is the temperature, and for momentum flow C is the velocity.

At scales smaller than a millimetre, random molecular motion in combination with molecular forces form molecular viscosity. The effect of viscosity acting on the fluid flow is equivalent to a shearing stress that removes energy from the flow. Newton's law of friction for laminar flow states

$$\tau = \mu \frac{du}{dz*} \tag{2.2}$$

Where τ is the shear stress and μ is the dynamic viscosity. More commonly kinematic viscosity $\nu = \mu/\rho$ (ρ being the density) is used instead of dynamic viscosity, as acceleration due to viscous diffusion is proportional to ν. Kinematic viscosity could be called "momentum diffusivity" to make the analogy between heat and momentum diffusion clearer, as heat diffusivity is the equivalent to kinematic viscosity for the diffusion of temperature.

In general, shear stress is a second order tensor quantity, with nine components. This stress tensor is formulated using Reynolds decomposition, where a value is the sum of a mean and turbulent value. The turbulence closure problem is about relating the turbulent values in the decomposition to a known quantity, such as the mean flow values.

As estuaries are modelled at an eddy scale of metres to kilometres rather than the millimetre scale of molecular viscosity, the turbulence closure is the representation of the turbulent eddies that dissipate energy. The closure is achieved with an analogy to molecular viscosity using eddy viscosity, which is a crude approximation given the complexity of the turbulence it has to describe. Eddy viscosity is a flow property, unlike molecular viscosity that is a fluid property. In between eddy and molecular motion, as the eddy size diminishes, energy is transferred from larger to smaller eddies, until at a molecular scale the energy is lost as heat.

Molecular viscosity is negligible compared to eddy viscosity in estuaries, with two exceptions. Firstly, near density interfaces where turbulence is suppressed, and secondly during double diffusion, with salt fingers occurring where heat diffuses faster than salt. As the diffusivity values are assumed to be the same for heat and salt in the river model, the microstructure of salt fingers could not be modelled, even if the grid size was small enough to resolve their 20 - 30cm length and 1cm spacing (Knauss, 1978).

In an estuary, there is a large range of eddy viscosity and eddy diffusivity values, collectively called diffusion values. Vertical diffusion values used in this thesis are in the range $10^{-5}m^2/s$ to $10^{-2}m^2/s$ and horizontal values range from $10^{-1}m^2/s$ to $10^{3}m^2/s$. Momentum diffusion is greater vertically than horizontally, although the diffusion values are larger in the horizontal direction because the vertical gradients are much larger. Even so, the horizontal momentum diffusion is usually retained for the purpose of numerical stability (Koutitas, 1988). While with scalar quantities both horizontal and vertical diffusion are important, as scalar quantities have no large driving forces such as the pressure force that acts on momentum.

There are many schemes for numerically calculating diffusion values. Blumberg and Mellor (1987) used a prognostic turbulence model for POM. This involves two conservation equations, similar to the momentum or heat conservation equations, for modelling turbulence energy and turbulence macroscale. Compared to this, the river model in this thesis calculates diffusion values using the simpler diagnostic Prandtl mixing length model. The term "prognostic" refers to predicting future values, while "diagnostic" refers to calculating present values.

2.3.4 Boundary conditions

The system considered for a model comprises the solution space and the surrounding space. Boundary conditions relate surroundings to the solution space. In the case of an estuary, boundaries exist where the estuary water has an interface with the land, open sea, atmosphere, and inflowing rivers. As a model predicts what will happen in the future, it has to know at some point in time what the conditions in the solution space are. These conditions are called the initial conditions of the model. Each problem in numerical

modelling of estuaries is different from another only by its geometry, initial conditions, and boundary conditions.

In a model most of the effort goes into solving the solution space, with only a small part devoted to solving the boundary conditions. Boundary conditions can be based on either equations of motion, field data, or a combination of both. The difficulty is that boundary conditions not only have to model everything that surrounds the solution space, but to do so with a simpler model than those used for the solution space. Usually the surroundings are much more complex than the solution space, making it even more difficult to accurately achieve with a simpler model. The solution space boundaries should be chosen where the boundary conditions can be accurately defined. This is seldom possible and is a limitation of numerical modelling.

Boundary conditions are required for each variable in the system, but will vary in accuracy due to the limited information available on each variable. A quantity like temperature can be accurately modelled in the surroundings of a study area, allowing a well defined boundary condition (Kim and Chapra, 1997). The hardest boundary conditions are open boundaries, where it is not known what is happening outside the solution space. For example, a surface elevation boundary at the open sea side of an estuary model is an open boundary. If the sea state is unknown at the boundary, the sea is assumed infinite and ideally the boundary condition should not cause a reflection back into the solution space from outgoing waves.

In the model of Macquarie Harbour, open boundaries are required upstream of the river models and on the open ocean side of the sea model. The rivers extend upstream further than the salt wedges, so salinity conservation is simpler at the boundary.

Davies (1983) assessed some common lateral boundary conditions used in meteorological models. These were the boundary zones of diffusive damping, tendency modification, flow relaxation, and a pseudo-radiation scheme. Similar schemes are used in estuary and ocean modelling, with flow relaxation and radiation schemes being popular. Engedahl (1995) used flow relaxation in the Nordic Seas, and Holloway (1996) used it for modelling the Australian North West Shelf (both authors used POM). Flow relaxation is designed to force values near the boundary towards a specified value.

A radiation boundary condition scheme allows waves to move out of the solution space, leaving the wave and interior unhindered. Sommerfeld (1964) conceived the radiation condition and Orlanski (1976) implemented it for ocean modelling. As noted by Raymond and Kuo (1984), the term "radiation condition" does not refer to the radiation as it is traditionally used in mathematics and physics, but rather as a numerical procedure for determining inflow and outflow from a solution space. The term radiation is retained as the

procedure predicts how a wave radiates. The difficulty with the radiation condition lies in determining a value for the phase speed of the wave.

There have been many schemes proposed for modelling the radiation condition, each one being tuned to solve a particular problem. Orlanski (1976) used a phase speed based on local function slopes. This was modified by Camerlengo and O'Brien (1980) to work more efficiently for Kelvin waves, but not as well for Rossby waves, and Israeli and Orszag (1981) combined the radiation condition with damping functions. At a similar time Miller and Thorpe (1981) reviewed previous radiation conditions for meteorological modelling and formulated a more accurate condition. This scheme was generalised by Carpenter (1982) to allow for waves entering the solution space, as well as the existing outgoing waves. Røed and Smedstad (1984) continued this work for forced waves in a rotating fluid, using a similar wave speed to Orlanski (1976).

Blumberg and Kantha (1985) used the shallow water wave celerity for the phase speed and included an external forcing, which used a similar form for the external forcing to Carpenter (1982). With so many radiation schemes proposed, many researchers started combining existing schemes. Shulman and Lewis (1995) optimised three radiation conditions using an inverse approach to minimise differences between model and observed values. Other advancements to the radiation condition where made by Tang and Grimshaw (1995), who compared six radiation condition schemes based on the Orlanski radiation condition, using a two-dimensional depth averaged model for studying coastally trapped waves. They found five to work well, with an explicit version of Orlanski's radiation condition not performing well. This explicit version was used in Miller and Thorpe's (1981) scheme.

While all these radiation schemes work well for the problem being solved, they do not generalise well. This is because the radiation condition not only has to get the hydraulics correct, but it also has to work with the response of a particular numerical scheme. As numerical schemes are as diverse as the hydraulics they model, it is reasonable that the radiation condition needs to be formulated for each problem. Kantha, Blumberg and Mellor (1990) assessed several methods for calculating phase speed based on local surface elevation differences, and proposed a recursive filter to help where waves where not well resolved – making the scheme more robust. Even with this more elaborate approach, some changes would be required for a particular problem.

2.4 Solution technique

It is not possible to directly solve a model's analytical equations using mathematical manipulation, except under simplified situations. With a numerical solution, the continuous

functions are replaced by functions known at discrete grid points in space and time. The derivatives of functions known at discrete points are only an approximation of the original continuous derivative expressions, which allows for a linear solution to the model equations. Although only approximate, the numerical equations should still accurately predict the flow. To do this the finite difference equations must be:

1. consistent with the physics of the analytical equations
2. convergent with the analytical equations in the limit of the space and time grid
3. numerically stable, so cumulative errors do not override the solution and caused it to break down

A numerical scheme consists of derivative approximations and a method for solving the resulting equations. Most numerical techniques substitute the derivatives from a truncated version of a Taylor Series expansion. The derivative approximations commonly use either finite difference, finite volume, or finite element methods. In estuary modelling finite difference and finite volume methods are used in preference to finite element methods, because finite element methods are more complicated to implement and offer no computational effectiveness or efficiency over the other two methods except when the solution space has a complex geometry. Finite difference methods have been used for the river model in this thesis.

At the heart of a finite difference scheme are the finite difference operators that approximate the terms in the analytical equation. These operators are based on a truncated Taylor series. After the finite difference operators are substituted into the analytical equations, the unknown values make a system of equations at the future time step. Depending on the nature of the finite difference operators, the system of equations can be solved either explicitly or implicitly. Explicit schemes calculate a value directly for a future time step based on the values in the surrounding grids. Implicit schemes generate an equation for the entire solution space, which is solved for all values at once. As the conservation equations model the conservation of a quantity in one region (point, plane, or volume) in space and time, all finite difference operators in the equation should be centred at the same region in space and time.

Implementation of an implicit scheme is more difficult than an explicit scheme, due the requirement for solving a set of linear equations. Using a von-Neumann analysis, it is possible to determine the stability of a simple numerical scheme, which can be locally linearised (Chaudhry, 1993). This analysis predicts whether errors will decay or grow. In many cases, such an analysis is not practical due to the complexity of a scheme, and stability is usually found by trial and error. Assuming a frictionless channel, which simplifies analysis, it is possible to show that implicit schemes, such as the Preissmann scheme, are unconditionally stable when their time weighting coefficient $\theta > 0.5$. This means they can

step forward in time at greater than the CFL limit. Hence implicit schemes are preferred over explicit schemes, except where a model implementation is required quickly.

Approximations made to form the finite difference operators and numerical rounding during solving, lead to errors that propagate as waves in the solution space. It is important that this error propagation be minimised, as it results in inaccuracy and instability. Errors propagate according to the terms that generate them. Besides numerical errors, instability is caused in explicit operators when the time step is greater than the CFL limit, where the CFL limit is the time it would take a wave to advect across a numerical grid. The "wave" could be a numerical artefact or a representation of a physical wave. There is a similar time limit for the diffusion terms. These time limits are required for stability of explicit schemes and are only used as a guide for time steps in an implicit scheme, which are unconditionally stable for the CFL limit. It is more accurate to step the implicit numerical schemes forward in time at the CFL limit time step as this is equivalent to moving through the solution space at the wave speed, which reduces amplitude and phase errors.

Within a given system, each phenomenon of fluid flow has a different wave speed. For example, salt advects and diffuses at different rates. This wave speed will change in space and time, as the fluid changes. As the time step in a numerical model is usually fixed and it is best to step in time at the wave speed, there is need for a compromise. The difficulty is in choosing a time step that will give stability for the explicit parts of a scheme, not introduce amplitude and phase errors, and solve the problem in an acceptable time period.

The CFL limit for a surface wave is $\Delta t_x \le \Delta x/(|u| + c_x)$ where $c_x = \sqrt{gD}$ is the celerity of a surface gravity wave, and the diffusion limits are $\Delta t_{Dx} \le (2A_f/\Delta x^2 + |u|/\Delta x)^{-1}$ and $\Delta t_{Dz} \le (2K_f/\Delta z^2 + |w|/\Delta z)^{-1}$. To find which time step controls stability, typical estuary values are substituted into the time step equations: $\Delta x = 250$m, u = 1.0m/s, w = 10^{-5}m/s, A_f =10m^2/s, and K_f= 10^{-3}m^2/s. The results from this substitution are shown in Table 2.1, indicating that in shallow water the time step is controlled by vertical diffusion and in deeper water it is controlled by gravity waves.

In the fluid problem being solved, the wave speed is finite and the solution steps forward in

D (m)	Δz (m)	Δt_x (s)	Δt_{Dx} (s)	Δt_{Dz} (s)
1.0	0.1	61	230	5.0
30	3.0	14	230	4400

Table 2.1 Maximum time steps, with 10 vertical levels

time. A finite wave speed means that a value at one grid is only influenced by surrounding values. Hence, the matrix that is solved in an implicit scheme is banded. With a three point finite difference derivative approximation, the matrix is tri-diagonal. As banded matrices, tri-diagonal matrices can be solved with schemes more efficient than a full matrix inversion, such as an adapted Gaussian elimination procedure commonly called the Thomas algorithm (Roache, 1976, appendix A). As some boundary conditions in the river model use three grids, where a tri-diagonal matrix would only use two, the matrix is solved with the Naval Surface Warfare Centre (NSWC) FORTRAN library subroutine "BTSLV" (NSWC, 1993).

Errors can be reduced with better derivative approximations, although a compromise has to be made between accuracy and the number of grids required. Higher order derivative approximations require more grids, making a scheme slower to solve and causing complications at boundaries. At boundaries, it is only possible to use grids inside the solution space, making it difficult to have the same accuracy as the internal finite difference operators. In most cases, the accuracy of a model is limited by the accuracy of its boundary conditions. Also, if the wave length of a phenomenon is similar to the grid size it will not be well resolved, and using higher order derivative approximations with grids away from the wave will not improve accuracy. While a derivative is required at a specific point in space and time, the more "accurately" it is calculated by using more surrounding grids, the more of an average the value becomes.

With a limited number of grids used to construct a finite difference operator from, there is a limit to which higher order derivatives can be expressed. Using a predictor corrector method with explicit schemes can better utilise a limited number of grid points, as the two step process effectively creates an extra grid between every pair of grids. In another approach to improving accuracy, Verwey and Ilic (1993) retained more higher order derivatives by transforming them via the analytical version of the conservation equation, into lower order derivatives that could be implemented. The transformation involved differentiating the conservation equations with respect to time and space variables several times. This gave relationships between higher order derivatives and the lower order ones. Verwey and Ilic (1993) used this method with an implicit scheme on a one-dimensional water hammer problem. The author tried to apply a similar scheme to the two-dimensional laterally average river model equations but the difference equations became unwieldy when diffusion was included. Difference expressions for coefficients of a solving matrix were over a page long, making them very hard to code without mistakes. As numerical approximations were required for the transformed derivatives, there was no apparent gain in accuracy.

Rounding errors are reduced with more real number floating point precision and using relative differences in finite difference operators. Using relative differences can be to

remove a mean or a long term bias from values, or calculate temporal derivatives based on the difference from the current to the future time step.

2.5 Computer resources

Advances in computer technology have fuelled developments in numerical modelling. Faster computers with more memory can now solve more complex problems in a shorter time. Parallel processor computers are used for computational hydraulics (Davies, Grzonka, and Stephens, 1992; Ashworth and Davies, 1993) with gigabytes of RAM (random access memory) and hundreds of megahertz of clock frequency. Desktop personal computers (PCs) are becoming more competitive with machines that rival the big UNIX boxes for speed at a much lower price. This opens up the number of organisations that can do top end modelling.

The bulk of the modelling in this thesis was done using a desktop PC: an Intel Pentium – 133 MHz processor (with a GA-586HX motherboard) over clocked to 166MHz, 64Mb of RAM, and a 6.5Gb hard drive. Some final modelling was done on a dual 195MHz processor Origin 200 SGI with 500Mb of RAM. On the PC, the model ran under both the Slackware Linux v2.0.0, using Gnu FORTRAN g77, and Windows 95a (Win95a) operating systems, using Lahey FORTRAN F77L3 v5.0. The main visualisation package used, VIS5D v4.3, runs under Linux. Linux, the PC version of UNIX, provides a good multi-tasking and multi-user environment with lower system overheads than Win95a.

A numerical model is not a useful tool without good visualisation of the model's output. Visualisation is about modelling the model's output with audio and video means. This is done by representing the values from the various quantities with colours, symbols and sounds. Visualisation is important during model development and to present results from a working model. Visualisation sophistication has developed along with numerical model sophistication, starting with tables of numbers, line and contour graphs, surface and volume rendering, and now includes multimedia cyber-space fly throughs of a solution space.

VIS5D was designed for meteorological data visualisation, but works equally well for estuary data. A draw back with VIS5D is it uses a Cartesian vertical projection, while the model data used σ vertical projection, so interpolation is required. VIS5D can be controlled interactivity with a mouse and keyboard, or with a tool command language (Tcl) script. The Tcl scripting function was useful for generating graphs with the same scale.

VIS5D can generate contour slices, colour slices, iso-surfaces, and volume rendering of the solution space. These graphics can be animated in time or space to allow users a full appreciation of the model dynamics. In this thesis only still frames can be reproduced, which is a limitation of a hardcopy form of thesis.

2.6 Existing models

There are several forms of numerical models that can be applied to the study of estuaries. These range from a description in a journal article to expert computer programs that can manage and model a hydraulic system. The commercial model market is increasing, with models available that are useable by professionals who are not necessarily computational hydraulic experts (Abbott, Havnø, and Lindberg, 1991). There is a large investment to be made in implementing a model, involving many specialists. The high pricing of the commercial modelling packages reflects this investment. Fortunately there is still a strong community of researchers who share their knowledge and working models freely. POM is freely available upon registering with the authors.

Depending on the problem, one-dimensional, two-dimensional (depth or laterally averaged) or three-dimensional models could be appropriate.

2.6.1 One-dimensional models

As early as 160 years ago, Laplace and Lagrange were interested in one-dimensional unsteady flow (Cunge, Holly, and Verwey, 1980). In 1871 Saint-Venant formed a set of equations for modelling unsteady flow, although they could not be solved in general until the advent of modern digital computers in the 1950s. One-dimension models have been used for flooding in river networks (Terry, 1992), tides and surges (Wolf, 1978), and estuaries (James and Horne, 1969).

The one-dimensional equations have been solved with explicit and implicit finite difference methods and the method of characteristics (Wylie, 1970). The method of characteristics is also used for the boundary conditions of finite difference schemes. The method of characteristics simplifies the Saint-Venant equations by changing the reference frame from absolute, to relative to the wave front. The resulting equations give a more intuitive feel for the dynamics of the flow and are useful for hand calculations.

2.6.2 Two-dimensional, depth averaged models

When flow is no longer constrained to a river and spreads out into a lake or estuary, the one-dimensional model is inadequate in predicting the circulation and a two-dimensional depth averaged model (2DDAM) is required. The difficulty of solving 2DDAMs over one-dimensional models is the inter-dependence of the conservation equations from the two horizontal directions. That is, equations like the momentum equations in the x^* and y^* directions have common terms that mean the equations should be solved at the same time for each time step. However, this would create a large matrix inversion problem when using implicit schemes and usually an alternating direction implicit (ADI) scheme is used instead.

An ADI scheme alternates between implicit and explicit methods for solving in each direction during successive time steps. Each direction with the ADI equations is solved using similar techniques to one-dimensional models.

2.6.3 Two-dimensional, laterally averaged models

Where the flow along the minor axis of an estuary is insignificant compared to the flow along the major axis, then a two-dimensional laterally averaged model (2DLAM) is appropriate. Such a situation is the mouth of a river estuary that has a slowly changing cross section. 2DLAMs are also appropriate for highly stratified water, such as some reservoirs (Martin, 1988). Blumberg (1977b) studied the Potomac River Estuary with a 2DLAM. This estuary flows 185 km into Chesapeake Bay from north west of Washington D.C. Previously Blumberg (1977a) had studied the whole Chesapeake Bay system with a 2DDAM. The Potomac River Estuary gradually widens and deepens, with various tributaries, a 120km salt intrusion, and an annual mean freshwater inflow of $300m^3/s$. In another study, Boericke and Hogan (1977) applied a 2DLAM to a 89km section of the lower Hudson River from Poughkeepsie to Dobbs Ferry with a 2DLAM. The section of the lower Hudson River studied varies from being 500m wide and 450m deep, to 1300m wide and 9m deep. Flows vary from 100 – $7000m^3/s$, typically 200 – $1100m^3/s$. Even for this diverse range of estuaries, the 2DLAM successfully modelled the circulation and water quality.

In this thesis a 2DLAM is used to model sections of the Gordon River, King River, and sea. The configuration of these models is given in Table 2.2. As 2DLAMs have been used successfully for similar hydraulic situations to the thesis study area, confidence can be placed using similar techniques.

Perrels and Karelse (1981) reviewed five 2DLAMs and then created their own. The models reviewed were based on versions of the conservation laws, with variations between them in the inclusion or exclusion of longitudinal and dispersion terms. Turbulence closure is based

	Gordon River	King River	sea
length (km)	40	10	20
depth range (m)	5 - 25	1.0 - 1.6	5.5 - 90
width range (m)	70 - 250	30 - 250	75 - 1000
flow range (m^3/s)	5 - 3000	1 - 300	0 - 5000
typical flow (m^3/s)	300	70	-
feature	38km salt intrusion	polluted	tidal

Table 2.2 2DLAM overviews studied in this thesis

on either average velocity or mixing length, with a stability function based on Richardson number to modify the viscosity for gravity and buoyancy effects.

The finite difference schemes are solved with various methods, usually on a spatially staggered grid. Boericke and Hogan (1977) had a temporally and spatially staggered grid. To avoid the CFL and diffusion time constraints, implicit schemes are used vertically with an explicit scheme horizontally. Leonard (1977) in a review discussion, felt the Boericke and Hogan's (1977) upstream differencing would introduce artificially high diffusion, estimated at $u\Delta x/2 \sim 300 m^2/s$ for a velocity of 0.5m/s.

More recently, Stacey, Pond, and Nowak (1995) modelled the circulation in Knight Inlet, British Columbia, Canada. Their model used a laterally averaged version of the level 2.5 turbulence closure scheme of Mellor and Yamada (1982), with an extra term for internal wave breaking.

2.6.4 Three-dimensional models

The 2DDAMs were building blocks for three-dimensional models (Davies, 1987). Initially the two-dimensional layers were impermeable and connected with shear stresses, but during upwelling and downwelling the layers could end up through the top or bottom surface. Using a fixed vertical grid, the grid box model improved the situation, but was limited by lower vertical resolution in the shallows (Pritchard, 1969; Madala and Piacsek, 1977). As mentioned in the section of co-ordinate systems, the σ transformation was introduced to handle varying bathymetry with equal vertical resolution (Phillips, 1957; Freeman, Hale, and Danard, 1972).

As all estuary and ocean circulation is three-dimensional in nature, it is better to represent them using a three-dimensional model. With increases in affordable computing power that can run three-dimensional models, three-dimensional models are becoming the standard. Three-dimensional models are used for problems from shallow lakes (Falconer, George, and Hall, 1991) to tides in the Irish Sea (Davies and Jones, 1992; Davies and Aldridge, 1993; Davies and Gerritsen, 1994).

2.6.5 The Princeton Oceanographic Model

The Princeton Oceanographic Model (POM) was used to model Macquarie Harbour. POM was designed to model mesoscale problems typical of estuaries (1 – 100km length, tidal to 30 day time scales). POM is described in Blumberg and Mellor (1987) and Mellor (1993; 1996), with readers referred to the FORTRAN code for details on the implementation of the finite difference scheme. In summary, POM is a free surface, three-dimensional estuary and coastal ocean circulation model that uses time dependant primitive equations. It uses σ co-

ordinates vertically and curvilinear orthogonal co-ordinates horizontally (with an "Arakawa C" differencing). For grid sizes less then 50km Batteen and Han (1981) recommended the staggered Arakawa C grid over the Arakawa B grid. It contains a second moment turbulence closure known as the Mellor – Yamada 2.5 level turbulence closure, which models turbulence kinetic energy and turbulence macroscale. The turbulence closure is fully described in Mellor (1973), and Mellor and Yamada (1974; 1982), and is based on turbulence hypotheses by Kolmogoroff (1942) and Rotta (1951). As POM would be considered a third generation model according to Abbott, Havnø, and Lindberg (1991), users require a firm grasp of FORTRAN and computational hydraulics to work the model.

POM's solving algorithm is divided into an internal and external mode. The external mode is a two-dimensional depth averaged model, which is limited by the CFL time step, and used for faster moving surface waves. The internal mode, which calculates the three-dimensional variables, is more time consuming than the external mode. Typically the external mode loop will step forward in time 10 to 30 steps for every one internal mode loop to speed up the computations. This is called the external to internal mode split. When downloaded from the Internet, POM is set up with an open basin or sea mount problem depending on which version is downloaded. There are some predefined boundary conditions and output is with text based tables.

There are currently over 300 registered users of POM. As examples, it has been used as a basis for modelling the

- Mediterranean Sea circulation using 16 vertical sigma levels, 8 – 60km horizontal grid, and 24min time step (Zavatarelli and Mellor, 1995)
- Australian North West Shelf using 31 sigma levels, 2.5km and 10km horizontal grid, 7.5s time step, and an external to internal mode split of 30 (Holloway, 1996)
- North Sea with a chemical – biological model to predict primary production, using 11 σ levels, 20km horizontal grid, 30s time step, and an external to internal mode split of 30 (Skogen *et al.*, 1995)
- Delaware Bay and River system using 11 σ levels, 1 – 5km horizontal grid, 24s time step, and an external to internal mode split of 10 (Galperin and Mellor, 1990)

In this thesis POM has been used to study Macquarie Harbour using 23 σ levels, 250m horizontal grid and 3.0s time step, with an external to internal mode split of 20.

2.6.6 Numerical modelling of Macquarie Harbour

There are no published numerical modelling studies of Macquarie Harbour. As part of the MLRRDP, Computational Fluid Mechanics International (CFMI) in Adelaide, Australia was contracted to model the physical and chemical behaviour of the harbour. When this thesis

was published the CFMI modelling work was not finished, although it was meant to be completed by January 1996.

CFMI was using a three-dimensional model called H3, with a mode split that allows time steps independent of the CFL limit (up to 2min) and a flux-corrected transport algorithm (CFMI, 1995b). The model has been set up with a 400m horizontal grid (5250 surface cells) and 14 horizontal vertical levels (6×2m, 1×3m, and 7×5m).

In model output from interim reports (CFMI, 1995b), the King River plume looks reasonable but the velocity field does not resemble the complex harbour circulation very well. It gives an almost uniform velocity distribution across the harbour and does not show the expected strong Gordon River flow up the western side of the harbour, or its recirculation off Liberty Pt. Instead, in the CFMI model the Gordon River water starts up the eastern side of the harbour, as if the sign on the Coriolis force terms was reversed.

Resolution and boundary conditions could be the problem with the CFMI. The model in this thesis did not work very well when it was set up with a similar resolution (Section 5.2.5) and boundary conditions (Section 5.4.1). When the resolution and boundary conditions were changed, the model in this thesis worked successfully.

Chapter Three
River model equations

3.1 Introduction

The river model developed by the author has been used to represent the Gordon River, King River, and the sea in the numerical model of the Macquarie Harbour system. For simplicity of notation, the sea is called a river. The river model is general to the three rivers, differing only in boundary and initial conditions. It is based on two-dimensional laterally averaged conservation equations. This chapter derives these equations so they can be solved using an implicit finite difference scheme and boundary conditions described in Chapter Four.

Conservation of water mass is used as a basis for the continuity equation, which in turn is used to solve for surface elevation (η) and σ vertical velocity (ω). The σ vertical velocity is the velocity normal to the σ surfaces and is transformed from the Cartesian vertical velocity (Blumberg and Mellor, 1987; Mellor, 1996). Conservation of momentum, temperature (T), salinity (S), and pollution concentration (C) are used as a basis for the momentum, heat, salt, and pollution equations respectively. Horizontal velocity (u) is solved with the momentum equation. Vertical acceleration is ignored to give a hydrostatic pressure variation as there are no large water surface curvatures in the problem to be solved. This approximation is common to many estuary models (Koutitas, 1988).

The two-dimensional laterally averaged equations are obtained by integrating the three-dimensional equations with respect to y, the direction across the river. This integration will introduce river width (B) in the equations. The rivers have a small depth (D) compared to their widths, that is D/B is small: 0.005 - 0.05 for the King River, 0.04 - 0.07 for the Gordon River, and 0.06 - 0.09 for the sea. B varies vertically and along the river, although the vertical variation can be ignored without significant loss of accuracy (Section 3.3.1). This rectangular section approximation is described in Section 3.3.1. Other simplifications ignore lateral inflow and assume subcritical flow.

The rectangular section approximation ($\partial B/\partial z = 0$) makes a large simplifications to the theory and its implementation. While it could be assumed that the width is invariant with time in a Cartesian co-ordinate system, because the model uses a σ co-ordinate system (Section 3.2) the width would vary within the co-ordinate system as the water depth varied.

3.2 Co-ordinate system

Before conservation equations can be developed a co-ordinate system is required. Surface elevations, $z^* = \eta$, are taken with positive up from a horizontal datum ($z^* = 0$) and the bathymetry at $z^* = -H$ (Figure 3.1).

Most equations have been defined in the σ co-ordinate system. An asterisk has been used to denote terms defined with vertical Cartesian co-ordinates (e.g. x^*) and terms with no asterisk are defined with σ co-ordinates (e.g. x). The transformation from Cartesian to σ co-ordinates (Blumberg and Mellor, 1987) is

$$x = x^* \qquad y = y^* \qquad \sigma = z = \frac{z^* - \eta}{H + \eta} \qquad t = t^* \tag{3.1}$$

Note the asterisk notation used here is consistent with Mellor and Ezer (1995), but the reverse of Blumberg and Mellor (1987). The values of σ range from $\sigma = 0$ at $z^* = \eta$ at the top surface, to $\sigma = -1$ at $z^* = -H$ at the bottom (Figure 3.1). As $t = t^*$, $x = x^*$ and $y = y^*$, the horizontal velocities are the same between the Cartesian and σ co-ordinates. Blumberg and Mellor (1987) introduce a transformed vertical velocity ω, the velocity normal to the σ

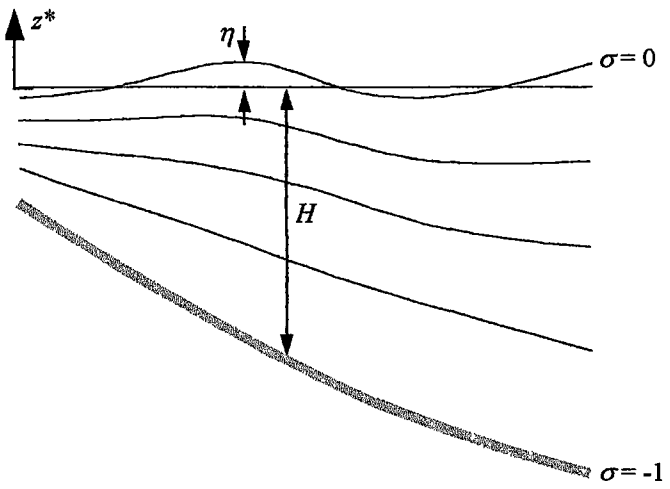

Figure 3.1 Co-ordinate system for river model and POM

surfaces

$$\omega = w - u\left(\sigma\frac{\partial D}{\partial x}+\frac{\partial \eta}{\partial x}\right)-v\left(\sigma\frac{\partial D}{\partial y}+\frac{\partial \eta}{\partial y}\right)-\left(\sigma\frac{\partial D}{\partial t}+\frac{\partial \eta}{\partial t}\right) \tag{3.2}$$

This vertical velocity is used to simplify the momentum and heat equations after they have been transformed from Cartesian to σ co-ordinates. At both the top surface ($\sigma = 0$) and bottom ($\sigma = -1$), $\omega = 0$.

Derivatives from conservation equations are transformed using the chain rule. In anticipation of this, derivatives of σ are required. The substitution $D = \eta + H$ is used. Firstly the derivative of σ with respect to η

$$\frac{\partial \sigma}{\partial \eta} = -\frac{1}{D} \tag{3.3}$$

With respect to D

$$\frac{\partial \sigma}{\partial D} = -\frac{\sigma}{D} \tag{3.4}$$

With respect to z^*

$$\frac{\partial \sigma}{\partial z^*} = \frac{1}{D} \tag{3.5}$$

With respect to x^* using chain rule, (3.3), (3.4), with $\frac{\partial z^*}{\partial x^*} = 0$ and $\frac{\partial x}{\partial x^*} = 1$, become

$$\begin{aligned}\frac{\partial \sigma}{\partial x^*} &= \frac{\partial \sigma}{\partial z^*}\frac{\partial z^*}{\partial x^*}+\frac{\partial \sigma}{\partial D}\frac{\partial D}{\partial x}\frac{\partial x}{\partial x^*}+\frac{\partial \sigma}{\partial \eta}\frac{\partial \eta}{\partial x}\frac{\partial x}{\partial x^*}\\ &= -\frac{1}{D}\left(\sigma\frac{\partial D}{\partial x}+\frac{\partial \eta}{\partial x}\right)\end{aligned} \tag{3.6}$$

Similarly,

$$\frac{\partial \sigma}{\partial y^*} = -\frac{1}{D}\left(\sigma\frac{\partial D}{\partial y}+\frac{\partial \eta}{\partial y}\right) \text{ and } \frac{\partial \sigma}{\partial t^*} = -\frac{1}{D}\left(\sigma\frac{\partial D}{\partial t}+\frac{\partial \eta}{\partial t}\right) \tag{3.7}$$

Applying the chain rule on an arbitrary variable f with (3.6) gives

$$\frac{\partial f}{\partial x^*} = \frac{\partial f}{\partial x}+\frac{\partial f}{\partial \sigma}\frac{\partial \sigma}{\partial x^*} = \frac{\partial f}{\partial x}-\frac{\partial f}{\partial \sigma}\frac{1}{D}\left(\sigma\frac{\partial D}{\partial x}+\frac{\partial \eta}{\partial x}\right) \tag{3.8}$$

And with (3.5) and (3.7)

$$\frac{\partial f}{\partial y^*} = \frac{\partial f}{\partial y}-\frac{\partial f}{\partial \sigma}\frac{1}{D}\left(\sigma\frac{\partial D}{\partial y}+\frac{\partial \eta}{\partial y}\right) \tag{3.9}$$

$$\frac{\partial f}{\partial z^*} = \frac{1}{D}\frac{\partial f}{\partial \sigma} \tag{3.10}$$

$$\frac{\partial f}{\partial t^*} = \frac{\partial f}{\partial t}-\frac{\partial f}{\partial \sigma}\frac{1}{D}\left(\sigma\frac{\partial D}{\partial t}+\frac{\partial \eta}{\partial t}\right) \tag{3.11}$$

3.3 Continuity equation

The continuity equation is derived by considering water mass flow in a rectangular control volume. Following Knauss (1978, page 270), a control volume within a larger body of water with small sides lengths Δx^*, Δy^*, and Δz^* is used (Figure 3.2).

With a density of water ρ, the mass of the control volume $m = \rho \Delta x^* \Delta y^* \Delta z^*$. Hence the mass flow in the x^* direction is

$$\frac{\partial m}{\partial t^*} = \frac{\partial}{\partial t^*_x}(\rho \Delta x^* \Delta y^* \Delta z^*) = \rho_1 u_1 \Delta y^* \Delta z^* - \rho_2 u_2 \Delta y^* \Delta z^* \tag{3.12}$$

The x subscript on $\frac{\partial}{\partial t^*_x}$ indicates the derivate is only due to change in the x direction. Dividing (3.12) by $\Delta y^* \Delta z^*$ gives

$$\frac{\partial \rho}{\partial t^*_x} = \frac{\rho_1 u_1}{\Delta x^*} - \frac{\rho_2 u_2}{\Delta x^*} \tag{3.13}$$

Where the subscripts *1* and *2* refer to the upstream and downstream sides on the y^* - z^* faces of the control volume. As the control volume is small, density and velocity are assumed to vary linearly across it, so

$$u_2 = u_1 + \Delta u,\ u_2 = u + \Delta u/2, \text{ and } u_1 = u - \Delta u/2 \tag{3.14}$$

$$\rho_2 = \rho_1 + \Delta \rho,\ \rho_2 = \rho + \Delta \rho/2, \text{ and } \rho_1 = \rho - \Delta \rho/2 \tag{3.15}$$

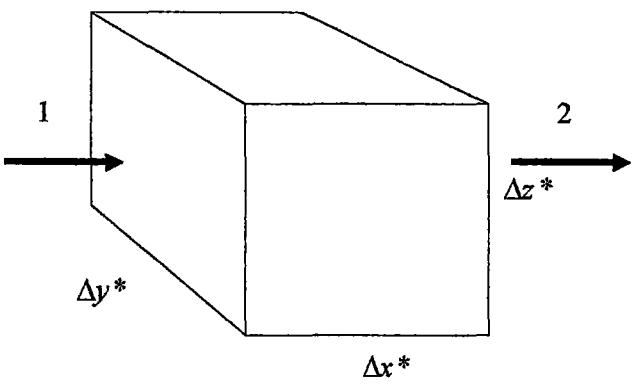

Figure 3.2 Control volume

Substituting (3.14) and (3.15) in (3.13) gives

$$\frac{\partial \rho}{\partial t^*_x} \Delta x^* = (u - \Delta u/2)(\rho - \Delta \rho/2) - (u + \Delta u/2)(\rho + \Delta \rho/2) \tag{3.16}$$

Simplifying

$$\frac{\partial \rho}{\partial t^*_x} = -\rho \Delta u/\Delta x^* - u \Delta \rho/\Delta x^* \tag{3.17}$$

Taking the control volume to the limit reduces the terms on the right of (3.17) to a differential form

$$\frac{\partial \rho}{\partial t^*}_x = -\rho\frac{\partial u}{\partial x^*} - u\frac{\partial \rho}{\partial x^*} = -\frac{\partial \rho u}{\partial x^*} \tag{3.18}$$

Similarly, the other directions are completed to give the total partial derivative

$$\frac{\partial \rho}{\partial t^*} = -\frac{\partial \rho u}{\partial x^*} - \frac{\partial \rho v}{\partial y^*} - \frac{\partial \rho w}{\partial z^*} \tag{3.19}$$

When (3.19) is rearranged, this is the non-Boussinesq continuity equation

$$\frac{\partial \rho}{\partial t^*} + \frac{\partial \rho u}{\partial x^*} + \frac{\partial \rho v}{\partial y^*} + \frac{\partial \rho w}{\partial z^*} = 0 \tag{3.20}$$

In this thesis, non-Boussinesq does not refer to the full non-Boussinesq dynamics, which might include acoustic waves. The Boussinesq approximation is to only assume density is locally constant and ignore density variations (except where associated with gravity)

$$\frac{\partial \rho}{\partial t^*} = \frac{\partial \rho}{\partial x^*} = \frac{\partial \rho}{\partial y^*} = \frac{\partial \rho}{\partial z^*} = 0 \tag{3.21}$$

This makes the Boussinesq continuity equation from (3.20) using (3.21)

$$\frac{\partial u}{\partial x^*} + \frac{\partial v}{\partial y^*} + \frac{\partial w}{\partial z^*} = 0 \tag{3.22}$$

This is now an equation of conservation of volume rather than conservation of mass. Because water is essentially incompressible, the Boussinesq approximation is widely used (Blumberg, 1977b; Koutitas, 1987; Davies, 1987). In estuaries, density variations are not always caused by fluid compression. Large salinity and temperature variations found in estuaries will cause significant density variations. Using the density subroutines in POM, that Mellor (1993;1996) based on the United Nations Educational, Scientific, and Cultural Organisation (UNESCO) equation of state (Mellor, 1991), it is possible to calculate the order of magnitude of spatial density variations due to temperature, salinity and depth. In 10 m deep water of a uniform salinity (20‰) and temperature (15°C), density changes at 4.49×10^{-3} kg/m^3/m (vertically). While in 10m deep water with a salinity stratification (typical of Macquarie Harbour) of 5‰/m (vertically) centred on 20‰ and a constant temperature (15°C), density changes at 3.84kg/m^3/m (vertically).

Mellor and Ezer (1995) checked the Boussinesq approximation in a global ocean model with seasonal thermal variations using a variation of POM. The temperature changes gave rise to density variations causing small (1cm) changes in surface elevation and a reversal of flow direction in the idealised flat bottom ocean. Mellor and Ezer (1995) proposed a spatially independent, time dependent correction to counter the effect of the Boussinesq

approximation. The surface elevation (η) can be broken into its Boussinesq and other components

$$\eta(x,y,t)=\eta_B(x,y,t)+\eta_E(t)+\eta_{GS}(x,y,t) \tag{3.23}$$

In (3.23) η_B is the Boussinesq solution, η_E is due to expansion or compression of water column, and η_{GS} is an unknown small error term that is neglected (attributed to "Goldsbrough-Stommel gyres"). After neglecting η_{GS} in (3.23) and introducing instead a spatially independent surface elevation η_T, it is possible to correct the Boussinesq solution

$$\eta(x,y,t)=\eta_B(x,y,t)+\eta_E(t)+\eta_T(t) \tag{3.24}$$

Area integrals and divergence theorem are used for the correction terms η_T and η_E respectively. This correction would need field observations to be calibrated (Mellor and Ezer, 1995). The correction is based on the assumption that the timescale for redistribution (L/c) of surface changes due to density induced changes in the continuity equation, is much less than the important model timescale; where L is the basin lateral size and $c=\sqrt{gH}$ is the barotropic wave speed (Mellor and Ezer, 1995). This might be appropriate in a global ocean model where the timescale is seasonal, measured in months. In such a global model L = 1000 km and H = 200m (used by Mellor and Ezer, 1995), so L/c = 22s. In an estuary there is a tidal timescale, measured in hours. For an estuary with L = 8km and H = 25m, the redistribution timescale L/c = 510s. A timescale of 510s is comparable to a tidal period, that is 1.1% of a M_2 tide period (12.42h). This means the redistribution of density induced surface elevations will be marginally noticeable compared to tidally induced surface changes.

3.3.1 Sigma transformation

Transforming the non-Boussinesq continuity equation from Cartesian to σ co-ordinates gives

$$\begin{aligned}&\frac{\partial\rho}{\partial t}-\frac{\partial\rho}{\partial\sigma}\frac{1}{D}\left(\sigma\frac{\partial D}{\partial t}+\frac{\partial\eta}{\partial t}\right)+\frac{\partial\rho u}{\partial x}-\frac{\partial\rho u}{\partial\sigma}\frac{1}{D}\left(\sigma\frac{\partial D}{\partial x}+\frac{\partial\eta}{\partial x}\right)\\&+\frac{\partial\rho v}{\partial y}-\frac{\partial\rho v}{\partial\sigma}\frac{1}{D}\left(\sigma\frac{\partial D}{\partial y}+\frac{\partial\eta}{\partial y}\right)+\frac{1}{D}\frac{\partial\rho w}{\partial\sigma}=0\end{aligned} \tag{3.25}$$

Substitution of the transformed vertical velocity (3.2) gives

$$\begin{aligned}\frac{\partial \rho}{\partial t}-\frac{\partial \rho}{\partial \sigma}\frac{1}{D}\left(\sigma\frac{\partial D}{\partial t}+\frac{\partial \eta}{\partial t}\right)+\frac{\partial \rho u}{\partial x}-\frac{\partial \rho u}{\partial \sigma}\frac{1}{D}\left(\sigma\frac{\partial D}{\partial x}+\frac{\partial \eta}{\partial x}\right)\\ +\frac{\partial \rho v}{\partial y}-\frac{\partial \rho v}{\partial \sigma}\frac{1}{D}\left(\sigma\frac{\partial D}{\partial y}+\frac{\partial \eta}{\partial y}\right)\\ +\frac{1}{D}\frac{\partial}{\partial \sigma}\left(\rho\omega+\rho u\left(\sigma\frac{\partial D}{\partial x}+\frac{\partial \eta}{\partial x}\right)+\rho v\left(\sigma\frac{\partial D}{\partial y}+\frac{\partial \eta}{\partial y}\right)\right.\\ \left.+\rho\left(\sigma\frac{\partial D}{\partial t}+\frac{\partial \eta}{\partial t}\right)\right)=0\end{aligned} \tag{3.26}$$

Which simplifies to

$$\frac{\partial \rho}{\partial t}+\frac{\partial \rho u}{\partial x}+\frac{\partial \rho v}{\partial y}+\frac{1}{D}\left(\frac{\partial \rho\omega}{\partial \sigma}+\rho\left(u\frac{\partial D}{\partial x}+v\frac{\partial D}{\partial y}+\frac{\partial D}{\partial t}\right)\right)=0 \tag{3.27}$$

Multiplying (3.27) by D and combining derivatives gives the non-Boussinesq continuity equation in σ co-ordinates

$$\frac{\partial \rho D}{\partial t}+\frac{\partial \rho u D}{\partial x}+\frac{\partial \rho v D}{\partial y}+\frac{\partial \rho\omega}{\partial \sigma}=0 \tag{3.28}$$

To derive the Boussinesq continuity equation, local density variations are neglected in (3.28). The river bathymetry is assumed constant with time, so $\partial H/\partial t=0$ and $\partial D/\partial t=\partial \eta/\partial t$, which gives for the Boussinesq continuity equation in σ co-ordinates as

$$\frac{\partial \eta}{\partial t}+\frac{\partial u D}{\partial x}+\frac{\partial v D}{\partial y}+\frac{\partial \omega}{\partial \sigma}=0 \tag{3.29}$$

The river model is laterally averaged by integrating the continuity equations with respect to y. As $\partial B/\partial z=0$ (rectangular section) and in general $\partial B/\partial x\neq 0$, the non-Boussinesq and Boussinesq equations are

$$\frac{\partial \rho D}{\partial t}+\frac{\partial \rho u D}{\partial x}+\frac{\rho u D}{B}\frac{\partial B}{\partial x}+\frac{\partial \rho\omega}{\partial \sigma}=0 \tag{3.30}$$

$$\frac{\partial \eta}{\partial t}+\frac{\partial u D}{\partial x}+\frac{u D}{B}\frac{\partial B}{\partial x}+\frac{\partial \omega}{\partial \sigma}=0 \tag{3.31}$$

Whenever a two-dimensional laterally averaged equation is given, the terms are lateral averages. That is the terms u, ω, ρ, and D in (3.30) and (3.31) are lateral averages, even though they use the same symbol as the terms used in the three-dimensional equations.

The inaccuracy introduced with the rectangular approximation can be estimated by considering a typical flow scenario. The term ignored with the approximation in (3.31) is $\frac{\omega}{B}\frac{\partial B}{\partial \sigma}$ on the left hand side of the equation. The typical flow scenario is a reach of river that changes from a velocity of 1.0m/s and a depth of 10.0m to 1.1m/s and 10.1m in 250m, while

width is constant along river at 100m, $\omega = 10^{-3}s^{-1}$ and $\frac{\partial B}{\partial \sigma} = 1.0$m. In this case the effect of using the rectangular approximation on $\frac{\partial \eta}{\partial t}$ is a 0.0225% difference and hence the rectangular approximation does not cause any significant inaccuracy.

3.3.2 Transformed sigma vertical velocity

The transformed σ vertical velocity (ω) is calculated by vertically integrating the continuity equation from either the top or bottom boundary, where $\omega = 0$, to where the velocity is required. Integrating the non-Boussinesq continuity equation (3.30) between ω_L and ω_U gives

$$(\rho\omega)\Big|_{\sigma_L}^{\sigma_U} = -\frac{\partial D\int_{\sigma_L}^{\sigma_U}\rho d\sigma}{\partial t} - \frac{\partial D\int_{\sigma_L}^{\sigma_U}\rho u d\sigma}{\partial x} - \frac{D\int_{\sigma_L}^{\sigma_U}\rho u d\sigma}{B}\frac{\partial B}{\partial x} \tag{3.32}$$

If $\Delta\sigma = \sigma_U - \sigma_L$ is small then the density and velocity can be assumed to vary linearly between ω_L and ω_U so

$$(\rho\omega)\Big|_{\sigma_U} = (\rho\omega)\Big|_{\sigma_L} - \Delta\sigma\left(\frac{\partial D\rho}{\partial t} + \frac{\partial D\rho u}{\partial x} + \frac{D\rho u}{B}\frac{\partial B}{\partial x}\right)\Bigg|_{\sigma_0} \tag{3.33}$$

Where ω_0 is between ω_L and ω_U. Similarly the Boussinesq version from (3.31) is

$$\omega\Big|_{\sigma_U} = \omega\Big|_{\sigma_L} - \Delta\sigma\left(\frac{\partial \eta}{\partial t} + \frac{\partial Du}{\partial x} + \frac{Du}{B}\frac{\partial B}{\partial x}\right)\Bigg|_{\sigma_0} \tag{3.34}$$

Mellor (1996) stated for POM that typically $\omega \approx 10^{-11}$ m/s using a similar Boussinesq version and both horizontal direction derivatives (as POM is three-dimensional). While this value might be typical for oceans, it can be as high as $\omega = 10^{-2}$ m/s in a fast moving river like the King River ($u = 1.5$m/s) or with sharply changing bathymetry like the Gordon River (curvatures of $10^{-5}m^{-1}$).

3.3.3 Surface elevation

Surface elevation (η) is solved by vertically integrating the continuity equation from the top to the bottom of the river. This removes any vertical structure from the equation and means it does not matter which direction the equation is integrated, as occurs with ω. Vertically integrating the non-Boussinesq (3.30) and Boussinesq (3.31) continuity equation gives

$$\frac{\partial \overline{\rho} D}{\partial t} + \frac{\partial \overline{\rho u} D}{\partial x} + \frac{\overline{\rho u} D}{B}\frac{\partial B}{\partial x} = 0 \tag{3.35}$$

$$\frac{\partial \eta}{\partial t} + \frac{\partial \overline{u} D}{\partial x} + \frac{\overline{u} D}{B}\frac{\partial B}{\partial x} = 0 \tag{3.36}$$

Where $\overline{\rho}=\int_{-1}^{0}\rho d\sigma$, $\overline{\rho u}=\int_{-1}^{0}\rho u d\sigma$, and $\overline{u}=\int_{-1}^{0}u d\sigma$. These averages are derived from values in the two-dimensional laterally averaged equations. The derivatives of products have been separated, as the density terms are not known at the future time step when η is being solved; which means some terms are centred at different locations in the numerical implementation. Separating the derivatives of products allows each term to be handled individually according to the limitations of what is known about it. Noting $\partial D/\partial t=\partial\eta/\partial t$ as $D=H+\eta$ and $\partial H/\partial t=0$, this makes the non-Boussinesq surface elevation equation after dividing by $\overline{\rho}$

$$\frac{\partial\eta}{\partial t}+\frac{\overline{\rho u}}{\overline{\rho}}\frac{\partial D}{\partial x}+\frac{D}{\overline{\rho}}\left(\frac{\partial\overline{\rho}}{\partial t}+\frac{\partial\overline{\rho u}}{\partial x}+\frac{\overline{\rho u}}{B}\frac{\partial B}{\partial x}\right)=0 \tag{3.37}$$

Similarly the Boussinesq surface elevation equation is

$$\frac{\partial\eta}{\partial t}+\overline{u}\frac{\partial D}{\partial x}+D\left(\frac{\partial\overline{u}}{\partial x}+\frac{\overline{u}}{B}\frac{\partial B}{\partial x}\right)=0 \tag{3.38}$$

3.4 The conservation equations

The equations for momentum, salt, heat, and pollution transport are derived using the same approach, with the momentum equation having extra terms for pressure and Coriolis forces. In light of this, a function f is used in the derivation that could be either horizontal velocity, salinity, temperature, or pollution concentration.

3.4.1 Components of conservation equations

The terms in the conservation equations are derived separately then combined. Each term represents a physical process that effects the water and its constituents. The advection term is due to bulk movement of water, the pressure term is due to hydrostatic pressure, the Coriolis force is due to rotation of the earth, and diffusion is due to the turbulent nature of estuary water flow. The momentum equation is made up of the advection, pressure, Coriolis and diffusion terms. While the scalar conservation equation contains only the advection and diffusion terms. In scalar equations there can also be source and sink terms, for such things as non-conservative biological contaminants, or short wave penetrative solar radiation. In this river model, the pollutant is conservative so there is no source or sink term, and solar radiation is handled with a heat flux boundary condition. In the momentum equation the bed friction term could be considered a sink term, this is discussed in the diffusion Section 3.4.1.4 below.

The general equation for the temporal derivative of f is made up of the contribution from the different forcings

$$\frac{\partial f}{\partial t} = \frac{\partial f}{\partial t}_A + \frac{\partial f}{\partial t}_D + \underbrace{\frac{\partial f}{\partial t}_C + \frac{\partial f}{\partial t}_P}_{\text{only for momentum}} \tag{3.39}$$

Where in (3.39) the subscripts on the temporal derivatives refer to A for advection, D for diffusion, C for Coriolis, and P for pressure.

3.4.1.1 Advection

The conservation equation is based on the same control volume used for the continuity equation (Figure 3.2). The flow of f in the x^* direction through the y^*-z^* side of the control volume at face one is $\rho_1 u_1 f_1 \Delta y^* \Delta z^*$, and at face two is $\rho_2 u_2 f_2 \Delta y^* \Delta z^*$. The basic conservation of f is analogous to the continuity equation in Section 3.3 so

$$\frac{\partial \rho f}{\partial t^*}_A \Delta x^* \Delta y^* \Delta z = \rho_1 u_1 f_1 \Delta y^* \Delta z^* - \rho_2 u_2 f_2 \Delta y^* \Delta z^* \tag{3.40}$$

and

$$\frac{\partial \rho f}{\partial t^*}_A = -\frac{\partial \rho u f}{\partial x^*} \tag{3.41}$$

Using the same approach as (3.40) and (3.41) for flow in the other two directions gives the total advective expression for f

$$\frac{\partial \rho f}{\partial t^*}_A = -\frac{\partial \rho u f}{\partial x^*} - \frac{\partial \rho v f}{\partial y^*} - \frac{\partial \rho w f}{\partial z^*} \tag{3.42}$$

Which expands to

$$\rho \frac{\partial f}{\partial t^*}_A + f \frac{\partial \rho}{\partial t^*}_A = -\rho \frac{\partial u f}{\partial x^*} - f \frac{\partial \rho u}{\partial x^*} - \rho \frac{\partial v f}{\partial y^*} - f \frac{\partial \rho v}{\partial y^*} - \rho \frac{\partial w f}{\partial z^*} - f \frac{\partial \rho w}{\partial z^*} \tag{3.43}$$

After rearranging and dividing by ρ, (3.43) becomes

$$\frac{\partial f}{\partial t^*}_A = -\frac{\partial u f}{\partial x^*} - \frac{\partial v f}{\partial y^*} - \frac{\partial w f}{\partial z^*} - \frac{f}{\rho}\left(\frac{\partial \rho}{\partial t^*} + \frac{\partial \rho u}{\partial x^*} + \frac{\partial \rho v}{\partial y^*} + \frac{\partial \rho w}{\partial z^*}\right) \tag{3.44}$$

Substituting in the continuity equation (3.20) eliminates the last term from (3.44) gives

$$\frac{\partial f}{\partial t^*}_A = -\frac{\partial u f}{\partial x^*} - \frac{\partial v f}{\partial y^*} - \frac{\partial w f}{\partial z^*} \tag{3.45}$$

With the substitution to give (3.45), the density only appears in the diffusion terms. Mellor and Ezer (1995), who used both Boussinesq and non-Boussinesq conservation equations, did not make the last simplification of substituting in the continuity equation. It is assumed this was done for ease of modifying their model (POM) from the Boussinesq form it had been coded. This would be done by multiplying the horizontal velocities by the density and

adding the density's temporal derivative. This would lead to a minimum change of code, and allow for switching between the Boussinesq and non-Boussinesq cases.

3.4.1.2 Pressure force

The pressure gradient acting on the control volume is evaluated with a force balance, $\sum force = m\frac{\partial u}{\partial t^*_P}$. The pressure force in the x^* direction on face one is $F_1 = p_1 \Delta y^* \Delta z^*$ and on face two is $F_2 = p_2 \Delta y^* \Delta z^*$. With $m = \rho \Delta x^* \Delta y^* \Delta z^*$ and $p_2 = p_1 + \Delta p$ the force balance gives

$$\rho \Delta x^* \Delta y^* \Delta z^* \frac{\partial u}{\partial t^*_P} = F_1 - F_2 = p_1 \Delta y^* \Delta z^* - (p_1 + \Delta p)\Delta y^* \Delta z^* \tag{3.46}$$

$$\frac{\partial u}{\partial t^*_P} = -\frac{1}{\rho}\frac{\Delta p}{\Delta x^*} \tag{3.47}$$

When the control volume diminishes to the limit (3.47) becomes

$$\frac{\partial u}{\partial t^*_P} = -\frac{1}{\rho}\frac{\partial p}{\partial x^*} \tag{3.48}$$

3.4.1.3 Coriolis force

The Coriolis force term comes from changing between a rotating and fixed reference frame, while on the surface of the earth. Letting $\mathbf{R}$ be a vector location of a point on the Earth's surface with an origin at the Earth's centre. So the temporal change of $\mathbf{R}$ is $\frac{d\mathbf{R}}{dt^*} = \dot{\mathbf{R}} + \Omega \times \mathbf{R}$, where Ω is the angular velocity of the earth and $\dot{\mathbf{R}} = \frac{\partial \mathbf{R}}{\partial t^*}$. Assuming Ω is constant, the total acceleration is

$$\frac{d^2\mathbf{R}}{dt^{*2}} = \ddot{\mathbf{R}} + 2\Omega \times \dot{\mathbf{R}} + \Omega \times \Omega \times \mathbf{R} \tag{3.49}$$

In (3.49), $\ddot{\mathbf{R}}$ is what an observer on the Earth's surface would measure as acceleration, as this observer (usually) ignores the Earth's rotation. The $2\Omega \times \mathbf{R}$ term is the Coriolis acceleration. The $\Omega \times \Omega \times \mathbf{R}$ term is usually considered part of the Earth's gravitational field (Knauss, 1978, page 278). Translating the total acceleration to a fixed co-ordinate system on the Earth's surface (ignoring the "gravitational field" term) at latitude ϕ, with $f_c = 2\Omega \sin\phi$ gives,

$$\frac{du}{dt^*_C} = f_c v - 2w\Omega\cos\phi \tag{3.50}$$

$$\frac{dv}{dt^*_C} = -f_c u \tag{3.51}$$

The $-2w\Omega\cos\phi$ term in (3.50) is usually ignored as it is small compared to $f_c v$. In the river model, as it is laterally averaged and does not contain any transverse velocity v, and as w is

small, there is no Coriolis term used. Even though it is not a term of the river model, the description of the Coriolis force was included here because it is incorporated into POM.

3.4.1.4 Diffusion

The Boussinesq approximation of the Reynolds stress tensor is used for diffusive terms. The horizontal eddy diffusion value (A_f) is assumed the same in both horizontal directions, and is different from the vertical eddy diffusion value (K_f). The diffusive stresses for the x^* direction are

$$\tau_{x^*x^*} = \rho A_f \frac{\partial f}{\partial x^*} \tag{3.52}$$

$$\tau_{x^*y^*} = \rho A_f \frac{\partial f}{\partial y^*} \tag{3.53}$$

$$\tau_{x^*z^*} = \rho K_f \frac{\partial f}{\partial z^*} \tag{3.54}$$

As with the pressure term, a force balance is used to find the acceleration caused by these stresses (3.52)-(3.54) giving

$$\frac{\partial u}{\partial t^*}_D = \frac{1}{\rho}\left(\frac{\partial \tau_{x^*x^*}}{\partial x^*} + \frac{\partial \tau_{x^*y^*}}{\partial y^*} + \frac{\partial \tau_{x^*z^*}}{\partial z^*}\right) \tag{3.55}$$

3.4.2 Momentum conservation equation

Including the advection, pressure, Coriolis, and diffusion terms with $f = u$ in (3.39) gives the momentum equation in non-Boussinesq form

$$\begin{aligned}\frac{\partial u}{\partial t^*} + \frac{\partial u^2}{\partial x^*} + \frac{\partial vu}{\partial y^*} + \frac{\partial wu}{\partial z^*} &= -\frac{1}{\rho}\frac{\partial p}{\partial x^*} + f_c v \\ &+ \frac{1}{\rho}\left(\frac{\partial}{\partial x^*}\left(\rho A_M \frac{\partial u}{\partial x^*}\right) + \frac{\partial}{\partial y^*}\left(\rho A_M \frac{\partial u}{\partial y^*}\right) + \frac{\partial}{\partial z^*}\left(\rho K_M \frac{\partial u}{\partial z^*}\right)\right)\end{aligned} \tag{3.56}$$

The Boussinesq form is

$$\begin{aligned}\frac{\partial u}{\partial t^*} + \frac{\partial u^2}{\partial x^*} + \frac{\partial vu}{\partial y^*} + \frac{\partial wu}{\partial z^*} &= -\frac{1}{\rho}\frac{\partial p}{\partial x^*} + f_c v \\ &+ \left(\frac{\partial}{\partial x^*}\left(A_M \frac{\partial u}{\partial x^*}\right) + \frac{\partial}{\partial y^*}\left(A_M \frac{\partial u}{\partial y^*}\right) + \frac{\partial}{\partial z^*}\left(K_M \frac{\partial u}{\partial z^*}\right)\right)\end{aligned} \tag{3.57}$$

Laterally averaging the non-Boussinesq form (3.56), that is integrating with respect to y^* gives

$$\begin{aligned}\frac{\partial u}{\partial t^*} + \frac{\partial u^2}{\partial x^*} + \frac{\partial wu}{\partial z^*} &= -\frac{1}{\rho}\frac{\partial p}{\partial x^*} + \frac{1}{\rho}\left(\frac{\partial}{\partial x^*}\left(\rho A_M \frac{\partial u}{\partial x^*}\right) + \frac{\partial}{\partial z^*}\left(\rho K_M \frac{\partial u}{\partial z^*}\right)\right) \\ &+ \lambda u|u| + \frac{1}{B}\frac{\partial B}{\partial x^*}\left(A_M \frac{\partial u}{\partial x^*} - u^2\right)\end{aligned} \tag{3.58}$$

As with the continuity equation, whenever a two-dimensional laterally averaged equation is given, the terms are lateral averages. That is, the terms u, w, p, A_M, K_M, ρ, and D in (3.58) are lateral averages, even though they use the same symbol as the terms used in the three-dimensional equations.

In (3.58) λ is a friction factor based on Manning's equation $\lambda = gn^2 R_h^{-4/3}$, where n is Manning's n, g is acceleration due to gravity, and R_h is the hydraulic radius of the river section. The $\lambda u|u|$ term is only due to the side wall friction and the top and bottom shear stresses are incorporated in the boundary conditions (see Chapter Four).

There is not a pressure width variation term in (3.58) as there is for velocity, because pressure is in balance with river side walls and pressure is a function of depth, not width.

This laterally averaged equation (3.58) is now transformed from Cartesian to σ co-ordinates using (3.8), (3.10), and (3.11) with the substitution of ω (as done with continuity equation) from (3.2) giving

$$\begin{aligned}\frac{\partial u}{\partial t}+\frac{\partial u^2}{\partial x}+\frac{1}{D}\left(\frac{\partial \omega u}{\partial \sigma}+u\frac{\partial \eta}{\partial t}+u^2\frac{\partial D}{\partial x}\right)&=-\frac{1}{\rho}\left(\frac{\partial p}{\partial x}+\frac{\partial p}{\partial \sigma}\frac{\partial \sigma}{\partial x}\right)+\frac{1}{\rho}\frac{\partial \rho A_M \dfrac{\partial u}{\partial x}}{\partial x}\\&+\frac{1}{\rho}\frac{\partial}{\partial \sigma}\left(\rho A_M\frac{\partial u}{\partial x}\right)\frac{\partial \sigma}{\partial x}+\frac{1}{\rho D^2}\frac{\partial}{\partial \sigma}\left(\rho K_M\frac{\partial u}{\partial \sigma}\right)+\lambda u|u|\\&+\frac{1}{B}\frac{\partial B}{\partial x}\left(A_M\frac{\partial u}{\partial x}-u^2\right)\end{aligned} \tag{3.59}$$

Multiplying by D and contracting derivatives on left hand side of (3.59) gives

$$\begin{aligned}\frac{\partial uD}{\partial t}+\frac{\partial u^2 D}{\partial x}+\frac{\partial \omega u}{\partial \sigma}&=-\frac{D}{\rho}\left(\frac{\partial p}{\partial x}+\frac{\partial p}{\partial \sigma}\frac{\partial \sigma}{\partial x}\right)+\frac{D}{\rho}\frac{\partial}{\partial x}\left(\rho A_M\frac{\partial u}{\partial x}\right)\\&+\frac{D}{\rho}\frac{\partial}{\partial \sigma}\left(\rho A_M\frac{\partial u}{\partial x}\right)\frac{\partial \sigma}{\partial x}+\frac{1}{\rho D}\frac{\partial}{\partial \sigma}\left(\rho K_M\frac{\partial u}{\partial \sigma}\right)+\lambda D u|u|\\&+\frac{D}{B}\frac{\partial B}{\partial x}\left(A_M\frac{\partial u}{\partial x}-u^2\right)\end{aligned} \tag{3.60}$$

The pressure term in (3.60) needs further manipulation to make it more accurate in its numerical implementation, because the extra terms in the horizontal pressure gradient introduced in the σ transformation, will increase diapycnal diffusion (Gerdes, 1993). The most common cause of error in a numerical scheme is rounding when differencing similar large values. As the pressure values are large, the numerical implementation of the pressure derivatives using finite differences will introduce rounding errors. It is therefore preferable to change the pressure derivatives to be derivatives of relative density. Relative density (ρ_0') is

based on the fluid density (ρ), $\rho' = \rho'_0 + \kappa_{\rho_2}$ and $\rho' = \rho\kappa_{\rho_1}$. Where κ_{ρ_1} and κ_{ρ_2} are constants chosen to make ρ'_0 close to zero, typically $\kappa_{\rho_1} = 10^{-3}$ and $\kappa_{\rho_2} = 1.025$.

To manipulate the pressure term in (3.60) the hydrostatic pressure relation is used, $\rho g = -\partial p/\partial z = -\partial p/\partial\sigma/D$. Assuming the atmospheric pressure (p_0) is constant, the pressure $p = p_0 - \int_0^\sigma \rho g D d\sigma = p_0 - Dg\int_0^\sigma \rho d\sigma$.

From these expressions, the pressure derivative term in (3.60), $\frac{D}{\rho}\left(\frac{\partial p}{\partial x} + \frac{\partial p}{\partial\sigma}\frac{\partial\sigma}{\partial x}\right)$, is manipulated

$$\begin{aligned}\frac{D}{\rho}\left(\frac{\partial p}{\partial x} + \frac{\partial p}{\partial\sigma}\frac{\partial\sigma}{\partial x}\right) &= \frac{D}{\rho}\frac{\partial}{\partial x}\left(Dg\int_\sigma^0 \rho d\sigma\right) + D^2 g\frac{1}{D}\left(\sigma\frac{\partial D}{\partial x} + \frac{\partial\eta}{\partial x}\right) \\ &= \frac{D^2 g}{\rho}\left(\int_\sigma^0 \frac{\partial\rho}{\partial x}d\sigma + \frac{1}{D}\frac{\partial D}{\partial x}\left(\sigma\rho + \int_\sigma^0 \rho d\sigma\right)\right) + gD\frac{\partial\eta}{\partial x} \\ &= \frac{D^2 g}{\rho}\left(\int_\sigma^0 \frac{\partial\rho}{\partial x}d\sigma + \frac{1}{D}\frac{\partial D}{\partial x}\left(-\int_\sigma^0 \sigma\frac{\partial\rho}{\partial\sigma}d\sigma\right)\right) + gD\frac{\partial\eta}{\partial x} \\ &= \frac{D^2 g}{\rho}\int_\sigma^0\left(\frac{\partial\rho}{\partial x} - \frac{1}{D}\frac{\partial D}{\partial x}\sigma\frac{\partial\rho}{\partial\sigma}\right)d\sigma + gD\frac{\partial\eta}{\partial x}\end{aligned} \tag{3.61}$$

Substituting relative density in (3.61) gives a similar expression to Mellor (1996)

$$\frac{D}{\rho}\left(\frac{\partial p}{\partial x} + \frac{\partial p}{\partial\sigma}\frac{\partial\sigma}{\partial x}\right) = \frac{D^2 g}{\rho'}\int_\sigma^0\left(\frac{\partial\rho'_0}{\partial x} - \frac{1}{D}\frac{\partial D}{\partial x}\sigma\frac{\partial\rho'_0}{\partial\sigma}\right)d\sigma + gD\frac{\partial\eta}{\partial x} \tag{3.62}$$

When solved with a finite difference scheme the horizontal and vertical derivatives of relative density will have less rounding than the absolute density equivalents. Note the κ_{ρ_1} constant was cancelled out, and is only used when calculating the pressure from the relative density.

3.4.3 Scalar conservation equation

This section changes a generic scalar conservation equation from Cartesian to σ co-ordinates. The generic conservation equation for the scalar quantities includes the advection and diffusion terms from sections 3.4.1.1 and 3.4.1.4 with $f = \theta$ (where θ is either *T*, *S*, or *C*). The non-Boussinesq form is

$$\begin{aligned}&\frac{\partial\theta}{\partial t^*} + \frac{\partial u\theta}{\partial x^*} + \frac{\partial v\theta}{\partial y^*} + \frac{\partial w\theta}{\partial z^*} \\ &\quad = \frac{1}{\rho}\left(\frac{\partial}{\partial x^*}\left(\rho A_H\frac{\partial\theta}{\partial x^*}\right) + \frac{\partial}{\partial y^*}\left(\rho A_H\frac{\partial\theta}{\partial y^*}\right) + \frac{\partial}{\partial z^*}\left(\rho K_H\frac{\partial\theta}{\partial z^*}\right)\right)\end{aligned} \tag{3.63}$$

Which is transformed from Cartesian to σ co-ordinates using (3.8), (3.10), and (3.11) with the substitution of ω from (3.2) giving

$$\frac{\partial\theta}{\partial t}+\frac{\partial u\theta}{\partial x}+\frac{1}{D}\left(\frac{\partial\omega\theta}{\partial\sigma}+\theta\frac{\partial\eta}{\partial t}+u\theta\frac{\partial D}{\partial x}\right)=\frac{1}{\rho}\frac{\partial}{\partial x}\left(\rho A_H\frac{\partial\theta}{\partial x}\right)$$
$$+\frac{1}{\rho}\frac{\partial}{\partial\sigma}\left(\rho A_H\frac{\partial\theta}{\partial x}\right)\frac{\partial\sigma}{\partial x}+\frac{1}{\rho D^2}\frac{\partial}{\partial\sigma}\left(\rho K_H\frac{\partial\theta}{\partial\sigma}\right) \quad (3.64)$$
$$+\frac{1}{B}\frac{\partial B}{\partial x}\left(A_H\frac{\partial\theta}{\partial x}-u\theta\right)$$

Multiplying (3.64) by D and contracting derivatives on left hand side of equation gives

$$\frac{\partial\theta D}{\partial t}+\frac{\partial u\theta D}{\partial x}+\frac{\partial\omega\theta}{\partial\sigma}=\frac{D}{\rho}\frac{\partial}{\partial x}\left(\rho A_H\frac{\partial\theta}{\partial x}\right)$$
$$+\frac{D}{\rho}\frac{\partial}{\partial\sigma}\left(\rho A_H\frac{\partial\theta}{\partial x}\right)\frac{\partial\sigma}{\partial x}+\frac{1}{\rho D}\frac{\partial}{\partial\sigma}\left(\rho K_H\frac{\partial\theta}{\partial\sigma}\right)+\frac{D}{B}\frac{\partial B}{\partial x}\left(A_H\frac{\partial\theta}{\partial x}-u\theta\right) \quad (3.65)$$

The Boussinesq form of (3.65) in σ co-ordinates does not have density in the diffusion terms, giving

$$\frac{\partial\theta D}{\partial t}+\frac{\partial u\theta D}{\partial x}+\frac{\partial\omega\theta}{\partial\sigma}=D\frac{\partial}{\partial x}\left(A_H\frac{\partial\theta}{\partial x}\right)$$
$$+D\frac{\partial}{\partial\sigma}\left(A_H\frac{\partial\theta}{\partial x}\right)\frac{\partial\sigma}{\partial x}+\frac{1}{D}\frac{\partial}{\partial\sigma}\left(K_H\frac{\partial\theta}{\partial\sigma}\right)+\frac{D}{B}\frac{\partial B}{\partial x}\left(A_H\frac{\partial\theta}{\partial x}-u\theta\right) \quad (3.66)$$

In the momentum equation (3.60), a wall friction term $\lambda u|u|$ appears after it had been laterally averaged, with no equivalent in the scalar conservation equation. This is because it is assumed no diffusion of scalar quantities occur through the river side and bottom boundary, while momentum is diffused by losing energy through viscous dissipation. While salinity and pollution concentration are conservative at the top and bottom boundaries, temperature is only conservative at the bottom boundary. At the top surface a heat flux is introduced as a boundary condition in the heat equation, but penetrative radiation is ignored. The temperature boundary condition models the diurnal solar temperature variations.

POM (Mellor, 1996) allows for several top surface thermal boundary conditions. Users have the option of using penetrative short wave radiation, and prescribing heat input through specifying a surface temperature or a heat flux. For the model in this thesis, POM is set with no penetrative short wave radiation and a heat flux is specified at the top surface.

3.4.4 Turbulence closure

With the Boussinesq approximation of the Reynolds stress tensor, the crux of the diffusion problem is deriving a value for the diffusion constants. Empirical values are used in a turbulence closure, due to the complexity and problems of resolution with modelling turbulence. Complexity arises from the random, non-linear, and diffusive nature of turbulent flow. The problem of resolution is due to the scales that turbulence is apparent at, ranging from less than millimetre to hundreds of metres. Current computer technology running

numerical models can not cope with modelling all these scales simultaneously. Direct numerical simulation, models the interactions between individual molecules. It is possible to model molecular scale turbulence with direct numerical simulation on a centimetre scale, but to model the molecular turbulence directly on an estuary scale is decades away.

The Prandtl mixing length model provides a zero-dimension turbulence closure equation based on a mixing length and velocity gradient for diffusion values. The vertical diffusion value is reduced by a stability function (ϕ_f) based on the Richardson number (R_i). The stability function models the turbulence suppressing ability of stable stratification. This is where an eddy of stably stratified water initiating upward movement will be denser than the surrounding water and is returned to its original location due to gravity; whereas an eddy moving down will be less dense than the surrounding water and be returned to its original location due to buoyancy. For unstable stratification ($R_i < 0$) the same forces will promote turbulent mixing. The horizontal diffusion value does not have a corresponding stability function, as there are no buoyancy or gravity effects in the horizontal plane.

For kinematic eddy viscosity

$$A_M = l_h^2 \left|\frac{\partial u}{\partial x}\right| \text{ and } K_M = \frac{l_v^2}{D\phi_M}\left|\frac{\partial u}{\partial \sigma}\right| \tag{3.67}$$

For eddy diffusivity

$$A_H = l_h^2 \left|\frac{\partial u}{\partial x}\right| \text{ and } K_H = \frac{l_v^2}{D\phi_H}\left|\frac{\partial u}{\partial \sigma}\right| \tag{3.68}$$

The diffusion values are capped to maintain numerical stability, $A_{f\,\min} \le A_f \le A_{f\,\max}$ and $K_{f\,\min} \le K_f \le K_{f\,\max}$. With typical values of the limits: $A_{f\,\min} = 5.0\text{m}^2/\text{s}$, $A_{f\,\max} = 250\text{m}^2/\text{s}$, $K_{f\,\min} = 1.0\times10^{-5}\,\text{m}^2/\text{s}$, and $K_{f\,\max} = 5.0\times10^{-3}\,\text{m}^2/\text{s}$. In (3.67) and (3.68), l_h and l_v are the horizontal and vertical mixing lengths, the cross-stream distance a fluid particle moves on average before giving up its momentum and loses its identity. The horizontal diffusion values are assumed the same, and the vertical values are the same for stable stratification $R_i > 0$, but ϕ_H is amplified for unstable stratification $R_i \le 0$.

$$\phi_M = \phi_H = \left(1+\kappa_{\phi_1} R_i\right)^{\kappa_{\phi_2}} \text{ for } R_i > 0 \tag{3.69}$$

$$\phi_M = \left(1+\kappa_{\phi_3} R_i^{\kappa_{\phi_4}}\right) \text{ and } \phi_H = \phi_M \Big/ \left(1+\kappa_{\phi_5} R_i^{\kappa_{\phi_6}}\right) \text{ for } R_i \le 0 \tag{3.70}$$

Typically

$$\kappa_{\phi_1} = 10,\ \kappa_{\phi_2} = 1.5 \tag{3.71}$$

$$\kappa_{\phi_3} = 0.520951,\ \kappa_{\phi_4} = 0.0592195 \tag{3.72}$$

$$\kappa_{\phi_5} = 2.381596,\ \kappa_{\phi_6} = 0.2519296 \tag{3.73}$$

The first two values (3.71) are based on the work by Munk and Anderson (1948), and various similar numbers were tried. The last four values (3.72) and (3.73) are from curve fitting a graph of Boericke and Hogan's (1977), based on the Monin-Obukov length used by Charnock (1967). For these relationships, R_i is capped $-10 < R_i < 10^6$, where typically $10 < R_i < 10^4$ for the stratified areas of the rivers, and $-5 < R_i < 10$ for the well mixed regions.

The expressions for the vertical and horizontal Prandtl mixing lengths are

$$l_v = -k\sigma D\sqrt{1+\sigma} \tag{3.74}$$

$$l_h = -k\sigma K_{l_h} B\sqrt{1+\sigma} \tag{3.75}$$

The mixing lengths are capped $0 < l_v \le l_{v\max}$ and $0 < l_h \le l_{h\max}$, typically $l_{v\max} = 1.0\text{m}$ and $l_{h\max} = 200\text{m}$. In (3.74) and (3.75) the von-Karman constant $k = 0.40$, and to make the eddy size is a fraction of the river width $0 < K_{l_h} \le 1$, typically $K_{l_h} = 0.8$. The minus signs in (3.74) and (3.75) make the mixing lengths positive, as $-1 \le \sigma_k \le 0$.

Another expression investigated for the horizontal diffusion values was from Fischer (1967), in which diffusion is due to wall shear stress. Fischer's scheme was depth integrated, hence uniform with depth, while the scheme used (3.68) allowed a variation of the horizontal diffusion with depth. An arbitrary depth variation was tried with Fischer's scheme by multiplying it with $-\sigma\sqrt{1+\sigma}$, but with no improvement over the scheme used.

Boericke and Hogan (1977) started using the Fischer (1967) formulation, but ended up using horizontal diffusion to calibrate their model. Odd (1981) also chose diffusion values to calibrate a one-dimensional model. Blumberg (1977b) used a different stability function and compared others, but used the same mixing length as Boericke and Hogan (1977). Perrels and Karelse (1981) tried a linear variation of mixing length with depth, which had a small roughness length at the bottom and a maximum length at the surface. They also used an exponential stability function that did not work well, being too severe at high Richardson numbers thus causing artificially low diffusion.

A low level model used for complex phenomenon will inevitably require calibration. In the case of this river model, the stability function coefficients were modified until the vertical mixing was reduced to a sensible level with $\kappa_{\phi_1} = 20$, $\kappa_{\phi_2} = 2.0$.

Chapter Four
River model implementation

4.1 Introduction

This chapter describes the numerical implementation of the continuous equations derived in Chapter Three, for the two-dimensional laterally averaged model (2DLAM). While numerical modelling is portrayed with the sequential chapters of this thesis as a one directional process, the process is actually iterative (Abraham, van Os, and Verboom, 1981). What is described in this chapter is the result of many attempts, some of which are also described.

In the context of this river model implementation, a term is explicit if it does not contain any variables at the next time step and can be evaluated directly using the known values. While the river model equations are solved implicitly, they can contain derivatives that are expressed explicitly. A whole scheme is said to be an explicit scheme when it only contains one term in the equation at the next time step. For example when solving for horizontal velocity the scheme is solved implicitly in the vertical direction, and contains explicit derivatives in the horizontal direction and implicit derivatives in the vertical direction. The horizontal derivatives have to be explicit as the solution matrix is being set up to contain unknowns for the vertical grids at the one horizontal position. If when solving vertically, there were unknowns at different horizontal positions, then the matrix for the solution would be a three-dimensional rather than two-dimensional, and time consuming to solve.

The finite difference operators used are centred in time and space. This allows the solution of the surface elevation and velocity to be separated by expressing explicitly the unknown derivatives that are not being solved in that equation. For example, the surface elevation is solved before the horizontal velocity. So when solving for surface elevation all the derivative expressions for the horizontal derivatives will be explicit, but still centred at the

same point as the surface elevation derivatives (that are implicit). Similarly when solving for horizontal velocity the pressure terms, based on surface elevation and density, are explicit.

Horizontal velocity is solved vertically because of the stability of implicit schemes, as usually the vertical CFL limit is smaller than the horizontal. If solved horizontally the CFL time step limit would be too restrictive due to the small vertical grid spacing in the shallow up stream ends of the rivers. The author attempted to use an alternating direction implicit (ADI) scheme alternating between the horizontal and vertical directions, but it was not stable enough when solving explicitly in the vertical direction. The ADI schemes are usually used for horizontal schemes, where the x and y directions are alternated between with implicit and explicit methods and are of similar scales. However, the vertical and horizontal scales are so different there is nothing to be gained by using explicit schemes vertically.

4.2 Grid arrangement

Finite difference schemes are based on a spatial and temporal grid. The temporal grid is not staggered and is indexed by n, where variables at time n-1 and n are known, and variables at time n+1 are the unknowns to be solved for (Figure 4.1). The spatial grid is indexed horizontally by i on a staggered fixed size grid and vertically by k on a non-staggered variably spaced grid, which are positive in the x and σ directions respectively. Terms in a finite difference expression are indexed with superscript for the temporal index and subscripts for the spatial index (using: x, σ). For example, $f^{n+1}_{i-\frac{1}{2},k}$ is a function f at time n+1, x at the $i-\frac{1}{2}$ horizontal grid, and σ at the k vertical grid. While the vertical grid spacing can be variable, in this thesis it is even except for near the top and bottom where the spacing is half the mid values. Details of the vertical σ grid values are given in Appendix D.

This river model has the surface elevation (1D) and two-dimensional (2D) variables horizontally offset by half a grid, with surface elevation on the limits of the solution space (Figure 4.2). In Figure 4.2 the surface elevation grid is denoted by i_{1D} and the two-dimensional grid is denoted by i_{2D}; the *harbour* grid are values from Macquarie Harbour; *KB* is the maximum number of vertical grids, and *IM* is the maximum number of horizontal grids. All the two-dimensional variables in the river model are on the same grid, as they are solved with the same scheme. This improves the final implementation with smaller, more accurate code. Most variables are then interpolated at the half grid points for use in the solution routines, so in the finite difference expressions later, any variables had half grid locations have been calculated before they are used to improve solution performance. The surface-elevation is solved at half a horizontal grid offset from where the horizontal velocity

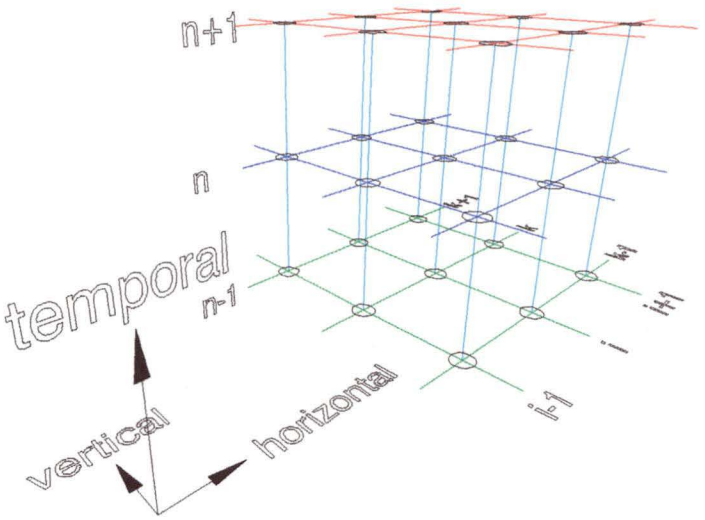

Figure 4.1 Time – 2D space grid definition

is solved, to improve the numerical accuracy of the difference operators with the pressure terms.

There can be confusion with the notation as the one and two-dimensional variables both use i for their horizontal index, but are offset by half a grid. The distinction is not that important, as after a variable is solved on one grid, it is interpolated at the half grid offset from where it was solved. In a finite difference equation all the horizontal indexes refer to the same horizontal grid, which is centred on the variable that is being solved. For example, when solving for surface elevation, η_i^{n+1}, a depth averaged horizontal velocity like u_i^n is centred at the same horizontal position as the surface elevation; and when solving for horizontal velocity, $u_{i,k}^{n+1}$, a surface elevation like $\eta_{i-\frac{1}{2}}^n$ is centred half a horizontal grid upstream of the horizontal velocity. Note the difference in notation used between depth averaged variables (one-dimensional) and the non depth averaged version (two-dimensional), as shown with the omission or inclusion of the vertical index (k) used with the horizontal velocity.

4.3 Difference operators

The finite difference operators are based on a spatially centred box scheme. A forward in time box scheme is added to a back in time box scheme with the aim for removing some of the truncation errors similar to Verwey and Ilic (1993). This makes the scheme second order centred in time and space, with a temporal weighting (θ) away from the current time step, typically $\theta = 0.62$. To be stable, a frictionless implicit scheme must have $\theta > 0.5$. When

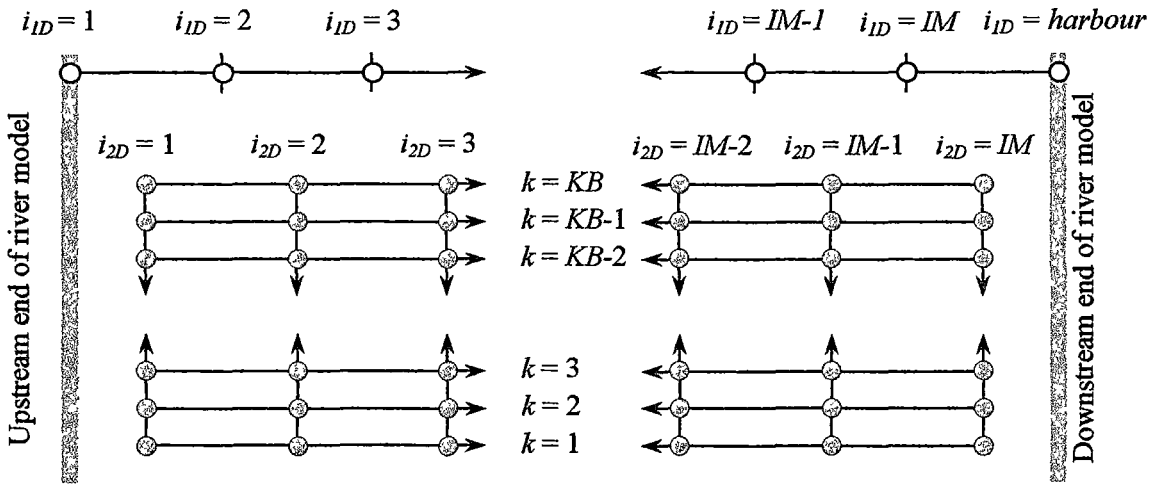

Figure 4.2 Horizontal grid offset between 1D (O) and 2D (⊛) variables

solving vertically, the horizontal derivatives are explicit (setting $\theta=0$), and when solving horizontally, the vertical derivatives are explicit.

The η and u variables are staggered by half a grid to be consistent with POM. Such that the equations for η are half a grid out from the equations for the two-dimensional variables (u, S, T, and C).

In an attempt to improve the condition of the terms in the elements of the solution matrix, define a relative term

$$f^{\Delta n+1}=f^{n+1}-f^{n} \text{ and } f^{\Delta n-1}=f^{n-1}-f^{n} \tag{4.1}$$

The difference equations are solved for $f^{\Delta n+1}$, then f^{n} is added back after to give f^{n+1}. As the scheme is only solving for the temporal difference in the function, the terms in the solution matrix are better conditioned for rounding errors. For example, consider a simple advection formula for a function f (units U) solved with an implicit scheme and three significant figures of floating point accuracy

$$\frac{\partial f}{\partial t}+\frac{\partial fu}{\partial x}=0 \tag{4.2}$$

At some point in space and time (i,n): $\Delta t=3.00\text{s}$, $f^{n}=20.0\text{U}$, $f^{n-1}=19.9\text{U}$, $\partial f/\partial x\big|_i^n=0.01\text{U/m}$, $u_i^n=1.00\text{m/s}$, and $\partial u/\partial x\big|_i^n=0.05\text{s}^{-1}$. While the problem is being solved with an implicit scheme, it is possible look at the rounding errors at this one point with an explicit approximation of (4.2) giving

$$\partial f/\partial t=\left(f_i^{n+1}-f_i^{n-1}\right)/2\Delta t$$
$$f_i^{n+1}=f_i^{n-1}-2\Delta t\left(\partial fu/\partial x\right)=19.9-1.26=18.64$$

So f_i^{n+1} = 18.6U with a 0.04U rounding error. This rounding error is carried through the entire solution space, with consequential errors in the other values. That is, the surrounding values will "see" the value at $(i, n+1)$ to be 18.6U and not 18.64U, and change accordingly. Instead, using the substitution $f_i^{n+1} = f_i^{\Delta n+1} + f_i^n$ and $f_i^{n-1} = f_i^{\Delta n-1} + f_i^n$ from (4.1), then solving for $f_i^{\Delta n+1}$

$$\partial f/\partial t = \left(f_i^{\Delta n+1} - f_i^{\Delta n-1}\right)/2\Delta t$$
$$f_i^{\Delta n+1} = f_i^{\Delta n-1} - 2\Delta t(\partial fu/\partial x) = -0.10 - 1.26 = -1.36$$

There is no rounding error at this stage and no consequential errors in the surrounding values. When f_i^n is added to $f_i^{\Delta n+1}$ after the implicit solution, f_i^{n+1} = 20.0 - 1.36 = 18.64 =18.6U, there is the same 0.04U rounding error. However, it is a local error and did not effect the neighbouring values. That is, while the implicit scheme was solving it would "see" the value as -1.36U, which is equivalent to 18.64U. The method is important when the value of the function is large, such as with salinity and temperature values. With salinity and temperature, the changes each time step are a magnitude less than of the original value.

Using the $f_i^{\Delta n+1}$ and $f_i^{\Delta n-1}$ definitions (4.1), with the box difference operators for a function value is

$$f = (1-\theta)f_{i,k}^n + \tfrac{1}{2}\theta\left(f_{i,k}^{n+1} + f_{i,k}^{n-1}\right) = f_{i,k}^n + \tfrac{1}{2}\theta\left(f_{i,k}^{\Delta n+1} + f_{i,k}^{\Delta n-1}\right) \tag{4.3}$$

The temporal derivative is

$$\frac{\partial f}{\partial t} = \frac{f_{i,k}^{n+1} - f_{i,k}^{n-1}}{2\Delta t} = \frac{f_{i,k}^{\Delta n+1} - f_{i,k}^{\Delta n-1}}{2\Delta t} \tag{4.4}$$

And a horizontal derivative is

$$\frac{\partial f}{\partial x} = (1-\theta)\frac{\partial f}{\partial x}\bigg|_{i,k}^{n} + \tfrac{1}{2}\theta\left(\frac{\partial f}{\partial x}\bigg|_{i,k}^{n+1} + \frac{\partial f}{\partial x}\bigg|_{i,k}^{n-1}\right) \tag{4.5}$$
$$= \frac{2(1-\theta)\left(f_{i+1,k}^n - f_{i-1,k}^n\right) + \theta\left(f_{i+1,k}^{n+1} - f_{i-1,k}^{n+1} + f_{i+1,k}^{n-1} - f_{i-1,k}^{n-1}\right)}{4\Delta x}$$

Now substitute in $f_i^{\Delta n+1}$ and $f_i^{\Delta n-1}$ from (4.1) in (4.5) to give

$$\frac{\partial f}{\partial x} = \frac{2\left(f_{i+1,k}^n - f_{i-1,k}^n\right) + \theta\left(f_{i+1,k}^{\Delta n+1} - f_{i-1,k}^{\Delta n+1} + f_{i+1,k}^{\Delta n-1} - f_{i-1,k}^{\Delta n-1}\right)}{4\Delta x} \tag{4.6}$$

The horizontal diffusive operator is only ever used in its explicit form

$$\frac{\partial A_f \dfrac{\partial f}{\partial x}}{\partial x} = \frac{1}{\Delta x^2}\left(A_{f\,i+\frac{1}{2},k}\left(f_{i+1,k}^n - f_{i,k}^n\right) - A_{f\,i-\frac{1}{2},k}\left(f_{i,k}^n - f_{i-1,k}^n\right)\right) \tag{4.7}$$

The vertical derivative is similar to the horizontal in its time centring

$$\frac{\partial f}{\partial \sigma} = (1-\theta)\frac{\partial f}{\partial \sigma}\bigg|_{i,k}^{n} + \tfrac{1}{2}\theta\left(\frac{\partial f}{\partial \sigma}\bigg|_{i,k}^{n+1} + \frac{\partial f}{\partial \sigma}\bigg|_{i,k}^{n-1}\right) \tag{4.8}$$

The horizontal grids are a constant size and the difference operator is horizontally centred using a linear approximation for the function. The vertical σ grids vary in size, so the vertical difference operator would not be vertically centred if a linear approximation was used for the function. Hence, the function is assumed to vary parabolically between the grid points for the vertical difference operator. An expression is derived (Appendix A.1) that is vertically centred even if the vertical grid spacing varies between adjacent cells

$$\frac{\partial f}{\partial \sigma}\bigg|_{i,k}^{n} = \frac{1}{\Delta\sigma_T}\left(\left(f_{i,k+1}^{n} - f_{i,k}^{n}\right)\frac{\Delta\sigma_L}{\Delta\sigma_U} + \left(f_{i,k}^{n} - f_{i,k-1}^{n}\right)\frac{\Delta\sigma_U}{\Delta\sigma_L}\right) \tag{4.9}$$

$\Delta\sigma_T = \Delta\sigma_U + \Delta\sigma_L$, $\Delta\sigma_U = \sigma_{k+1} - \sigma_k$ and $\Delta\sigma_L = \sigma_k - \sigma_{k-1}$

Substituting (4.9) in (4.8) gives

$$\begin{aligned}\frac{\partial f}{\partial \sigma} = {} & (1-\theta)\frac{1}{\Delta\sigma_T}\left(\left(f_{i,k+1}^{n} - f_{i,k}^{n}\right)\frac{\Delta\sigma_L}{\Delta\sigma_U} + \left(f_{i,k}^{n} - f_{i,k-1}^{n}\right)\frac{\Delta\sigma_U}{\Delta\sigma_L}\right) \\ & + \frac{\theta}{2\Delta\sigma_T}\left(\left(f_{i,k+1}^{n+1} - f_{i,k}^{n+1} + f_{i,k+1}^{n+1} - f_{i,k}^{n+1}\right)\frac{\Delta\sigma_L}{\Delta\sigma_U}\right. \\ & \left. + \left(f_{i,k}^{n+1} - f_{i,k-1}^{n+1} + f_{i,k}^{n+1} - f_{i,k-1}^{n+1}\right)\frac{\Delta\sigma_U}{\Delta\sigma_L}\right)\end{aligned} \tag{4.10}$$

Now substitute in $f_i^{\Delta n+1}$ and $f_i^{\Delta n-1}$ from (4.1) in (4.10) to give

$$\begin{aligned}\frac{\partial f}{\partial \sigma} = \frac{1}{\Delta\sigma_T}\Bigg(\Bigg(f_{i,k+1}^{n} - f_{i,k}^{n} + \frac{\theta}{2}\left(f_{i,k+1}^{\Delta n+1} - f_{i,k}^{\Delta n+1} + f_{i,k+1}^{\Delta n-1} - f_{i,k}^{\Delta n-1}\right)\Bigg)\frac{\Delta\sigma_L}{\Delta\sigma_U} \\ + \left(f_{i,k}^{n} - f_{i,k-1}^{n} + \frac{\theta}{2}\left(f_{i,k}^{\Delta n+1} - f_{i,k-1}^{\Delta n+1} + f_{i,k}^{\Delta n-1} - f_{i,k-1}^{\Delta n-1}\right)\right)\frac{\Delta\sigma_U}{\Delta\sigma_L}\Bigg)\end{aligned} \tag{4.11}$$

To keep the solution matrix tri-diagonal, the scheme should only use three grids at the unknown (future) time step. Therefore, for diffusive terms the vertical derivatives can not use the quadratic differencing, as it would take five grids. The alternative is the linear differencing (that is not vertically centred when $\Delta\sigma_U \neq \Delta\sigma_L$)

$$\frac{\partial K_f \dfrac{\partial f}{\partial \sigma}}{\partial \sigma} = (1-\theta)\frac{\partial K_f \dfrac{\partial f}{\partial \sigma}}{\partial \sigma}\bigg|_{i,k}^{n} + \tfrac{1}{2}\theta\left(\frac{\partial K_f \dfrac{\partial f}{\partial \sigma}}{\partial \sigma}\bigg|_{i,k}^{n+1} + \frac{\partial K_f \dfrac{\partial f}{\partial \sigma}}{\partial \sigma}\bigg|_{i,k}^{n-1}\right) \tag{4.12}$$

Where

$$\frac{\partial K_f \dfrac{\partial f}{\partial \sigma}}{\partial \sigma}\bigg|_{i,k}^{n} = \frac{2}{\Delta\sigma_T}\left(\frac{K_{f\,i,k+\frac{1}{2}}}{\Delta\sigma_U}\left(f_{i,k+1}^{n} - f_{i,k}^{n}\right) - \frac{K_{f\,i,k-\frac{1}{2}}}{\Delta\sigma_L}\left(f_{i,k}^{n} - f_{i,k-1}^{n}\right)\right) \tag{4.13}$$

Now substituting in $f_i^{\Delta n+1}$ and $f_i^{\Delta n-1}$ from (4.1) in (4.12) using (4.13) to give

$$\frac{\partial K_f \frac{\partial f}{\partial \sigma}}{\partial \sigma} = \frac{2}{\Delta\sigma_T}\left(\frac{K_{f_{i,k+\frac{1}{2}}}}{\Delta\sigma_U}\left(f_{i,k+1}^{n} - f_{i,k}^{n} + \tfrac{1}{2}\theta\left(f_{i,k+1}^{\Delta n+1} - f_{i,k}^{\Delta n+1} + f_{i,k+1}^{\Delta n-1} - f_{i,k}^{\Delta n-1}\right)\right)\right. \\ \left. - \frac{K_{f_{i,k-\frac{1}{2}}}}{\Delta\sigma_U}\left(f_{i,k}^{n} - f_{i,k-1}^{n} + \tfrac{1}{2}\theta\left(f_{i,k}^{\Delta n+1} - f_{i,k-1}^{\Delta n+1} + f_{i,k}^{\Delta n-1} - f_{i,k-1}^{\Delta n-1}\right)\right)\right) \tag{4.14}$$

4.4 Difference equations

The difference operators are substituted in the continuous equations from Chapter Three to give finite different equations. The general form of a vertical prognostic equations is

$$A_{f_k} f_{i,k+1}^{\Delta n+1} + B_{f_k} f_{i,k}^{\Delta n+1} + C_{f_k} f_{i,k-1}^{\Delta n+1} = K_{f_{v,k}} \tag{4.15}$$

While a horizontal prognostic equation is

$$A_{f_i} f_{i+1,k}^{\Delta n+1} + B_{f_i} f_{i,k}^{\Delta n+1} + C_{f_i} f_{i-1,k}^{\Delta n+1} = K_{f_{h,i}} \tag{4.16}$$

Where A_f, B_f, and C_f are expressions for the coefficients of $f^{\Delta n+1}$ at the future time step. $K_{f_{v,k}}$ and $K_{f_{h,i}}$ are expressions containing all the known values in the equation, and are not a vertical diffusion value (that is generically referred to as K_f). The three coefficients for each grid make up the tri-diagonal matrix. Such that for the vertical prognostic equations

$$\begin{bmatrix} B_{f_1} & C_{f_1} & A_{f_1} & & & \\ A_{f_2} & B_{f_2} & C_{f_2} & & \mathbf{0} & \\ & A_{f_3} & B_{f_3} & C_{f_3} & & \\ & \ddots & \ddots & \ddots & & \\ \mathbf{0} & & A_{f_{k_{\max}-1}} & B_{f_{k_{\max}-1}} & C_{f_{k_{\max}-1}} & \\ & & C_{f_{k_{\max}}} & A_{f_{k_{\max}}} & B_{f_{k_{\max}}} & \end{bmatrix} \times \begin{bmatrix} f_{i,1}^{\Delta n+1} \\ f_{i,2}^{\Delta n+1} \\ f_{i,3}^{\Delta n+1} \\ \vdots \\ f_{i,k_{\max}-1}^{\Delta n+1} \\ f_{i,k_{\max}}^{\Delta n+1} \end{bmatrix} = \begin{bmatrix} K_{f_{v,1}} \\ K_{f_{v,2}} \\ K_{f_{v,3}} \\ \vdots \\ K_{f_{v,k_{\max}-1}} \\ K_{f_{v,k_{\max}}} \end{bmatrix} \tag{4.17}$$

The off diagonal elements are zero and $k_{\max}$ is the maximum value for k. With the inclusion of the A_{f_1} and $C_{f_{k_{\max}}}$ elements the matrix is called an almost block tri-diagonal matrix. Usually these coefficients are zero, but with some boundary conditions they are not. The horizontal prognostic equation is very similar to the vertical (where i_{max} is the maximum value of i)

$$\begin{bmatrix} B_{f_1} & C_{f_1} & A_{f_1} & & & \\ A_{f_2} & B_{f_2} & C_{f_2} & & \mathbf{0} & \\ & A_{f_3} & B_{f_3} & C_{f_3} & & \\ & \ddots & \ddots & \ddots & & \\ \mathbf{0} & & A_{f_{i_{\max}-1}} & B_{f_{i_{\max}-1}} & C_{f_{i_{\max}-1}} & \\ & & C_{f_{i_{\max}}} & A_{f_{i_{\max}}} & B_{f_{i_{\max}}} & \end{bmatrix} \times \begin{bmatrix} f_{1,k}^{\Delta n+1} \\ f_{2,k}^{\Delta n+1} \\ f_{3,k}^{\Delta n+1} \\ \vdots \\ f_{i_{\max}-1,k}^{\Delta n+1} \\ f_{i_{\max},k}^{\Delta n+1} \end{bmatrix} = \begin{bmatrix} K_{f_{h,1}} \\ K_{f_{h,2}} \\ K_{f_{h,3}} \\ \vdots \\ K_{f_{h,i_{\max}-1}} \\ K_{f_{h,i_{\max}}} \end{bmatrix} \tag{4.18}$$

The equations (4.17) and (4.18) are solved with a NSWC FORTRAN library subroutine BTSLV (NSWC, 1993) for solving almost block-diagonal systems of linear equations. Then the next time step in calculated with $f_{i,k}^{n+1} = f_{i,k}^{\Delta n+1} + f_{i,k}^{n}$.

In the following sections the relative density (ρ') is used,

$$\rho = \rho' / \kappa_{\rho 1} \text{ where } \rho' = \rho_0' + \kappa_{\rho 2}. \tag{4.19}$$

4.4.1 Surface elevation

Non-Boussinesq surface elevation equation is solved horizontally. See Appendix A.2 for the derivation

$$A_{\eta_{NB}} \eta_{i-1}^{\Delta n+1} + B_{\eta_{NB}} \eta_i^{\Delta n+1} + C_{\eta_{NB}} \eta_{i+1}^{\Delta n+1} = K_{\eta_{NB}} \tag{4.20}$$

Where

$$A_{\eta_{NB}} = -\frac{\overline{\rho' u_i}^n}{\overline{\rho'}_i^n} \frac{\theta}{4\Delta x} \tag{4.21}$$

$$B_{\eta_{NB}} = \frac{1}{2}\left(\frac{1}{\Delta t} + \theta Z_{\eta_{NB}}\right) \tag{4.22}$$

$$C_{\eta_{NB}} = \frac{\overline{\rho' u_i}^n}{\overline{\rho'}_i^n} \frac{\theta}{4\Delta x} \tag{4.23}$$

$$K_{\eta_{NB}} = \frac{\eta^{\Delta n-1}}{2\Delta t} - \frac{\overline{\rho' u_i}^n}{\overline{\rho'}_i^n} \times \frac{2\left(D_{i+1}^n - D_{i-1}^n\right) + \theta\left(\eta_{i+1}^{\Delta n-1} - \eta_{i-1}^{\Delta n-1}\right)}{4\Delta x} - \left(D_i^n + \tfrac{1}{2}\theta\eta_i^{\Delta n-1}\right) Z_{\eta_{NB}} \tag{4.24}$$

$$Z_{\eta_{NB}} = \frac{1}{\overline{\rho'}_i^n}\left(\frac{\overline{\rho'_0}_i^n - \overline{\rho'_0}_i^{n-1}}{\Delta t} + \frac{\overline{\rho' u}_{i+\frac{1}{2}}^n - \overline{\rho' u}_{i-\frac{1}{2}}^n}{\Delta x} + \frac{\overline{\rho' u}_i^n}{B_i} \times \frac{B_{i+\frac{1}{2}} - B_{i-\frac{1}{2}}}{\Delta x}\right) \tag{4.25}$$

$$\eta_i^{\Delta n-1} = \eta_i^{n-1} - \eta_i^n \tag{4.26}$$

Note the $\partial\rho/\partial t$ term in (4.25) is centred at $\left(i, n-\frac{1}{2}\right)$, not (i,n) as is the rest of the equation. This is because when η is being solved for, density is only known at the current and past time steps. The Boussinesq equations are similar

$$A_{\eta_B} \eta_{i-1}^{\Delta n+1} + B_{\eta_B} \eta_i^{\Delta n+1} + C_{\eta_B} \eta_{i+1}^{\Delta n+1} = K_{\eta_B} \tag{4.27}$$

Where

$$A_{\eta_B} = -\overline{u_i}^n \frac{\theta}{4\Delta x} \tag{4.28}$$

$$B_{\eta_B} = \frac{1}{2}\left(\frac{1}{\Delta t} + \theta Z_{\eta_B}\right) \tag{4.29}$$

$$C_{\eta_B} = \overline{u_i}^n \frac{\theta}{4\Delta x} \tag{4.30}$$

$$K_{\eta_B} = \frac{\eta^{\Delta n-1}}{2\Delta t} - \bar{u}_i^n \times \frac{2\left(D_{i+1}^n - D_{i-1}^n\right) + \theta\left(\eta_{i+1}^{\Delta n-1} - \eta_{i-1}^{\Delta n-1}\right)}{4\Delta x} - \left(D_i^n + \tfrac{1}{2}\theta\eta_i^{\Delta n-1}\right) Z_{\eta_B} \tag{4.31}$$

$$Z_{\eta_B} = \frac{\bar{u}_{i+\frac{1}{2}}^n - \bar{u}_{i-\frac{1}{2}}^n}{\Delta x} + \frac{\bar{u}_i^n}{B_i} \times \frac{B_{i+\frac{1}{2}} - B_{i-\frac{1}{2}}}{\Delta x} \tag{4.32}$$

4.4.2 Conservation of momentum & scalar variables

For ease of derivation and later of coding, a generic conservation equation is used for both momentum and scalar variables. This reduces human error in both stages. The same equation is used for non-Boussinesq and Boussinesq equations, with the Boussinesq equations $\rho_0' = 0$ except in the pressure terms.

$$\begin{aligned}\frac{\partial Df}{\partial t} + \frac{\partial Duf}{\partial x} + \frac{\partial \omega f}{\partial \sigma} &= \frac{D}{\rho}\frac{\partial \rho A_f \dfrac{\partial f}{\partial x*}}{\partial x} + \frac{D}{\rho}\frac{\partial \rho A_f \dfrac{\partial f}{\partial x*}}{\partial \sigma}\frac{\partial \sigma}{\partial x} \\ &+ \frac{1}{\rho D}\frac{\partial \rho K_f \dfrac{\partial f}{\partial \sigma}}{\partial \sigma} + \frac{D}{B}\frac{\partial B}{\partial x}\left(A_f \frac{\partial f}{\partial x*} - uf\right) \\ &- M\left(\frac{D^2 g}{\rho' + \kappa_{\rho_2}}\int_\sigma^0 \left(\frac{\partial \rho'}{\partial x} - \frac{1}{D}\frac{\partial D}{\partial x}\sigma\frac{\partial \rho'}{\partial \sigma}\right)d\sigma + gD\frac{\partial \eta}{\partial x} - \lambda Df|u|\right)\end{aligned} \tag{4.33}$$

Where

$$\frac{\partial f}{\partial x*} = \frac{\partial f}{\partial x} + \frac{\partial f}{\partial \sigma}\frac{\partial \sigma}{\partial x} \tag{4.34}$$

The function f could be u, S, T, or C. When $f = u$ then $A_f = A_M$, $K_f = K_M$, and $M = 1$; and when $f = S$, T, or C then $A_f = A_H$, $K_f = K_H$, and $M = 0$. Appendix A.3 contains the expansion of the derivatives using the finite difference operators and the coefficients of the solution matrix. When solved vertically $\theta = 0$ in the finite difference operators for the horizontal derivatives, and the solution is of the form

$$A_{f_k} f_{i,k-1}^{\Delta n+1} + B_{f_k} f_{i,k}^{\Delta n+1} + C_{f_k} f_{i,k+1}^{\Delta n+1} = K_{f_{v,k}} \tag{4.35}$$

Where

$$A_{f_k} = \frac{\theta}{\Delta\sigma_T}\left(-\tfrac{1}{2}\omega_{i,k-1}^n \frac{\Delta\sigma_U}{\Delta\sigma_L} - \frac{\rho_{i,k-\frac{1}{2}}'^n}{\rho_{i,k}'^n}\frac{K_{f_{i,k-\frac{1}{2}}}}{D_i^n \Delta\sigma_L}\right) \tag{4.36}$$

$$\begin{aligned}B_{f_k} = \frac{D_i^{n+1}}{2\Delta t} &+ \frac{\theta D_i^n u_{i,k}^n}{2B_i^n \Delta x}\left(B_{i+\frac{1}{2}}^n - B_{i-\frac{1}{2}}^n\right) + \frac{\theta}{\Delta\sigma_T}\left(\tfrac{1}{2}\omega_{i,k}^n\left(\frac{\Delta\sigma_U}{\Delta\sigma_L} - \frac{\Delta\sigma_L}{\Delta\sigma_U}\right)\right. \\ &\left. + \frac{1}{D_i^n \rho_{i,k}'^n}\left(\rho_{i,k+\frac{1}{2}}'^n \frac{K_{f_{i,k+\frac{1}{2}}}}{\Delta\sigma_U} + \rho_{i,k-\frac{1}{2}}'^n \frac{K_{f_{i,k-\frac{1}{2}}}}{\Delta\sigma_L}\right)\right) - M\tfrac{1}{2}\theta\lambda_i^n D_i^n \left|u_{i,k}^n\right|\end{aligned} \tag{4.37}$$

$$C_{f_k} = \frac{\theta}{\Delta\sigma_T}\left(\tfrac{1}{2}\omega^n_{i,k+1}\frac{\Delta\sigma_L}{\Delta\sigma_U} - \frac{\rho'^n_{i,k+\frac{1}{2}}}{\rho'^n_{i,k}}\frac{K_{f\,i,k+\frac{1}{2}}}{D^n_i\Delta\sigma_U}\right) \tag{4.38}$$

$$K_{f_k} = \sum_{L=1}^{11} K^L_{f_k} \tag{4.39}$$

$$K^1_{f_k} = \frac{D^{n-1}_i f^{\Delta n-1}_i - \left(D^{n+1}_i - D^{n-1}_i\right)f^n_{i,k}}{2\Delta t} \tag{4.40}$$

$$K^2_{f_k} = -\frac{D^n_{i+1}u^n_{i+1,k}f^n_{i+1,k} - D^n_{i-1}u^n_{i-1,k}f^n_{i-1,k}}{2\Delta x} \tag{4.41}$$

$$K^3_{f_k} = -\frac{1}{\Delta\sigma_T}\left(\left(\omega^n_{i,k+1}f^n_{i,k+1} - \omega^n_{i,k}f^n_{i,k} + \tfrac{1}{2}\theta\left(\omega^n_{i,k+1}f^{\Delta n-1}_{i,k+1} - \omega^n_{i,k}f^{\Delta n-1}_{i,k}\right)\right)\frac{\Delta\sigma_L}{\Delta\sigma_U} + \left(\omega^n_{i,k}f^n_{i,k} - \omega^n_{i,k-1}f^n_{i,k-1} + \tfrac{1}{2}\theta\left(\omega^n_{i,k}f^{\Delta n-1}_{i,k} - \omega^n_{i,k-1}f^{\Delta n-1}_{i,k-1}\right)\right)\frac{\Delta\sigma_U}{\Delta\sigma_L}\right) \tag{4.42}$$

$$K^4_{f_k} = -D^n_i u^n_{i,k}\left(f^n_{i,k} + \tfrac{1}{2}\theta f^{\Delta n-1}_{i,k}\right)\frac{B^n_{i+\frac{1}{2}} - B^n_{i-\frac{1}{2}}}{B^n_i\Delta x} \tag{4.43}$$

$$K^5_{f\,k} = \frac{D^n_i}{2\rho'^n_{i,k}\Delta x}\left(\rho'^n_{i+1,k}A_{f\,i+1,k}\frac{\partial f^{\,n}}{\partial x^*_{i+1,k}} - \rho'^n_{i-1,k}A_{f\,i-1,k}\frac{\partial f^{\,n}}{\partial x^*_{i-1,k}}\right) \tag{4.44}$$

$$K^6_{f_k} = \frac{1}{\rho'^n_{i,k}\Delta\sigma_T}\left(\left(\rho'^n_{i,k+1}A_{f\,i,k+1}{}^n\frac{\partial f^{\,n}}{\partial x^*_{i,k+1}} - \rho'^n_{i,k}A_{f\,i,k}{}^n\frac{\partial f^{\,n}}{\partial x^*_{i,k}}\right)\frac{\Delta\sigma_L}{\Delta\sigma_U} + \left(\rho'^n_{i,k}A_{f\,i,k}{}^n\frac{\partial f^{\,n}}{\partial x^*_{i,k}} - \rho'^n_{i,k-1}A_{f\,i,k-1}{}^n\frac{\partial f^{\,n}}{\partial x^*_{i,k-1}}\right)\frac{\Delta\sigma_U}{\Delta\sigma_L}\right) \times\left(\sigma_k\left(D^n_{i+\frac{1}{2}} - D^n_{i-\frac{1}{2}}\right) + \eta^n_{i+\frac{1}{2}} - \eta^n_{i-\frac{1}{2}}\right) \tag{4.45}$$

$$K^7_{f_k} = \frac{2}{D^n_i\rho'^n_{i,k}\Delta\sigma_T}\left(\rho'^n_{i,k+\frac{1}{2}}\frac{K_{f\,i,k+\frac{1}{2}}}{\Delta\sigma_U}\left(f^n_{i,k+1} - f^n_{i,k} + \tfrac{1}{2}\theta\left(f^{\Delta n-1}_{i,k+1} - f^{\Delta n-1}_{i,k}\right)\right) - \rho'^n_{i,k-\frac{1}{2}}\frac{K_{f\,i,k-\frac{1}{2}}}{\Delta\sigma_L}\left(f^n_{i,k} - f^n_{i,k-1}\right) + \tfrac{1}{2}\theta\left(f^{\Delta n-1}_{i,k} - f^{\Delta n-1}_{i,k-1}\right)\right) \tag{4.46}$$

$$K^8_{f_k} = \frac{D^n_i A_{f\,i,k}{}^n}{4B_i\Delta x^2}\left(B_{i+1} - B_{i-1}\right)\left(f^n_{i+1,k} - f^n_{i-1,k}\right) \tag{4.47}$$

$$K^9_{f_k} = -M\frac{D^{n2}_i g}{\rho'^n_{i,k}}\sum_{k=1}^{k_{\max}}\frac{\Delta\sigma_k}{2\Delta x}\left(\rho'^n_{0i+1,k} - \rho'^n_{0i-1,k} - \frac{D^n_{i+1} - D^n_{i-1}}{D^n_i}\sigma_k\frac{\partial\rho'^{\,n}}{\partial\sigma_{\,i,k}}\right) \tag{4.48}$$

$$K^{10}_{f_k} = -MgD^n_i\frac{\eta^n_{i+\frac{1}{2}} - \eta^n_{i-\frac{1}{2}}}{\Delta x} \tag{4.49}$$

$$K^{11}_{f_k} = M\lambda^n_i D^n_i\left(f^n_{i,k} + \tfrac{1}{2}\theta f^{\Delta n-1}_{i,k}\right)\left|u^n_{i,k}\right| \tag{4.50}$$

$$\frac{\partial\rho'^{\,n}}{\partial\sigma_{\,i,k}} = \frac{1}{\Delta\sigma_T}\left(\left(\rho'^n_{0i,k+1} - \rho'^n_{0i,k}\right)\frac{\Delta\sigma_L}{\Delta\sigma_U} + \left(\rho'^n_{0i,k} - \rho'^n_{0i,k-1}\right)\frac{\Delta\sigma_U}{\Delta\sigma_L}\right) \tag{4.51}$$

$$\frac{\partial f^{\,n}}{\partial x^*_{i,k}} = \frac{f^n_{i+1,k} - f^n_{i-1,k}}{2\Delta x} + \frac{1}{\Delta\sigma_T}\left(\left(f^n_{i,k+1} - f^n_{i,k}\right)\frac{\Delta\sigma_L}{\Delta\sigma_U} + \left(f^n_{i,k} - f^n_{i,k-1}\right)\frac{\Delta\sigma_U}{\Delta\sigma_L}\right)\frac{\partial\sigma}{\partial x} \tag{4.52}$$

$$\lambda_i^n = gn^2\left(\frac{B_i D_i^n}{B_i + 2D_i^n}\right)^{-4/3} \tag{4.53}$$

For solving horizontally $\theta = 0$ in the finite difference operators for the vertical derivatives, see Appendix A.3.1.2 for details.

4.4.3 Vertical velocity

The continuity equation is integrated vertically to get the vertical velocity. In the river model, vertical velocity is usually much higher than in the harbour due to the higher horizontal velocity and quickly changing bathymetry. Errors in the numerical integration for large vertical velocities become significant. Such that when integrating from the bottom, the vertical velocities at the top are usually the same order of magnitude of the mid depth vertical velocities and not zero. Also integrating from the top or bottom will give different results, with the vertical velocity profile being a similar shape, but just offset. It is unclear if integrating from the top or the bottom is correct, and several combinations have been tried

1. integrating from top (Figure 4.3)
2. integrating from bottom (Figure 4.4)
3. arithmetic average of 1. and 2. (Figure 4.5)
4. geometric average of 1. and 2. (Figure 4.6)
5. value with the minimum magnitude of either 1. or 2. (Figure 4.7)

The method 2 gave the best compromise for both ω and $\partial\omega/\partial\sigma$. For the illustration of the different methods, the King River is used due to its simple bathymetry, with similar differences show for the other rivers.

Initially ω is calculated with half a vertical grid offset from u, then interpolated to be on the same grid as u. From (2.35),

$$\omega_{i,k+\frac{1}{2}}^n = \left(\overset{1}{K}_{\omega_k} - \Delta\sigma_k\left(\overset{2}{K}_{\omega_k} + \overset{3}{K}_{\omega_k} + \overset{4}{K}_{\omega_k}\right)\right)\Big/\rho'^n_{i,k+\frac{1}{2}} \tag{4.54}$$

Where

$$\overset{1}{K}_{\omega_k} = \omega^n_{i,k-\frac{1}{2}}\rho'^n_{i,k-\frac{1}{2}} \tag{4.55}$$

$$\overset{2}{K}_{\omega_k} = \left(u^n_{i+\frac{1}{2},k}\rho'^n_{i+\frac{1}{2},k}D^n_{i+\frac{1}{2}}B_{i+\frac{1}{2}} - u^n_{i-\frac{1}{2},k}\rho'^n_{i-\frac{1}{2},k}D^n_{i-\frac{1}{2}}B_{i-\frac{1}{2}}\right)\Big/B_i\Delta x \tag{4.56}$$

$$\overset{3}{K}_{\omega_k} = D_i^n\left(\rho'^{n+1}_{0i,k} - \rho'^{n-1}_{0i,k}\right)\Big/2\Delta t \tag{4.57}$$

$$\overset{4}{K}_{\omega_k} = \rho'^n_{i,k}\left(\eta_i^{n+1} - \eta_i^{n-1}\right)\Big/2\Delta t \tag{4.58}$$

$$\Delta\sigma_k = \sigma_{k+\frac{1}{2}} - \sigma_{k-\frac{1}{2}} \tag{4.59}$$

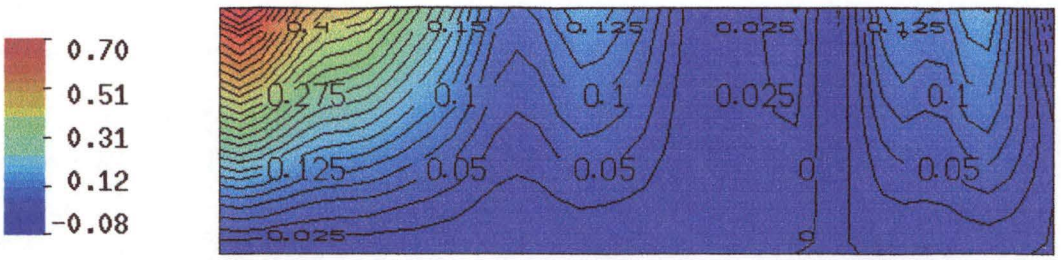

Figure 4.3 ω (mm/s) in σ co-ordinates, using integration from top

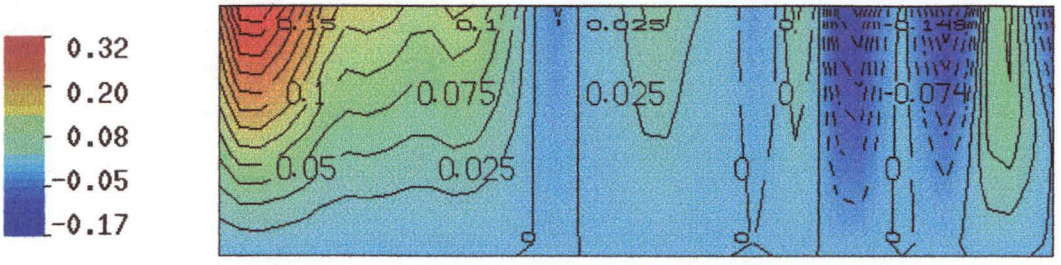

Figure 4.4 ω (mm/s) in σ co-ordinates, using integration from bottom

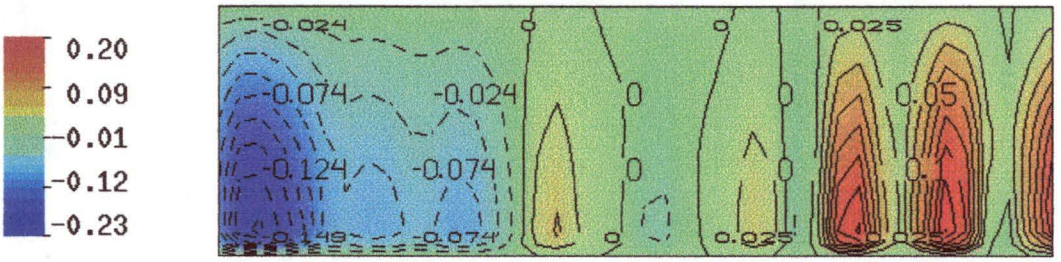

Figure 4.5 ω (mm/s) in σ co-ordinates, using arithmetic average of integration of top and bottom methods

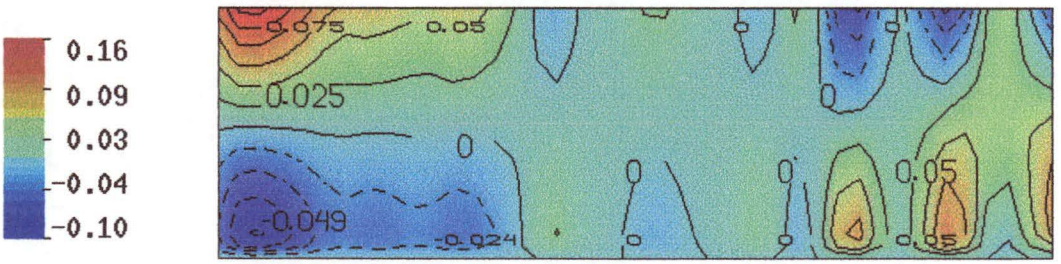

Figure 4.6 ω (mm/s) in σ co-ordinates, using geometric average of integration from top and bottom methods

For the Boussinesq version of $\omega, \rho_0' = 0$, so $\rho' = \kappa_{\rho_2}$ in the above equations. Note ω is calculated after the surface elevation and density, so the expressions above can contain values for surface elevation and density at the future time step.

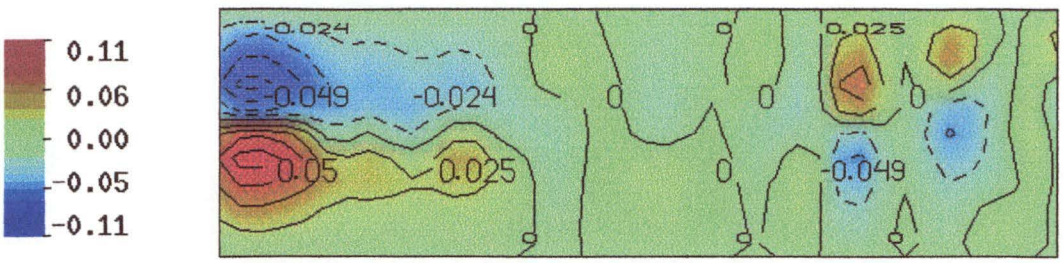

Figure 4.7 ω (mm/s) in σ co-ordinates, using absolute minimum value of integration from top and bottom methods

4.4.4 Boundary conditions

External boundary conditions are applied at the upstream ends of each river model; the downstream end being connected with an internal boundary condition to Macquarie Harbour described in Section 3.6. The river models for the Gordon River and King River are extended upstream of Macquarie Harbour far enough so there is always positive flow at the upstream boundary. This means no scalar quantities (salt, heat, or pollution concentration) from Macquarie Harbour are advected out across the boundary, which simplifies the boundary conditions. Should the upstream boundary have been too close to Macquarie Harbour, salt and heat would move back and forth across the rivers' upstream boundaries from tidal action and density driven currents, and storage boundary equations would have been required.

The upstream boundaries of the 2DLAM become the important external water boundaries when the 2DLAMs are attached to the three-dimensional POM. Below the boundary conditions for the different variables are considered separately for the river model.

4.4.4.1 Surface elevation boundary conditions

In the 2DLAM, surface elevation is on the physical boundaries of the river model, with the two-dimensional variables offset half a grid inside the boundaries (Figure 4.2). This makes the surface elevation the primary boundary condition, the momentum boundary condition being a weak condition. As the upstream river flow is driven by gravity surface waves, having the surface elevation on the river boundaries makes it easier to accurately implement the boundary conditions. Surface elevation is calculated at the upstream boundary and taken from the harbour model at the downstream boundary. The surface elevation is usually calculated from a prescribed flow rate.

Several surface elevation boundary conditions were tried at the upstream boundary of the river model, including using

1. Reservoir:

$$\eta_1^{n+1} = \eta_{res} - (1+\kappa_{res})\frac{{u_1^n}^2}{2g} \tag{4.60}$$

Where η_{res} is the reservoir level and κ_{res} is a loss coefficient. The depth average horizontal velocity, u_1^n, is extrapolated to the model boundary using $\partial^2 u/\partial x^2 = 0$, that is $u_1^n = \frac{3}{2}u_{\frac{3}{2}}^n - \frac{1}{2}u_{\frac{5}{2}}^n$.

2. Flow rate:

$$\eta_1^{n+1} = \eta_1^n + \left(Q_1^{n+1} - Q_1^n\right)\frac{\Delta t}{B_1 \Delta x} \tag{4.61}$$

Where Q_1^{n+1} is the defined flow rate at the boundary and Q_1^n is the current flow rate. The new surface elevation (η_1^{n+1}) is the current surface elevation (η_1^n) plus a term that, assuming the velocity is constant, will change the volume in the last grid to make the flow rate equal to the defined flow rate. This change in volume is calculated using a simple storage equation, that is change in storage volume is due to the difference in water flowing in and out. If the defined flow rate was constant the surface elevation would converge to the normal depth, but as the flow rate usually changes with time, the surface elevation changes as well.

3. Tide based on surface elevation:

$$\eta_1^{n+1} = \eta_{offset} + \eta_{amp}\sin(2\pi t\omega_{tide}) \tag{4.62}$$

Where η_{amp} is the amplitude, ω_{tide} is the angular frequency, t is the time, and η_{offset} is an offset to stop the harbour surface elevation from increasing on a long term basis - with more flow going in than coming out.

The King and Gordon Rivers are generally controlled by specifying a flow rate upstream, while the sea uses this sinusoidal surface elevation. This means to keep the long term average surface elevation (in the middle of the harbour) approximately equal to zero, the sea surface elevation needs to be offset below zero to create a net flow out to sea. If this offset is arbitrary the harbour will eventually fill or drain, so the offset is active and changes with the harbour's surface elevation. The averaging over a time period stops feedback, although as the system is heavy damped with the viscosities used this is only a small problem.

To keep the long term average of the harbour surface elevation close to zero the offset is the negative of the average harbour surface elevation, averaged over the previous three hours.

The tide equation allows for a single tide component. As the tide is mixed, for the purposes of the general circulation modelling and as the BB-ADCP data used to verify the harbour model was recorded when the harbour had a semi-diurnal tide, an M_2 (principal lunar semidiurnal) tide with a tidal period of 12.42h ($\omega_{tide} = 2.236536 \times 10^{-5}$ rad/s) is used.

4. Tide based on flow rate: same as number 2 with

$$Q_1^{n+1} = Q_{offset} + Q_{amp} \sin(2\pi t \omega_{tide}) \tag{4.63}$$

Where Q_{amp} is the amplitude of the tidal flow rate, and Q_{offset} is a flow rate version of η_{offset} in number 3.

The Gordon River and King River models are typically driven with the second scheme based on a known flow rate. This flow rate can be varied to simulate floods and to ramp in the flow when starting from initially still water. The sea model was tried with both the third and forth scheme using a tide based on either surface elevation or flow rate. Amplitudes in (4.62) and (4.63) are picked to match know tidal variations within the harbour. The surface elevation approach is stiffer than the flow rate approach, giving a more predictable tide. This is because the flow rate is a function of velocity as well as surface elevation, and one value of flow rate can be obtained with more than one value of surface elevation. The advantage of using flow rate in a boundary condition is that it is a smoother function in space and time than either surface elevation or velocity. This makes flow rate less prone to numerical noise and less reflective of waves leaving the solution space. For the final model (4.62) was used for the sea model as it was easier to produce tides in the harbour that corresponded to field measurements.

An additional approach is required to counter the tidally derived waves, even though using flow rate to predict the upstream Gordon River and King River boundary conditions does absorb some outgoing waves. The King River in particular requires a non-reflective approach, due to its proximity to the sea entrance. The approach taken was to use a forced radiation boundary condition, with a phase speed based on the phase speed of a shallow water gravity wave (Blumberg and Kantha, 1985).

$$\frac{\partial \eta}{\partial t} + c\frac{\partial \eta}{\partial x} = -\frac{\eta - \eta_k}{t_f} \tag{4.64}$$

Where the phase speed $c=\sqrt{gD}$, η_k is the known boundary surface elevation, and t_f is the time scale over which the radiation boundary condition forces the surface elevation to η_k. Most work by other researchers using radiation conditions has been with unforced boundaries that only have to transmit outgoing waves without reflection. This gives rise to a well behaved boundary, where the phase speed can be calculated from temporal and spatial derivatives of the function, in this case surface elevation. In the river model, the phase speed was tested with both the phase speed from the shallow gravity wave, and the phase speed from derivatives of the function. When the boundary is forced and there are irregular waves generated internally from a complicated geometry, and using derivatives of the function to calculate the phase speed is too numerically noisy and unstable. While the phase speed from the shallow water gravity wave makes a boundary condition that is more robust and numerically stable, and so is the one used.

For the upstream boundary condition of the sea model, several radiation conditions where unsuccessfully tried, as the boundary surface elevation was changing too quickly. If the time scale is large ($t_f > 1000$s) the forced value will never catch up to the radiated value, and if the time scale is small ($t_f \cong O(\Delta t)$) it makes the radiation condition unable to work as a non-reflected boundary condition. Fortunately, there is little reflection off the upstream end of the sea model, due its bathymetry and viscosity.

In terms of the matrix coefficients for the implicit solution routine used with the non-Boussinesq equation, an upstream boundary value is set using a version of (4.20) without a coefficient for $\eta_{i-1}^{\Delta n+1}$ as it is outside the solution space,

$$B_{\eta_{NB}}\eta_i^{\Delta n+1}+C_{\eta_{NB}}\eta_{i+1}^{\Delta n+1}=K_{\eta_{NB}} \tag{4.65}$$

Where for a fixed boundary value using η_i^{n+1} from (4.60)-(4.63),

$$B_{\eta_{NB}}=1 \tag{4.66}$$

$$C_{\eta_{NB}}=0 \tag{4.67}$$

$$K_{\eta_{NB}}=\eta_i^{n+1}-\eta_i^n \tag{4.68}$$

For the radiation boundary condition centred at $\left(1,n+\frac{1}{2}\right)$, using the same η_i^{n+1} values,

$$B_{\eta_{NB}}=1-\frac{\Delta t}{\Delta x}\sqrt{gD_1^n} \tag{4.69}$$

$$C_{\eta_{NB}}=\frac{\Delta t}{\Delta x}\sqrt{gD_1^n} \tag{4.70}$$

$$K_{\eta_{NB}}=\left(\eta_i^{n+1}-\eta_i^n\right)\frac{1}{t_f\Delta t} \tag{4.71}$$

4.4.4.2 Horizontal velocity boundary conditions

At the upstream boundary, horizontal velocity is solved using the momentum equation, as it is elsewhere. When solving horizontally, the horizontal derivatives need to be explicit, as there are no velocity values to be solved outside the boundary. For vertical solving there is no difference in the solution scheme, as the horizontal derivatives are already explicit. However, in both cases to calculate the horizontal derivative, a value for horizontal velocity is required at the half a grid space upstream of the first velocity grid. This point is the limit of the solution space and the first grid for the surface elevation. To extrapolate for this value, two derivative approximations where tried. They were $\partial u/\partial x = 0$ $(u^n_{\frac{1}{2},k} = u^n_{1,k})$ and $\partial^2 u/\partial x^2 = 0$ $(u^n_{\frac{1}{2},k} = \frac{3}{2}u^n_{1,k} - \frac{1}{2}u^n_{2,k})$. The first approximation was more robust than the second under quickly changing boundaries, but introduced more errors for gradually varying flow.

The pressure terms are accurately known at the upstream boundary, because of the grid offset between the surface elevation and horizontal velocity. With the velocity grid half a grid inside the physical limits of the model solution space, the boundary pressure terms are no different to the internal values. This is important, as the pressure terms are the largest forcing terms in the fast moving upstream end of the rivers.

Stresses are applied at the top and bottom surfaces for the boundary conditions, as in POM. The top stress, τ_t, is due to the wind

$$\rho_t K_{Mt} \frac{1}{D}\frac{\partial u}{\partial \sigma_t} = \tau_t \tag{4.72}$$

$$\tau_t = \rho_t \kappa_{wind} u_w |u_w| \tag{4.73}$$

Where u_w is the wind velocity 10m above the water surface and κ_{wind} is a roughness coefficient that represents the interaction between the moving air and the water surface. Typically, $\kappa_{wind} = 1\times10^{-6}$ to 3×10^{-6}. When solving the momentum equation horizontally, (4.72) is used to get an expression for the velocity at the surface in terms of the velocity in the next level down. This expression is used to explicitly calculate the surface velocity. However, when the momentum equation is solved vertically, the shear stress from (4.73) is added directly into the momentum equation at the top level.

The bottom stress, τ_b, is due to friction calculated from a roughness parameter z_0,

$$\rho_b K_{Mb} \frac{1}{D}\frac{\partial u}{\partial \sigma_b} = \tau_b \tag{4.74}$$

$$\tau_b = \rho_b \kappa_{bottom} u_b |u_b| \tag{4.75}$$

$$\kappa_{bottom} = \max\left[\frac{k^2}{(\ln((1+\sigma_{KB-1})H/z_0))^2}, \kappa_{bottom_{MIN}}\right] \tag{4.76}$$

Where variables with a subscript b refer to values in the grid closest to the bottom. A value of $\kappa_{bottom_{MIN}} = 0.0025$ is suggested by Mellor (1996), but to reduce damping of the tide a value of $\kappa_{bottom_{MIN}} = 0.001$ was used. The roughness parameter was set to $z_0 = 0.005$m. Without extensive field calibration these values remain arbitrary, although fortunately the model is insensitive to their value (due mainly to the large momentum of the rivers). To test the sensitivity of the model output to z_0, the magnitude of the harbour's velocity was averaged at the end of a ten day simulation for $z_0 = 0.004$m, 0.005m and 0.006m. The 20% variation in z_0 only changed the average harbour velocity by 2%.

4.4.4.3 Scalar boundary conditions

The scalar quantities are defined at the upstream boundary using a simple advection equation. This allows the solution space to be driven by changing external values; unlike the horizontal velocity boundary condition, that is controlled by surface elevation and internal values. In the following expressions, the variable f is used for salinity, temperature, and pollution concentration. The advection equation is used to calculate a new boundary value $\overset{new}{f_b}$ at each time step with a FORTRAN assignment statement

$$2 \qquad \text{for } u^n_{1,k} > 0 \tag{4.77}$$

$$\overset{new}{f_b} = \overset{old}{f_b} - u^n_{1,k}\frac{\Delta t}{\Delta x}\left(f^n_{2,k} - f^n_{1,k}\right) \qquad \text{for } u^n_{1,k} \le 0 \tag{4.78}$$

$$f_{ext} = f_{top} - \kappa_{ext}\sigma D \tag{4.79}$$

The boundary value at the future time step $f^{n+1}_{1,k} = f_b$. In (4.79) f_{top} is the external value at the top surface. The κ_{ext} value allows a linear variation with depth, in units of the variable f per metre. To change smoothly from the initial conditions, f_{top} and κ_{ext} are varied with time with a linear interpolation routine.

At the top and bottom boundaries, there is zero flux of scalar quantities - except for temperature, that has an imposed heat flux at the top surface. The zero flux is obtained by assuming $\partial f/\partial\sigma = 0$ at the bottom, which is

$$f^n_{i,-\frac{1}{2}} = f^n_{i,\frac{1}{2}} \tag{4.80}$$

Where $f^n_{i,\frac{1}{2}}$ is just below the physical bottom of the river, and is a numerical construction used to calculate derivatives at $\left(i,\frac{1}{2}\right)$. The heat flux is due to solar radiation and is approximated to a sinusoidal variation, from zero at midnight to a maximum at midday. It is

included as a source term in the scalar conservation equation, and is limited so the temperature of the water surface is less than the air temperature (which has a sinusoidal variation from midnight to midday).

POM allows for short wave radiation, that can be penetrative or not, through imposing a heat flux or a surface temperature. For this model, POM is set to use non-penetrative radiation with the same imposed sinusoidal heat flux variation used in the river model.

4.5 Solution algorithm

After all the finite difference equations are formulated, they are solved with a computer program, written in the FORTRAN computer language. As a computer program, the river model is called from POM as a separate subroutine in POM's external loop, which in turn calls several other subroutines. The essential attributes of the solution algorithm used in the river model are, the scheme should be

1. accurate and robust, able to model the range of situations the exist in the problem area without crashing
2. efficient, to be fast enough, so solution times are practical
3. easy to implement and change, so coding errors are reduced

While the primary focus is to create an accurate scheme, the implementation required for these attributes often conflicts, so the final code will be a compromise.

In the river model subroutine, the order of variable calculation is important because the some variables need to be solved before others. This makes a sequential process that could not be optimised greatly by using multiple processors or multi-threading (using a computer architecture that handles independent tasks simultaneously). There are several possible combinations for the order of variable calculation that were tried for the river model, but the finite difference equations need to be derived with one order of calculation in mind. For example, as the surface elevation is calculated before the horizontal velocity, when solving for the surface elevation all the horizontal velocity terms have to be at the current or previous time step, and when solving for the horizontal velocity there can temporal derivatives of surface elevation that use the terms at the future time step.

The order of variable calculation used is given in Table 4.1, with the solution at steps 11 and step 15 detailed in Table 4.2. The BTSLV subroutine mentioned in step 3 of Table 4.2, is routine for solving almost banding matrices, from the NSWC FORTRAN library (NSWC, 1993).

Mild smoothing is required to keep the model stable, especially with the large density gradients and surface slopes. Seven schemes are tried on different variables in the river

model. The approach is to calculate a smoothed value $\overset{smooth}{f_i}$ from a scheme in Table 4.4, then the final new value $\overset{new}{f_i}$ is found with weighting κ_{weight} to the old value $\overset{old}{f_i}$,

$$\overset{new}{f_i} = \frac{1}{1+\kappa_{weight}}\left(\overset{smooth}{f_i} + \kappa_{weight}\overset{old}{f_i}\right) \tag{4.81}$$

Typical values for κ_{weight} used for variables in the river model, are given in Table 4.3. The methods in Table 4.4 are for horizontal smoothing, and similar schemes are used for vertical smoothing. The linear smoothing scheme (method 1 from Table 4.4) was the most robust scheme and used for most of the variables; it is a simpler case of the diffusive smoothing (method 2 from Table 4.4). The more severe smoothing schemes (method 4 to 7 from Table 4.4) are useful at times for the diagnostic variables, calculated diagnostically from derivatives of current values (such as ω and diffusion values), because these variables tend to be numerically noisy. It was found that by tuning the smoothing on the prognostic variables, the severe smoothing was not required on the diagnostic variables.

Part I ***Preliminary calculations***

1. Boundary values for two-dimensional variables
2. Variables at half grid offset
3. Density, ρ^n
4. Vertical derivatives for horizontal velocity, $\partial u/\partial\sigma$
5. Horizontal pressure derivatives, $\partial p/\partial x$
6. Richardson number, R_i
7. Vertical diffusion values, K_m and K_h
8. Horizontal diffusion values, A_m and A_h
9. Flow rate along river, Q

Part II ***One-dimensional solving***

10. Surface elevation boundary condition values at future time step, η_1^{n+1} and η_{IM}^{n+1}
11. Solve for surface elevation at future time step, η_i^{n+1}

Part III ***Two-dimensional solving***

12. First order salinity vertical derivatives, $\partial S/\partial\sigma$
13. Second order vertical diffusion derivatives for salinity, $\partial K_h \dfrac{\partial S}{\partial\sigma}\Big/\partial\sigma$
14. Transform horizontal salinity derivatives, $\dfrac{\partial S}{\partial x}+\dfrac{\partial S}{\partial\sigma}\dfrac{\partial\sigma}{\partial x}$
15. Solve for salinity at future time step, S_i^{n+1}
16. Repeat steps 12 – 15 for temperature, pollution concentration, and horizontal velocity

Part IV ***Post solving calculations***

17. Density at future time step, ρ^{n+1}
18. Vertical σ velocity at future time step, ω
19. Rotate variables between future, present, and past time steps
20. Update boundary values

Table 4.1 Order of variable solving in river model, with all calculations at current time step unless stated otherwise.

1. Subtract present value of past value, $f^{\Delta n-1} = f^{n-1} - f^{n}$
2. Calculate elements in solving matrix
3. Solve solution space with BTSLV subroutine for $f^{\Delta n+1}$
4. Add present values back to give value at future time step, $f^{n+1} = f^{\Delta n+1} + f^{n}$
5. Smooth values at future time step
6. Temporally filter values at present time step

Table 4.2 Steps for solving variables at future time step

Variable	κ_{weight}	
	horizontal smoothing	**vertical smoothing**
η	20	-
u	20	50
θ	30	no smoothing
ω	0	0
diffusion values	0	0

Table 4.3 Typical weighting values (κ_{weight}) for smoothing scheme, where θ is generic for *S*, *T*, or *C*

Diffusive smoothing in two-dimensions, similar to method 2 from Table 4.4, was applied to the surface elevation variables in POM. The smoothing was required to remove instabilities in surface elevation during ebb tides near Hells Gates. When applying the smoothing, care was required not to include any of the land grids in the calculation, which always had zero surface elevation, as this cause errors in the momentum balance. This was achieved using an edge mask variable, similar to the other masks used by POM. The edge mask is equal to zero over the land and one the grids just in the water, and equal to one over the rest of the water. The diffusive constant, α_x, is multiplying by the edge mask. A value of $\alpha_x = 0.01$ was used for the surface elevation in POM.

The aim of smoothing is only to suppress instability, without distorting the solution. The smoothing schemes effect the flow field as if extra diffusion is applied evenly over the solution space. It is as if the base diffusion values were increased slightly, independent of the flow field. When using diagnostic diffusion values, the model is more robust if there is extra diffusion that is independent of the flow field. This is because the diagnostic diffusion values are numerically noisy and have weak temporal inertia. Temporal inertia comes from calculating something prognostically, in that variables that are based on their past values will change is a smoother, more stable manner. The diffusion values have a weak temporal

inertia because the diffusion values are derived from velocity gradients, which are weakly influenced by the diffusion values. Smoothing could be reduced if diffusion values were calculated prognostically.

The procedure for determining smoothing values is to increase κ_{weight} for a variable until it becomes unstable. The smaller κ_{weight} is, the more severe the smoothing. Due to the interrelationship between variables, an iterative approach is required to find maximum values for κ_{weight}, and to find which smoothing scheme is the most suitable. Care must be taken with smoothing scalar quantities as they are greatly effected by diffusion. For all variables there is much less smoothing vertically as there is horizontally.

Temporal filtering, mentioned in step 6 of Table 4.2, is required because the schemes for solving future time steps are centred in time. Without temporal filtering, numerical oscillations are set up between odd time steps. Following Mellor (1996), the diffusive temporal filtering is

$$f^{new\,n} = f^{old\,n} + \alpha_t \left(f^{old\,n+1} - 2 f^{old\,n} + f^{old\,n-1} \right) \tag{4.82}$$

Typical values tried for α_t are $0.05 - 0.10$, with the river model using $\alpha_t = 0.10$.

4.6 Joining river and harbour models

The river model uses a similar numerical scheme to POM, so it could be joined easily to POM. The river model and POM use consistent variables and co-ordinate system, although POM needed modification to allow it to model the pollution concentration. The river model subroutine is called within POM's external loop separately for the Gordon River, King River, and the sea. Figure 4.8 gives the program structure for POM (Mellor, 1996). The external loop steps forward time at the external time step, Δt_E, for *ISPLIT* steps, then the internal mode loop steps forward in time once at the internal time step Δt_I; where $\Delta t_I = ISPLIT \times \Delta t_E$.

Before the river model subroutines are run, values from the harbour are taken as boundary conditions for the river. After the river model subroutines have run, values from the rivers are put back in the harbour variables.

1. **Linear**

$$f_i^{smooth} = \tfrac{1}{2} f_i^{old} + \tfrac{1}{4}\left(f_{i-1}^{old} + f_{i+1}^{old} \right) \text{ and } f_b^{smooth} = f_b^{old}$$

2. **Diffusive**

$$f_i^{smooth} = f_i^{old} + \tfrac{1}{2}\alpha_x \left(f_{i-1}^{old} - 2 f_i^{old} + f_{i+1}^{old} \right) \text{ and } f_b^{smooth} = f_b^{old}$$

3. **Quadratic**

$$f_i^{smooth} = \frac{1}{35}\left(-3 f_{i-2}^{old} + 12 f_{i-1}^{old} + 17 f_i^{old} + 12 f_{i+1}^{old} - 3 f_{i+2}^{old} \right) \text{ and}$$

$$f_b^{smooth} = \frac{1}{35}\left(31 f_b^{old} + 9 f_{b+1}^{old} - 3 f_{b+2}^{old} - 5 f_{b+3}^{old} + 3 f_{b+4}^{old} \right),$$

$$f_{b+1}^{smooth} = \frac{1}{35}\left(9 f_b^{old} + 13 f_{b+1}^{old} + 12 f_{b+2}^{old} + 6 f_{b+3}^{old} - 5 f_{b+4}^{old} \right)$$

4. **Outside envelope**

$$f_i^{smooth} = f_i^{average} \text{ for } f_i^{old} < f_i^{average} \text{ or } f_i^{smooth} = f_i^{old} \text{ for } f_i^{old} \geq f_i^{average} \text{ and}$$

$$f_b^{smooth} = f_b^{old} \text{ with } f_i^{average} = \tfrac{1}{2}\left(f_{i-1}^{old} + f_{i+1}^{old} \right)$$

5. **Inside envelope**

$$f_i^{smooth} = f_i^{average} \text{ for } f_i^{old} > f_i^{average} \text{ or } f_i^{smooth} = f_i^{old} \text{ for } f_i^{old} \leq f_i^{average} \text{ and}$$

$$f_b^{smooth} = f_b^{old} \text{ with } f_i^{average} = \tfrac{1}{2}\left(f_{i-1}^{old} + f_{i+1}^{old} \right)$$

6. **Five point average**

$$f_i^{smooth} = \tfrac{1}{5}\sum_{i-2}^{i+2} f_m^{old} \text{ and } f_b^{smooth} = f_b^{old},\ f_{b+1}^{smooth} = \tfrac{1}{3}\sum_{b}^{b+2} f_m^{old}$$

7. **Seven point average**

$$f_i^{smooth} = \tfrac{1}{7}\sum_{i-4}^{i+4} f_m^{old} \text{ and } f_b^{smooth} = f_b^{old},\ f_{b+1}^{smooth} = \tfrac{1}{3}\sum_{b}^{b+2} f_m^{old},\ f_{b+2}^{smooth} = \tfrac{1}{5}\sum_{b}^{b+4} f_m^{old}$$

Table 4.4 Smoothing functions for mid reach (f_i^{smooth}) and boundary (f_b^{smooth}) values

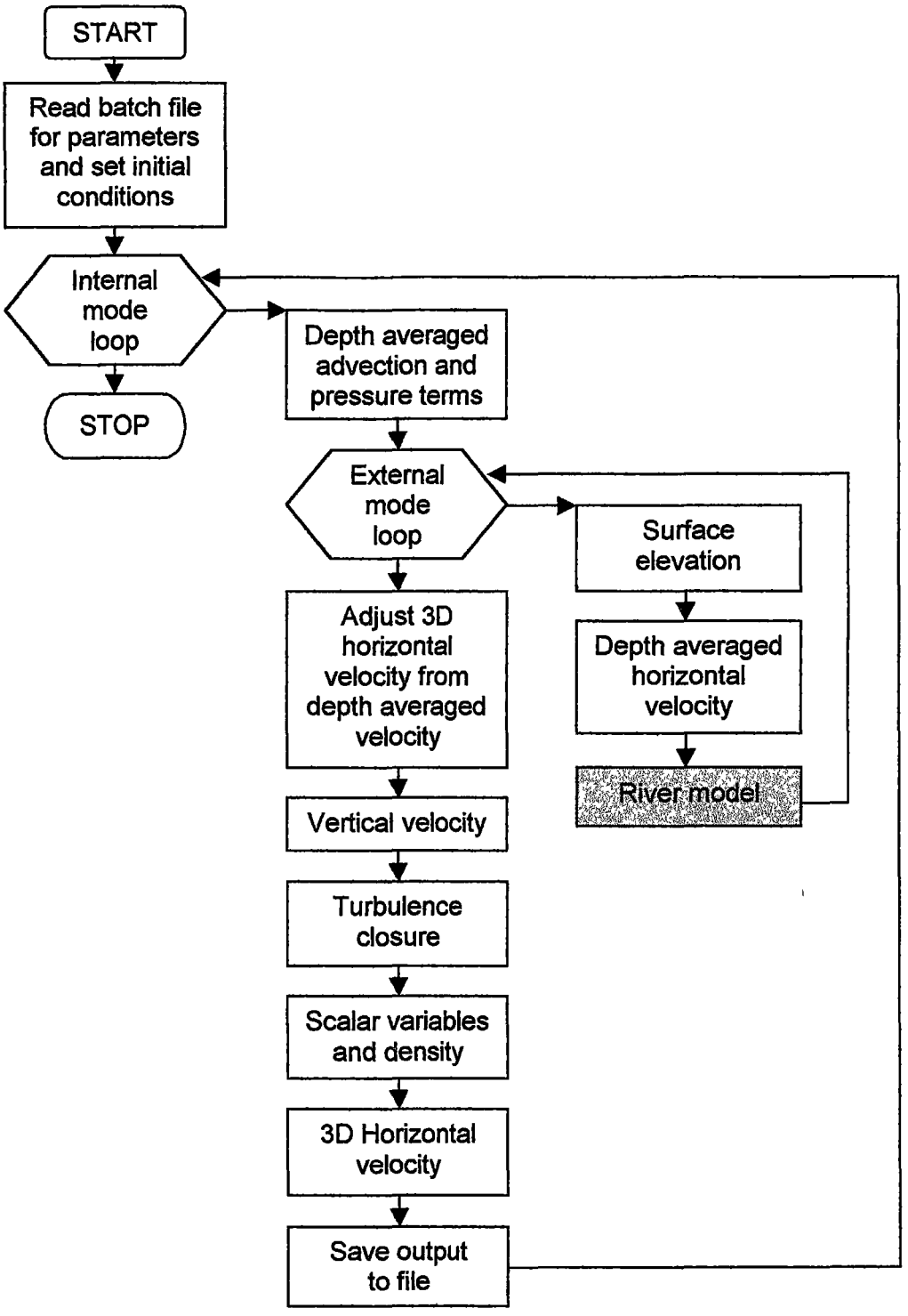

Figure 4.8 Program structure for modified POM, showing river model location

In POM's grid for the harbour, the mouths of the Gordon River, King River, and the sea are represented with three grid cells each (Figure 4.9). The variables in these river stubs are updated by the harbour and river models. If not updated correctly, the harbour would "see" the river stubs as having blocked ends, and waves would reflect off them. The grid index shown in Figure 4.9 is the same index shown on the river model grid in Figure 4.2. In Figure 4.9 the POM surface elevation and scalar variables are centred on the half grid, with the horizontal velocity centred horizontally on the full grid. Therefore, interpolation is required when transferring information between the river model and POM. For example, to transfer a scalar variable from the harbour to the river model,

$$\overset{river}{\theta}{}^{n}_{IM,k} = \frac{1}{2}\left(\overset{harbour}{\theta}{}^{n}_{R,k} + \overset{harbour}{\theta}{}^{n}_{R+1,k} \right) \tag{4.83}$$

while to transfer a scalar variable back from the river model to the harbour,

$$\overset{harbour}{\theta}{}^{n}_{R,k} = \frac{1}{2}\left(\overset{river}{\theta}{}^{n}_{IM-1,k} + \overset{river}{\theta}{}^{n}_{IM,k} \right) \tag{4.84}$$

The largest difficultly in joining the river model to POM, is calculating values through the water column at the downstream boundary of the river model. The problem is, the variables through the water column in the harbour are calculated less frequently than those in the river, by a factor of *ISPLIT*. As the river model is looping through POM's external mode loop, it needs to calculate horizontal and scalar variable values at the downstream boundary. The scalars are held fixed through the external mode loop for lack of information. Procedures for extrapolating scalar values from the river where tried, but they were not robust enough.

More information is available for the horizontal velocity at the downstream boundary, as POM calculates a depth averaged velocity for the harbour during the external mode loop. For the first loop through the external mode loop, the velocity distribution from the internal mode loop is used as a boundary condition for the river,

$$\overset{rivernew}{u}{}^{n}_{IM,k} = \overset{harbour}{u}{}^{n}_{R+\frac{1}{2},k} \tag{4.85}$$

Then for the other (*ISPLIT*-1) steps, two methods were tested for fabricating a horizontal velocity distribution ($\overset{rivernew}{u}{}^{n}_{IM,k}$) through the water column from a depth averaged harbour velocity ($\overset{harbour}{u}{}^{n}_{R+\frac{1}{2}}$) and a previous river velocity distribution ($\overset{riverold}{u}{}^{n}_{IM,k}$). The general form of the fabrication is

$$\overset{rivernew}{u}{}^{n}_{IM,k} = \overset{riverold}{u}{}^{n}_{IM,k} + \Delta u \tag{4.86}$$

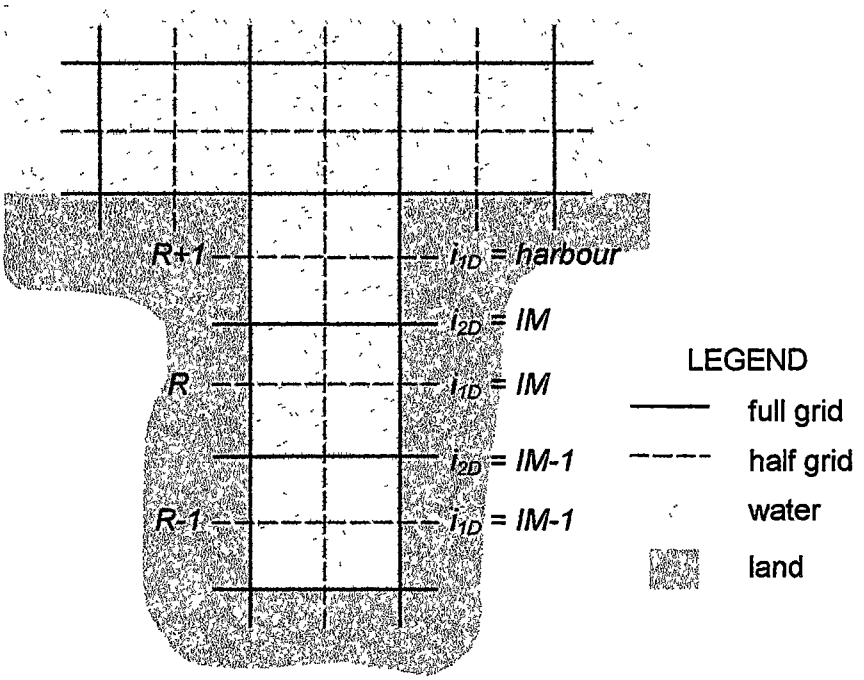

Figure 4.9 River – harbour connection grid cells in harbour, with grid indexes from river model one-dimensional (i_{1D}) and two-dimensional variables (i_{2D}). The *R* indexes refer to the harbour grid.

The first method for calculating the difference (Δu) between the previous and new velocities tested is

$$\Delta u_1 = u^{n\ harbour}_{R+\frac{1}{2}} - \sum_{k=1}^{KB} \sigma_k\, u^{n\ river}_{IM,k} \tag{4.87}$$

And based on (4.87), the second method is

$$\Delta u_2 = \Delta u_1 \frac{\left| u^{n\ harbour}_{R+\frac{1}{2},k} \right|}{\sum_{k=1}^{KB} \sigma_k \left| u^{n\ harbour}_{R+\frac{1}{2},k} \right|} \tag{4.88}$$

If the denominator in (4.88) was zero, then Δu_1 from (4.87) is used instead on Δu_2. Δu_2 is not conservative when there is flow reversal in the water column, because of the absolute value signs. Therefore, Δu_1 from (4.87) was used for Δu in (4.86). The difference between Δu_1 and Δu_2, is Δu_1 shifts the whole distribution by a constant value, while Δu_2 tries to change the slope of the distribution.

Chapter Five
Macquarie Harbour model

5.1 Introduction

To predict the general circulation and water quality in Macquarie Harbour, the numerical model needs appropriate bathymetry, initial conditions, and boundary conditions. These key elements are described in this chapter for the Macquarie Harbour system. The circulation of the harbour is described with velocity and surface elevation, while the water quality is described by the salinity, temperature, and pollution concentration.

The interrelationship between variables is a feature of estuaries. The circulation is in part driven by the water quality terms through the water density, which is a function of salinity, temperature, and pollution concentration. Conversely, the water quantity terms are advected by the circulation. Beyond the scope of this thesis, there are other interrelationships, such as chemical and biological relationships between the pollution, salinity, and temperature. In this thesis the pollution is considered conservative and is a good approximation for stable chemicals such as dissolved copper, but not good for biological contaminants such as *Escherichia coli* (*E. coli*).

The pollution variable in this model represents the conservative transport of sediments and heavy metals such as copper, iron, manganese, zinc, mercury, and lead. With one variable to represent the concentration of many contaminants, the pollution distribution needs to be scaled for each of the pollutants it represents with a calibration factor. Using a calibration factor will only give an approximate magnitude for the pollution concentration of each contaminant and the pollution variable is used mainly to indicate the general distribution of pollution in the harbour.

To work out the calibration factor the pollution concentration from the model is compared to known pollution values from field measurements. A pollution value of $10g/m^3$ is used as a constant source at the upstream end of the King River model. To work out a calibration

factor, pollution values from the model and field measurements are compared in Table 5.1. A typical model value at a depth of 15m in the harbour off Sophia Pt is $0.15g/m^3$, which is compared to field values for total copper, dissolved copper, and suspended sediment. The error introduced by using a calibration factor that is independent of the water density, when converting between units of g/m^3 and parts per billion (ppb) by mass, will not significantly effect the accuracy of using the factor, because of its approximate nature. The density should have been used because the conversion is been units of mass per volume and mass per mass.

To use the calibration factor in Table 5.1 just multiply it by the pollution concentration value from the model to get the pollution concentration of the appropriate pollutant. For example, a pollution concentration value from the model of $1.0g/m^3$ is equivalent to a dissolved copper at a concentration of 90ppb.

5.2 Bathymetry

The bathymetry for a numerical model of an estuary is defined at the grid points used in the finite difference equations. It needs to have enough resolution to model the important features and allow grid independence, while not being too detailed for the computer resources. Smaller spatial grid spacing requires more computer memory and smaller temporal steps because of the CFL stability criteria, and so the model takes longer to solve.

Complete grid independence is seldom possible as a numerical model will always use a grid or mesh, and so its output will always be a function of that grid. The aim is to minimise the impact of the grid on the output, while still maintaining practical limits on computer memory usage and solution time. In the following sections, the horizontal grids used in the harbour and river models are examined. The model is also checked for sensitivity to the vertical resolution and horizontal grid size.

Variable	Field Value	Calibration factor
Total Cu	100ppb	670
Dissolved Cu	13ppb	90
Suspended Sediment	21mg/l	140

Table 5.1 Comparison between field measurements (Koehnken, 1996) and model pollution concentration value of $0.15g/m^3$ ($\equiv$ 147ppb for water density of $1022kg/m^3$) at a depth of 15m in Macquarie Harbour off Sophia Pt

5.2.1 Macquarie Harbour

Four sources were combined for the bathymetry of Macquarie Harbour used in the model,

1. Sheet SK 55-7 Edition 1, from the National bathymetry map series. This is a 1 : 250 000 scale map of Macquarie Harbour and its surroundings with 10 m depth contours, referenced in longitude and latitude.
2. HEC depth soundings using a Deso 10 Echo Sounder, in the north half of the harbour (HEC, 1993a). These soundings were referenced to the Australian Map Grid (AMG) using a Wild System 200 GPS.
3. Admiralty map 3531, 1980 Edition, around entrance to the harbour. This is a 1 : 10 560 scale map, referenced in longitude and latitude.
4. Hobart Ports Corporation depth soundings around the Gordon River mouth. This is a hand drawn 1 : 5 000 scale map, referenced to local features (Grundy, 1983).

The approach was to digitalise depths from the National bathymetry map and transform it to a regular grid. The digitisation was done by the author using Arcinfo, a geographical information system (GIS), and the gridding was done using Surfer (version 3.0, 1987), a surveying computer program. The HEC (1993a) depth soundings where also gridded using Surfer, and combined with the National bathymetry map data on the AMG. These two sources formed the base harbour bathymetry. When putting the bathymetry onto a regular grid there are several parameters and different algorithms that can be altered. The primary parameter is the size of the grid spacing, and several were tried, ranging from 200m to 980m. The 250m grid spacing was chosen, as it was the best compromise between resolving the important features, and not having too many grid cells.

The base bathymetry was then rotated clockwise 45°, so the main axis of the harbour changed from a line running north-west/south-east, to a line running north/south. This transformation would better suit a rectangular grid, and have less wasted land grid cells. Measuring in the AMG (units of metres), the transformed co-ordinates are

$$x^{new} = x_0 + R\cos 45° \tag{5.1}$$

$$y^{new} = y_0 + R\sin 45° \tag{5.2}$$

$$R = \sqrt{\left(x^{old} - x_0\right)^2 + \left(y^{old} - y_0\right)^2} \tag{5.3}$$

Where $(x_0, y_0) = (368000, 5313300)$ is the point of rotation, and approximately the centre of the harbour. Birchs Inlet, joining in the south-east corner of the harbour, is excluded from the model, as it has a restricted passage to the harbour and very low flow rate. It would also be inefficient to include it on the rectangular grid, as it sticks out to the side of the harbour by almost the width of the harbour, once the harbour is rotated.

The Admiralty map and Hobart Ports Corporation soundings (Grundy, 1983) were then used to tune local features, such as the channel at the harbour entrance and the sand bar at the

mouth of the Gordon River. This tuning was done by hand editing the bathymetry data file. The depth is given for each harbour grid in Appendix B. Values of less than or equal to 0.1m are land, which are not set to zero to simplify the checking of depth when calculating friction terms in POM. This data is represented with a colour contour map with local features in Figure 5.1. The features are included to relate the map to the Macquarie Harbour location map in Figure 1.2 and Figure 1.3, and to show the feature resolution of the 250m grid spacing.

The features of Macquarie Harbour's bathymetry are

1. Surface area of 280km^2, depths up to 55m with an average of 25m.
2. Trench off Sophia Pt, containing the deepest part of the harbour.
3. Liberty Pt splits the harbour
4. Sandbars around entrance to harbour near Hells Gates.
5. Bar across Gordon River mouth to harbour at a depth of 3m.
6. Trailing wall inside and breakwater wall outside harbour, with both on the south-west side of harbour.
7. King River delta, with 2.5km^2 visible, has redirected the King River flow into the harbour since it formed, from being westerly to north-westerly.
8. Fish farms on the south side of Liberty Pt, and in the bays just north of Liberty Pt on the western side of the harbour. There are unused sites south of Liberty Pt mid way along the western side of the harbour, and further sites are planned off Yellow Bluff (Koehnken, 1998).
9. Islands in the shallows of the harbour: Sarah Is, Soldier Is, Philips Is, Elizabeth Is, Cat Is, and Neck Is.

All these features are included in the model of Macquarie Harbour, except the fish farms – which are discussed due to their location in the pollution plume rather than their effect on the hydraulics, which would be minimal. The sandbars in the model are assumed always submerged, and the King River delta is always exposed. This means there is no need to model the wetting and drying of these areas.

5.2.2 Gordon River

The Gordon River bathymetry is taken from a report on the lower Gordon River (HEC, 1979). The original bathymetry was smoothed, because with a 250m horizontal grid spacing, the river model became unstable when it could not resolve the large number of deep holes along the river bed. The model instability was due the derivatives from the conversion to σ co-ordinates dominating the solution, which were large because the bottom σ co-ordinate level follows the river bottom. Figure 5.2 gives the original bathymetry from the HEC (1979) report, and the smoothed version used in the river model. The upstream end is grid 1 and the downstream harbour end is grid 160. Using a 250m grid spacing, this reach of Gordon River is 40km. Refer to Appendix C for tables of the Gordon River bathymetry.

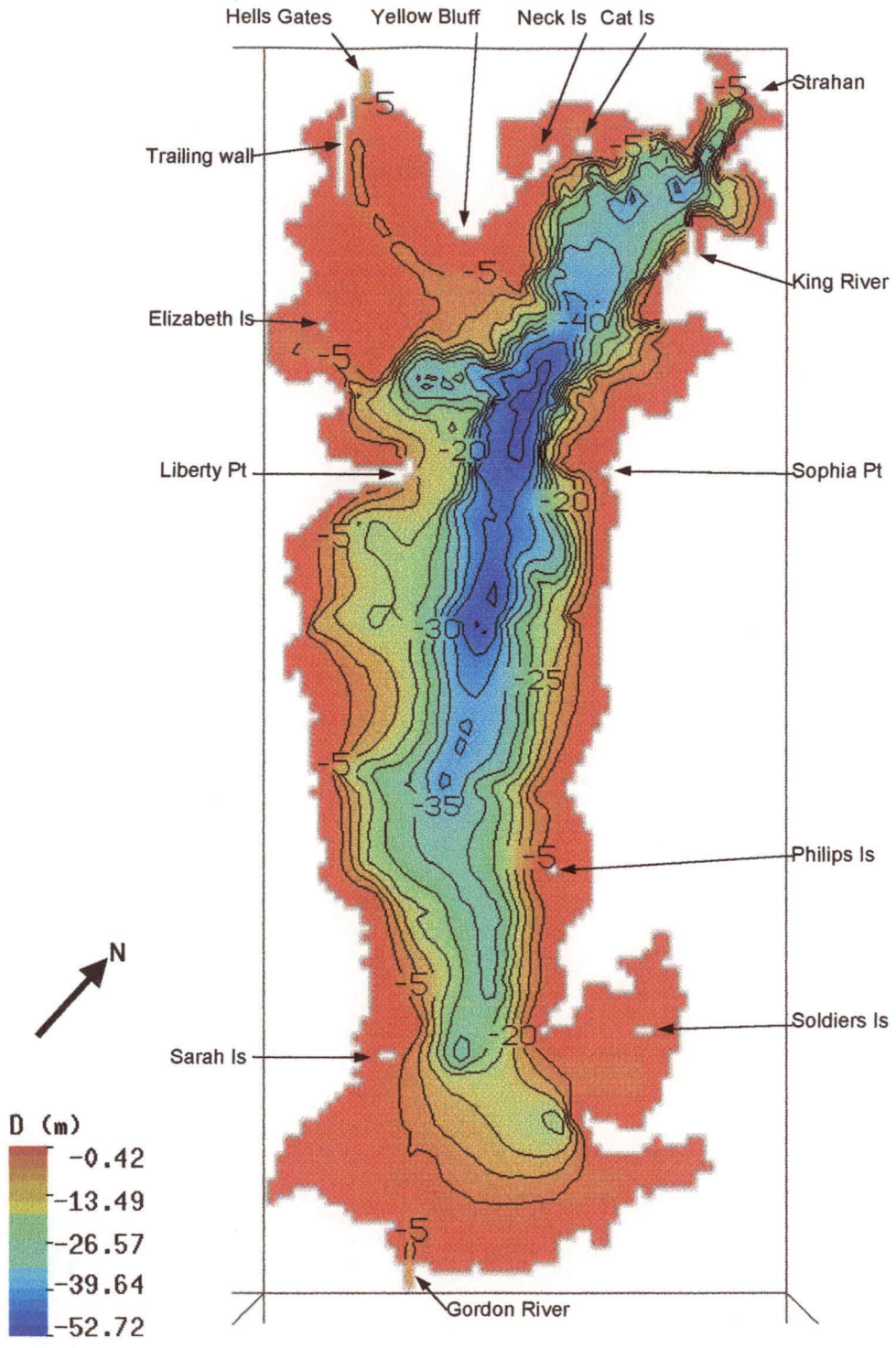

Figure 5.1 Macquarie Harbour bathymetry, 5 m contours, with features

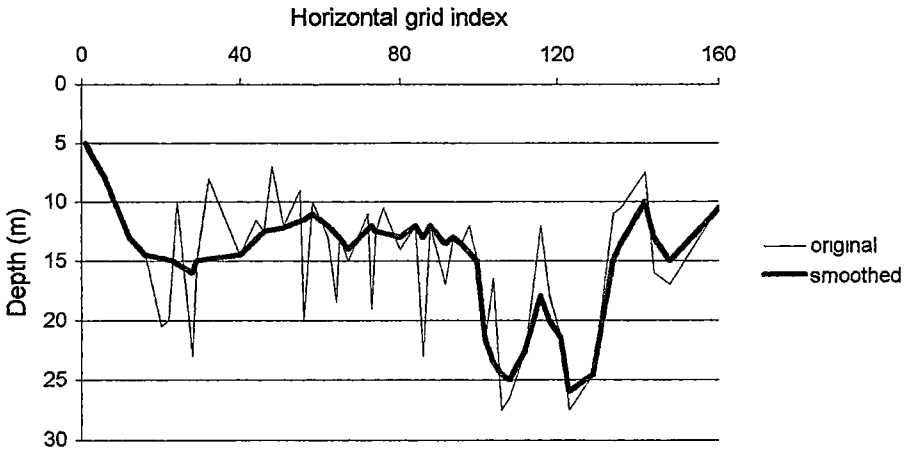

Figure 5.2 Gordon River depths, before and after smoothing

Depths from the bathymetry were scaled off a figure in the report (HEC, 1979). The bathymetry data file for the river model consists of triplets of: horizontal grid index, river depth, and river width. When the grid indexes are not consecutive, linear interpolation is used for the points in between. The river widths where taken off 1 : 25 000 scale maps of the area (DELM, 1989), and approximately linear width variation was found. Therefore, the model with width was varied linearly between 70m upstream to 250m downstream at the harbour end. The 250m downstream width was required to merge to the harbour grid.

5.2.3 King River

The King River bathymetry is taken from HEC depth soundings along the river (HEC, 1993b). These were taken in the same survey that the HEC found the bathymetry in the north half of Macquarie Harbour. Smoothing of some deeper holes was required, but not as extreme as the smoothing done in Gordon River, because the King River is essentially smooth. Figure 5.3 shows the King River bathymetry used in the river model. As for the Gordon River bathymetry, the upstream is at index 1 and the downstream harbour end is at index 40. Using a 250m grid spacing, this reach of King River is 10km. Refer to Appendix C for tables of the King River bathymetry.

The HEC (1993b) survey also contained river widths for mean flow levels, given in Figure 5.4. The lower section of the river is modelled as a single reach, although there is a smaller channel off the main reach, which is separated under lower flows.

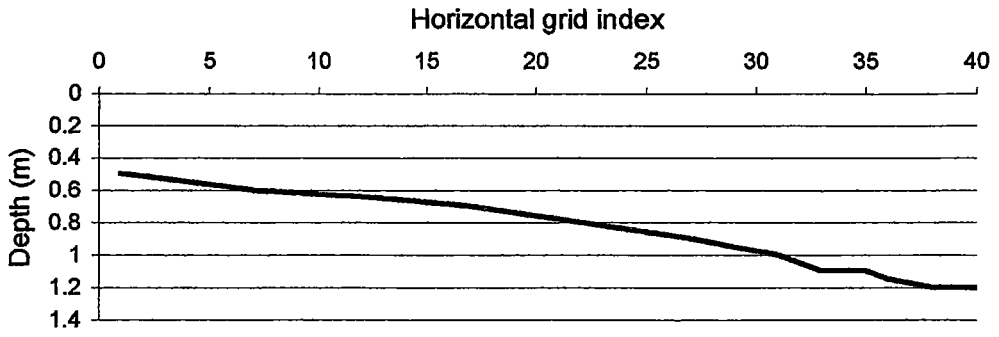

Figure 5.3 King River depth

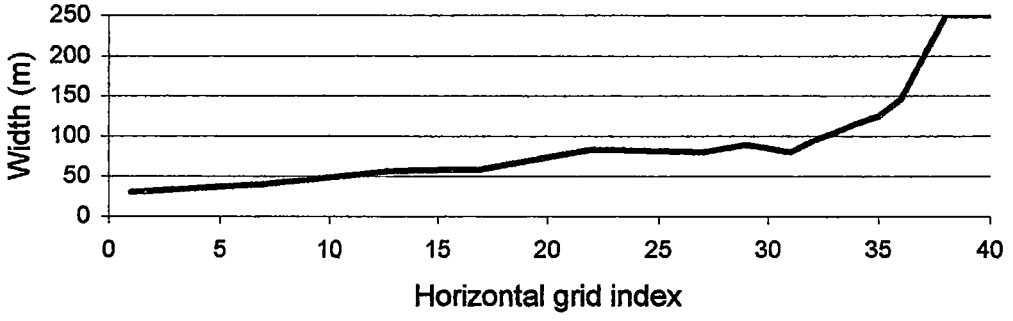

Figure 5.4 King River width

5.2.4 The sea

The bathymetry for the sea model was taken from Admiralty map 3531, 1980 Edition, for the 3km passage from Macquarie Harbour to the open sea; then Admiralty map 353, 1967 Edition, for the 17km of open sea surrounding the harbour that was modelled. In the model, the bathymetry around Hells Gates was smoothed slightly, because the large depth and width changes caused numerical instability during the peak tidal flows. The depths are shown in Figure 5.5. The minimum width at Hells Gates was increased from 75m to 150m, as shown in Figure 5.6. This was done to avoid width variation derivatives dominating the solution and causing numerical instability. Refer to Appendix C for tables of the sea bathymetry.

In the 3km passage from the harbour, channel widths were taken off the Admiralty map 3531, 1980 Edition. In the 17km reach outside the harbour, widths are more arbitrary, and represent the main corridor of the Southern Ocean that enters the harbour.

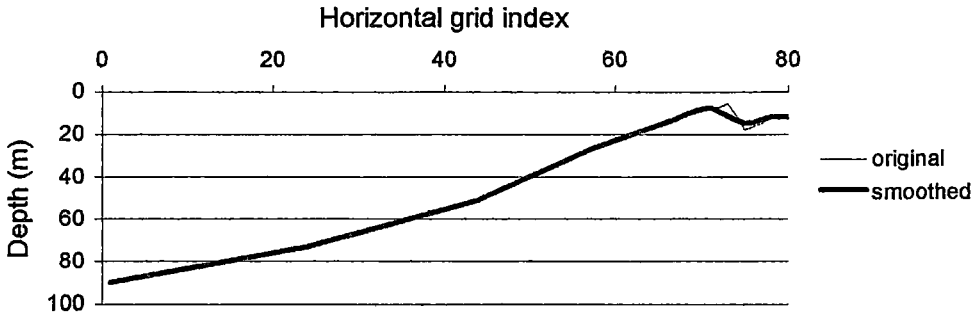

Figure 5.5 Sea depths, before and after smoothing

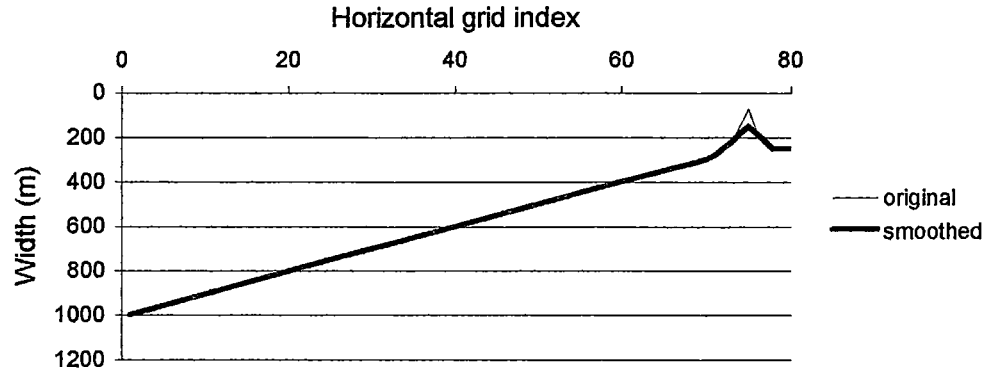

Figure 5.6 Sea widths, before and after smoothing

5.2.5 Grid independence

In order to investigate grid independence ten day simulations of Macquarie Harbour were conducted with different numbers of σ levels (KB) and horizontal grid size (Δx). As the harbour and rivers vary considerably more in depth than in plan, the vertical grid resolution is more important than the horizontal grid resolution. This variation exists in the hydraulic structure as well as geometry.

Checking vertical grid resolution is much easier than checking horizontal grid resolution. Changing the vertical grid resolution required editing a handful of parameters in the computer program and recompiling it, while changing the horizontal resolution requires regridding and changing boundary conditions. Horizontal and vertical resolutions were checked separately with the vertical described first.

The values for KB tried were 7, 13, 23, and 33, using Δx=250m. The velocity, salinity, and pollution at the harbour surface are used to compare the four simulations. From these three quantities, it was clear 7 levels was inadequate (Figure 5.7), 13 levels was barely adequate

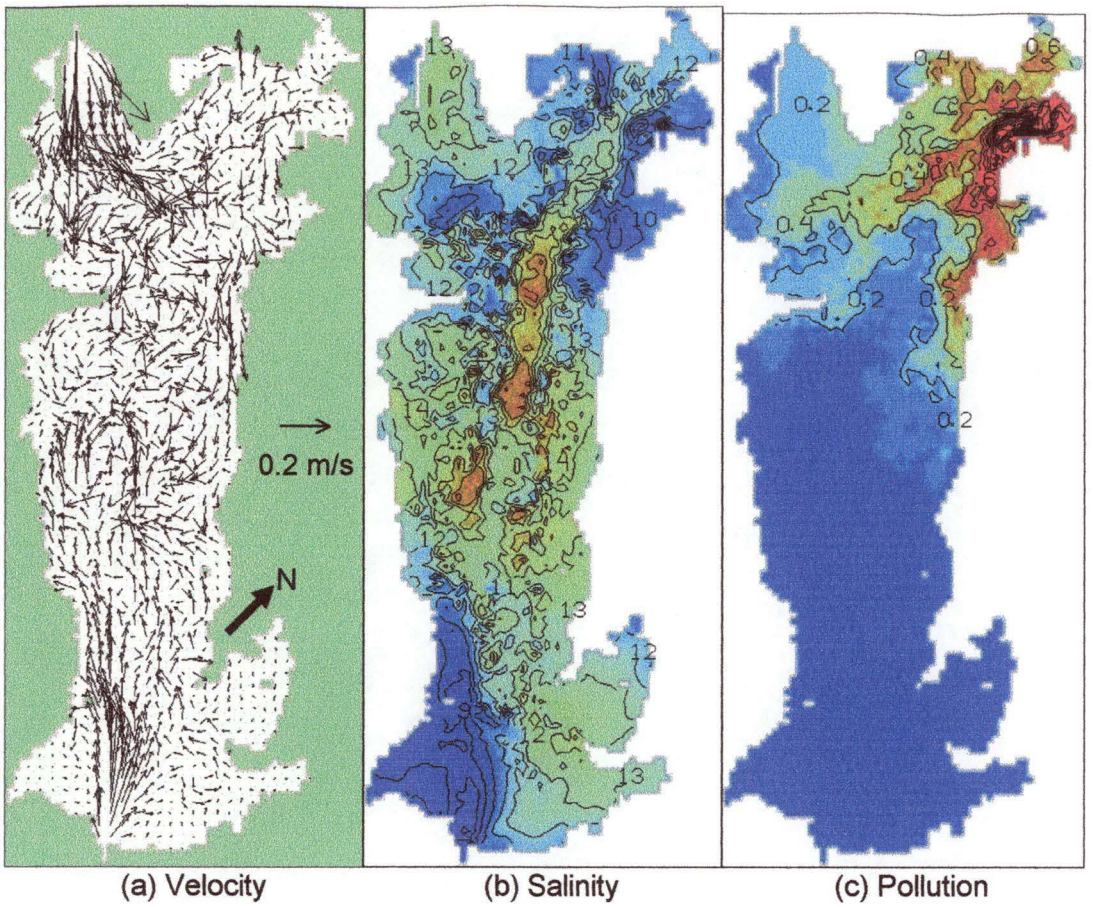

Figure 5.7 Surface values of velocity, salinity (‰) with 1.0‰ contours, and pollution (g/m^3) with 0.2g/m^3 contours; at day 10 for ***KB* = 7**

(Figure 5.8), and 33 levels required changing the time step from 3.0s to 2.0s to retain numerical stability (Figure 5.10). The same general circulation features where evident in the 13, 23, and 33 level simulations. The greater the number of levels, the smoother the result, although numerical rounding errors in the 33 level case caused by the smaller grid spacing and time steps, gave erroneously large pollution values in the harbour. The 7 level simulation was very numerically noisy and clearly not modelling the harbour very well. Therefore, 23 levels were chosen for the modelling, as a compromise between resolution and a practical time to solve the model (Figure 5.9).

The four figures (Figure 5.7, Figure 5.8, Figure 5.9, and Figure 5.10) all have the same scales, to allow a qualitative assessment of the four simulations. The length of the horizontal velocity vectors is proportional to the velocity magnitude. A 5mm vector is equivalent to a velocity of 0.2m/s. The salinity values are in grams of salt per kilogram of water, that is parts per thousand by mass (ppt) with the symbol ‰.

The ten day simulation had a Gordon River flow rate of 300m^3/s, King River flow rate of 70m^3/s, no wind, M_2 tide (12.42h period) with 1.2m amplitude at the out to sea (upstream

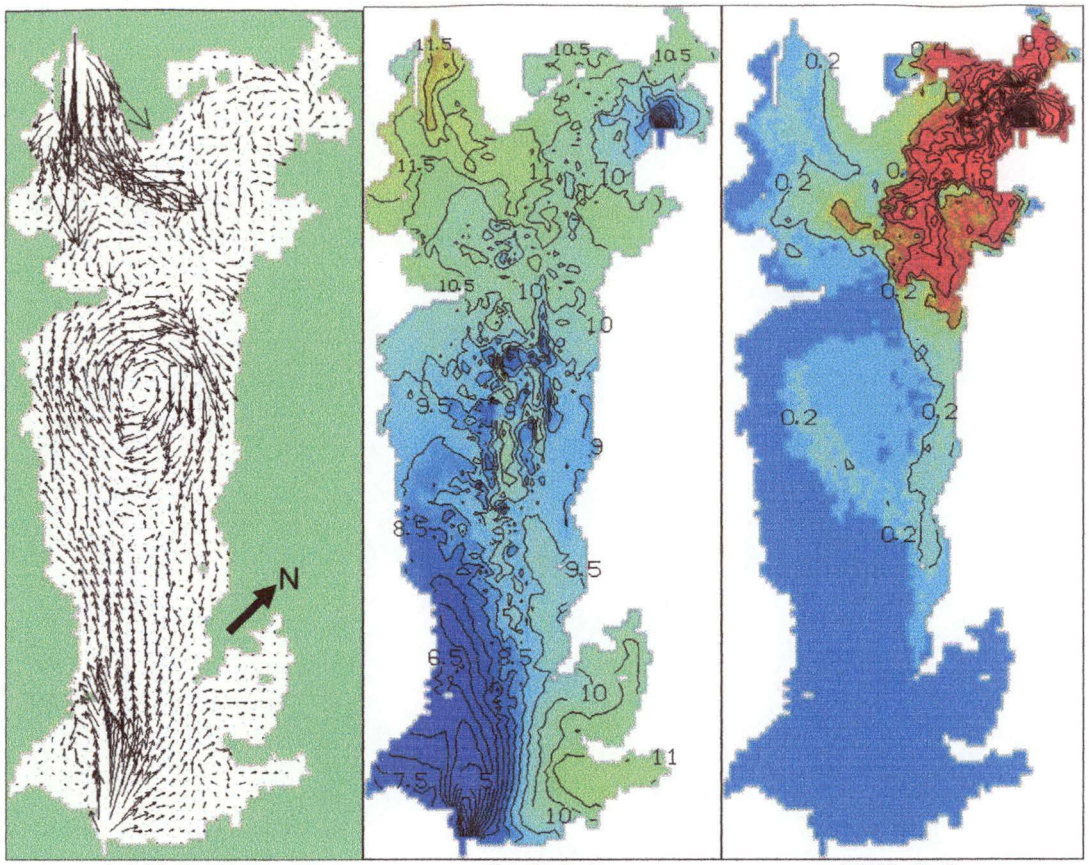

Figure 5.8 Surface values of velocity, salinity (‰) with 0.5‰ contours, and pollution (g/m^3) with 0.2g/m^3 contours; at day 10 for ***KB* = 13**

end of the sea model, giving a 0.2m amplitude just inside the harbour). The stationary initial conditions are described in section 5.3 and a list of typical model parameters is given in Appendix D.

The horizontal grid resolution was checked for Δx = 200m, 250m and 300m, using KB = 23. Horizontal grids larger than this could not represent the geometry of the estuary adequately and smaller grids had impractically large solving times. The conditions of the simulations were the same as for the vertical resolution comparison with a results given at the end of a ten day simulation, although at a different point in the tidal cycle. A 3.0s time step was used for Δx = 250m and 300m and a 2.0s time step was used for the 200m case to retain stability. The Δx = 300m model in given in Figure 5.11, Δx = 250m in Figure 5.12, and Δx = 200m in Figure 5.13.

Comparing Figure 5.11, Figure 5.12 and Figure 5.13 it is clear all the solutions give a similar general circulation and distribution of scalar quantities. The main difference is the salinity in Figure 5.11.b near Hells Gates (top right) that indicates the sea (river) model is moving salt much faster from the seaward boundary to the Macquarie Harbour boundary than the other

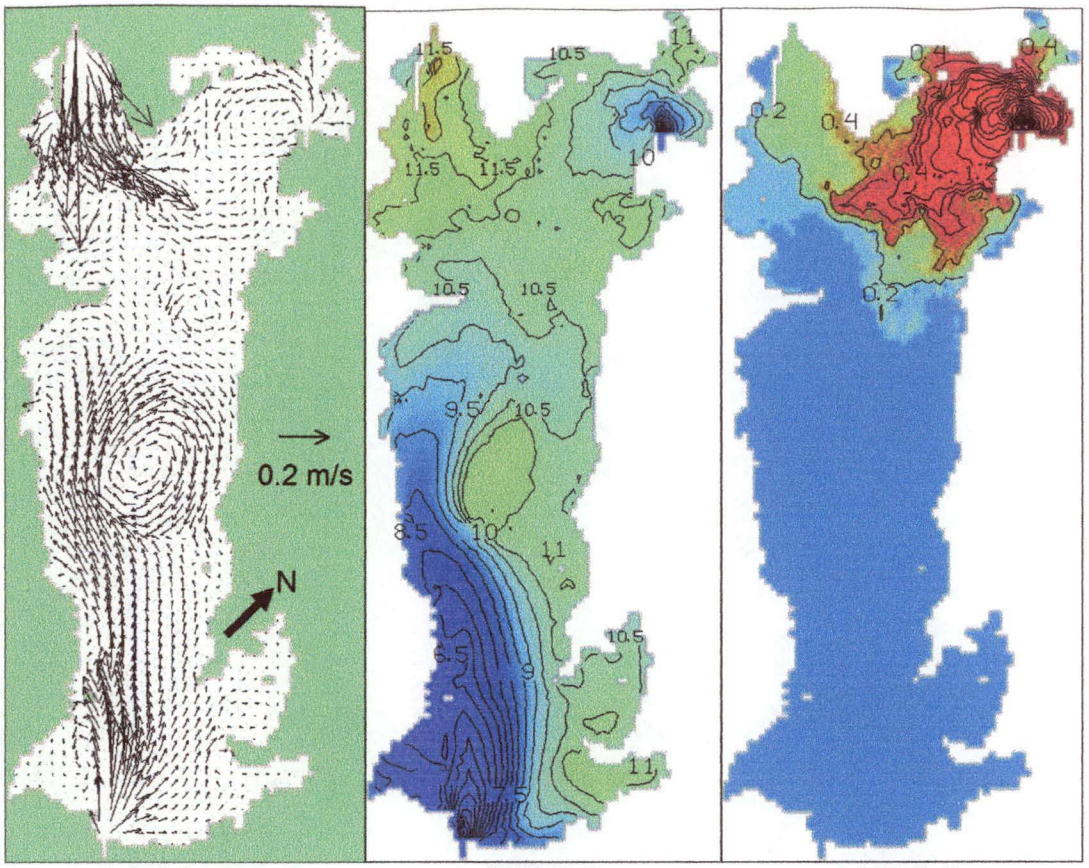

Figure 5.9 Surface values of velocity, salinity (‰) with 0.5‰ contours, and pollution (g/m^3) with 0.2g/m^3 contours; at day 10 for ***KB* = 23**

two models. This is a minor anomaly and averaging the salinity of the harbour model for the three grid scales the shows the $\Delta x = 200$m and $\Delta x = 250$m models are different by 0.60‰ (3.5% of $\Delta x = 250$m model average) and the $\Delta x = 250$m and $\Delta x = 300$m models are different by only 0.0098‰ (0.06% of $\Delta x = 250$m model average).

With the model output not very sensitive to the horizontal grid size, $\Delta x = 250$m is chosen as the horizontal grid size as it represents the geometry well and still allows the model solve in a practical time.

5.3 Initial conditions

Model simulation runs are started from a stationary initial condition or from the end point of a previous simulation run. The stationary initial condition has zero velocity and zero surface elevation, with a salinity and temperature structure shown in Figure 5.14. The salinity has a linear variation starting at the surface with 10‰, then 12‰ at 8m, 21‰ at 9m, up to 35‰ at

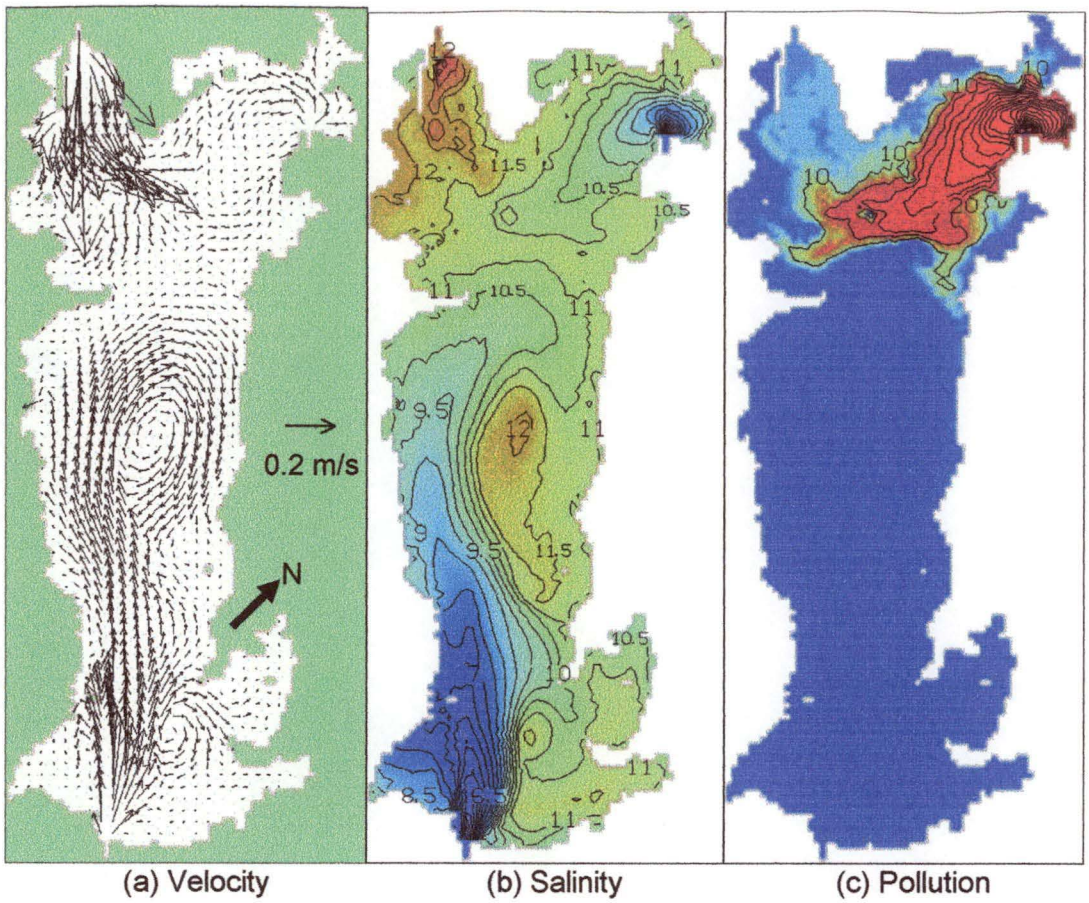

Figure 5.10 Surface values of velocity, salinity (‰) with 0.5‰ contours, and pollution (g/m^3) with 5.0g/m^3 contours; at day 10 for ***KB* = 33**

55m. The temperature (°C) has an exponential variation $T = 5 + 10e^{\sigma D/58}$, D is the total depth (m), and σ is the non-dimensional depth where the temperature is being calculated.

The initial conditions are the same throughout the harbour and the river models, so there is static equilibrium. When the model was not started with static equilibrium, the resulting unsteady flow can cause instability or inaccurate results. For example, an initial condition for salinity in the rivers was tested with a linear horizontal variation from 0‰ upstream to 20‰ at the harbour. This case produced large density currents that caused standing waves in the harbour and ended in numerical instability. To counter the density currents, the water surface in the rivers can be sloped, but it is difficult to tune the water surface slope to avoid other waves that cause instability. The simplest and most repeatable approach is to start with static equilibrium.

While the initial condition for salinity closely follows a typical water column, the initial condition for temperature decreases with depth in the top 20m where the actual temperature increases. The aim is to see if the temperature distribution will change from the initial distribution (Figure 5.14), to what is measured in the harbour. For Macquarie Harbour,

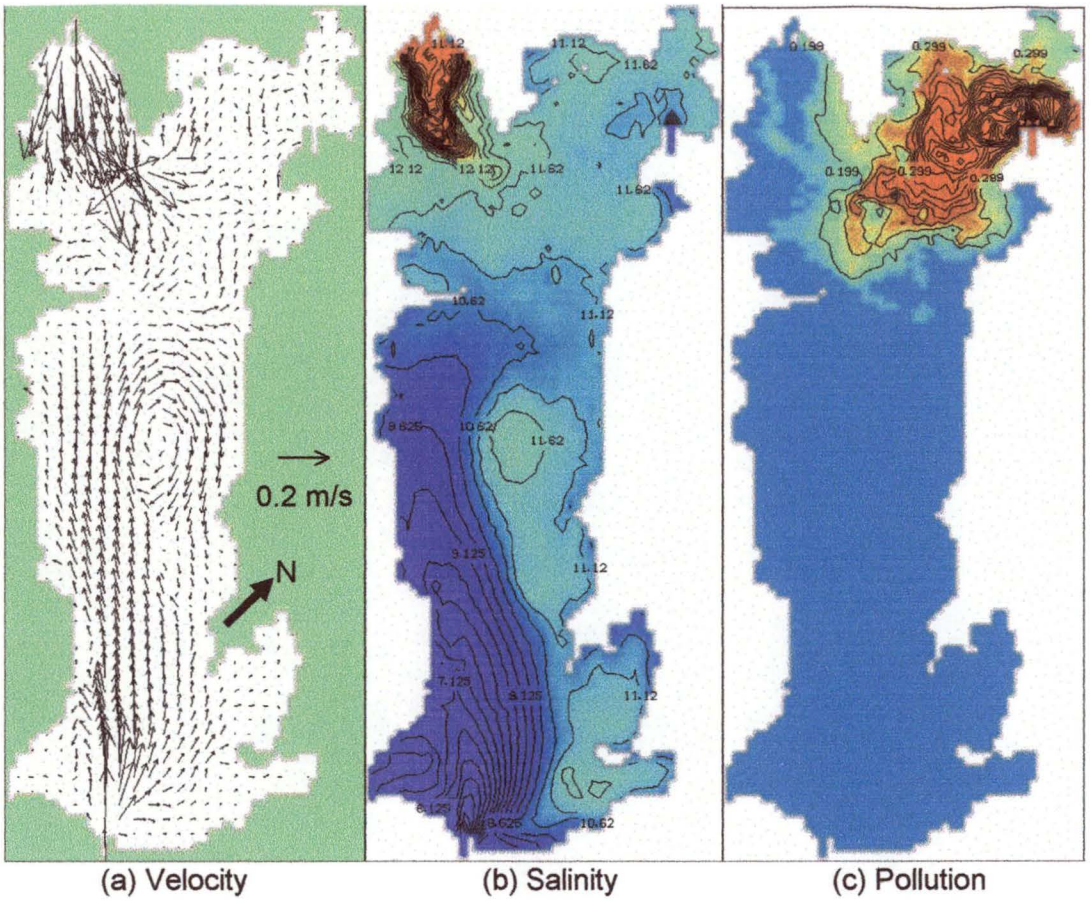

Figure 5.11 Surface values of velocity, salinity (‰) with 0.5‰ contours, and pollution (g/m^3) with 0.2g/m^3 contours; at day 10 for Δx = **300m**

density is a stronger function of salinity than temperature, so the differences in density due to the changed temperature distribution will not be enough to effect the circulation.

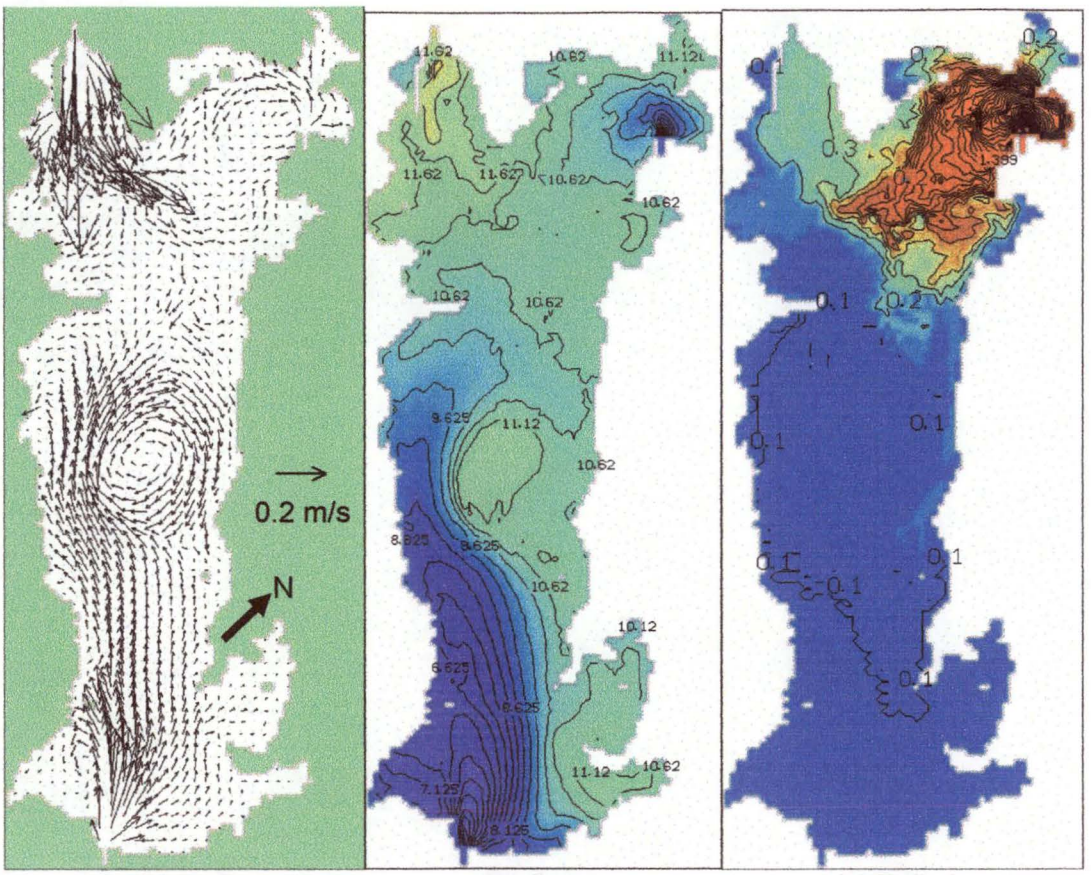

Figure 5.12 Surface values of velocity, salinity (‰) with 0.5‰ contours, and pollution (g/m^3) with 0.2g/m^3 contours; at day 10 for Δx **= 250m**

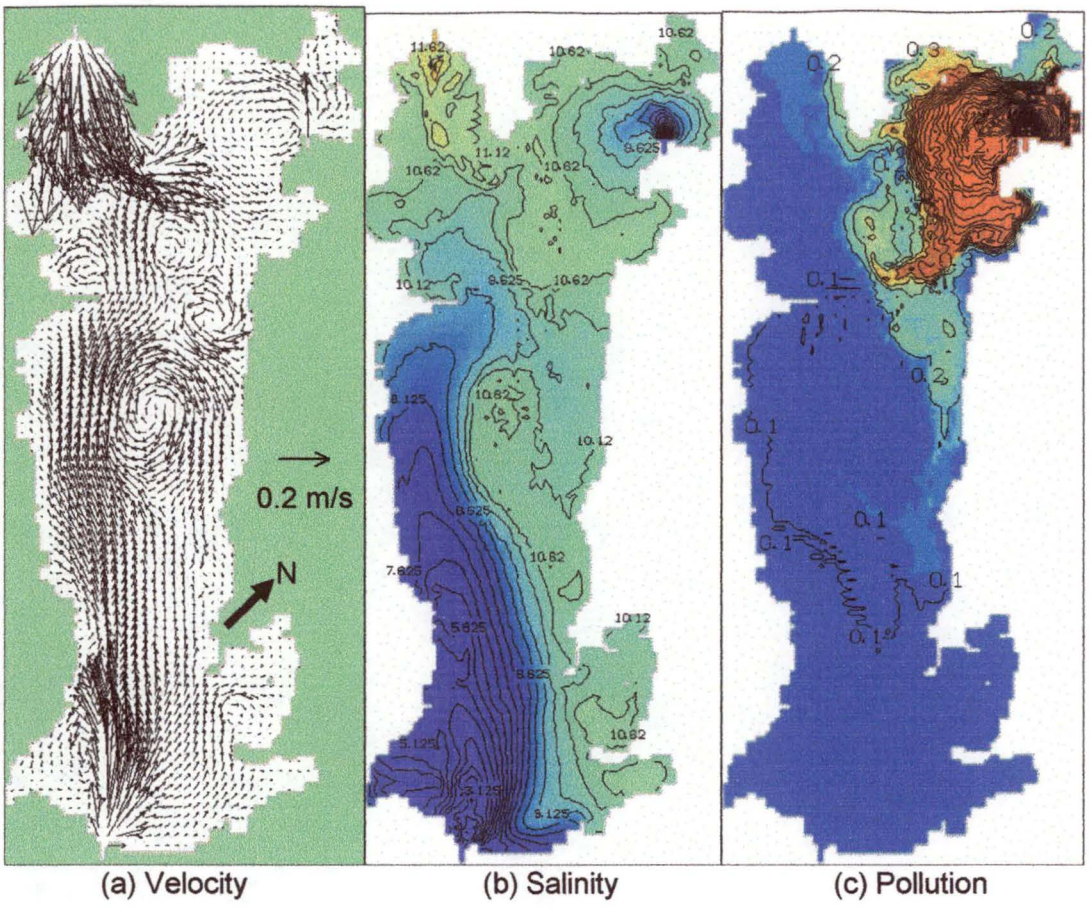

Figure 5.13 Surface values of velocity, salinity (‰) with 0.5‰ contours, and pollution (g/m^3) with 0.2g/m^3 contours; at day 10 for Δx = **200m**

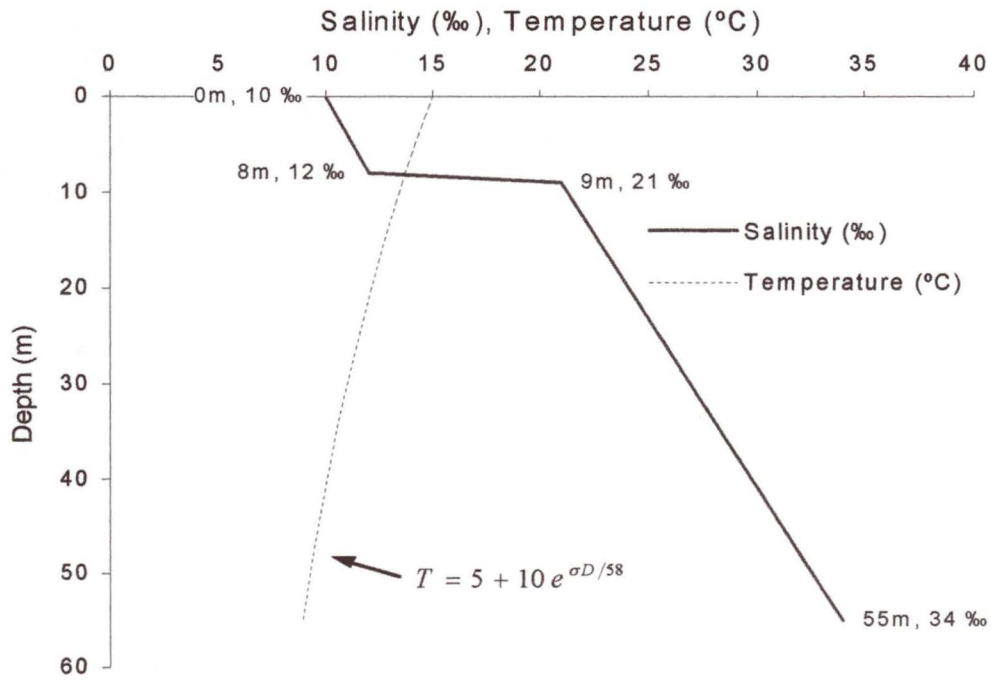

Figure 5.14 Initial condition for salinity and temperature

5.4 Boundary conditions

In Macquarie Harbour the Gordon River, King River, sea, and wind produce the most significant driving force, and their effect on the harbour must be accurately modelled. Initially the solution space of the model was limited to Macquarie Harbour, with the rivers and sea modelled with zero-dimension boundary condition equations. This proved unstable and these equations were replaced with separate river models. The formulation of river and sea boundary conditions for the Macquarie Harbour model has given the direction for this thesis, through the development of the river models.

After the description of an initial attempt at modelling the boundary conditions with zero-dimension equations (Section 5.4.1), the boundary conditions used with separate river models are described. With the addition of two-dimensional river models, the solution space was expanded to a point where the boundary conditions could be defined more accurately and stably.

5.4.1 Initial river boundary on harbour

In an earlier version of the Macquarie Harbour model, the boundary condition where the rivers and sea joined the harbour, was modelled with zero-dimension equations. That is, storage and flow equations were used to model the amount of water, salt, and heat in each river. At the river mouth, the water volumes gave a surface elevation, and Manning's equation was used to generate a velocity. This approach was inaccurate and unstable, but is included as an example of the model development.

The zero-dimension boundary equations control surface elevation and scalars at the river mouth and open sea boundary, leaving POM to calculate the velocity. The alternative of controlling the velocity and allowing POM to calculate the surface elevation was also tested, with the same lack of success. The surface elevation at the sea was set with a sinusoidal tide variation, and the surface elevation for the rivers was calculated from the water stored in the river from a geometry in Figure 5.15 assuming

1. rivers have a constant slope = S_0
2. change in volume of water stored in river (V_r) per second $\partial V_r/\partial t = Q_r + Q_h$; where Q_r is the river flow rate and Q_h is the net flow rate out of harbour
3. length of the storage wedge $L = D_s/S_0$ and the volume of storage $V_r = \frac{1}{2} D_s L B$, where B is the river width and D_s is the depth due to storage above the normal depth (D_n)
4. rearranging the equations in point 3 gives $D_s = \sqrt{2 S_0 V_r / B}$

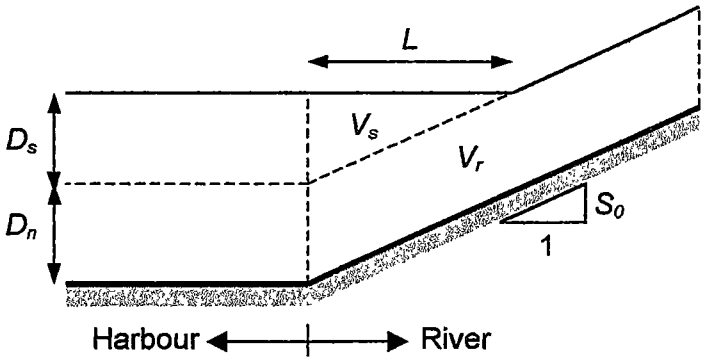

Figure 5.15 Schematic of zero-dimension river boundary condition geometry

5. normal depth (D_n) is calculated from Manning's equation, $Q_r = \frac{1}{n} A R_h^{2/3} S_o^{1/2}$; where n is Manning's n and the river section is rectangular, so cross sectional area $A = BD_n$ and hydraulic radius $R_h = BD_n/(B + 2D_n)$
6. salt water is mixed quickly with river storage water as water flows out of harbour

These assumptions gave the surface elevation at river mouth $\eta_r = D_n + D_s - H_r$, where H_r is the depth from the surface elevation datum at the river mouth.

The most unstable river was the King River, with its proximity to the tidal flow from the sea entrance through Hells Gates. Flood tides would cause flow back up the King River and as there was only a zero-dimension equation describing the flow in the river, the river flow was driven by the harbour. This would lead to the surface elevation dropping around the river mouth, leading to greater flow up the river. As the river equations did not model the momentum of the water flowing from further upstream, the river model was very sensitive to what was happening at the river mouth. This made the model unstable, and it usually crashed or at least became inaccurate, as shown in Figure 5.16. Figure 5.16 is a plot of surface velocity and surface salinity in the harbour surrounding the mouth of the King River using the zero-dimension equations. The simulation had been set up with a uniform 20‰ salinity in the harbour to simplify the hydraulics as part of testing the boundary conditions. Visible in the figure are the disorganised surface velocity vectors and the patchy salinity distribution.

To successfully model the system there was the need to create two-dimensional laterally averaged model for the Gordon River, King River, and the sea. This is the two-dimensional model described in this thesis.

Before the two-dimensional model was added, the sea was modelled as part of the three-dimensional harbour model (using POM) for 1km beyond Hells Gates with an open ocean

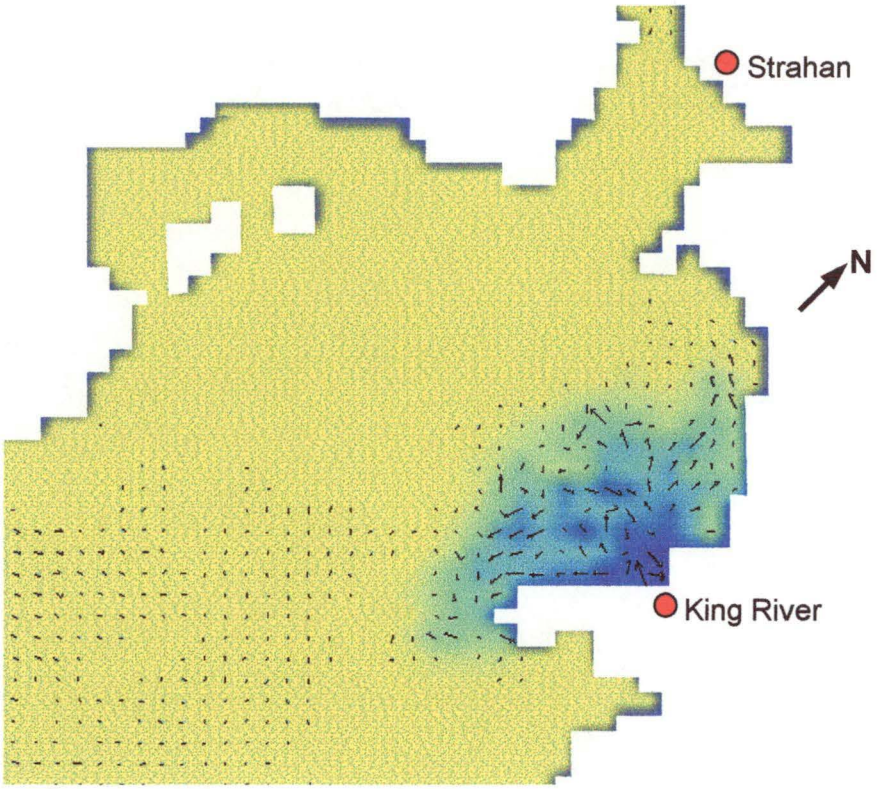

Figure 5.16 Surface velocity (black vectors) and surface salinity in Macquarie Harbour surrounding the mouth of the King River, using zero-dimension equations for the river boundary conditions. The brown colour is 20‰ of salt, and the blue is fresher water (< 5‰ salt)

boundary of 2km. When the two-dimensional models were added to the model system, the portion of the three-dimensional model outside Hells Gates was removed so the two-dimensional model could be joined at Hells Gates. This was because the narrows of Hells Gates were more "river like" than the 2km open ocean boundary.

5.4.2 Upstream river model

In the Gordon River and King River, the upstream surface elevation boundary is calculated from a prescribed flow rate. This flow rate can be linearly varied (ramped) from between values, allowing the model to start from a stationary initial condition and slowly introducing flow in the rivers, and to simulate flood events. At the 'upstream' end of the sea 'river' model, the surface elevation is a prescribed 1.2m amplitude M_2 tide (12.42h period) shown in Figure 5.17. This 1.2m amplitude produces a realistic tide amplitude inside Macquarie Harbour.

The scalar quantities are prescribed at the upstream end of the river model, with a capped linear variation. The capping is required because the quantities vary linearly with depth and during a flood event the large depths can cause unrealistic values. For example, temperature

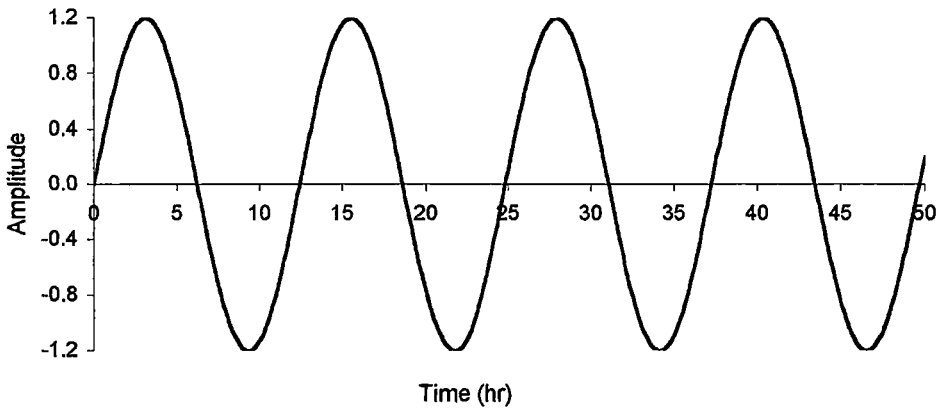

Figure 5.17 Amplitude of M_2 tide used for sea model

decreases with depth and during a flood without capping on the boundary values, the temperature can be unrealistically forced below freezing point.

As for all the boundary values, the scalars can be varied linearly between values in time. This avoids the problem of introducing fresh water at the upstream end of the Gordon River and King River model with a stationary initial condition. The problem is the fresh water is less dense than the saltier water downstream at the same depth (given in Figure 5.14) and density currents cause flow upstream instead of downstream. By ramping the salinity at the upstream boundary from the depth mean value in the surrounding water at the initial condition, to a less saline value when the flow is more developed, the flow's inertia can overcome the density forces.

The linear variation for a scalar f at the upstream boundary is

$$f(\sigma) = f_0 - mD\sigma > f_{\min} \tag{5.4}$$

Where f_0 is the surface value, m is the slope of the variation, D is the total depth, σ is the value of sigma, and $f_{\min}$ is the minimum capping value. Table 5.2 gives the f_0, m, and $f_{\min}$ values for the salinity, temperature, and pollution concentration in the three river models to be used at the start of simulation run with stationary initial conditions. The f_0 values are obtained by depth averaging the scalar distributions at the upstream ends from the initial conditions. As already mentioned, this avoids unwanted density currents. At the end of the ramping, when the circulation has stabilised, Table 5.3 gives the f_0, m, and $f_{\min}$ values. Note the Gordon River and King River has fresh water, the sea has salty water, and only the King River is polluted.

	Salinity			Temperature			Pollution		
	f_0	m	$f_{\min}$	f_0	m	$f_{\min}$	f_0	m	$f_{\min}$
Gord.	10.70	0	0	14.96	0	4	0	0	0
King	10.10	0	0	10.10	0	4	0	0	0
sea	26.30	0	0	14.58	0	4	0	0	0

Table 5.2 Coefficients for linear variation of scalars at river upstream boundaries at **start** of a ramp from stationary initial conditions

	Salinity			Temperature			Pollution		
	f_0	m	$f_{\min}$	f_0	m	$f_{\min}$	f_0	m	$f_{\min}$
Gord.	0.00	0	0	14.00	-1.00	4	0	0	0
King	0.00	0	0	10.00	-1.00	4	0.01	0	0
sea	32.00	0.07	0	14.00	-0.08	4	0	0	0

Table 5.3 Coefficients for linear variation of scalars at river upstream boundaries at **end** of a ramp from stationary initial conditions

5.4.3 Scalars at top and bottom boundaries

The top boundary of the model is the water/air interface and the bottom boundary is the land/water interface, corresponding to $\sigma = 0$ and $\sigma = -1$ respectively. All the scalars except temperature have no flux across the top and bottom boundaries. The temperature has a heat flux at the top surface and no flux at the bottom surface. The heat flux is used to simulate the diurnal solar radiation and convection from the surrounding air. A simple sinusoidal variation is used for heat flux and air temperature, with the maximum and minimum values given in Appendix D.

While the boundary condition is specified with the heat flux, the air temperature is used to ensure the water surface temperature does not unrealistically exceed the air temperature. The model does this by setting the heat flux boundary value to $\kappa_{cooling}\left(T_{surface} - T_{air}\right)$ when the water surface temperature exceeds the air temperature, which removes heat from the water. Using numerical testing, a value of $\kappa_{cooling} = 10^{-5}$ has been determined.. This capping of the heat flux models the water convecting heat back to the air. Although the model is simple, it gives realistic results.

5.4.4 Velocity at top and bottom boundaries

Shear stress is used at the top and bottom boundaries in the momentum equation to model the wind stress and bottom friction. In the harbour, POM uses a roughness length to calculate bottom friction via a quadratic stress expression. A roughness length of 5mm is used (variable *Z0B* in POM) with a minimum friction coefficient of 0.001. In the river model, Manning's n is used for the side friction, with the bottom stresses calculated with an expression similar to that used in POM. Typical values of Manning's n of 0.03 are used for the King River and sea, and a value of 0.04 is used for the Gordon River due to its many deep holes.

Wind stresses are included only in the harbour for simplicity, with a roughness coefficient between the waves and air of 1.0×10^{-6} (variable *KW* in POM). The sensitivity of the model to *Z0B* and *KW* was tested by comparing the model output at the end of a 10 day simulation with values 20% above and below the ones finally used.. For the *KW* test the wind was only applied for one hour at the end of the 10 day (windless) simulation - from the south west at 10m/s (from left in figures), ramped up over 15min. The model output was averaged throughout the harbour, with the magnitude of velocity used to represent the circulation. This comparisons shows for the 20% increase in *KW* there was a 5.5% increase in velocity (greater wind stresses accelerated water more), no variation in salinity or temperature, and a 0.3% increase in pollution (increased velocities changed circulation to draw more polluted King River water into the Harbour). A 20% increase in *Z0B* caused a 2.5% decrease in velocity (greater bottom friction slowed water), no variation in salinity and temperature, and a 3% increase in pollution. The effect of *KW* variations are shown in Figure 5.18 ($KW = 0.8\times10^{-6}$), Figure 5.19 ($KW = 1.0\times10^{-6}$) and Figure 5.20 ($KW = 1.2\times10^{-6}$). The effect of *Z0B* variations are shown in Figure 5.21 (*Z0B* = 4mm), Figure 5.22 (*Z0B* = 5mm) and Figure 5.23 (*Z0B* = 6mm). Note, there is a different velocity scale between the *KW* and *Z0B* sets of figures. The pattern of harbour circulation and distribution of scalar quantities are similarly as insensitive to variations in *KW* and *Z0B* as the average values.

Shielding from the land is included for the wind stresses in the harbour. That is, there is zero wind stress on the lee side of a landmass and the wind stress increases over the development length (L_d) to the current free air stress value. The wind stress is also set to zero in the grid cell just before the land on the wind side. The development length is the distance the wind has travelled over land before reaching water since the last region of water.

As the wind changes direction, the wind stresses need to be recalculated. To do this, the model loops through the variable containing the land/water mask in a direction parallel to the

wind. Every time the loop encounters land, it sets the wind stress back to zero and continues at zero until it reaches water, adding up L_d as it goes. At the water, it linearly varies the wind stress up to the free air value over L_d. In the loop L_d is set arbitrarily to 2.5km if the loop starts on land at the edge of the model. A schematic of the wind stress shielding is shown in Figure 5.24.

Wind velocities are recorded at Cape Sorell (outside Macquarie Harbour), Strahan airport (just west of Strahan), and Granville Harbour (45km north of Strahan). For this thesis wind velocities are taken from Matthews (1978) and CFMI (1995a). At Cape Sorell there is very little calm weather and over 60% of the annual wind speeds are greater than 3.3m/s, and over 25% at speeds greater than 8m/s (Matthews, 1978). Annually 80% of this wind blows from the SSW to NNW direction (Matthews, 1978). The percentage frequencies for velocity magnitude averaged from 1957 to 1971 is plotted in Figure 5.25 for 9am and Figure 5.26 for 3pm. The direction of the same wind data is plotted in Figure 5.27 for 9am and Figure 5.28 for 3pm. CFMI (1995a) found the Strahan airport had on average two-thirds the wind speed to Cape Sorell.

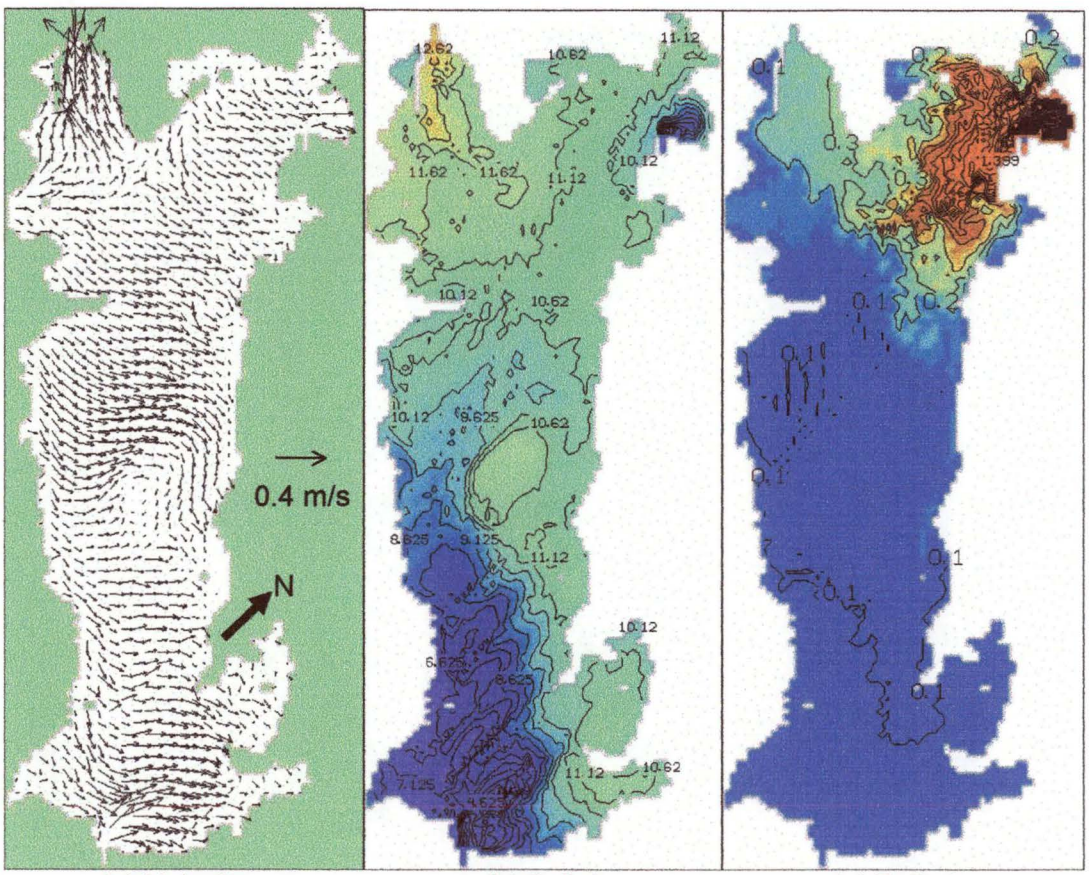

(a) Velocity (b) Salinity (c) Pollution

Figure 5.18 Surface values of velocity, salinity (‰) with 0.5‰ contours, and pollution (g/m^3) with 0.2g/m^3 contours; at day 10 (+1hr) for $KW = 0.8\times10^{-6}$

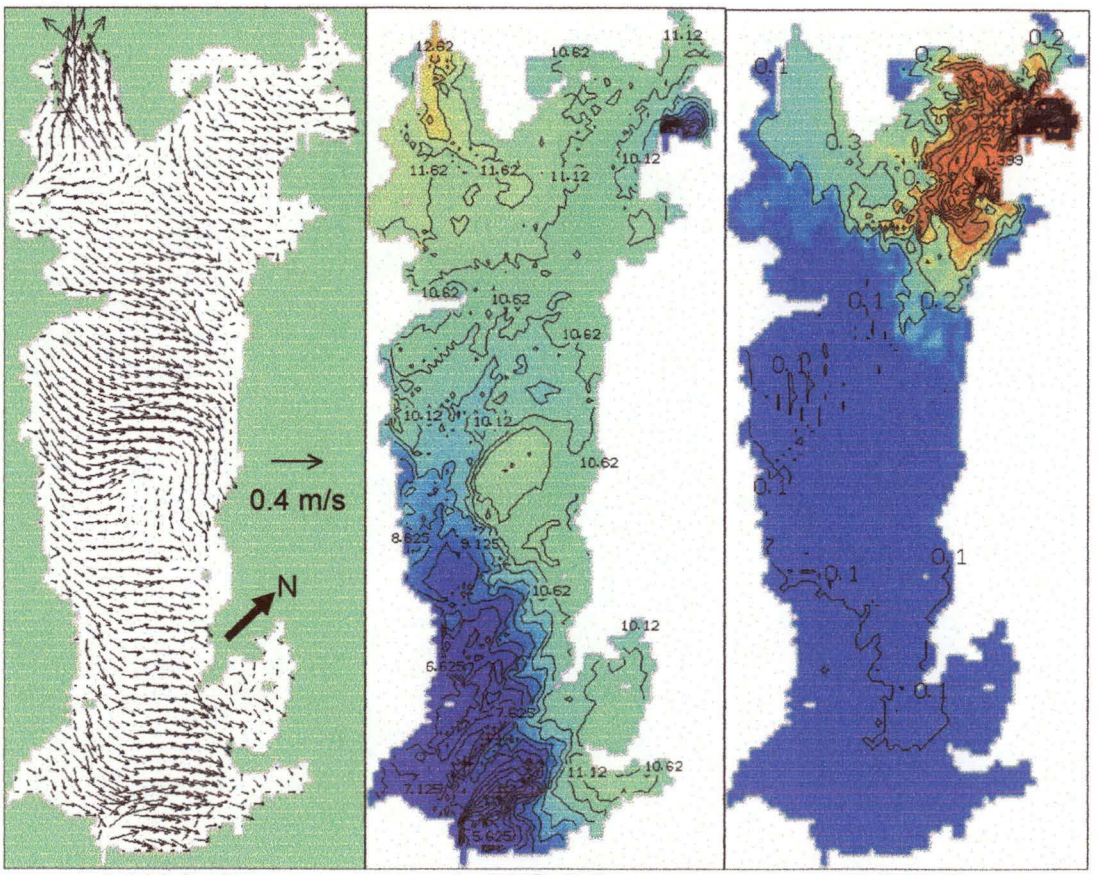

(a) Velocity (b) Salinity (c) Pollution

Figure 5.19 Surface values of velocity, salinity (‰) with 0.5‰ contours, and pollution (g/m^3) with 0.2g/m^3 contours; at day 10 (+1hr) for $\boldsymbol{KW = 1.0\times10^{-6}}$

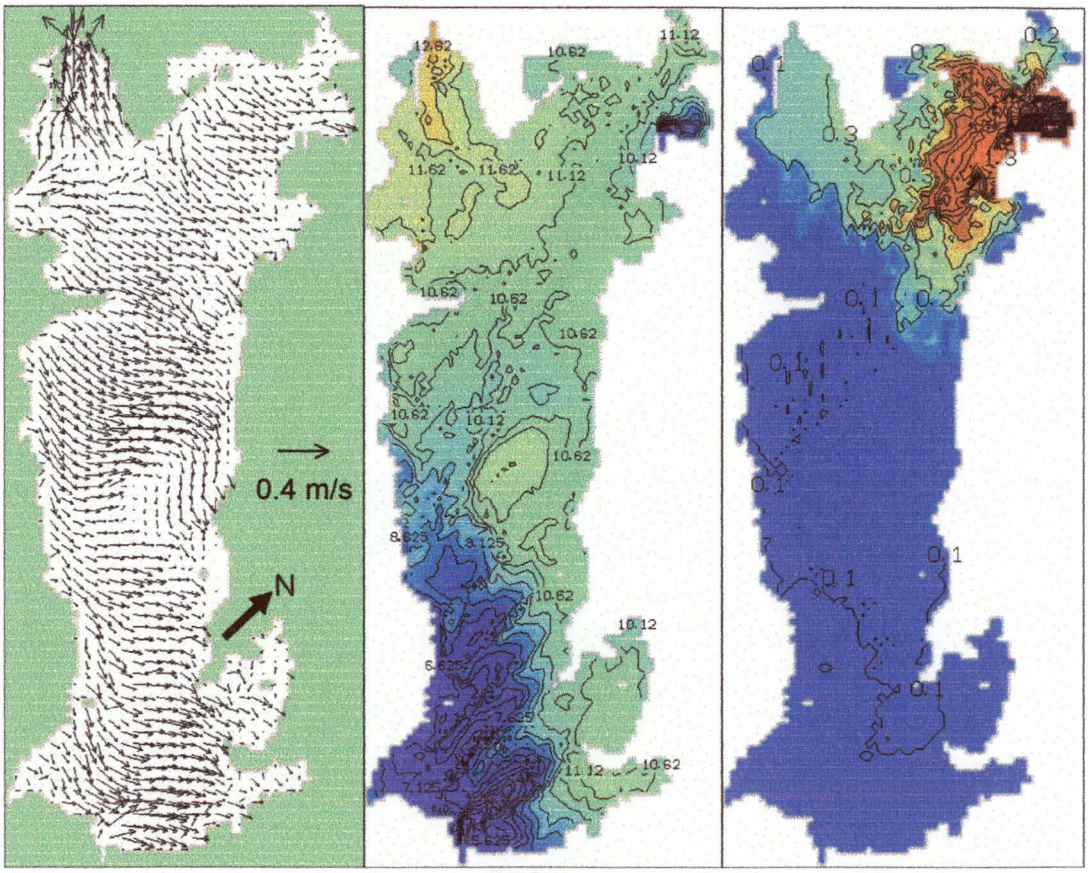

(a) Velocity (b) Salinity (c) Pollution

Figure 5.20 Surface values of velocity, salinity (‰) with 0.5‰ contours, and pollution (g/m^3) with 0.2g/m^3 contours; at day 10 (+1hr) for $KW = 1.2\times10^{-6}$

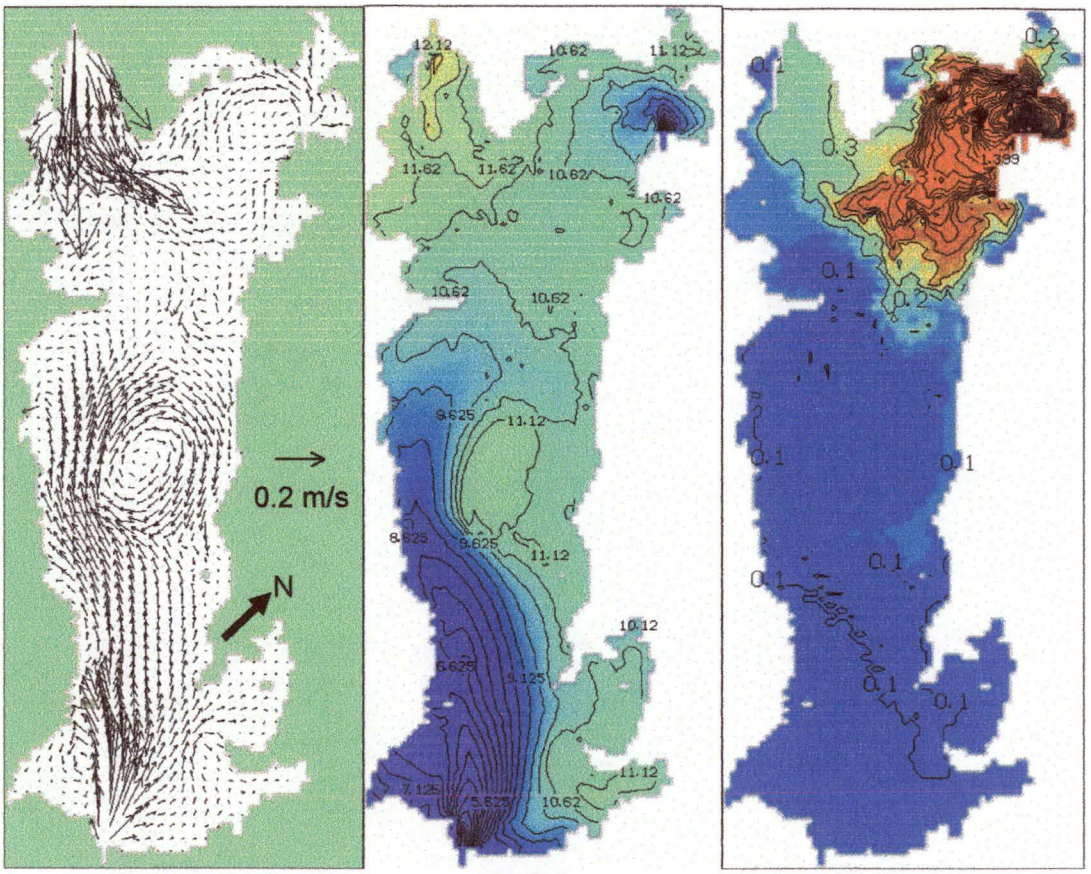

Figure 5.21 Surface values of velocity, salinity (‰) with 0.5‰ contours, and pollution (g/m^3) with 0.2g/m^3 contours; at day 10 for ***Z0B* = 4mm**

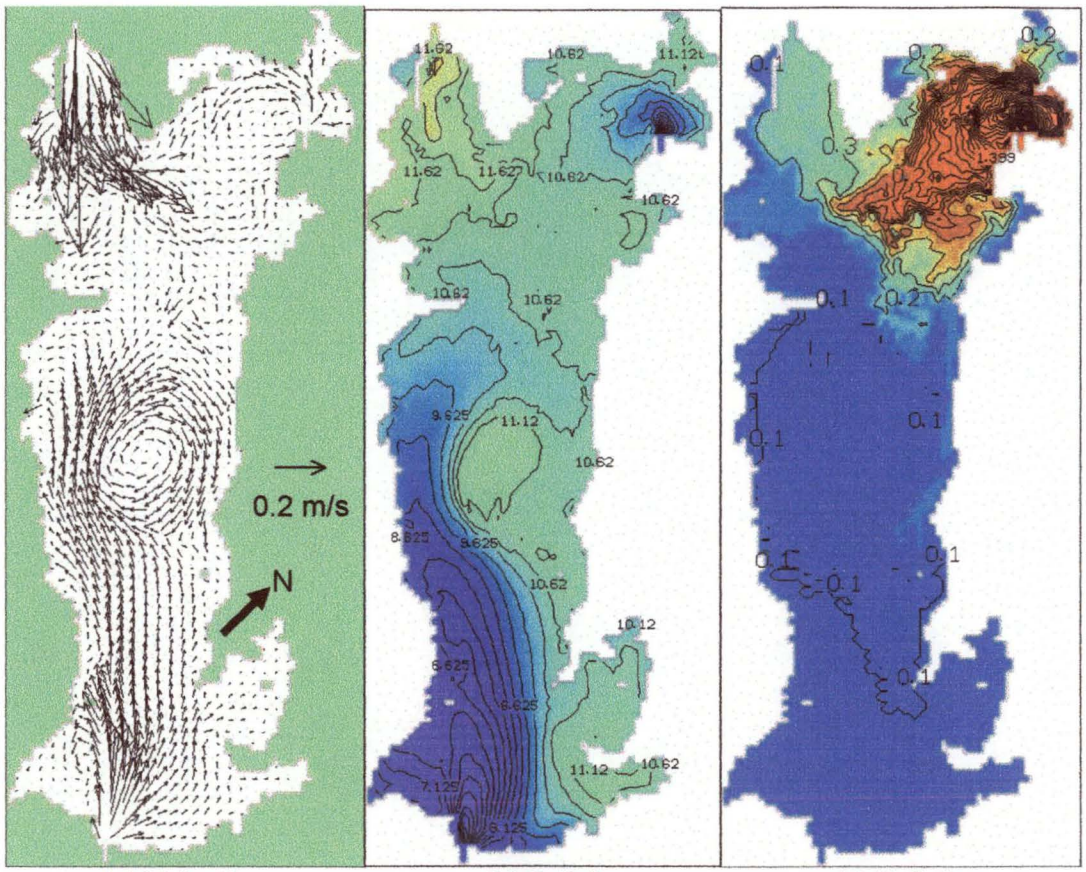

(a) Velocity (b) Salinity (c) Pollution

Figure 5.22 Surface values of velocity, salinity (‰) with 0.5‰ contours, and pollution (g/m^3) with 0.2g/m^3 contours; at day 10 for ***Z0B* = 5mm**

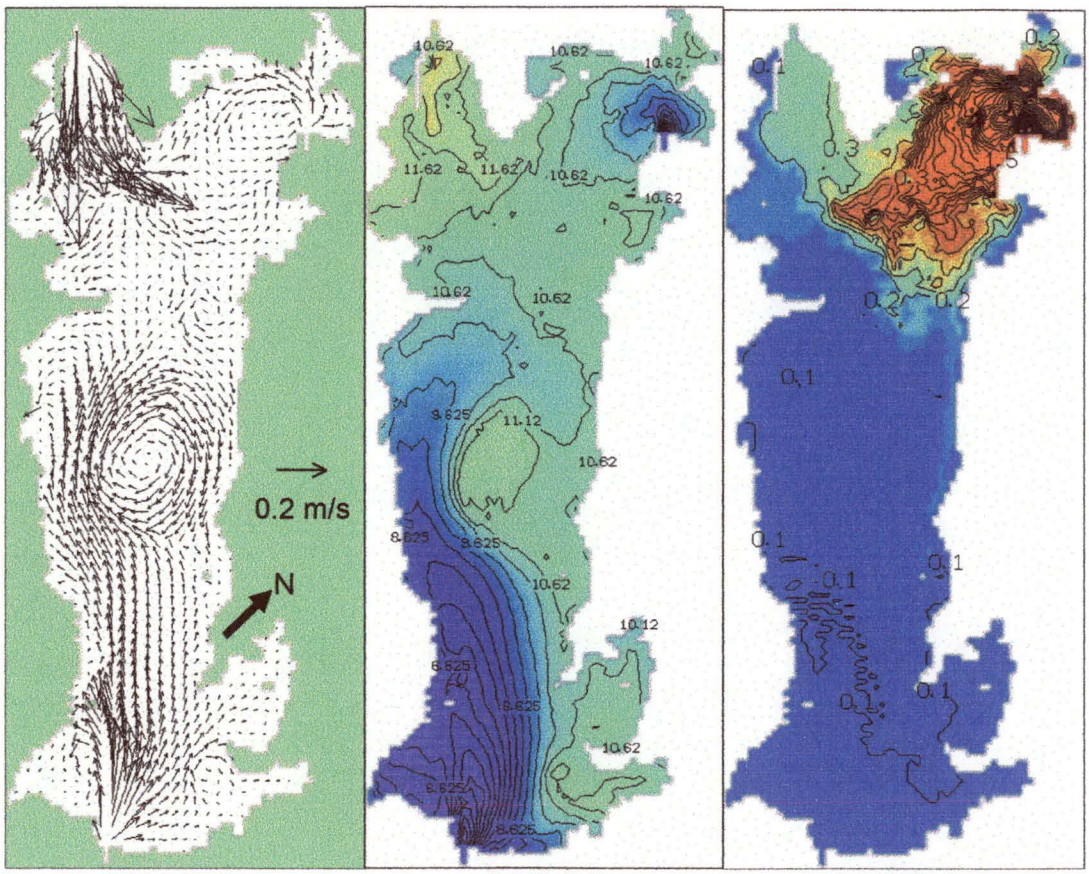

Figure 5.23 Surface values of velocity, salinity (‰) with 0.5‰ contours, and pollution (g/m^3) with 0.2g/m^3 contours; at day 10 for ***Z0B* = 6mm**

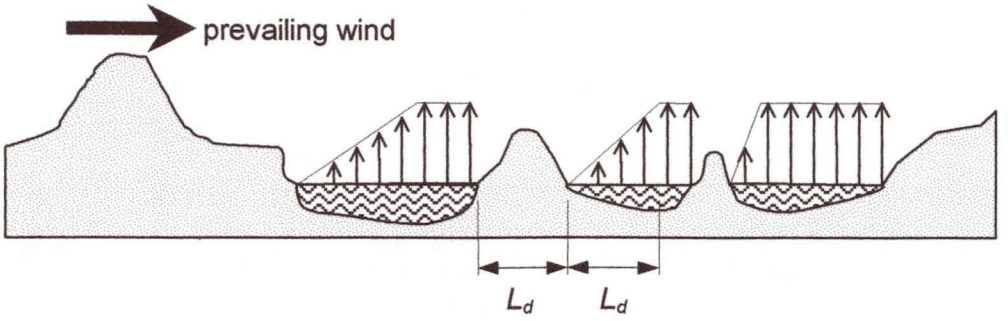

Figure 5.24 Schematic of wind stress over water showing the land shielding and development length L_d

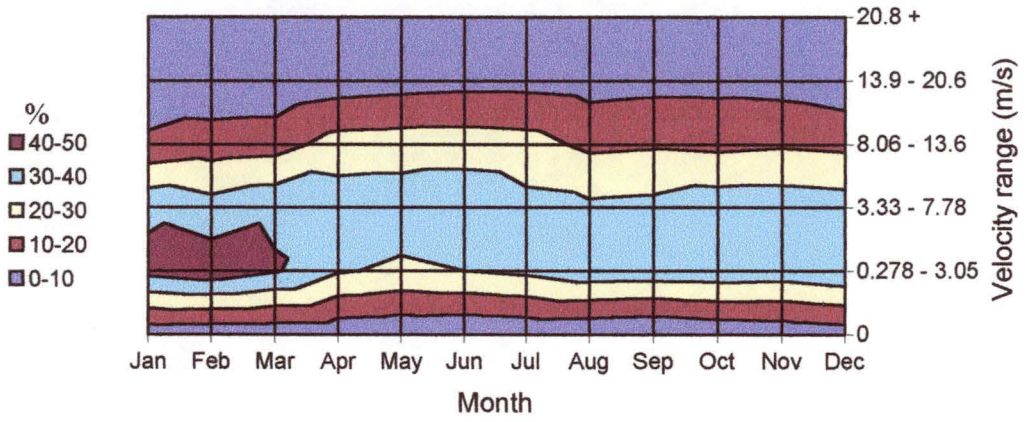

Figure 5.25 Percentage frequencies of wind speeds at Cape Sorell, 9am

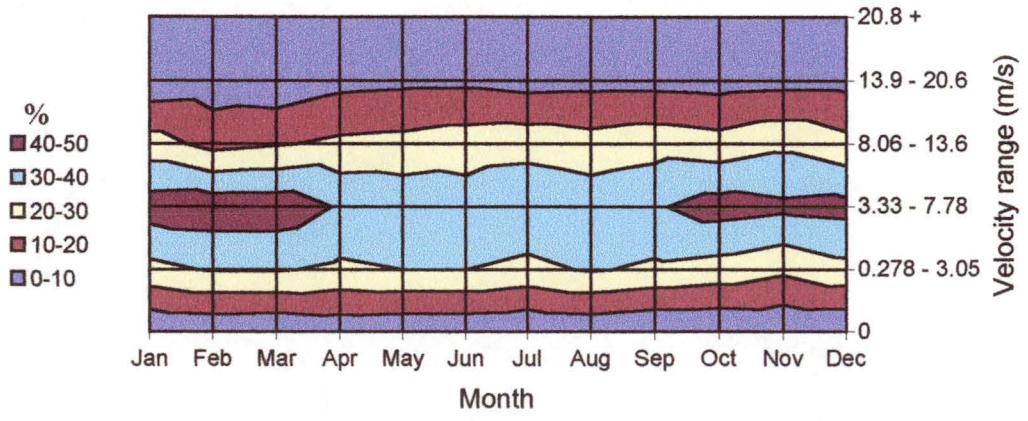

Figure 5.26 Percentage frequencies of wind speeds at Cape Sorell, 3pm

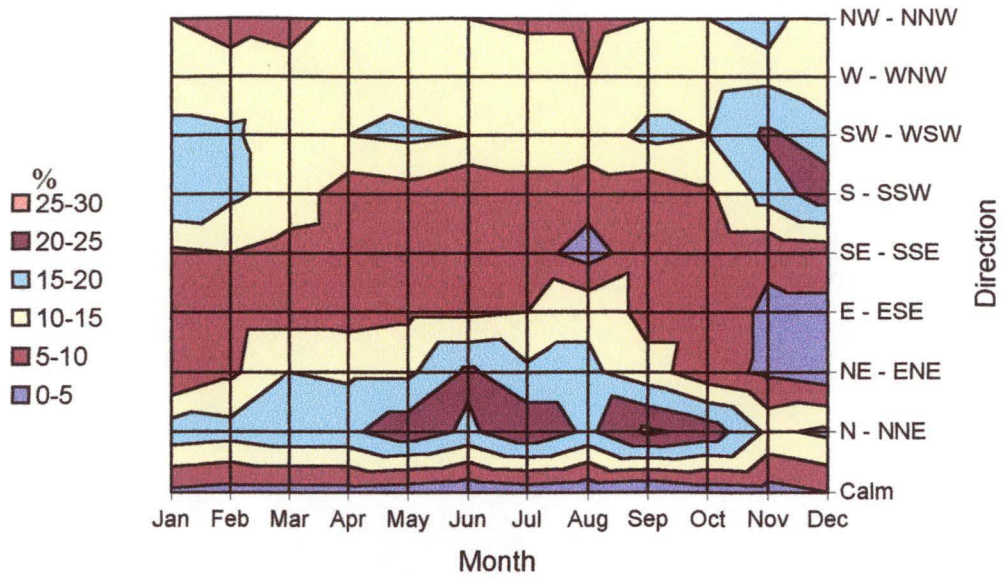

Figure 5.27 Percentage frequencies of wind direction at Cape Sorell, 9am

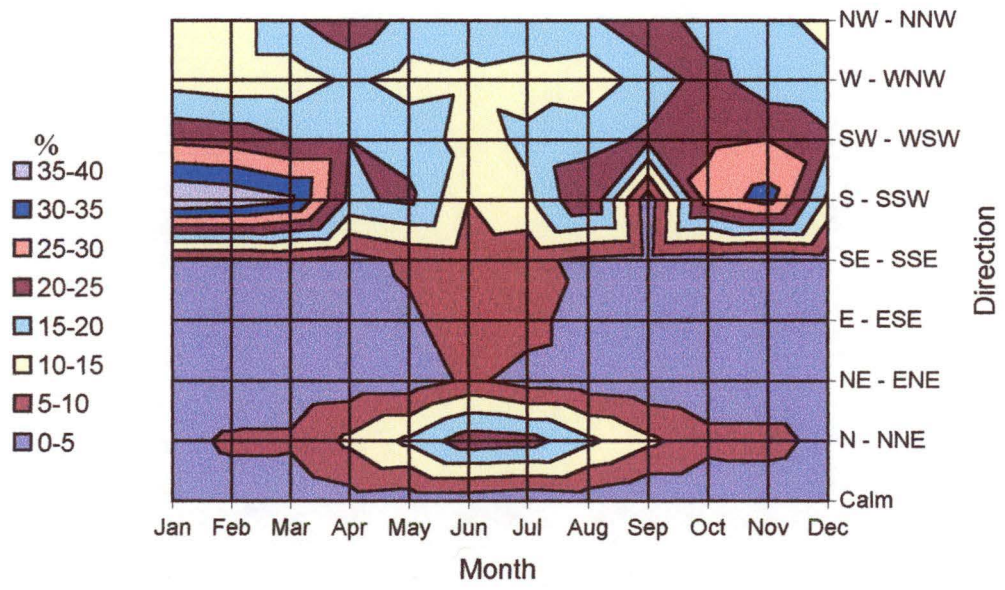

Figure 5.28 Percentage frequencies of wind direction at Cape Sorell, 3pm

Chapter Six
Macquarie Harbour behaviour

6.1 Introduction

The results from the modelling show Macquarie Harbour to have a complex circulation. The harbour is sensitive to several changeable forcings, which makes its behaviour difficult to succinctly define, given that a certain combination of forcings will evoke a response different to individual forcings. The three main forcings in the harbour are the tide, flow from the Gordon River and King River, and the wind. This chapter describes how the behaviour of the harbour's circulation and water quality is affected by these forcings, and validates the model's circulation against sparse field data in Section 6.5.

Typical model simulations will start from a stationary initial condition, as described in Section 5.3, with boundary values ramped over one day. In this context "ramped" means linearly varied with time. After approximately four days the Gordon River, King River, and sea models settle into a stable tidal ebb and flood cycle. It takes ten days for the harbour itself to develop a stable circulation after a change in the river flow rates, and so most model output is plotted after ten days of simulation. In Macquarie Harbour the important time scales are tidal, day/night heating, harbour circulation development time, and seasonal. Of these time scales, only the season variation is not modelled.

While the model output is generated as a time series, only still frames can be viewed in this printed thesis. Output in this chapter is mostly generated using the Vis5D computer program, with small amounts from Surfer and Microsoft Excel. When Vis5D is used for vertical sections through Macquarie Harbour, steps are evident around the land edges of the sections, even though the bottom σ level of the model follows the bathymetry. This is because Vis5D uses horizontal vertical levels and interpolation is required from the model output at a finite number of levels.

Colour and contour graphs are plotted for scalar variables on horizontal and vertical sections through the solution space. Velocity is often plotted using vectors, where the direction of the vector gives the direction of the velocity, and the length of the tail of the vector is proportion to the magnitude of the velocity. In the horizontal sections of velocity vectors, the density of vectors has been halved for clarity. That is, each velocity vector corresponds to two computational cells.

6.2 Circulation during ebb and flood tides

After a ten day simulation with a Gordon River flow rate of $200m^3/s$ and a King River flow rate of $70m^3/s$, the harbour circulation and water quality is investigated during a tidal cycle. In this simulation, wind velocity is set to zero and the tide is M_2 (12.42h period) with an amplitude of 1.2m at the ocean side of the sea model. Maximum velocities and surface elevations at Hells Gates occur at the peaks of the tidal cycle, while scalars have been transported to their extreme position as the tide turns and velocities are at a minimum. The tide has the most effect in the northern third of the harbour, although surface elevation changes occur throughout the harbour without any noticeable phase shift. The maximum velocities and surface elevations are found around Hells Gates, with flow reversal from the tide occurring in parts of northern harbour during the tidal cycle.

As described in previous sections, the water column in Macquarie Harbour shows significant density stratification, with a halocline at approximately 9m. This stratification, combined with the bathymetry and river locations produces a very complicated circulation that varies with the tide, changing river flow, and the wind. The simulations with varying river flow and wind are described later. Figure 6.1 and Figure 6.2 give a schematic representation of harbour circulation at the peak ebb and peak flood tides, where the arrow width is proportional to the flow rate. These figures have been derived from the velocity vector plots given in Appendix E. Appendix E also contains plots for surface elevation, salinity, temperature, and pollution concentration.

The Gordon River water flows north up the western harbour due to the Coriolis force. To check the effect of the Coriolis force, its sign was reversed and the water leaving the mouth of the Gordon River started up the eastern side of the harbour. Figure 6.3 compares the two cases at three days into a simulation from stationary initial conditions.

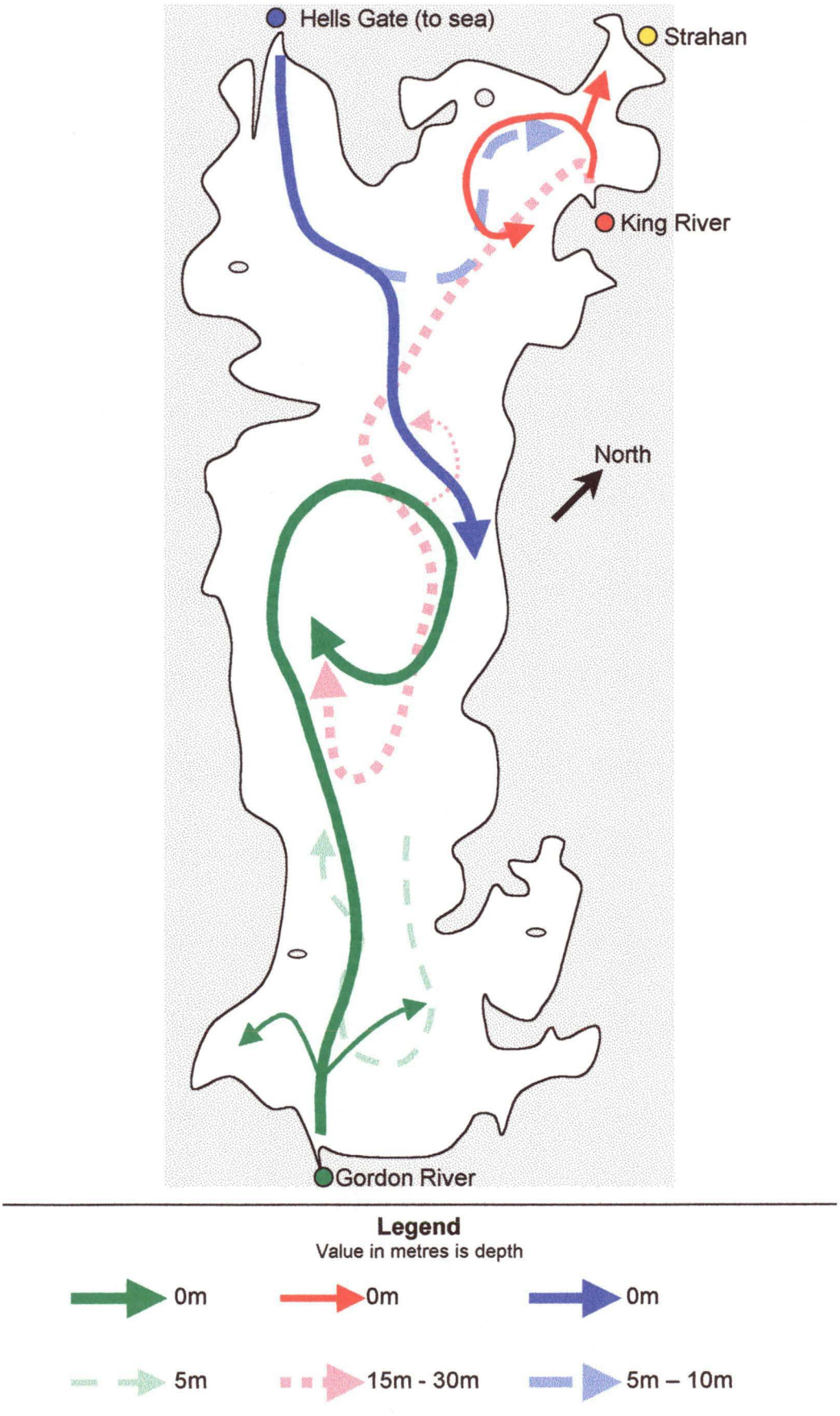

Figure 6.1 **Flood** tide in Macquarie Harbour, arrow width indicates flow rate and arrow colour indicates water source and depth

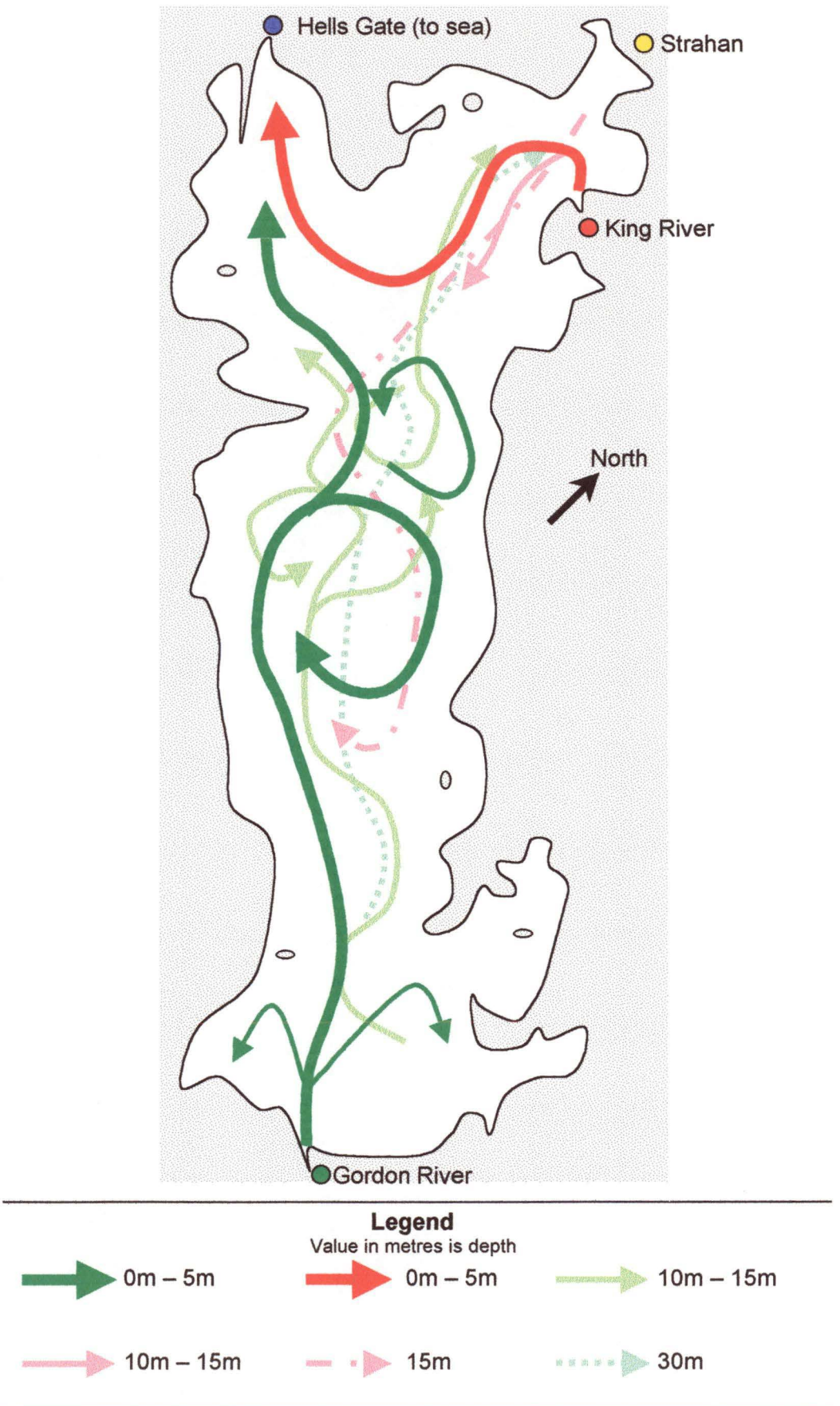

Figure 6.2 Ebb tide in Macquarie Harbour, arrow width indicates flow rate and arrow colour indicates water source and depth

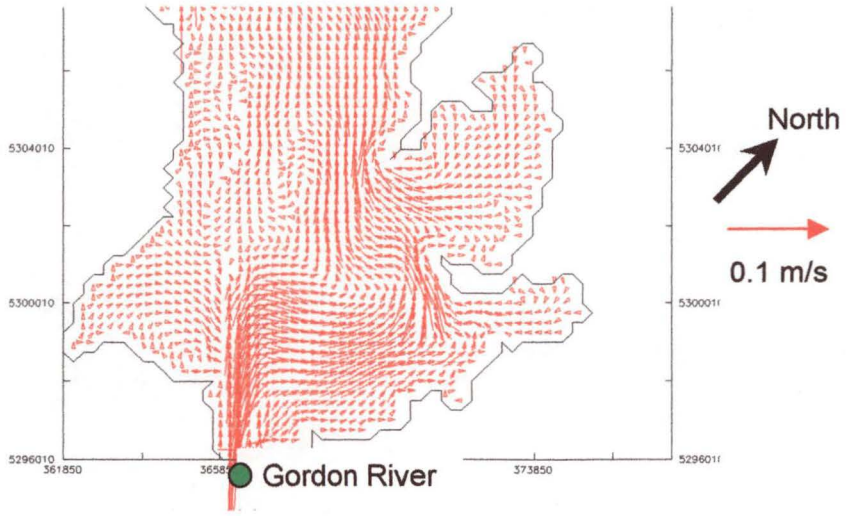

(a) Incorrect sign on Coriolis force (sign negative)

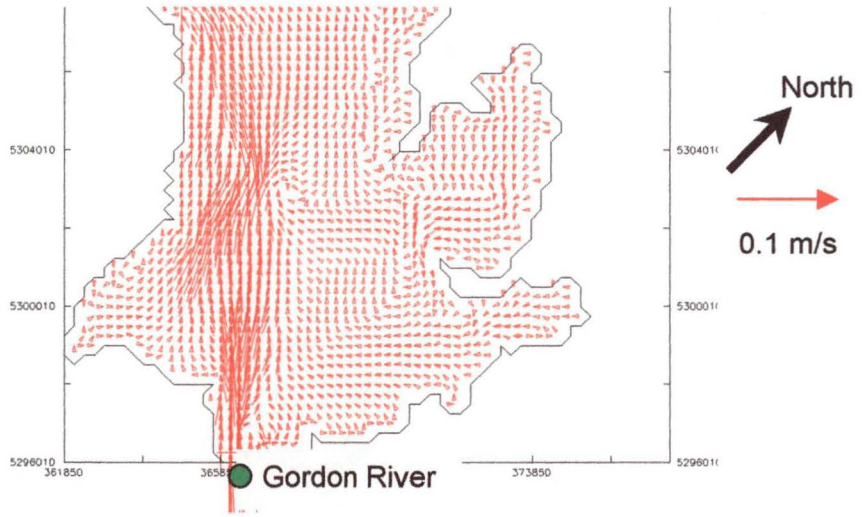

(b) Correct sign on Coriolis force (sign postive)

Figure 6.3 Effect of sign change on Coriolis force for southern Macquarie Harbour

The dominant surface feature of the harbour south of Liberty Pt is the clockwise recirculation of the Gordon River water. The Gordon River water flows up the western side of the harbour at the surface, and is redirected by Liberty Pt, the King River water and the tide, to flow back down the eastern side of the harbour. The surface elevation is depressed at the centre of the eddy south of Liberty Pt, just as air circulates clockwise around a low pressure system in the southern hemisphere. With the depressed surface elevation accessing the deeper saltier water, the surface salinity is higher at the centre of the eddy.

During an ebb tide, the Gordon River water can flow seaward at the surface, but a flood tide blocks this flow. In the deeper parts of the harbour, water from the southern end of the harbour flow northward during an ebb tide.

In the northern end of the harbour, water from the King River flows south at the surface and also below the halocline. During a flood tide the King River re-circulates at the surface as the tidal flow enters under it at 5m – 10m and blocks its seaward movement, the tidal flow then joins with the King River water and flows south at 15m – 30m. During an ebb tide the King River water flows out to sea at the surface, and into the southern harbour between 10m and 15m. In that 10m – 15m range, water from the large surface eddy south of Liberty Pt, flows into the northern harbour.

6.3 Scalar transport in harbour

The scalar quantities vary in the harbour on different time scales. As expected, during the day/night cycle the surface temperature will increase and decrease. On the tidal cycle the salinity in the shallows of the harbour near Hells Gates will increase and decrease, and the pollution changes with the harbour development time scale. The salt transport is important for the harbour circulation because the density is a stronger function of salinity than temperature or pollution. As the least significant in terms of harbour circulation, the pollution is of the most interest from a harbour management point of view, especially in relation to the location of fish farms within the harbour.

The salinity profile of Macquarie Harbour changes during both a tidal and seasonal time scale (Cresswell, Edwards, and Barker, 1989). The model simulation runs for this thesis, use periods of a week to a month and only show the tidal variation. During the tidal period, the salinity profile remains stratified and oscillates, as shown in Figure 6.4 by the depth to the 20‰ isohaline. Unlike the surface waves that have a density difference at the interface between the water and air of over 1000kg/m^3, the isohaline interface has a density difference of approximately 20kg/m^3. This means the isohaline does not have the same buoyancy and gravity forces acting on it, and while the surface elevation is changing only 0.1m to 0.2m, the 20‰ isohaline can vary in position up to 1.0m.

The structure is more complicated than represented by the simple line graph in Figure 6.4, as shown in the perspective projection of the 20‰ isohaline, shown with a vertical colour salinity section mid harbour in Figure 6.5. In Figure 6.5 the fresher (blue) water on the western (left) side of the harbour, shown in the vertical colour slice, is water from the Gordon River.

The extent of the low salinity water from the Gordon River and King River in the harbour, depends on the flow rate of the respective river. Higher flow rates will create a larger plume of river water at the surface of the harbour. The freshwater plume from the rivers and the salty seawater is shown at the turning points of the tide in Figure 6.6. As the tide turns from flood to ebb, the high surface salinity near Hells Gates is due to seawater. As the tide changes from ebb to flood, the river plumes are closer to Hells Gates (compared to when the tide changed from flood to ebb), due to the surface flow out to sea.

To investigate the effect of Gordon River flow on the salinity plume and general circulation, ten day simulations with the Gordon River flow rate at $10m^3/s$, $200m^3/s$, and $300m^3/s$, were compared. The river flows were ramped up to full flow over one day and left to run for a total of ten days. Figure 6.7 demonstrates that under low Gordon River flow there is a greater intrusion of sea water at Hells Gates. At the same time the pollution plume is pushed north (Figure 6.9). Interestingly the higher Gordon River flow also increases the fresh plume from the King River, because the Gordon River blocking the effects of the tide which usually effect the King River water.

The vertical section C-C' shown on Figure 6.6 is taken just north of Elizabeth Is to observe the salt entering the harbour from the sea. Figure 6.8 shows the salinity on section C-C', with the small intrusion of saline water on the flood tide when the Gordon River is flowing at $200m^3/s$, and a much saltier flood tide when the Gordon River is flowing at $10m^3/s$. This suggests that the Gordon River flow controls the salt flux at the harbour entrance. As a result of this, during a normal flow rate of $200m^3/s$, the Gordon River will produce a net out flow of salt in the harbour, while at a low flow rate of $10m^3/s$, the net salt flux is into the harbour from the sea. As the salt is leaving the harbour under normal flow rates, the saline water in the deeper parts of the harbour must have been transported there either in large seas that occur during storm events, or when there are low Gordon River flows.

To quantify the effect of the Gordon River flow on scalar transport, the pollution concentration and salinity where integrated on four vertical sections in the harbour: between Liberty Pt and Sophia Pt, the mouth of the Gordon River, the mouth of the King River, and the entrance to the harbour from the sea. This integration was performed for three flow conditions to give a flux in kg/min for each section. For the three sections where the river model joins the harbour, the integration between time t_1 and t_2 for a scalar f is

$$I_{river} = B\int_{t_1}^{t_2} D\int_{-1}^{0} Fu\, d\sigma\, dt \qquad (6.1)$$

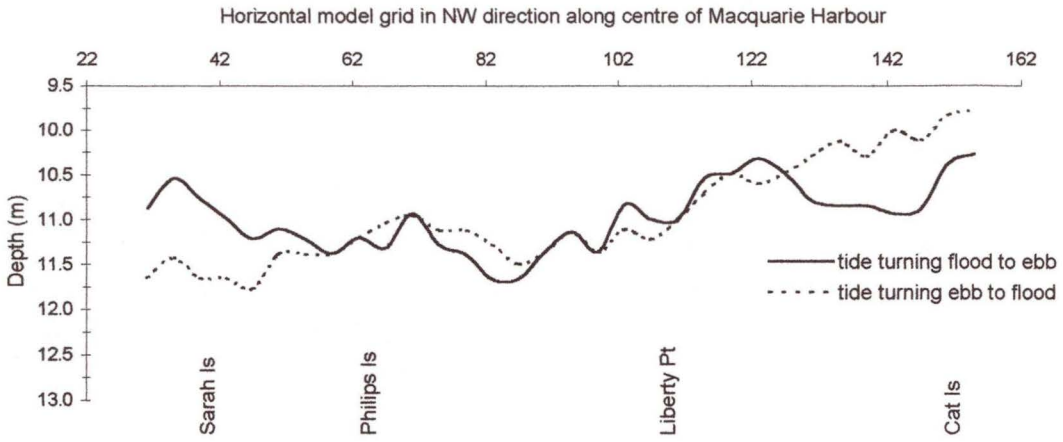

Figure 6.4 Depth to 20‰ isohaline on centre line of harbour for turning points during tidal cycle, with a Gordon River flow rate of 200m^3/s

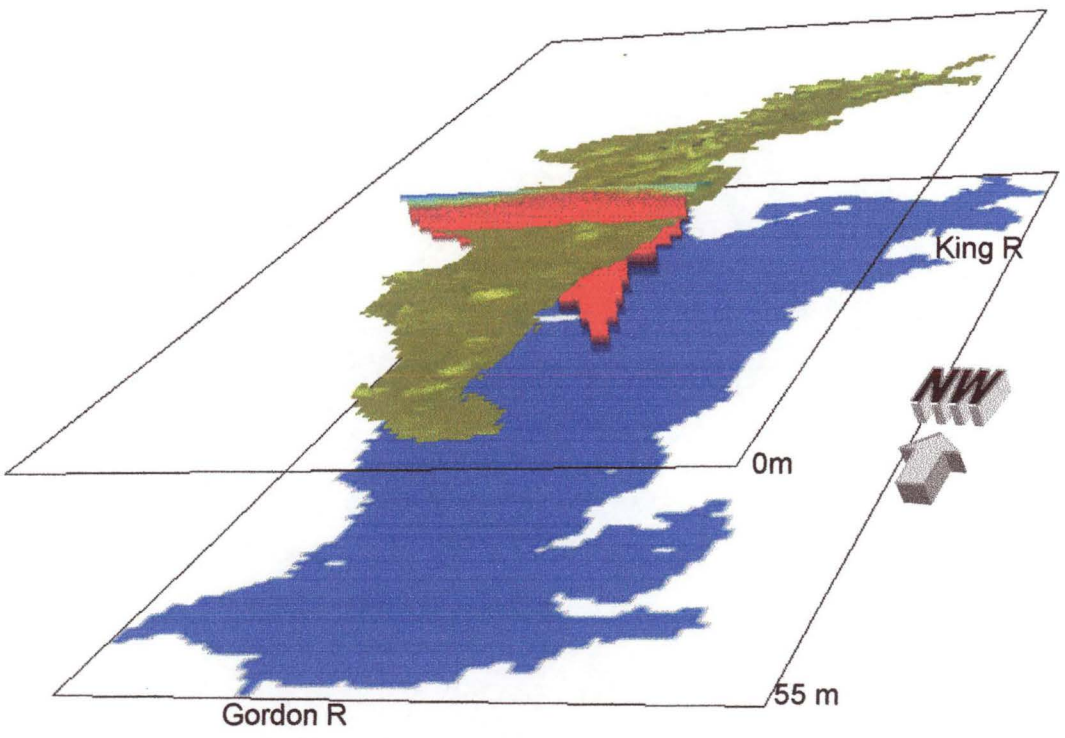

Figure 6.5 Perspective view of 20‰ isohaline (brown) in Macquarie Harbour at tide turning flood to ebb, located at a depth of approximately 11m. Shown also is a vertical salinity profile just north of Philip Is (red is saline water, blue is low salinity water). The large blue shape at 55m is a harbour outline.

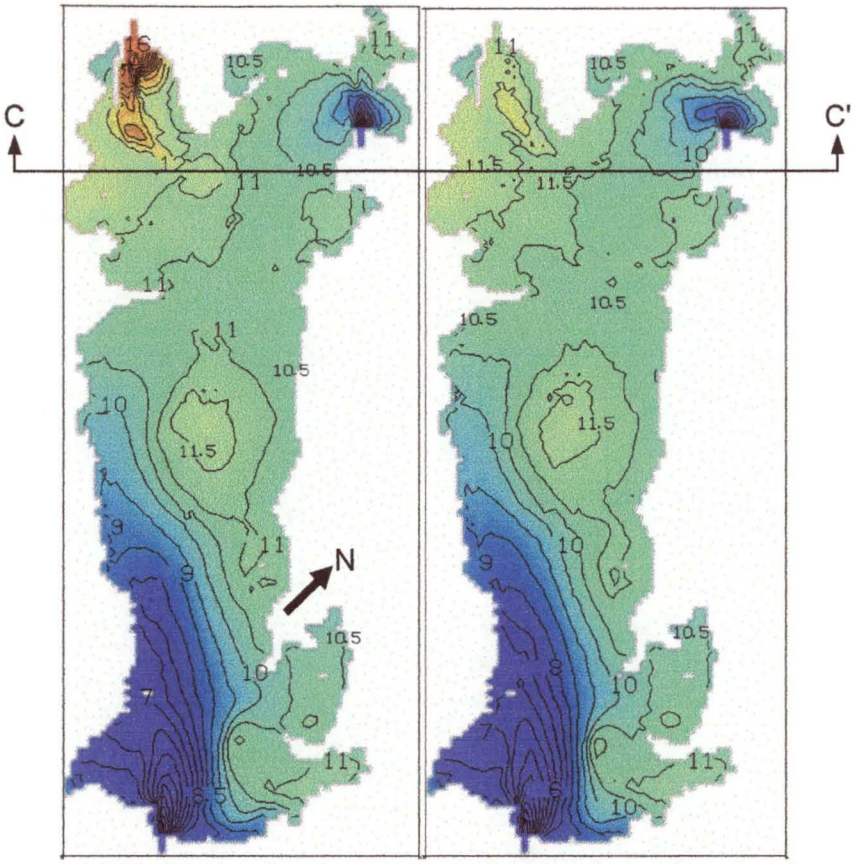

Figure 6.6 Surface salinity (‰) in Macquarie Harbour with 0.5‰ contours, a Gordon River flow of 200m^3/s and a King River flow of 70m^3/s

Where F is equal to f for pollution concentration or equal to $f\rho$ for salinity (to keep the flux in consistent units). Changing (6.1) to the discrete form used by the model makes the integration a summation

$$I_{river} = \Delta t BD \sum_{k=1}^{KB} (F_k u_k \Delta \sigma_k) \tag{6.2}$$

Where Δt is the internal time step equal to one minute. For the harbour integration, a section is defined by a line ξ, with ξ_i is a point on ξ. The line starts at grid point $\xi_s = (x_s, y_s)$ and finishing at grid point $\xi_f = (x_f, y_f)$, and the integration is

$$I_{harbour} = \int_{\xi_s}^{\xi_f} \int_{t_1}^{t_2} D \int_{-1}^{0} F u_\xi \, d\sigma \, dt \, d\xi \tag{6.3}$$

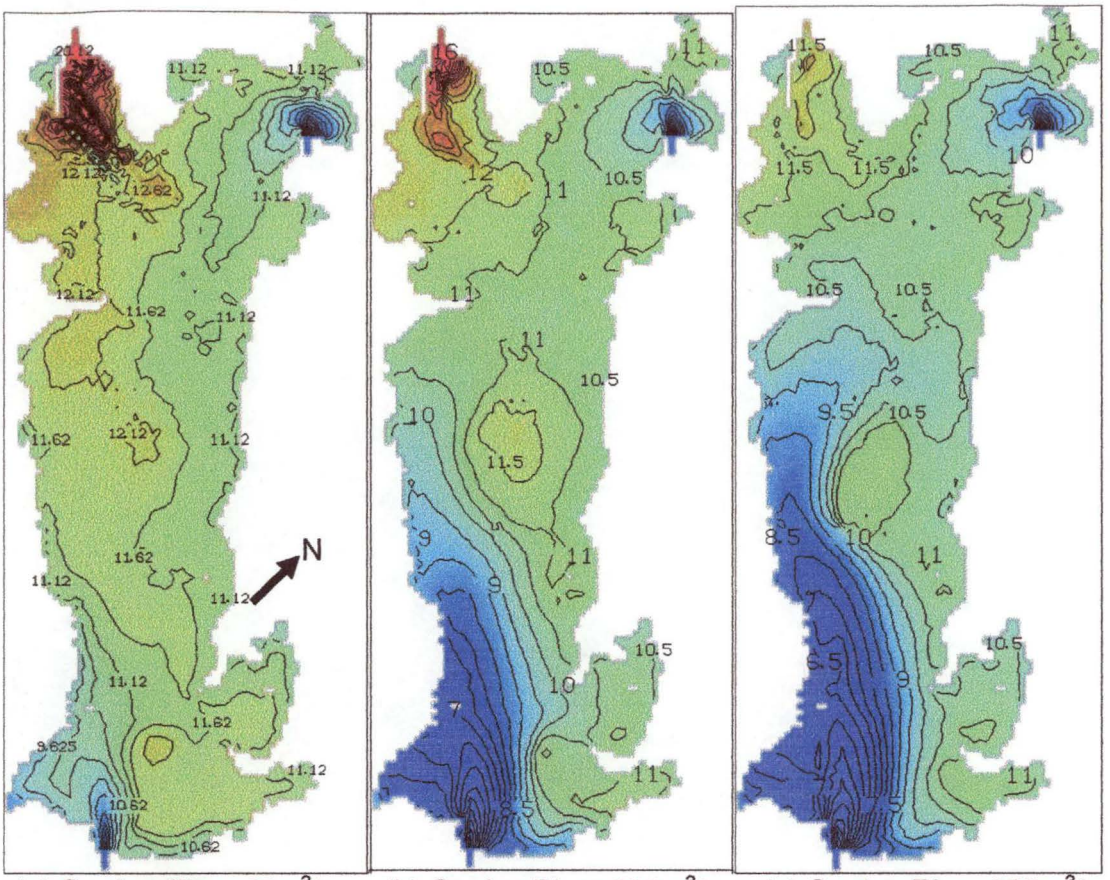

Figure 6.7 Surface salinity (‰) with 0.5‰ contours for different Gordon River flow rates, all with a King River flow rate of 70m³/s after 10 days of simulation

Where u_ξ is the velocity perpendicular to ξ, defined in terms of the x and y horizontal velocity components,

$$u_\xi = u\cos\theta - v\sin\theta \tag{6.4}$$

$$\theta = \arctan\left(\frac{y_f - y_s}{x_f - x_s}\right) \tag{6.5}$$

Changing (6.3) to a discrete form gives

$$I_{harbour} = \Delta t \sum_{\xi_i=\xi_s}^{\xi_f}\left(D\sum_{k=1}^{KB}\left(F_k u_{\xi k}\Delta\sigma_k\right)\right)_{\xi_i} \tag{6.6}$$

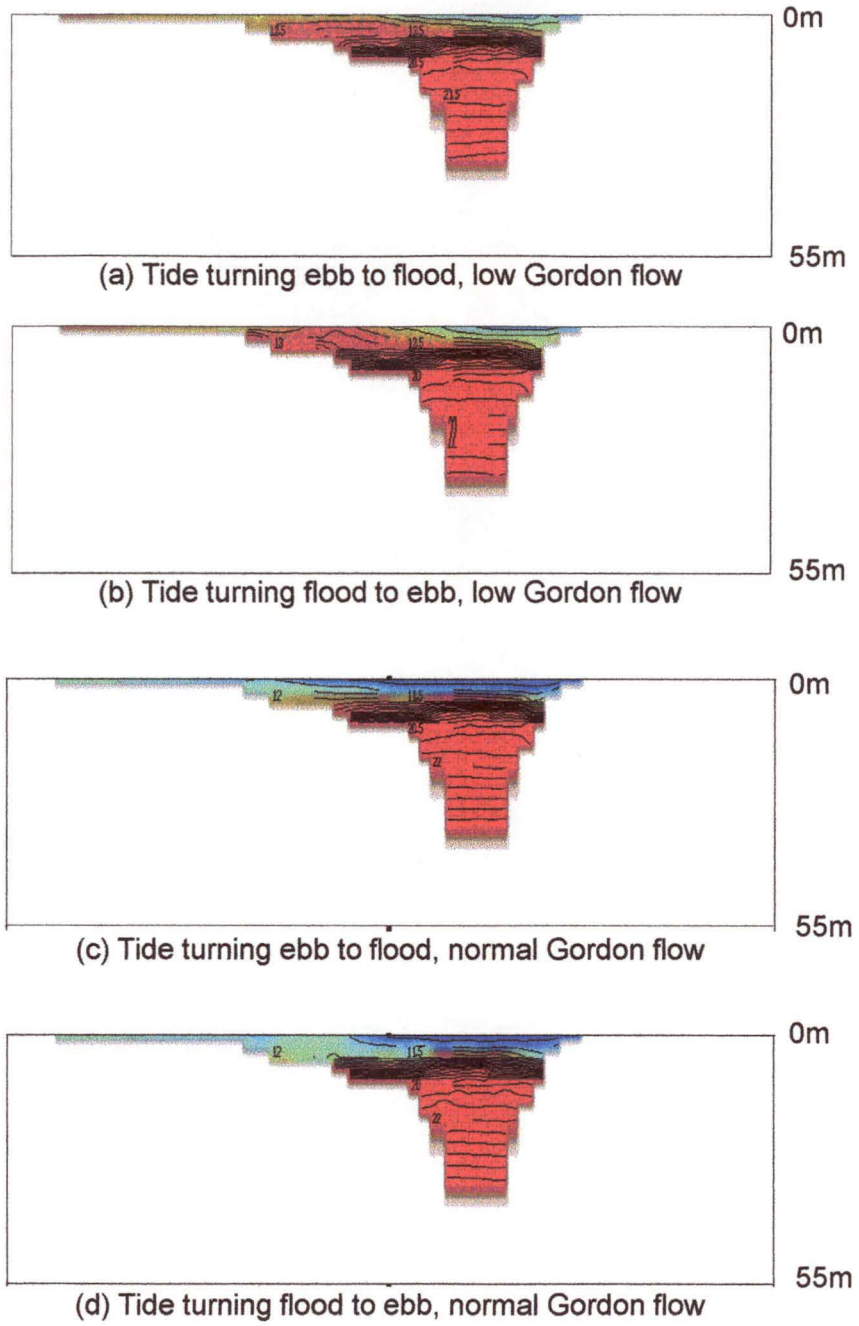

Figure 6.8 Salinity on section C-C' of Macquarie Harbour with 0.5‰ contours, for Gordon River flow of $10m^3/s$ in (a) and (b), and $200m^3/s$ in (c) and (d), King River flow is constant at $70m^3/s$

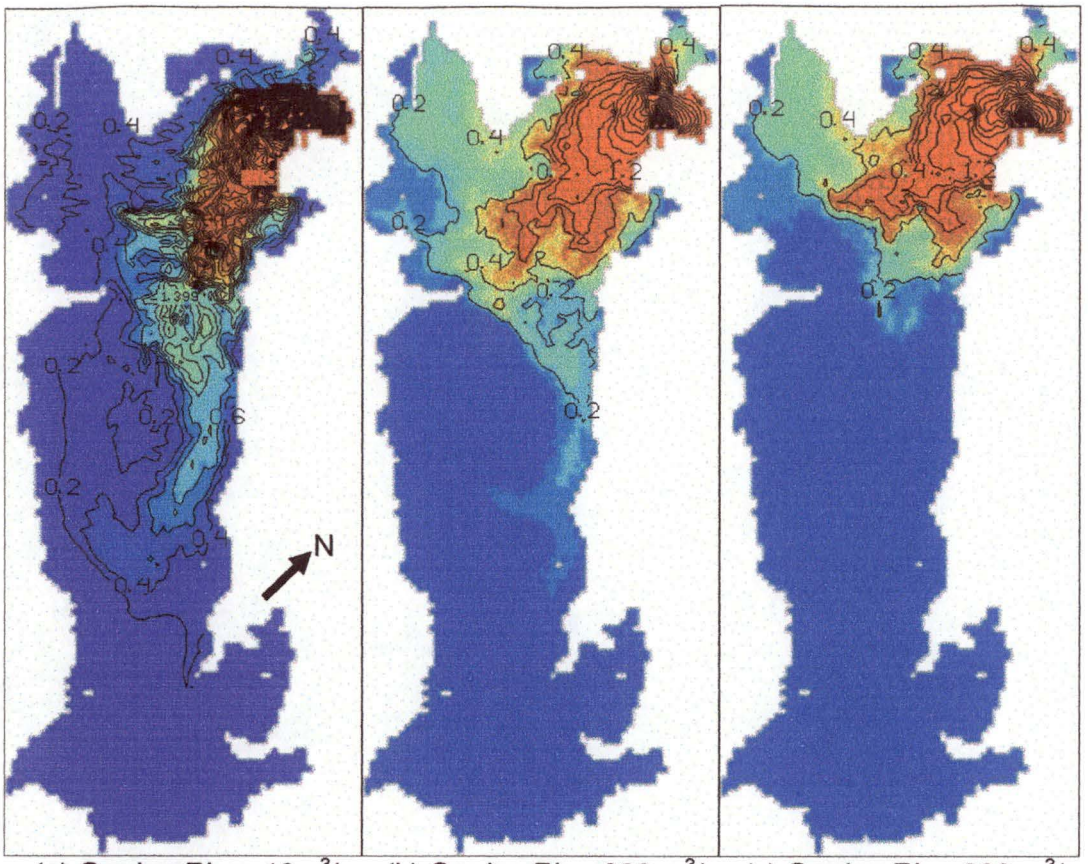

Figure 6.9 Surface pollution (g/m^3) with 0.2g/m^3 contours for different Gordon River flow rates, all with a King River flow rate of 70m^3/s after 10 days of simulation

The model was run for 10 days with a Gordon River flow of 200m^3/s and a King River flow of 70m^3/s (ramped over the first day). At this time the integration was done between days 10 and 12, keeping the river flow rates constant. The pollution fluxes are plotted for all sections in Figure 6.10, except the Gordon River mouth section because the flux was too small.

At day 12 the flow was ramped down over one day to a Gordon River flow rate of 10m^3/s and a King River flow rate of 5m^3/s. At day 22 the integration was calculated again over a 1.8 day period with the flow rates constant, with the results plotted in Figure 6.11.

Starting from day 22 again, an alternative flow regime was then used. This time the flow in the King was ramped up to 70m^3/s over one day and then keep constant. The Gordon River flow rate was kept at 10m^3/s. The fluxes from the integration carried out from the alternative day 22 to day 26 are shown in Figure 6.12.

The Gordon River pollution fluxes are plotted in Figure 6.13 for normal and low flow rates on an arbitrary time axis. The normal flow rate corresponds to Figure 6.10 and the low rate case corresponds to Figure 6.12. The data from Figure 6.11 is the same Gordon River flux as Figure 6.12 and so is not plotted in Figure 6.13.

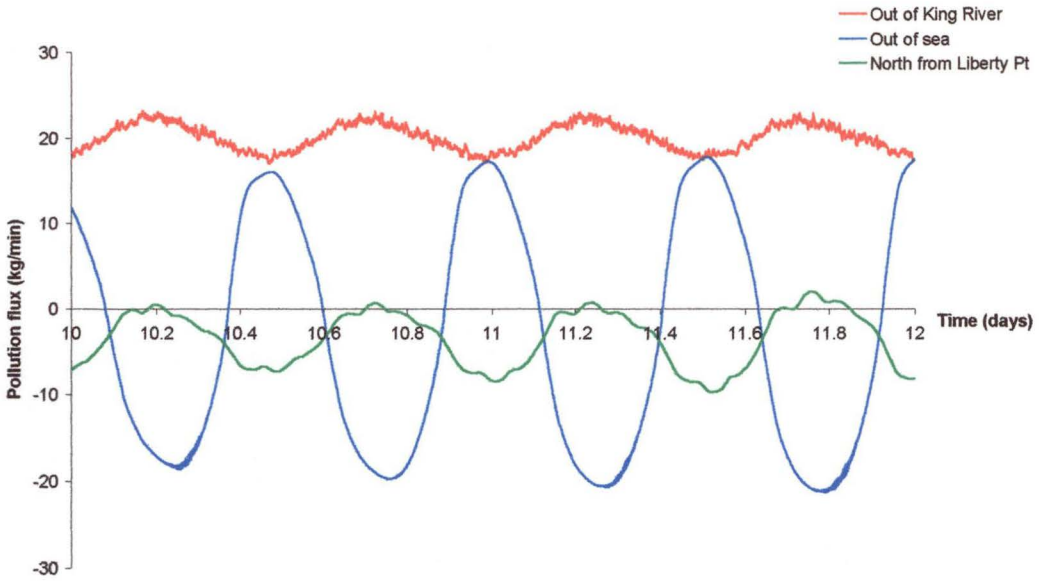

Figure 6.10 Pollution flux in Macquarie Harbour, day 10 to day 12, with a Gordon River flow of 200m/s³ and King River flow of 70m/s³, pollution in King River at 10g/m³

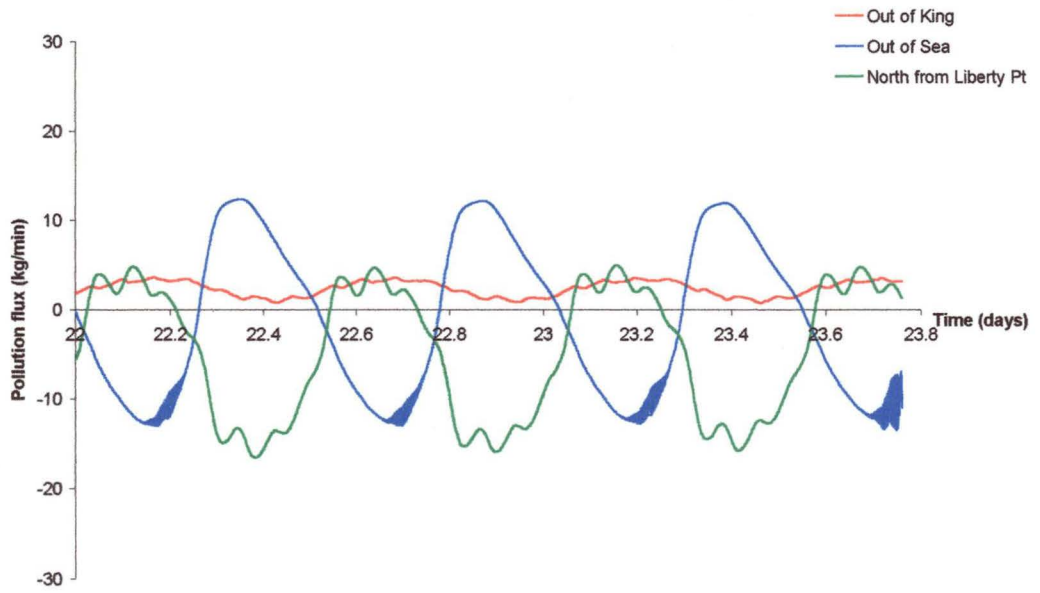

Figure 6.11 Pollution flux in Macquarie Harbour, day 22 to day 23.8, with a Gordon River flow of 10m/s³ and King River flow of 5m/s³, pollution in King River at 10g/m³

The dominant feature of the three figures (Figure 6.10, Figure 6.11, and Figure 6.12) is the tidal cycle, and in order to compare the figures a tidal average is required. In the case of Figure 6.12 this averaging was performed after the King River flow had been ramped up to 70m^3/s and pollution was being transported south of Liberty Pt (between days 27 and day 28). These tidal averages are given in Table 6.1. The Gordon River flux differs between

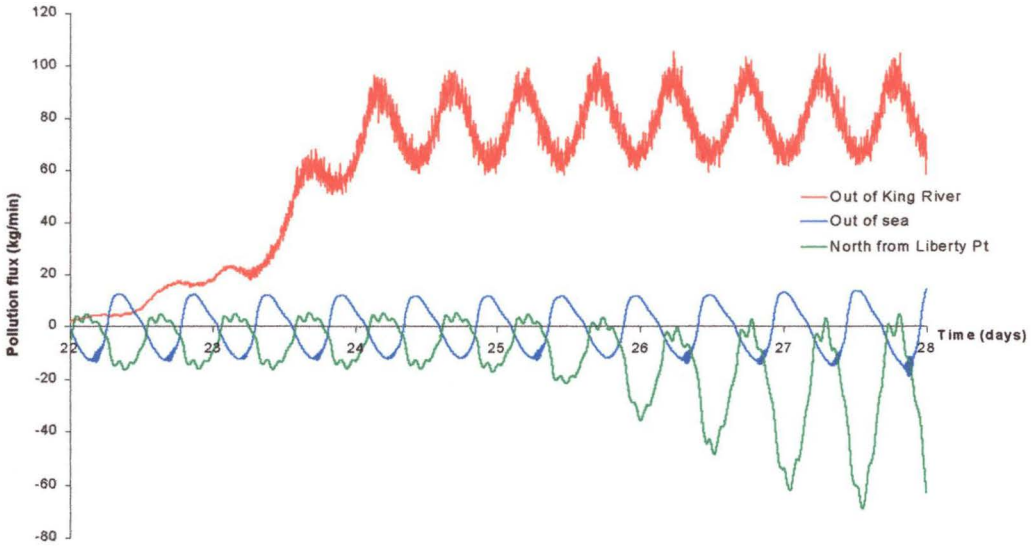

Figure 6.12 Pollution flux in Macquarie Harbour, alternate day 22 to day 28, with a Gordon River flow of 10m/s³ and King River flow linearly changes 5m/s³ to 70m/s³ during day 22 to day 23, then constant at 70m/s³, pollution in King River at 10g/m³

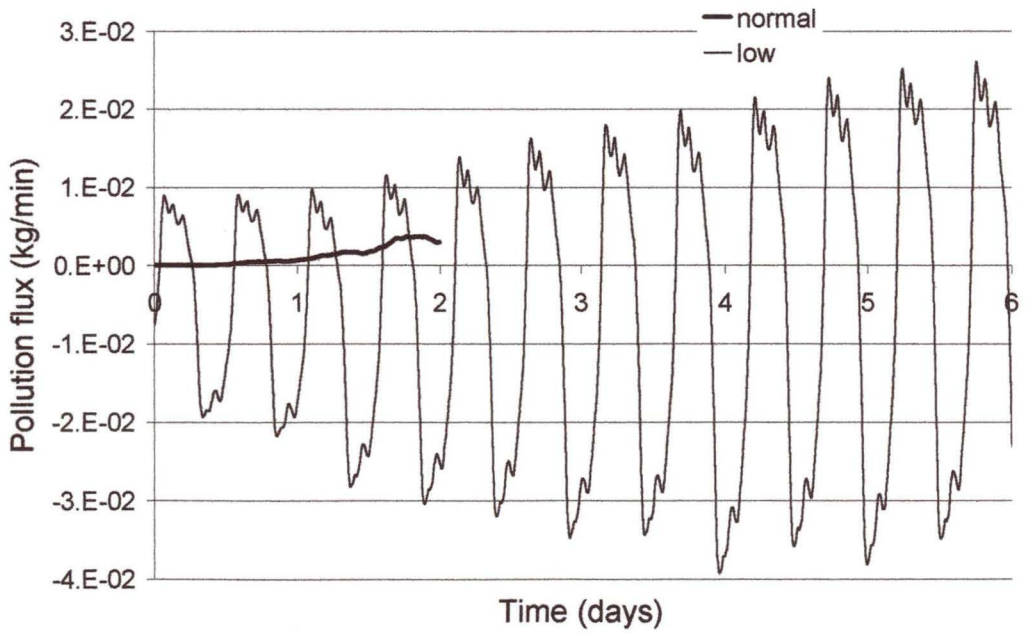

Figure 6.13 Gordon River pollution flux for flow rates that are normal (200m^3/s) and low (10m^3/s)

the second and third cases (although the flow rate is the same), because the third case is averaged over a longer time than the second case.

Table 6.1 shows how the pollution flux from the King River is reduced in value with the flow rate, but then increases above the original level when the flow rate is increased back to the

Section of harbour	Pollution flux (kg/min)		
	normal for both	**low for both**	**King R normal Gordon R low**
Out of King River	20.1	2.24	79.8
Out of sea	-2.74	-0.445	-0.862
North of Liberty Pt	-3.21	-5.43	-29.6
Out of Gordon River	1.84×10^{-3}	-3.58×10^{-3}	-4.71×10^{-3}

Table 6.1 Pollution fluxes in Macquarie Harbour after tidal averaging for three flow configurations of the King River and Gordon River, for Gordon River the normal flow rate is 200 m^3/s and low flow rate is 10 m^3/s, for King River the normal flow rate is 70 m^3/s and low is 5 m^3/s

normal flow rate. This highly polluted plume of water from the King River, typically occurs when the John Butters Power Station (on the King River) is turned on after a period of low flow rate. With low Gordon River flow, this highly polluted plume does not get transported out to sea, but instead resides in the northern harbour and also is transported south of Liberty Pt (Figure 6.9 a).

Even without the highly polluted plume of water from the King River, there is more polluted water transported south of Liberty Pt when the Gordon River has low flow. This is because the Gordon River, when flowing normally, blocks the King River water at Liberty Pt on the surface where most of the pollution resides (see Figure E.7 and Figure E.8 in Appendix E). When the Gordon River flow rate is reduced, the King River water flows south and transports the pollution with it, as the tide blocks most of the seaward flow.

The pollution flux at the mouth of the Gordon River is directed into the harbour for normal flows and into the river for low flows (Table 6.1). The noticeable feature in the low flow case is how tidally affected the pollution flux is. There are also higher frequency oscillations superimposed on top of the tidal frequency, due to wave reflection around the harbour from the various bays and points.

Using the same approach for salinity as was used for pollution concentration, Table 6.2 was generated for salt fluxes. Plots are not given as they have the same form as the pollution concentration flux graphs, but are more periodically regular. The King River salt flux from Table 6.2, is more dependant on the Gordon River flow rate than its own flow rate. This indicates the Gordon River is responsible for blocking the tidal flow and allowing the King to flow out to sea. A higher King River flow does not effect the Gordon River circulation significantly, as evident from the lack of effect it has on the pollution or salt fluxes.

Section of harbour	Salt flux (tonne/min)		
	normal for both	low for both	King R normal Gordon R low
Out of King River	12.2	5.01	6.72
Out of sea	-217	40.8	19.8
North of Liberty Pt	70.3	7.22	16.7
Out of Gordon River	107	-3.06	-3.02

Table 6.2 Salt fluxes in Macquarie Harbour after tidal averaging for three flow configurations of the King River and Gordon River, for Gordon River the normal flow rate is 200m^3/s and low flow rate is 10m^3/s, for King River the normal flow rate is 70m^3/s and low is 5m^3/s

The Gordon River flow rate is the factor determining the direction of salt fluxes at the mouth of the Gordon River and leaving the harbour to the sea. Normal Gordon River flow rates transport salt out of the Gordon River and out of the harbour, while the opposite occurs for low flow rates. Whereas the King River flow rate does not have a straight forward relationship with salt fluxes, due to the effect of the King River water on blocking the water from the Gordon River. Increasing the King River rate from low to normal will decrease the salt flux out to sea and increase its flux north of Liberty Pt. This confirms the harbour circulation results, that water from the King River has a complicated flow once it enters the harbour, flowing south at move than one depth.

The temperature distribution follows the same general pattern as the salinity. As the rivers are cooler than the harbour, a cool plume is evident – similar to the fresh water plume in the salinity distribution. The main features of the temperature distribution are the vertical distribution, the river plumes, and the heating/cooling near the surface of the diurnal cycle (Figure 6.14).

6.4 Wind response

The shallow nature of Macquarie Harbour make its circulation sensitive to passing weather patterns. This section investigates the circulation and water quality transport due to wind stress on the surface of the harbour. Two typical wind cases are used (where times given is simulated time):

1. A 2.5m/s north-west (NW) wind is applied for two days, followed by two days of a 10m/s NW wind, the change ramped over one hour.
2. Similar to case 1 for the first four days, with the wind from the SE not the NW. Then the wind swings clockwise to the NE over another four days, still at 10m/s.

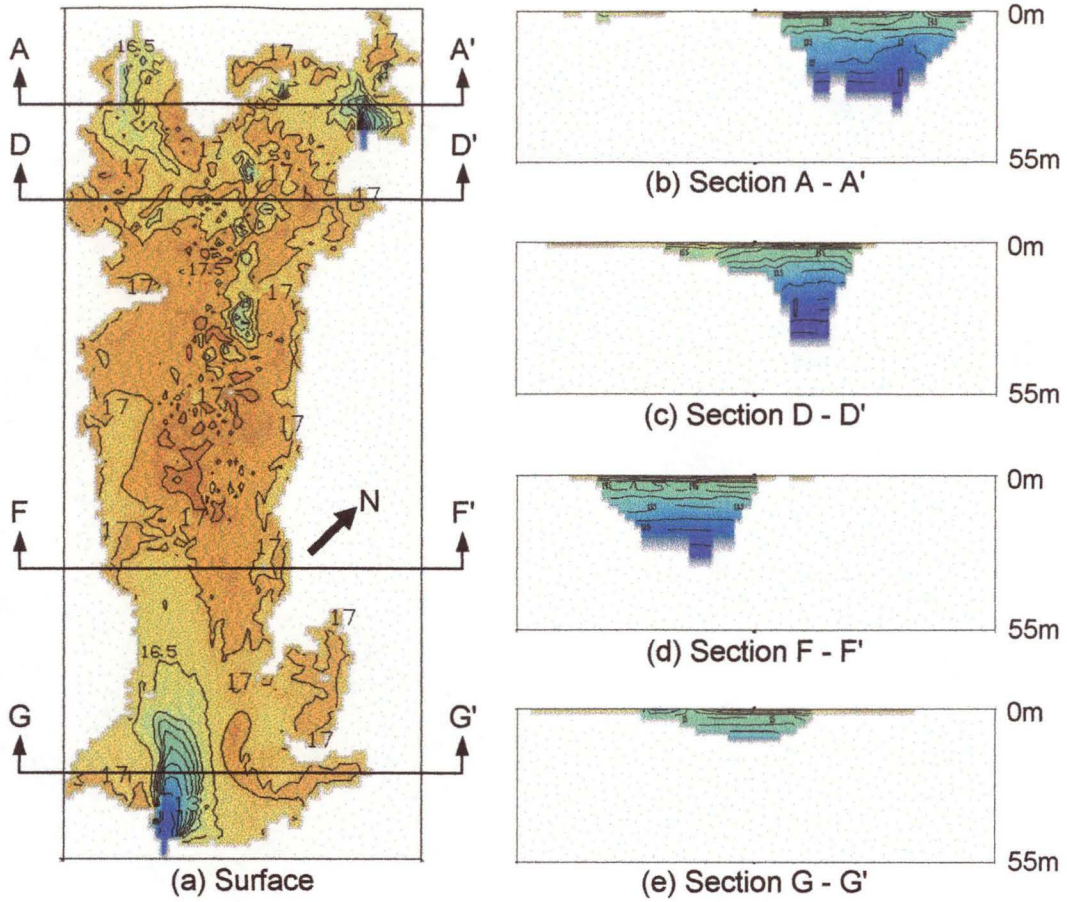

Figure 6.14 Temperature (°C) in Macquarie harbour during day with 0.5°C contours

The wind causes a change in the circulation, strong scalar mixing above the halocline, and transport of surface scalars. In both wind cases the river flow rates were keep constant, with a Gordon River flow rate of $200m^3/s$ and a King River flow rate of $70m^3/s$. Figure 6.15 shows the surface circulation and surface salinity from the first wind case during an ebb tide at the end of two days of 2.5m/s NW wind and end of two days of 10m/s NW wind. Note, when comparing the velocity plots in Figure 6.15 to the no wind case in Appendix E (Figure E.2 at 0m), that the velocity scales are different - a 5mm vector is 0.4m/s in Figure 6.15 and 0.2m/s in Appendix E.

The application of wind from the NW, changes the surface circulation to flow in the direction the wind is blowing. The surface elevation changes to maintain the momentum balance with the extra force created by the wind stress. The water surface is forced up against the downwind side of the harbour, increasing the surface elevation near the mouth of the Gordon River by approximately 0.3m between having and not having wind (Figure 6.16). The 2.5m/s and 10m/s cases increased the surface elevation a similar amount.

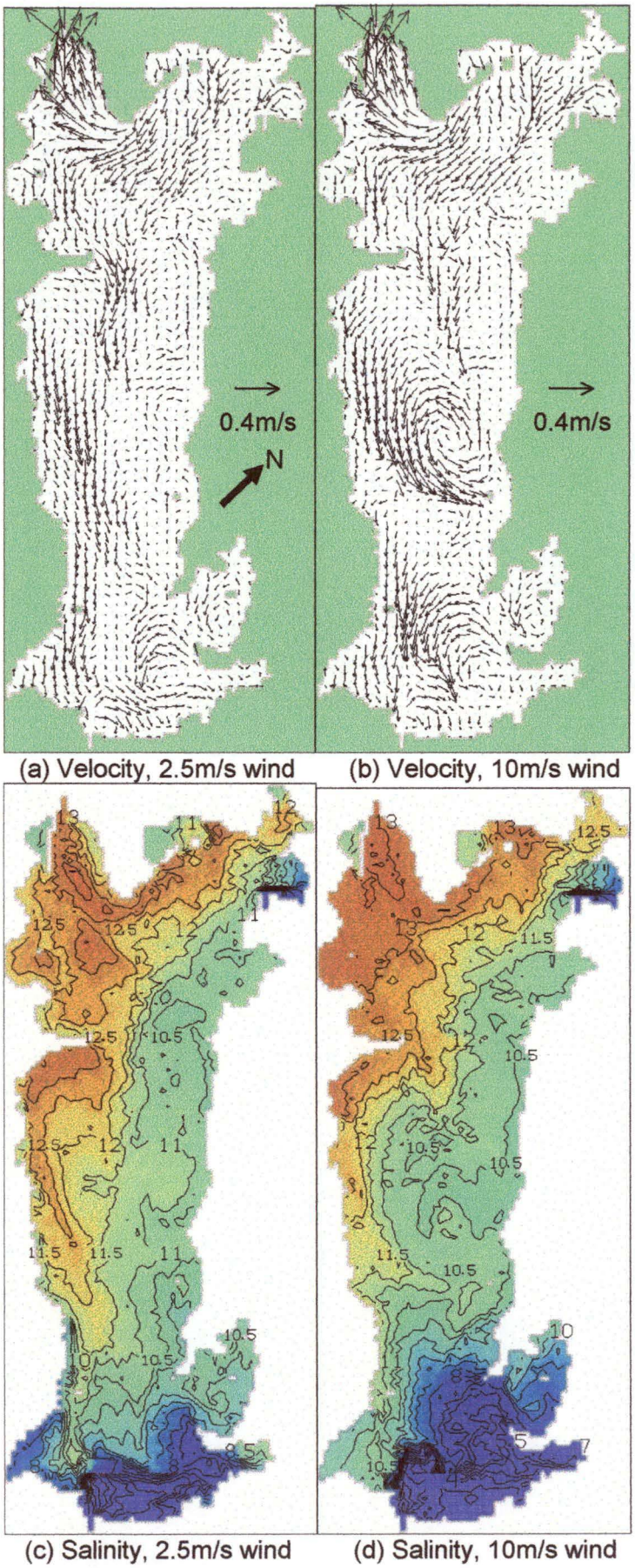

Figure 6.15 Surface velocity and surface salinity (‰) with 0.5‰ contours, at ebb tide in Macquarie Harbour for NW wind (speeds of 2.5m/s and 10m/s)

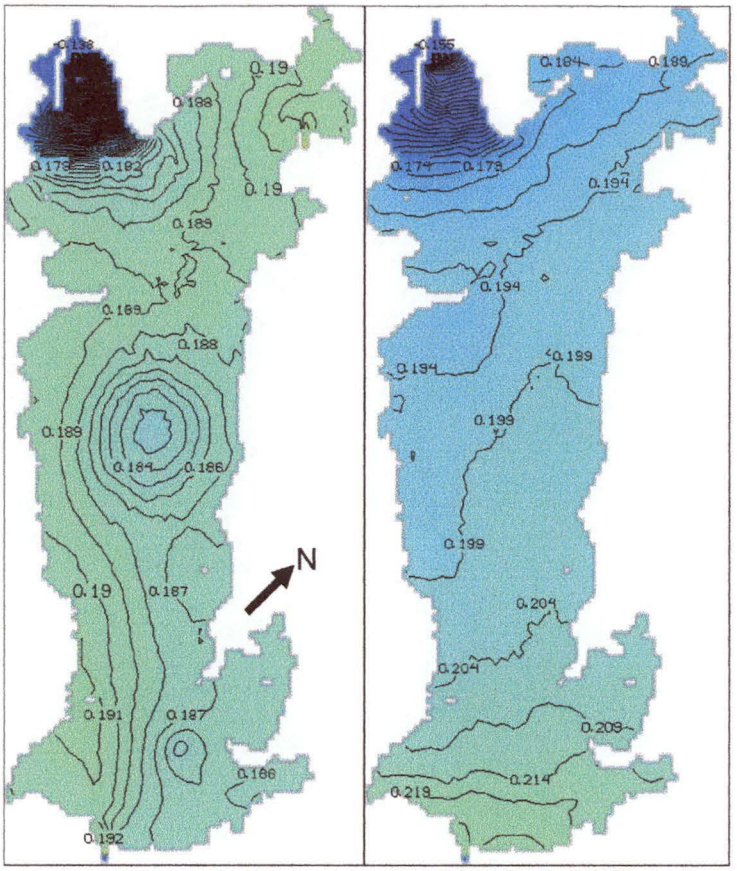

(a) no wind (b) 2.5m/s NW wind

Figure 6.16 Surface elevation during ebb tide, with 0.001m contours for no wind case and 0.005m contours for wind case

Changing the wind speed from 2.5m/s to 10m/s causes large surface eddies, as the circulation is changed deeper into the water column. There is also greater mixing through the water column as event in the surface salinity plot (Figure 6.15.c and Figure 6.15.d). The water is more saline near Hells Gates because the recirculating water, flowing in the opposite direction to the surface water, is transporting the deeper (saline) water to the surface.

In general, the wind causes the water just above the halocline to recirculates in the opposite direction to the surface flow to maintain continuity, with other flow reversals through the water column. This is shown clearly in some of the velocity plots from the second wind case. While the main output for the second wind case is given in Appendix F, Figure 6.17 gives typical horizontal velocity profiles off Liberty Pt.

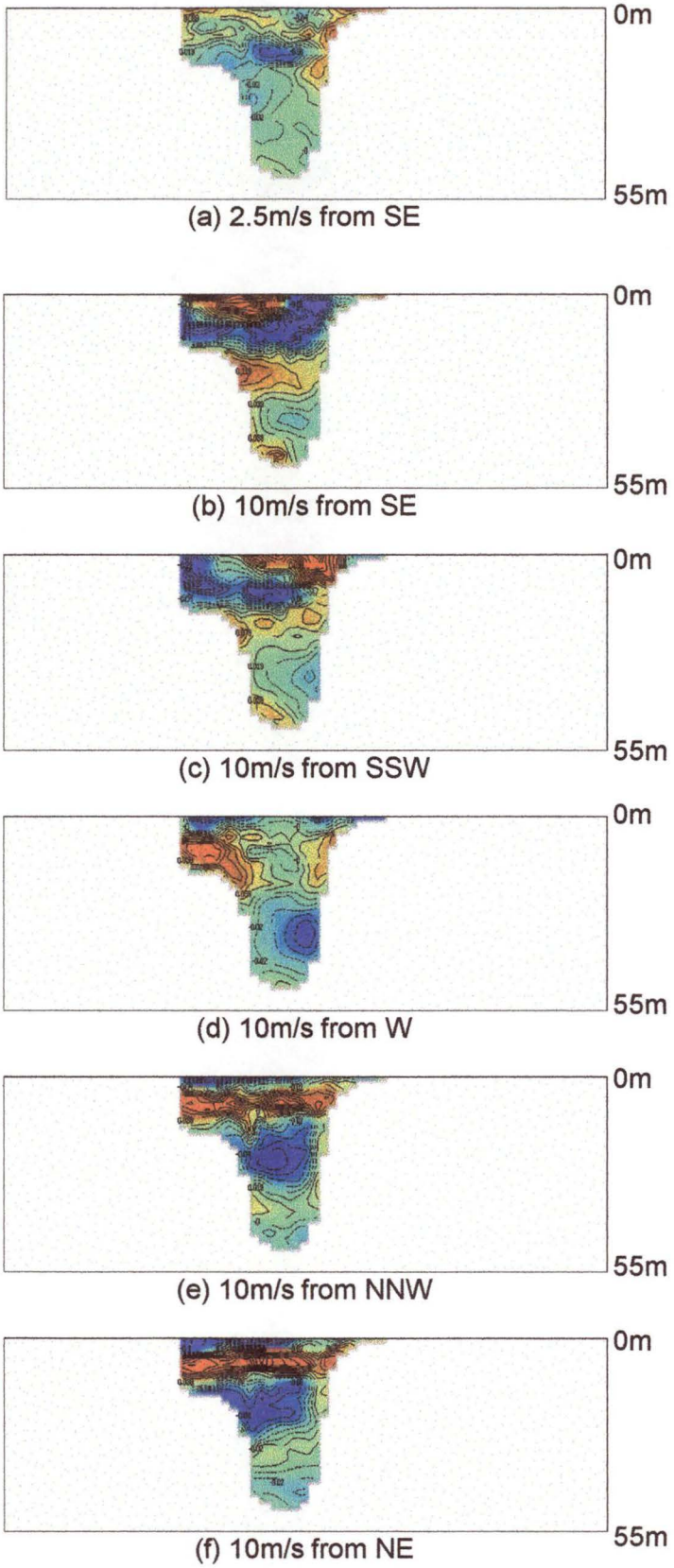

Figure 6.17 Horizontal velocity (NW direction) on section E-E' (near Liberty Pt defined in Figure E.4, Appendix E), contours in 0.02m/s, red is positive (into page), blue is negative (out of page)

Comparing the horizontal velocity profiles off Liberty Pt, between the second wind case (Figure 6.17) and when there is no wind (Figure E.5.c and Figure E.6.c in Appendix E), the effect of the wind is noticeable throughout the entire water column. The density stratification caused by the halocline, allows a degree of independence for the circulation above and below the stratification. As the wind swings clockwise around from SE to NE, the effect of the halocline (between 8m and 12m) is evident on the changing velocity profile, especially in Figure 6.17.b, Figure 6.17.c, Figure 6.17.e, and Figure 6.17.f.

In the more detailed output for the second wind case given in Appendix F, the horizontal sections in Figure F.1, Figure F.2, and Figure F.3 show the effect of the wind, indicated in the vertical profiles from Figure 6.17, are harbour wide. While the surface elevation (Figure F.4) and surface salinity (Figure F.5) give some indication of the wind's effect at the surface, the changes to the surface pollution concentration (Figure F.6) are more dramatic. The plume of pollution from the King River acts like a windsock, moving with the prevailing wind.

6.5 Verification of harbour circulation

The harbour circulation from the model was compared to field data collected over three days using a broadband acoustic doppler current profiler (BB-ADCP) (Koehnken, 1996). During these three days the tide in Macquarie Harbour was semi-diurnal, with daily wind averages at Granville Harbour indicating SSE to SSW wind at 5m/s to 10m/s (CFMI, 1995a). The BB-ADCP would only work in water up to 25m in depth, limiting the coverage of the harbour (Koehnken, 1996). Velocity was recorded on only 25 sections in the three days and all but one section was taken in the harbour north of Liberty Pt. The sections varied in length from 220m to 9380m and were usually curved in plan, which made is difficult to compare to the straight sections from the VIS5D output.

As the harbour is sensitive to the wind, and without knowing the accuracy of the BB-ADCP data and only knowing the approximate wind conditions during the measurement period, there can not be an accurate verification of the model. With the complexity of the harbour circulation indicated by the model, there would need to be hundreds of velocity sections measured over weeks, to verify the model accurately. As the aim of the modelling was to give the general circulation of the harbour, the BB-ADCP will indicate if the model is reasonable or unreasonable.

The velocity section that gave the clearest indication of the harbour circulation was recorded between Liberty Pt and Sophia Pt on a flood tide on 29 September 1993. Due to the BB-ADCP's depth limitation of 25m, the entire section was not recorded and two sections have been joined. As the BB-ADCP graphical output uses the same size graphics for a section

irrespective of the section length, the two parts of the Liberty Pt – Sophia Pt section needed to be scaled and cropped to be viewed together in Figure 6.18 (Lawson and Treloar, 1994). The dominate features of Figure 6.18 are the top 6m flowing towards Strahan (into page) and the water between 6m and 16m flowing away from Strahan (out of page).

Comparing Figure 6.18 to Figure 6.17, the best match between the BB-ADCP data and model output occur when the wind blowing is from the SE or SSW (Figure 6.17.b and Figure 6.17.c). As the sections in Figure 6.17 are during ebb tides, for a more accurate comparison Figure 6.19 gives the model output velocity on the Liberty Pt – Sophia Pt section when the tide is flooding. When comparing Figure 6.18 to Figure 6.19, note that only the top 25m is given in Figure 6.18, while Figure 6.19 shows the entire water column. The bathymetry looks slightly different as the sections are not in exactly the same place and due to the distortion and smoothing from the gridding techniques used to produce the model bathymetry. The three parts in Figure 6.19 are unsymmetrical by one degree because the data to generate the figures was saved hourly and the second wind case was used. As the wind changes direction with constant angular frequency and the tide has a period that is out of phase with the saving frequency, the figures are not at exactly the some point in the tidal phase.

Of the three parts of Figure 6.19, Figure 6.19.b is the closest fit to the field data given in Figure 6.18. The wind conditions in Figure 6.19.b are also the closest ones to those recorded at Granville Harbour, giving confidence in the model output. The minimum and maximum velocities in Figure 6.19.b are different by 36% and 20% respectively from the field values, and the general pattern of velocities is similar. That is, water is flowing similar directions in a particular region for both the model output and field data.

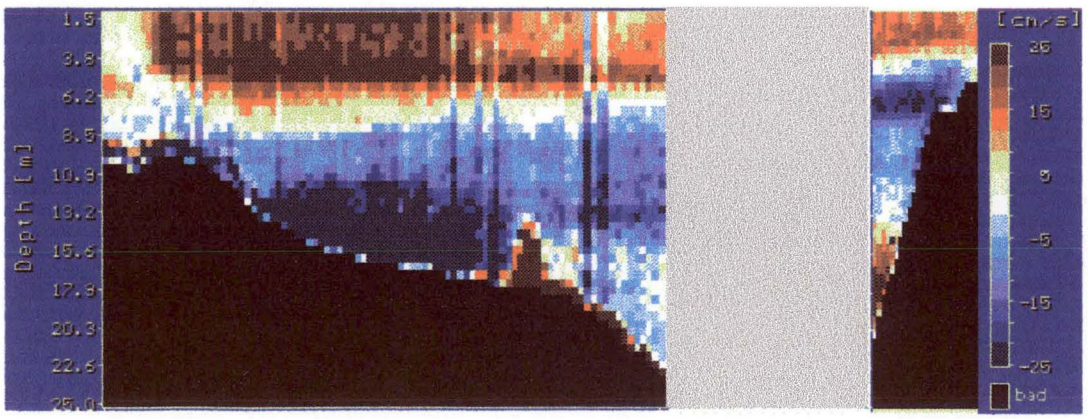

Figure 6.18 Horizontal velocity (north component) section compiled from BB-ADCP data on 29 September 1993 at 12:01pm (LHS) and 11:28am (RHS), between Liberty Pt and Sophia Pt (grey area was not covered by the BB-ADCP)

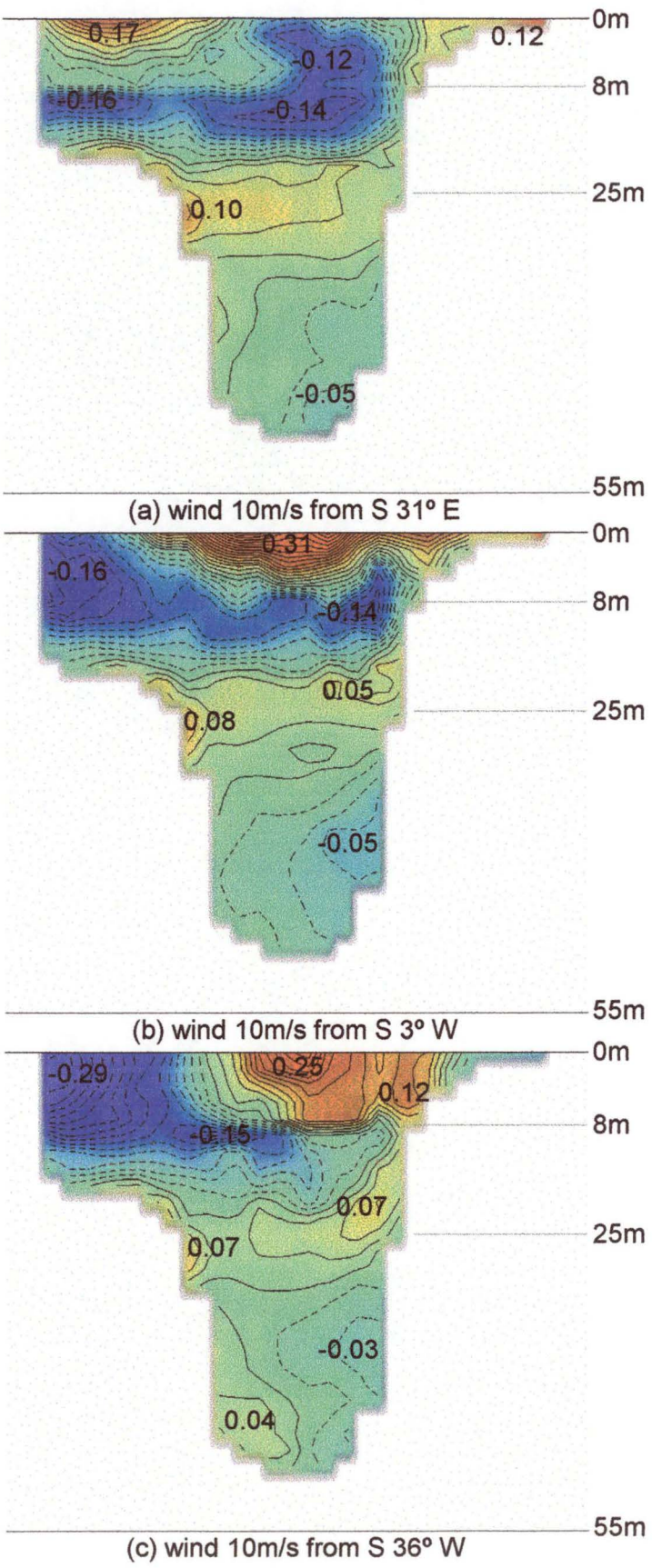

Figure 6.19 Horizontal velocity section from model at flood tide between Liberty Pt and Sophia Pt, with 0.02m/s contours and local maximum and minimums labelled in m/s

As the wind swings around from S 31° E (Figure 6.19.a) to S 36° W (Figure 6.19.c), the body of north bound water moves in an easterly direction – due to the circulation around Liberty Pt. This circulation is evident in the horizontal sections of Figure F.1.d and Figure F.2.a (Appendix F), although the figures are for ebb tides.

Around the halocline, at a depth of 8m to 9m, the velocities change dramatically - a feature common to the field data (Figure 6.18) and model output (Figure 6.19). This feature is more obvious when the data is animated by VIS5D, showing that the circulation is contained above and below the halocline. This flow containment is due to the density interface at the halocline, similar to the way that the fluid flow of air past water is contained to within the air and the water. While there is interaction between the fluids, their different densities allow them some independence of movement, with the stable density interface suppressing mass, momentum, and turbulence transport across the interface. The density interface at the halocline is not as strong as with the air/water interface, but is still a dominant feature of the harbour.

The BB-ADCP section between Yellow Bluff and Sophia Pt (reproduced from Chapter One in Figure 6.20) is another straight section that is compared to model output. The field data is compared to the model at approximately the same three points in the tide cycle as used in the previous Liberty Pt – Sophia Pt comparison. Once again the model output with the wind from S 3° W (Figure 6.21.b) is the closest to the field data in Figure 6.20, although the model output in Figure 6.21.a is also close. When comparing the model output and field data, note that the field data figure is only for the top 25m. The maximum and minimum velocities in the section are different by 28% and 35% respectively. The fit of the model output to the

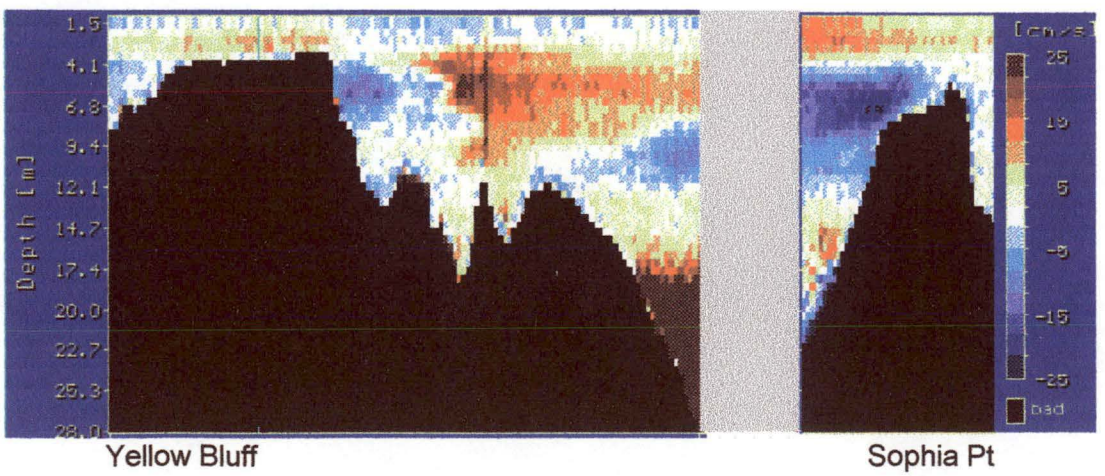

Figure 6.20 Horizontal velocity section compiled from BB-ADCP data on 29 September 1993 at 10:33am (LHS) and 11:18am (RHS), between Yellow Bluff and Sophia Pt (grey area was not covered by the BB-ADCP)

field data is not as good as it is for the previous comparison because the section is taken in a region that is more tidally effected. This makes velocities change more dramatically during the tidal cycle and makes comparisons more difficult. The bathymetry is also more variable in this region, which makes it harder to place the sections in the model output at the same position as the field data as recorded, especially as the field data was not taken on straight sections.

The circulation features are: the regions of north bound water (red) at the surface, and the south bound (blue) water beneath this to the west (left side of figure) and east (right side of figure). In the model output, the south bound water is stronger on the west of the section, compared to the field data where the south bound water is stronger on the east of the section. Even with these differences, the water from the model output is flowing in the same general direction as the field data in each region of the section.

The effect of the halocline is not as noticeable for the Yellow Bluff – Sophia Pt section (Figure 6.21) as it is for the Liberty Pt – Sophia Pt section (Figure 6.19). The water in Figure 6.19 flows predominantly horizontally, while the water in Figure 6.21 has a strong vertical component due to the water recirculation at the dead end of the harbour near Strahan. This recirculation is due to the flood tide water flowing north, then diving under the King River water to end up flowing south.

In future work, BB-ADCPs that can measure the entire water column should be used, as there are many interesting circulation features that need field measurements. The transects should be straight and taken at regular intervals through several tidal cycles. The difficultly is the area to be covered is many kilometres and the vessel transporting the BB-ADCP travels at only 3.5knots (1.8m/s). To measure these large areas quickly, aerial or satellite photogrammetry could be used. These techniques could measure surface elevations, temperature, and sediment plumes, but are limited to measuring near surface quantities.

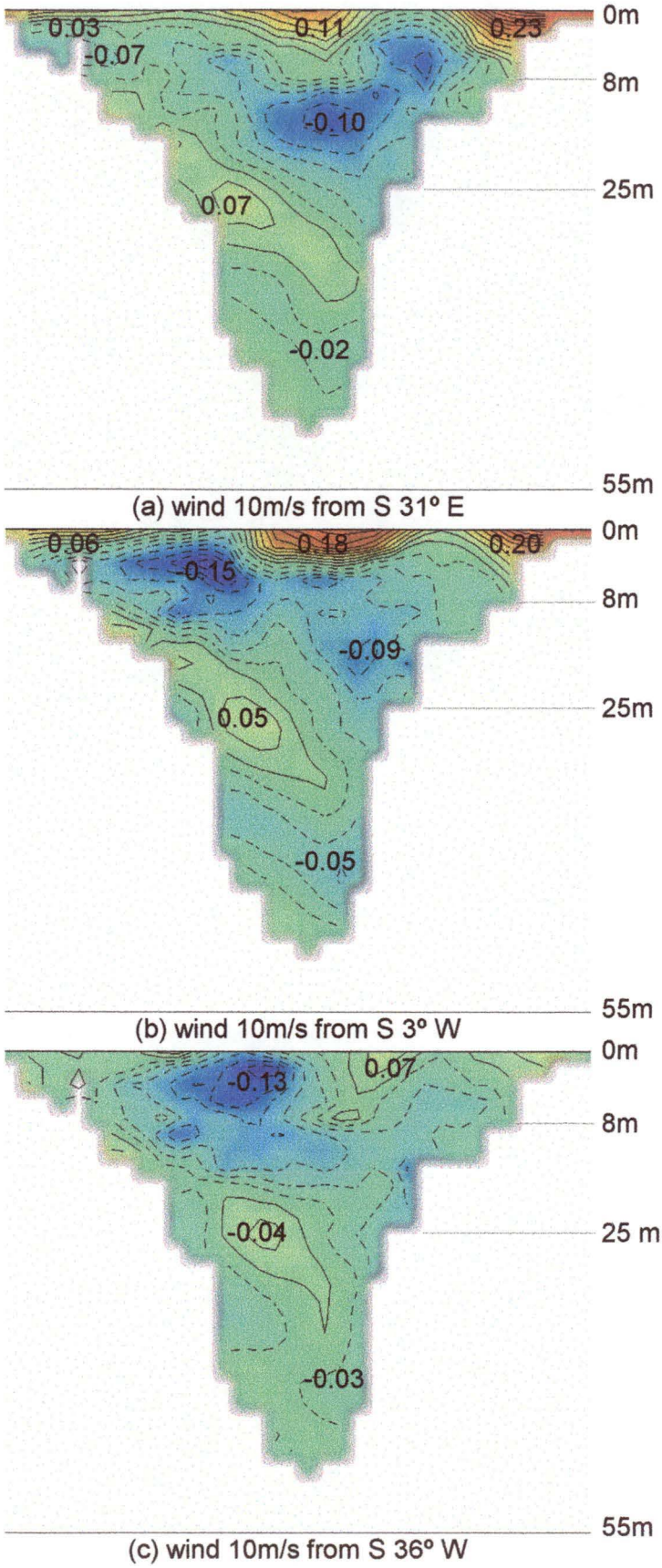

Figure 6.21 Horizontal velocity section from model at flood tide between Yellow Bluff and Sophia Pt, with 0.02m/s contours and local maximum and minimums labelled in m/s

Chapter Seven
River behaviour

7.1 Introduction

The river models are not individually as complex in their circulation or water quality structure, as the harbour model shown in Chapter Six, but there is a great diversity between the three models. The three "rivers" modelled are the Gordon River, King River and the sea. Each has different bathymetry and boundary conditions, leading to their diversity of behaviour. This diversity is a good test for the ability of the river model developed in this thesis.

The model output from the rivers in this chapter is created from day ten simulations using the same stationary initial conditions as Chapter Six. In the first part of this chapter typical flow conditions are described for the Gordon River, King River and the sea. Then the salinity from the Gordon River model is compared to sparse field data in Section 7.5, and in Section 7.6 the effect of not using the Boussinesq approximation in the river model is investigated.

7.2 Gordon River

The Gordon River is modelled from just after it is joined by the Franklin River, where it deepens and slows, for 40km to Macquarie Harbour. Figure 7.1 shows the velocity at flood and ebb tides, with a small difference evident in the downstream (D/S) half. Note that unlike the depth values at the right hand side (RHS) of the vertical sections in Chapter Six, the values in this chapter are not depths, but the z co-ordinate from the same datum as the surface elevation (the negative of depth).

Temperature and salinity do not vary noticeably during a tidal cycle and Figure 7.2 depicts typical values. As the Gordon River is not a pollution source, its pollution concentration is not plotted as it is only detected in ppm in the first few kilometres from the harbour.

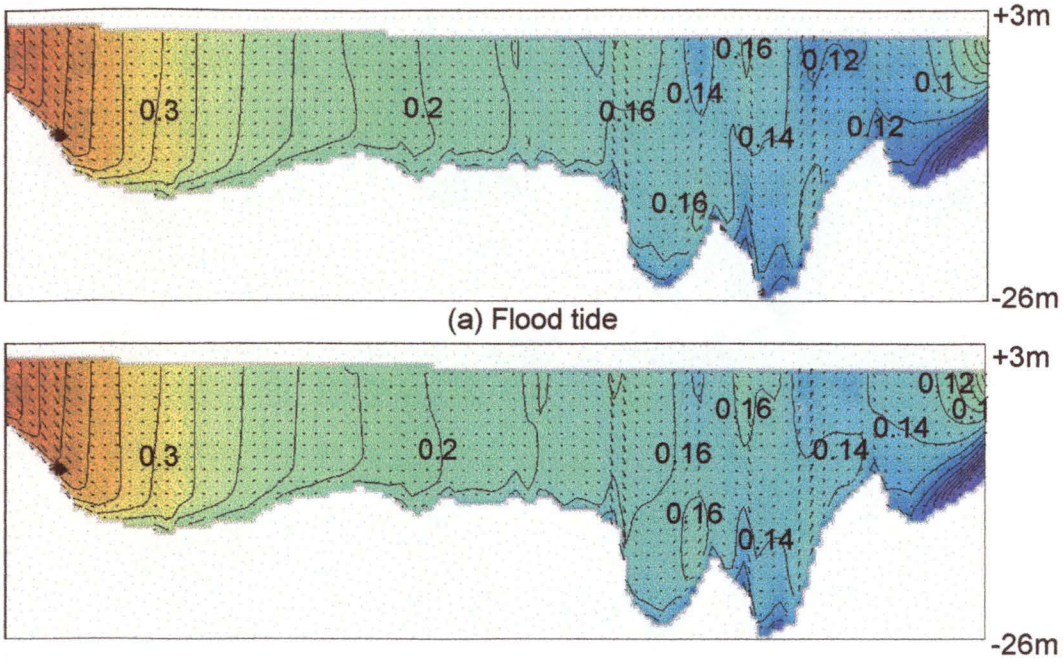

Figure 7.1 Velocity in Gordon River during flood and ebb tides on a vertical section along a 40km reach for a 200m^3/s flow rate, 0.02m/s contours of horizontal velocity (m/s), water flows left to right (U/S to D/S)

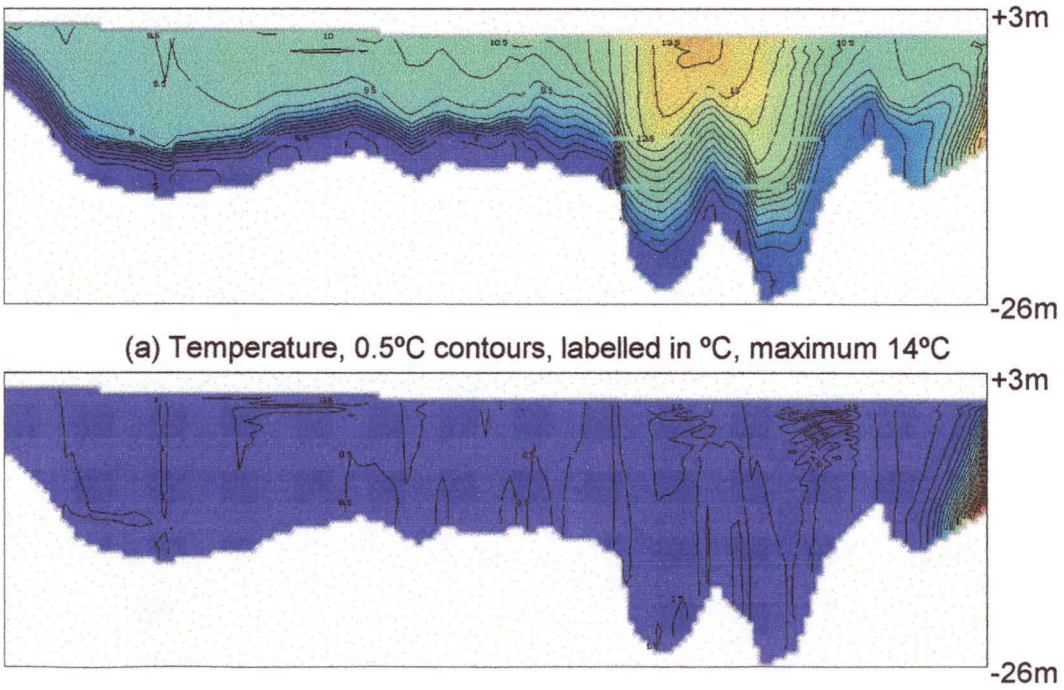

Figure 7.2 Typical temperature and salinity in Gordon River on a vertical section for a 200m^3/s flow rate

The Gordon River is deep enough that cool water from mountain catchments and the Gordon Dam storage, can flow most of the way along the bottom of the 40km reach that is modelled (Figure 7.2.a). The surface water is warmed by the sun and mixed through the water column more rapidly downstream in the more turbulent regions. At the downstream half, the deeper water allows larger eddies, increasing the diffusion. The slower moving harbour waters have longer to warm, as evidenced by the heat wedge on the downstream (RHS) of Figure 7.2. This heat wedge is caused by the salt wedge inducing density driven currents to flow upstream. Clearly the warmer harbour water is not going to cause a density driven current by itself, as it is less dense than the cooler river water.

The feature of interest in the salinity distribution, is the salt wedge from the harbour waters shown in Figure 7.2.b. At flow rates lower than the $200m^3/s$ used for these figures, the salt wedge intrudes further upstream, and under flood conditions ($2000m^3/s$ flow rate) there is no salt wedge in the river. In Section 7.5 the different salt wedge positions are shown when the model output is compared to field data.

The Gordon River's surface elevation is steeper upstream, tapering to the harbour. The upstream (U/S) and D/S surface elevations are given in Table 7.1, showing the maximum U/S change through the tidal cycle is 0.08m and the maximum D/S change is 0.12m. As expected, the maximum D/S change is the same as the tidal variation throughout the harbour.

7.3 King River

The King River is shallower, has a lower flow rate than the Gordon River, and being closer to Hells Gates the King River is effected more by the tidal activity. Figure 7.3 gives the velocities at the peak ebb and flood tides (extremes of velocity), while the scalars (Figure 7.4, Figure 7.5, and Figure 7.6) are given plotted at the turning points at the tide (extremes of surface elevation and minimum harbour velocities) where the scalars have been transported the furthest.

Tide phase	U/S (m)	D/S (m)
flood	1.64	0.194
turning flood to ebb	1.68	0.260
ebb	1.70	0.208
turning ebb to flood	1.65	0.141

Table 7.1 Surface elevation in Gordon River at U/S and D/S (harbour end) of the 40km reach, at different points in the tide cycle for a flow rate of $200m^3/s$

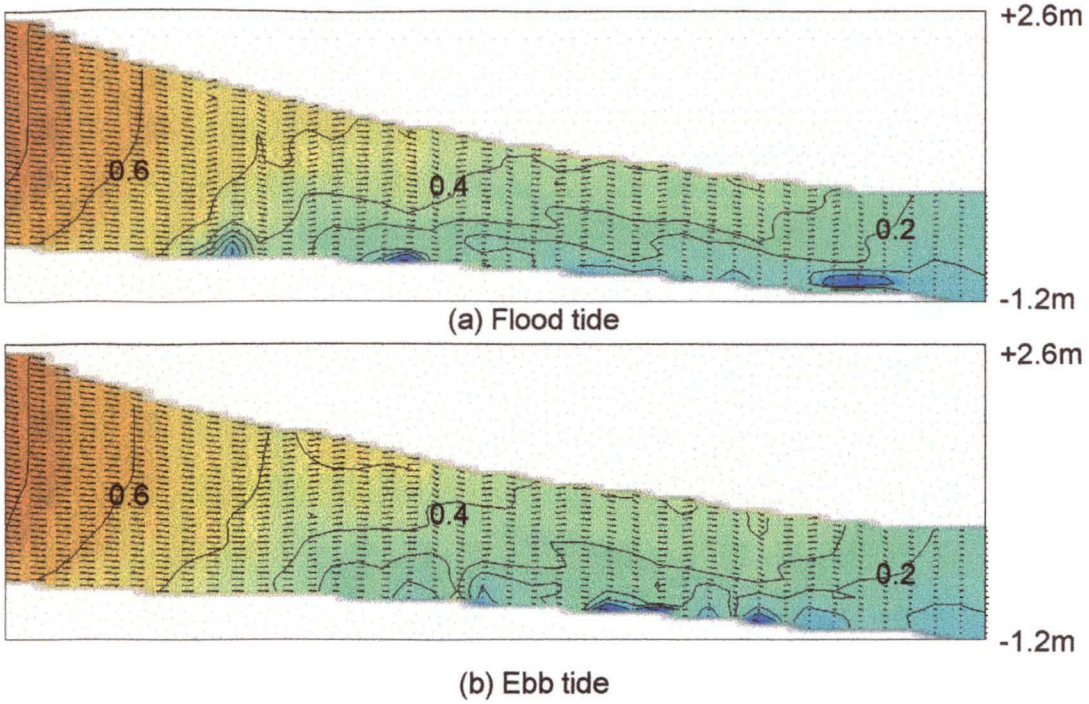

Figure 7.3 Velocity in King River during flood and ebb tides on a vertical section along a 10km reach for a 70m^3/s flow rate, 0.1m/s contours of horizontal velocity (m/s), U/S of model is on LHS, D/S of model at harbour is on RHS

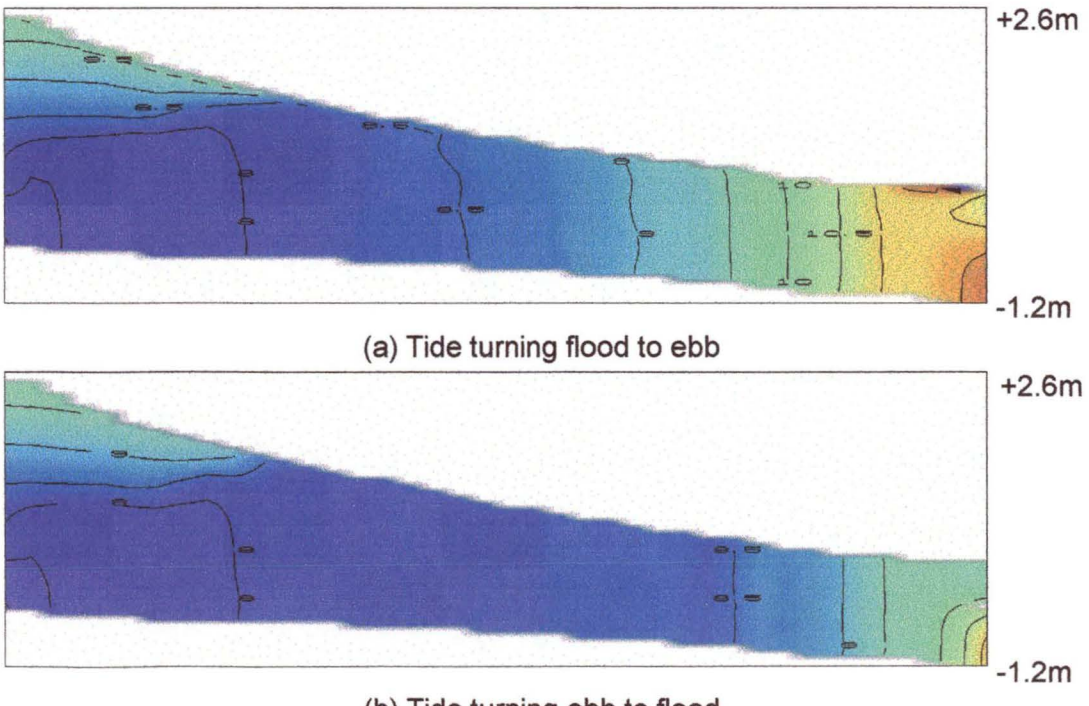

Figure 7.4 Temperature in King River for turning points in the tide cycle, 0.5°C contours labelled in °C, on a vertical section for a 70m^3/s flow rate

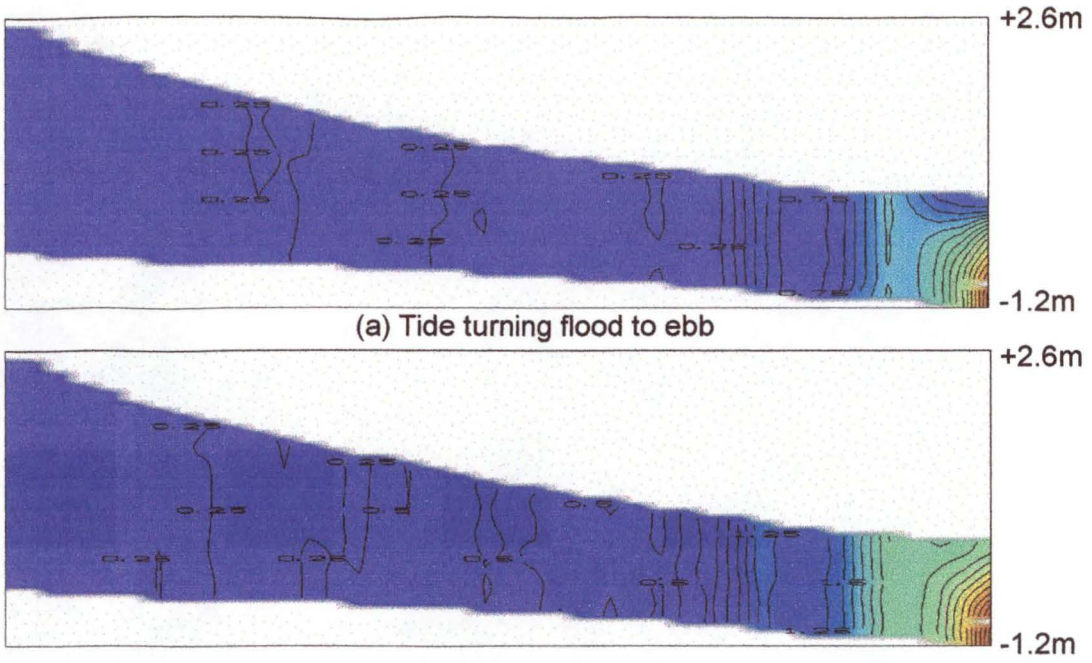

(a) Tide turning flood to ebb

(b) Tide turning ebb to flood

Figure 7.5 Salinity in King River for turning points in the tide cycle, 0.5‰ contours labelled in ‰, on a vertical section for a 70m^3/s flow rate

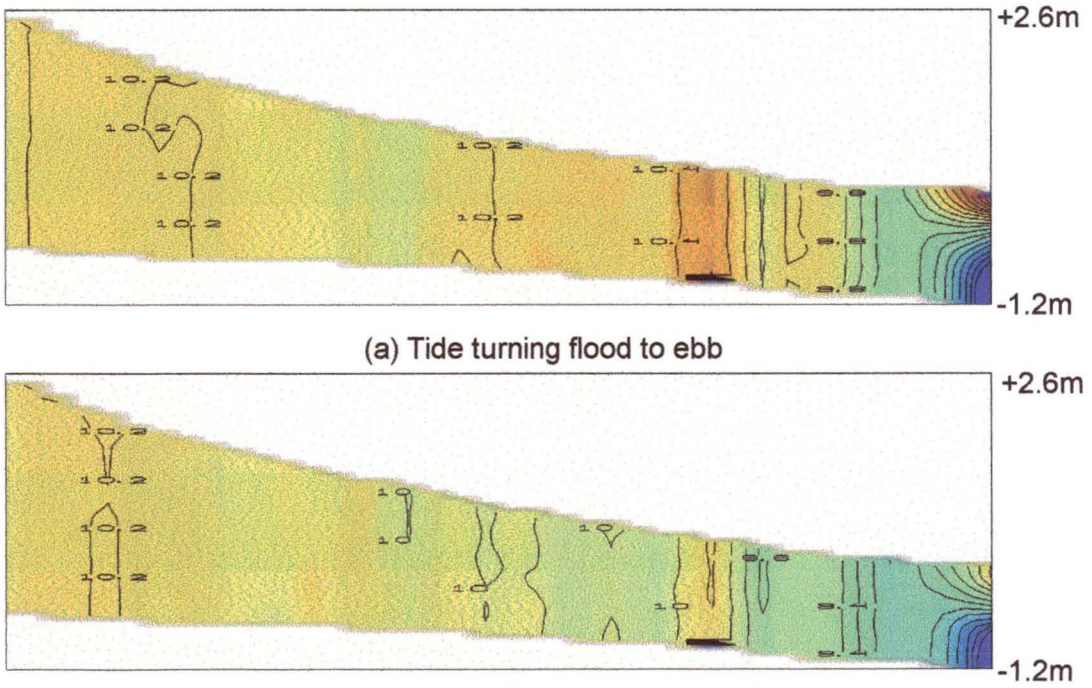

(a) Tide turning flood to ebb

(b) Tide turning ebb to flood

Figure 7.6 Pollution concentration in King River for turning points in the tide cycle, 0.2g/m^3 contours labelled in g/m^3, on a vertical section for a 70m^3/s flow rate

The King River is almost completely vertically mixed compared to the Gordon River, due to its faster and more turbulent flow. There is some structure at the D/S end of the river, with density induced currents producing a salt and heat wedge similar to the Gordon River.

The King River's surface elevation is steeper upstream, tapering to the harbour like the Gordon River. The U/S and D/S surface elevations are given in Table 7.2, showing the maximum U/S change through the tidal cycle is 0.02m and the maximum D/S change is 0.12m. The maximum D/S change is the same as the tidal variation throughout the harbour.

7.4 The sea

The river model of the sea is different in nature to both the Gordon River and King River as it is directly tidally effected. The Gordon River and King River are indirectly effected through the harbour water. Being directly effected by the tide, the sea model undergoes dramatic changes in circulation throughout the tide cycle, as shown with the velocity in Figure 7.7. The scalars are transported back and forward on the tide, although there is a net upstream movement (that is, out to the Southern Ocean) due to the flows from the Gordon and King rivers. The temperature is shown in Figure 7.8, salinity in Figure 7.9, pollution concentration in Figure 7.10, and the horizontal diffusion in Figure 7.11. The horizontal diffusion value is used for eddy viscosity in the momentum equation and eddy diffusivity in the scalar transport equations.

The transport of ocean water into the harbour can be seen at the shallows around Hells Gates as the tide turns from flood to ebb, in Figure 7.8.b for temperature and Figure 7.9.b for salinity. As discussed in Chapter Six, a Gordon River flow rate of $200m^3/s$ and a King River flow rate of $70m^3/s$ result in a net flux of salt out of the harbour. Hence the salt and cool water seen entering the harbour as the tide turns from flood to ebb will leave again, plus extra from the harbour, as the tide ebbs.

Tide phase	U/S (m)	D/S (m)
flood	2.46	0.204
turning flood to ebb	2.45	0.269
ebb	2.47	0.221
turning ebb to flood	2.45	0.148

Table 7.2 Surface elevation in King River at U/S and D/S (harbour end) of the 10km reach, at different points in the tide cycle for a flow rate of $70m^3/s$

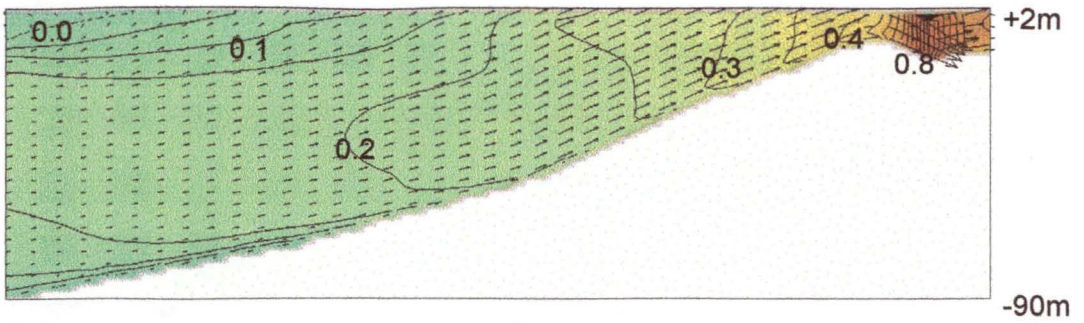

(a) Flood tide

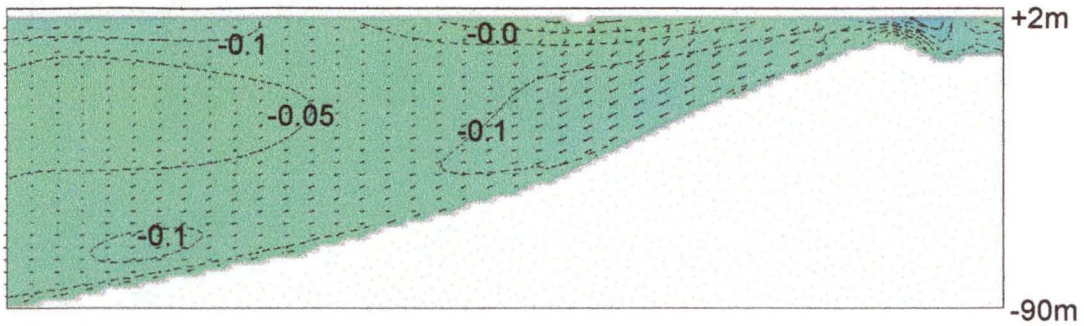

(b) Tide turning flood to ebb

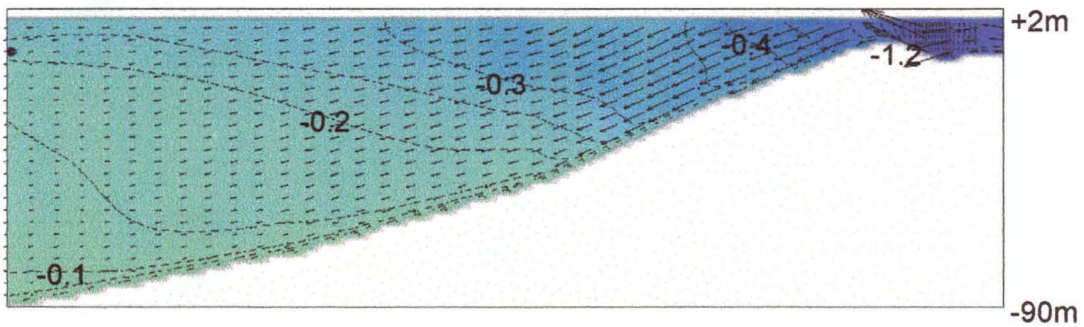

(c) Ebb tide

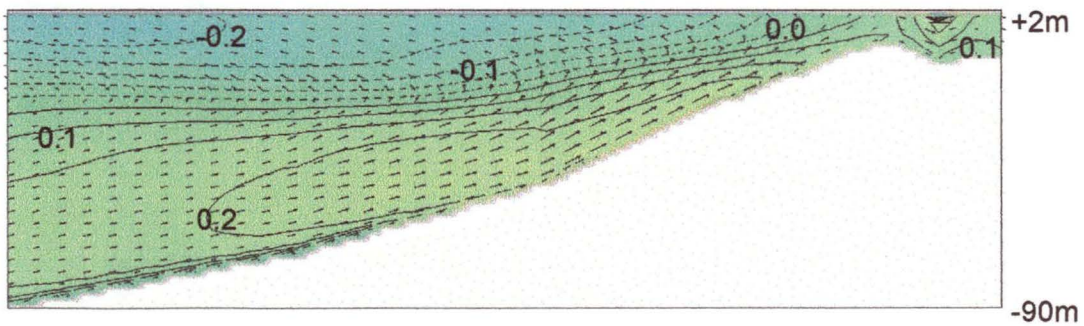

(d) Tide turning ebb to flood

Figure 7.7 Velocity in the sea at different points in the tide cycle, on a 20km vertical section for a tide period of 12.42h, 0.05m/s contours of horizontal velocity (m/s), U/S of model is on LHS, D/S of model at harbour is on RHS

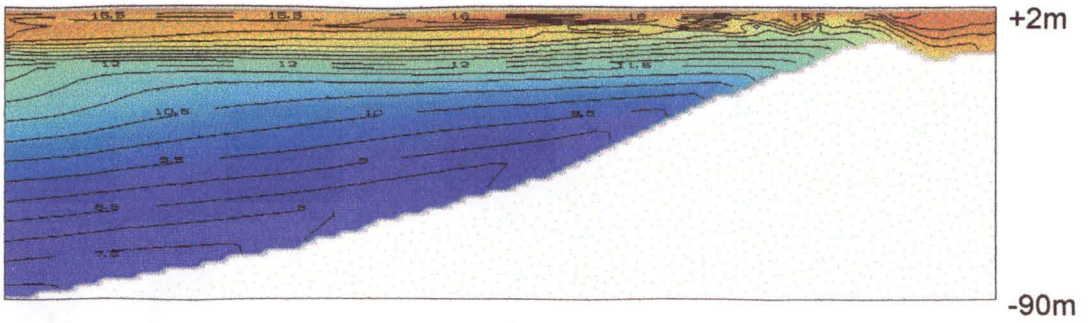

(a) Flood tide

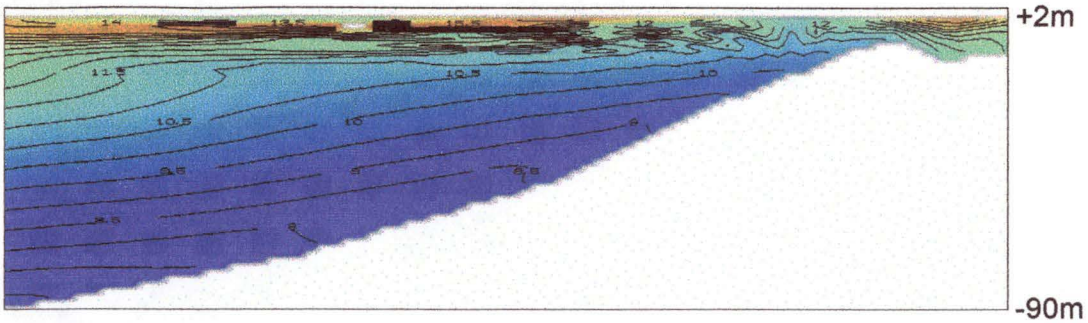

(b) Tide turning flood to ebb

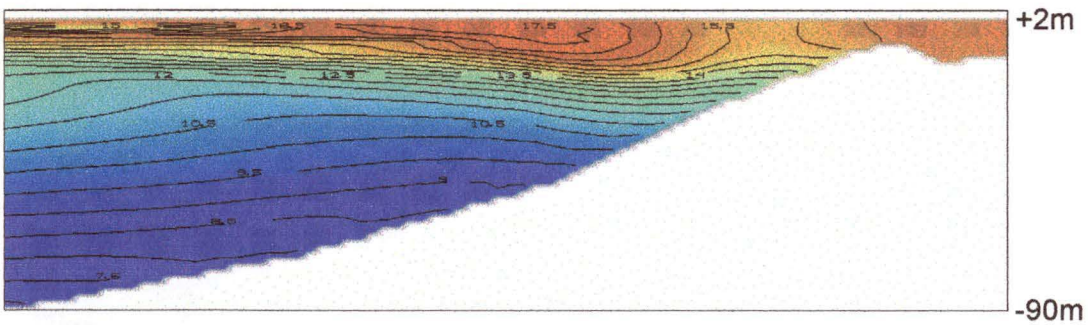

(c) Ebb tide

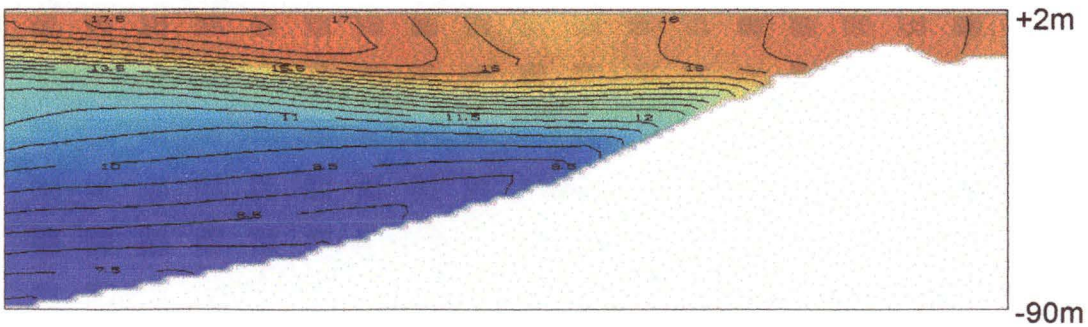

(d) Tide turning ebb to flood

Figure 7.8 Temperature in the sea at different points in the tide cycle on a 20km vertical section for a tide period of 12.42h, 0.5°C contours, labelled in °C

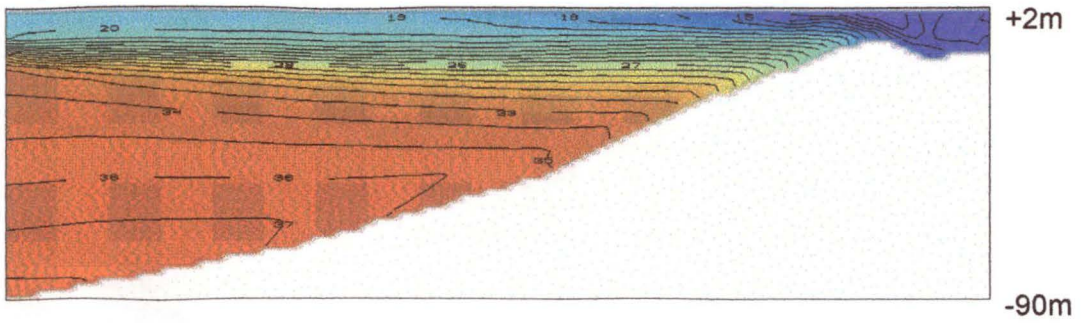

(a) Flood tide

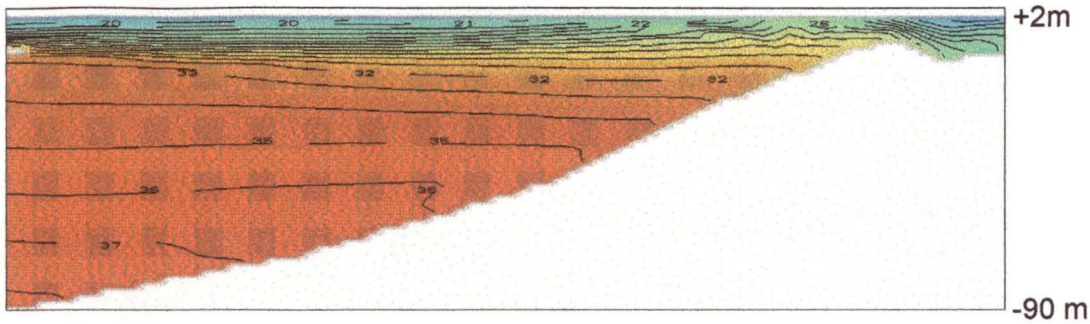

(b) Tide turning flood to ebb

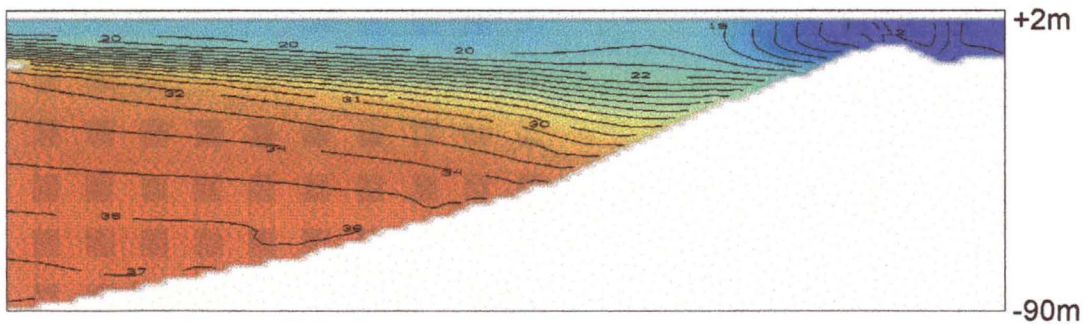

(c) Ebb tide

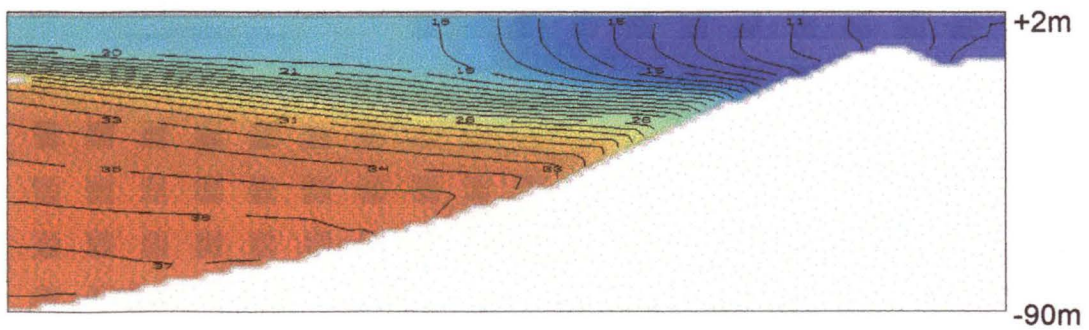

(d) Tide turning ebb to flood

Figure 7.9 Salinity in the sea at different points in the tide cycle on a 20km vertical section for a tide period of 12.42h, 0.5‰ contours, labelled in ‰

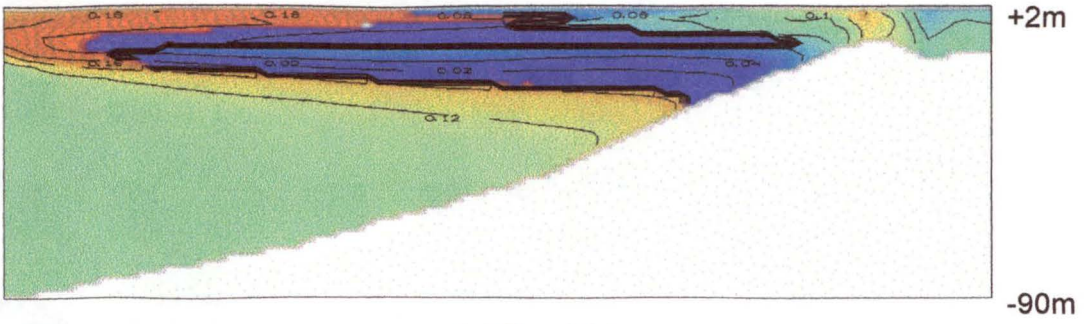

(a) Flood tide

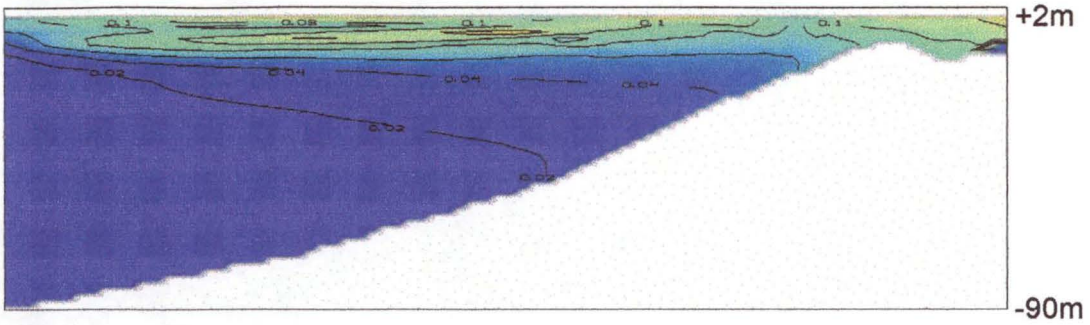

(b) Tide turning flood to ebb

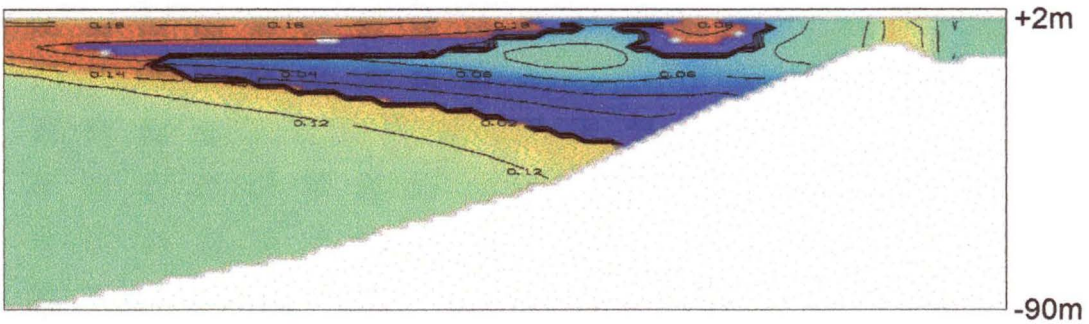

(c) Ebb tide

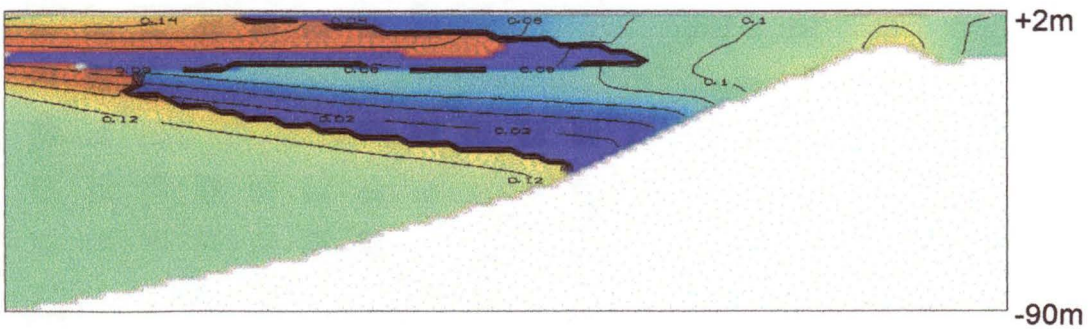

(d) Tide turning ebb to flood

Figure 7.10 Pollution concentration in the sea at different points in the tide cycle on a 20km vertical section for a tide period of 12.42h, 0.2g/m^3 contours, labelled in g/m^3

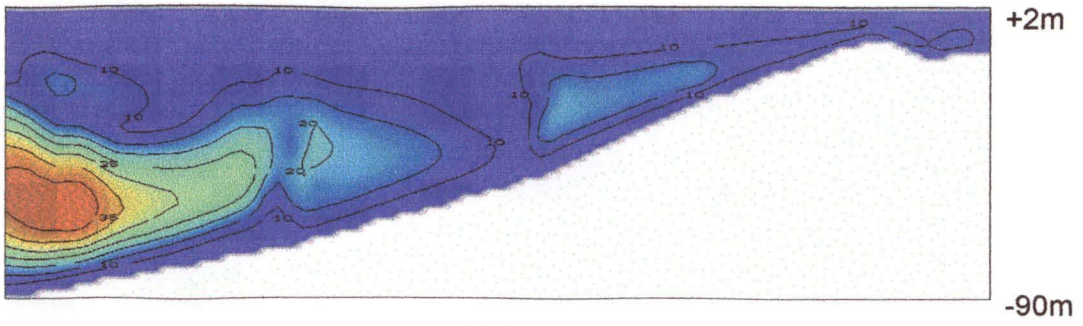

(a) Flood tide

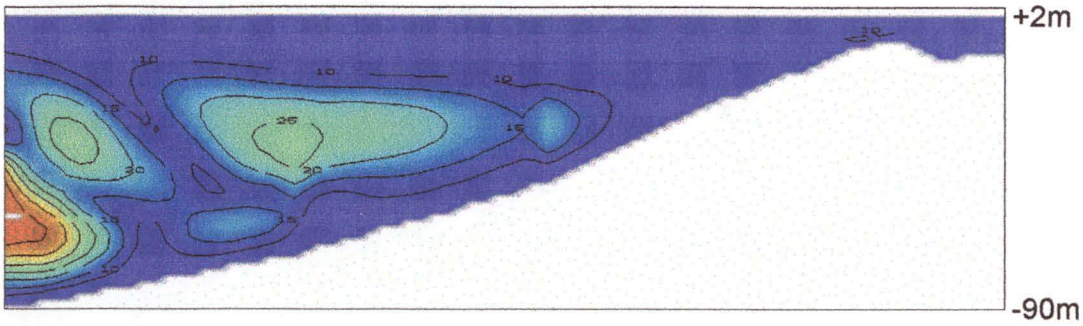

(b) Tide turning flood to ebb

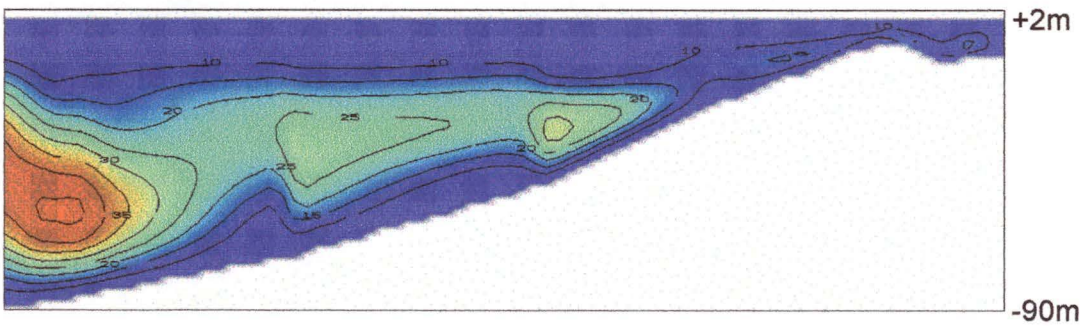

(c) Ebb tide

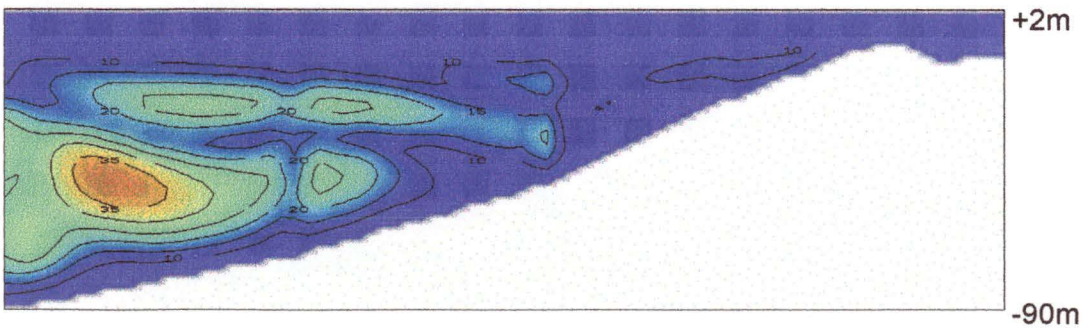

(d) Tide turning ebb to flood

Figure 7.11 Horizontal diffusion in the sea at different points in the tide cycle on a 20km vertical section for a tide period of 12.42h, 5m^2/s contours, labelled in m^2/s

The pollution concentration in Figure 7.10 has a different distribution through the water column compared to the salinity (Figure 7.9) and temperature (Figure 7.8). This is because the pollution has come from the harbour into the sea where there was no previous pollution. The pollution concentration values in the sea model are similar to those in the waters around Liberty Pt inside the harbour, and they move back and forward on the tide as do the other scalars.

The halocline in the sea model plays an important role in the scalar mixing, as it does in Macquarie Harbour. The density interface reduces mixing across the halocline, causing the halocline to oscillate on the tide, rather than diffusing the scalars through the water column. The halocline is created in the initial conditions, with the strong tidal flow attempting to disrupt the halocline's integrity. To negate this disruption the halocline is fed cool salty open sea water, from underneath and warm brackish harbour water from above.

The mixing is greatest in the deeper waters, as discussed already for the Gordon River. The diffusion will increase with larger eddy sizes, shown by the horizontal diffusion distribution in Figure 7.11. The divisions in the horizontal diffusion (Figure 7.11) spaced at approximately the quarter points along the reach, are due to small standing waves from reflection of the open boundary. These standing waves are not evident in quantities other than the horizontal diffusion, as the horizontal diffusion is sensitive to the horizontal velocity distribution, being a diagnostic variable based on horizontal derivatives of the horizontal velocity.

The surface elevation in the sea varies much more than the Gordon River and King River, and is the driving force in the sea model. The surface elevation at the U/S ocean end varies by 2.4m, as the tide has an amplitude of 1.2m. The mean surface elevation at the U/S is -0.17m, for the Gordon River flow rate of $200m^3/s$ and a King River flow rate of $70m^3/s$, to keep the harbour level approximately constant on an tidal average. This offset is described in Section 4.4.4.1. While the D/S harbour end varies by 0.66m, this tide is quickly attenuated through Hells Gates and the shallows just inside the Harbour, to give a 0.12m tide for most of

Tide phase	U/S (m)	D/S (m)
flood	1.04	0.410
turning flood to ebb	-0.133	0.110
ebb	-1.37	-0.249
turning ebb to flood	0.269	0.255

Table 7.3 Surface elevation in the sea at U/S and D/S (harbour end) of the 20km reach, at different points in the tide cycle for a 1.2m U/S tide amplitude

the harbour. This tidal range was required to compare the model output against the BB-ADCP harbour data in Chapter Six.

7.5 Verification of river salinity

A comparison was made between the model output and field data from an HEC survey of the Gordon River (HEC, 1979). The HEC survey measured salinity profiles along 40 km of the Gordon River upstream of Macquarie Harbour. Gordon River salinity measurements were made over three years, for flow rates of $17m^3/s$ (measured 16 February 1972), $102m^3/s$ (measured 29 October 1974), and $238m^3/s$ (measured 22 September 1971). For the comparison the model was run from a stationary initial condition, ramping the boundary conditions over 14 simulated days, ending with the Gordon River flow at $238m^3/s$.

The only quantity used by the model to make it simulate the field conditions was to have consistent flow rates. The flow rates were calculated in the field on a ten day average and in the model were calculated continuously at the U/S boundary. With no other knowledge of the field conditions and with different time scales between the model run time and field data measurement period, the comparison will only provide an approximate indication of the model's accuracy.

Figure 7.12 compares the salinity from the model output and field data at flow rates of $17m^3/s$, $102m^3/s$, and $238m^3/s$. The $34m^3/s$ case (Figure 7.12.b) is included to show the intermediate salinity distribution to aid understanding of the river dynamics, even though there is no field data for that flow rate.

In all parts of Figure 7.12 the isohalines from the field data are closer to horizontal than the model. This is because the model output was simulating a steadily increasing flow that was pushing the salt out of the river, while in the field the river had years to establish a stable horizontal salinity distribution. That is, under a prolonged constant flow rate, the isohalines are expected to converge to horizontal, and the isohalines from the model output are sloping because the model is simulating unsteady conditions.

Even with the model simulating unsteady conditions, it gives a reasonable representation of the transport and diffusion of the salt, comparing favourably with field data considering that the model was not calibrated by any field data. The model output gives consistently low salinity values, which may be caused by either the unsteady conditions or too much mixing.

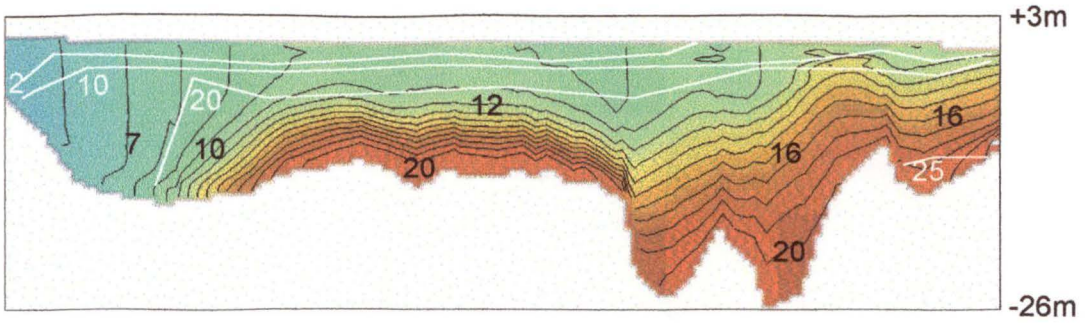

(a) flow rate of 17m^3/s, day 1

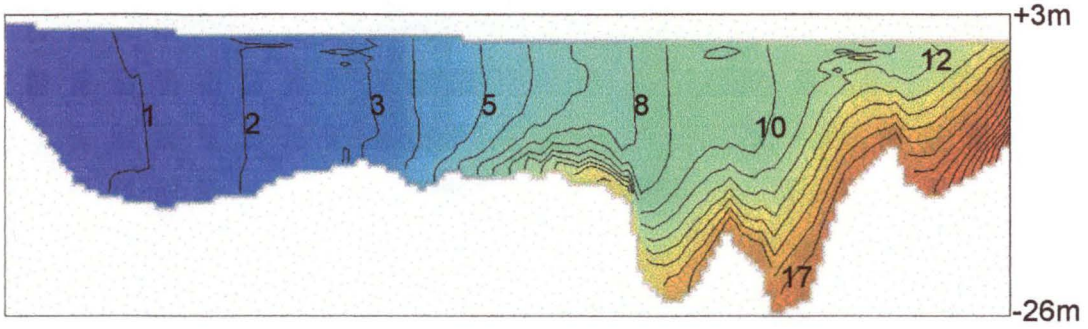

(b) flow rate of 34m^3/s, day 2 (no field data)

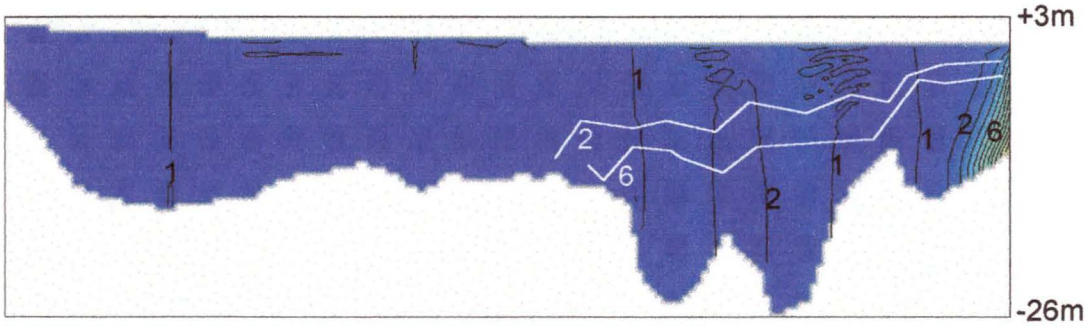

(c) flow rate of 102m^3/s, day 6

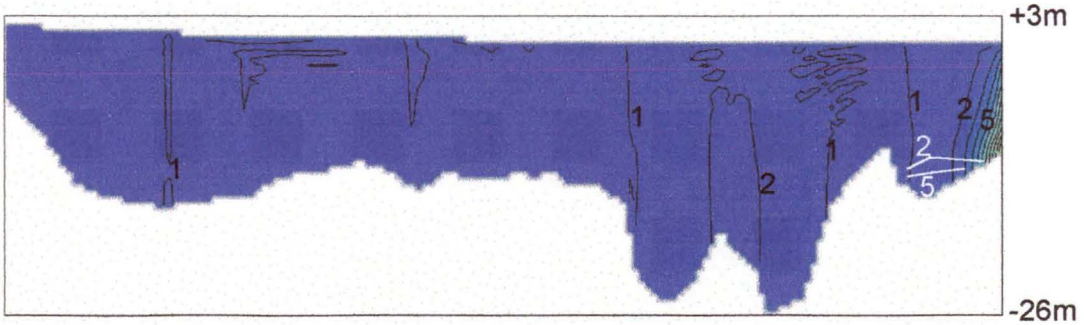

(d) flow rate of 238 m^3/s, day 14

Figure 7.12 Salinity in Gordon River for various flow rates that have been ramped over 14 days from an stationary initial condition, black 1‰ contours are model output, white contours are field data from HEC (1979), all labels in ‰

During a calibration with field data that might be done in future work, the diffusion values could be altered by changing the scaling value for the horizontal mixing length. The scaling value is a fraction of the river width (Boericke and Hogan, 1977), used to get a base value for horizontal mixing length. Currently the scaling value is set arbitrarily to 0.8 .

To illustrate the time scales involved in establishing a stable salinity distribution, a 2000m^3/s flood was simulated in the Gordon River, ramping the flow up and down over two days from a base of 200m^3/s. The salt wedge was completely pushed out of the river, and after the flood, the salt wedge took a week to re-establish itself.

More accurate comparisons with the HEC (1979) field data would need to have the flow rates changing over a month, rather than a week time scale. A six month simulation would take approximately 40 days on the SGI Origin 200 if the model was given sole use of a processor, but in practical terms would take twice that as it has many users, and so was not carried out.

7.6 Boussinesq approximation

The river model was principally used without the Boussinesq approximation in the derivation of its equations, and has been called a non-Boussinesq model. To find the effect of using the Boussinesq approximation, the model was coded to allow the option of using the Boussinesq approximation. The model was run from a stationary initial condition for 24h for both Boussinesq and non-Boussinesq cases. While the non-Boussinesq model ran well, the initial Boussinesq model crashed in the sea river model after 23.5h, so output is shown for before this time. At 23.5h the tide was at 93% of its ebb flow, so the flow from the harbour through Hells Gates would almost be at its maximum, the most difficult conditions to model.

The non-Boussinesq model has run stably for over twenty five days, and could conceivably run for much longer. However, during its development, the non-Boussinesq model has crashed, as the Boussinesq model did, from one time step to several days after starting. It was then a matter of fixing some bugs, tuning the mixing model, or changing the smoothing parameters to ensure it worked. Similarly, will a little tuning the Boussinesq model that crashed, could be made to run stably. Nevertheless, the fact the Boussinesq model crashed in a situation where the non-Boussinesq model did not crash, indicates the non-Boussinesq model is more stable for this situation.

Comparing the non-Boussinesq and Boussinesq model output in more detail there are noticeable differences. The non-Boussinesq model has less vertical mixing of scalars than the Boussinesq model, as shown in its more sharply defined salinity and temperature distributions in the Gordon River (Figure 7.13).

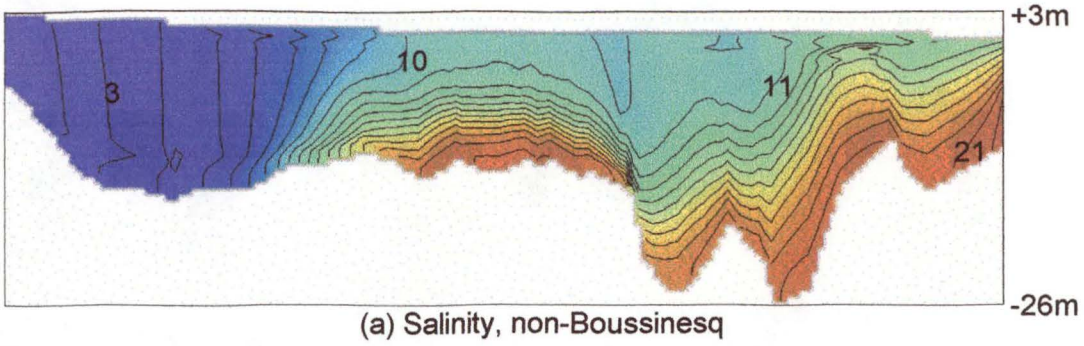

(a) Salinity, non-Boussinesq

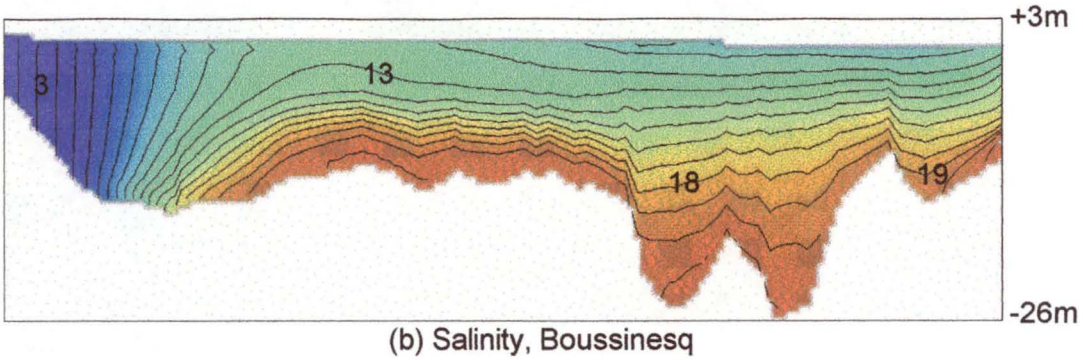

(b) Salinity, Boussinesq

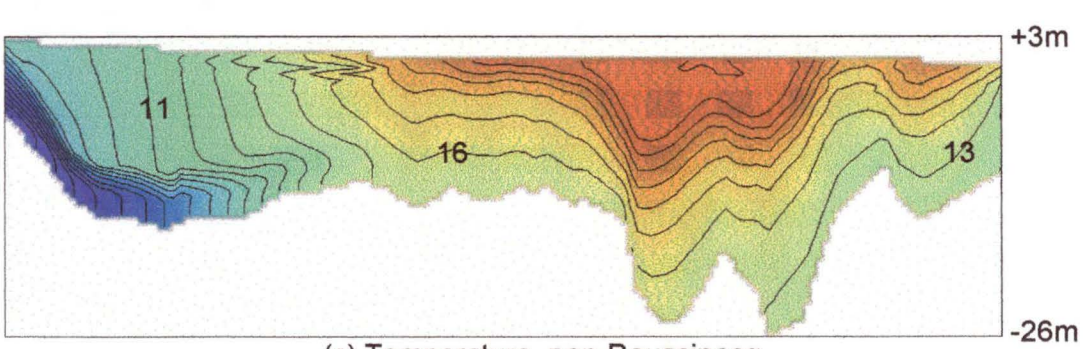

(c) Temperature, non-Boussinesq

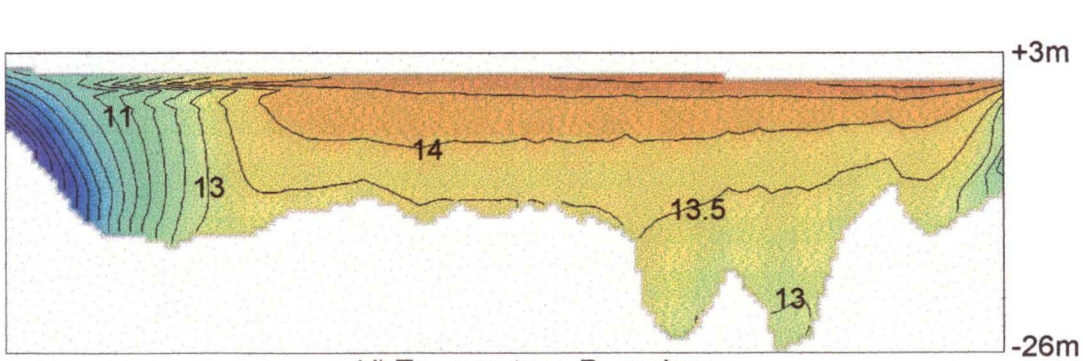

(d) Temperature, Boussinesq

Figure 7.13 Salinity and temperature in Gordon River, 21h after stationary initial conditions for non-Boussinesq and Boussinesq river model, salinity has 1‰ contours and labelled in ‰, temperature has 0.5°C contours and labelled in °C

There is greater horizontal transport of scalars in the Gordon River for the non-Boussinesq model than the in the Boussinesq model (Figure 7.13), but the opposite for the King River (Figure 7.14). This can be explained by looking at the river velocities (Figure 7.15), which indicate that transport is related to velocity. The non-Boussinesq model of the Gordon River has higher velocities and greater scalar transport, while the non-Boussinesq model of the King River has lower velocities and lower scalar transport.

The greater vertical mixing in the Boussinesq model results from the extra diffusion caused by neglecting the density terms in the conservation equations. Neglecting the density terms in making the Boussinesq approximation is non-conservative and introduces a smoothing similar to diffusion.

Often extra diffusion will create numerical stability, such as the horizontal diffusion on the momentum equation, but in the extremes of velocities and large density gradients around Hells Gates, the extra diffusion in the Boussinesq model caused instability. After the initial instability, the Boussinesq model was made to work with slightly different smoothing on the scalars.

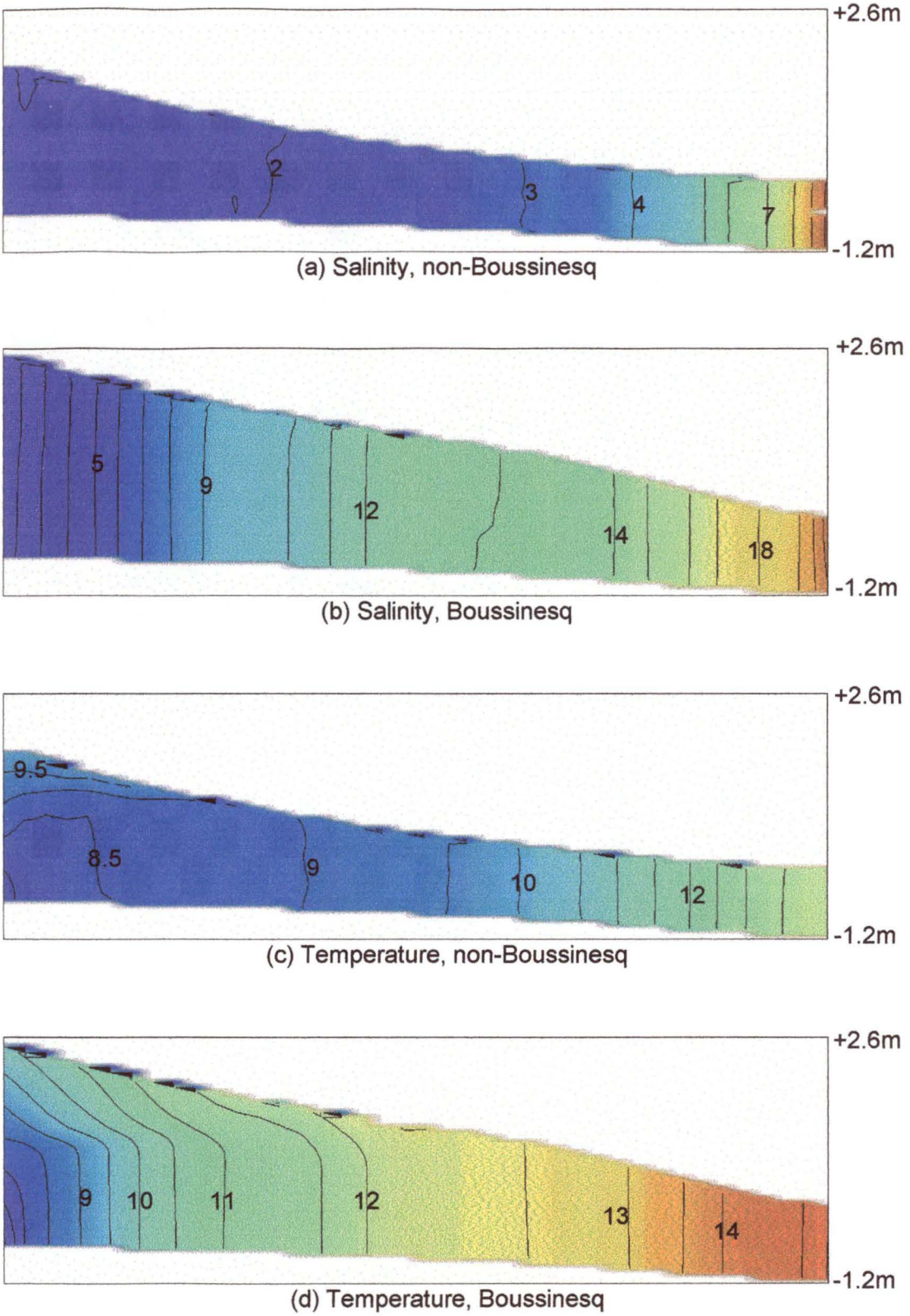

Figure 7.14 Salinity and temperature in King River, 21h after stationary initial conditions for non-Boussinesq and Boussinesq river model, salinity has 1‰ contours and labelled in ‰, temperature has 0.5°C contours and labelled in °C

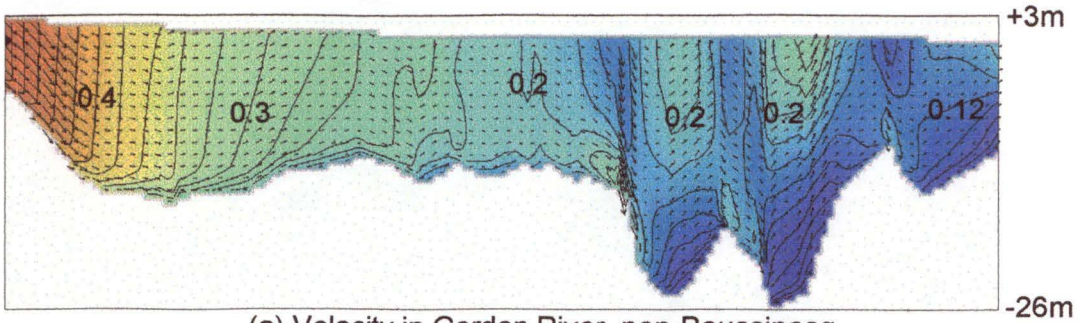

(a) Velocity in Gordon River, non-Boussinesq

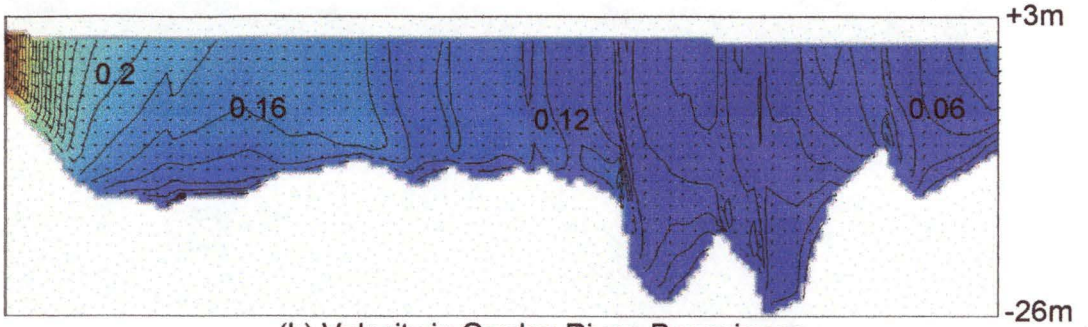

(b) Velocity in Gordon River, Boussinesq

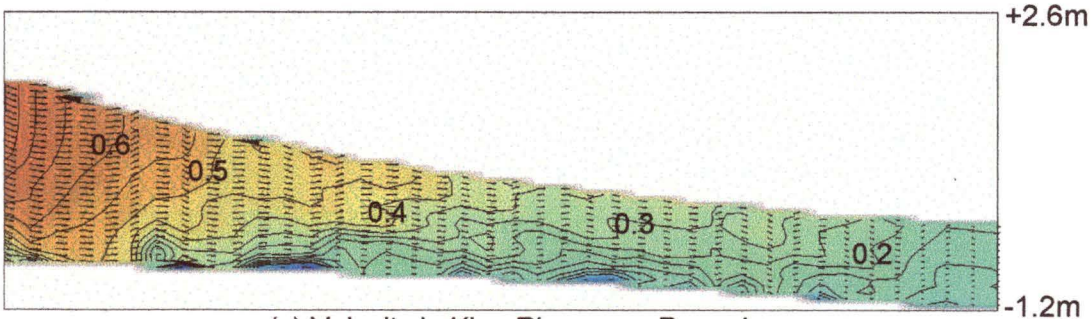

(c) Velocity in King River, non-Boussinesq

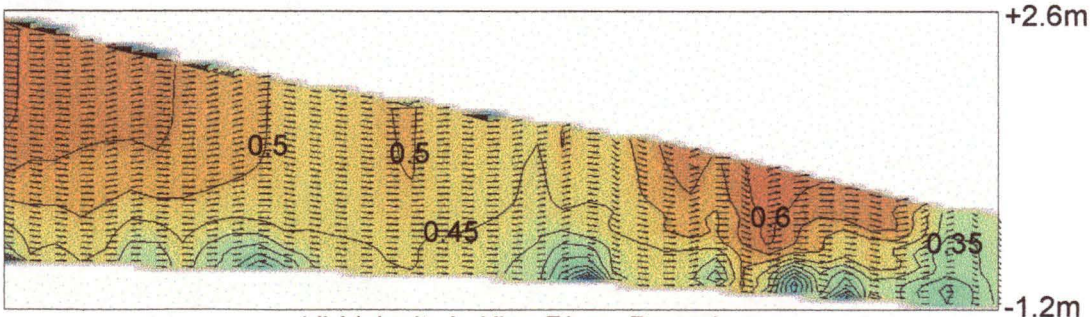

(d) Velocity in King River, Boussinesq

Figure 7.15 Velocity in Gordon River and King River, 21h after stationary initial conditions for non-Boussinesq and Boussinesq river model, Gordon River has 0.02m/s contours and King River has 0.05m/s contours, labels in m/s

Chapter Eight
Conclusions and future directions

8.1 Introduction

The numerical model of Macquarie Harbour described in this thesis has applications as a management tool to benefit both the environment and industry. The model has answered some questions and created many more. The harbour is more complex than previously realised, with model output giving direction to future field investigations.

8.2 Macquarie Harbour circulation

Macquarie Harbour is forced primarily by the Gordon River, the tide, and the strong north-westerly and westerly winds that are prominent in the local weather. The Gordon River water flows north up the western side of the harbour at the surface and also along the deeper parts of the central harbour. The King River effects the circulation in the northern third of the harbour, but it is primarily of interest because of the effect its polluted waters have on the harbour system. The predominant circulation pattern in the harbour, is a large clockwise eddy mid-way along the harbour south of Liberty Pt. This forms because the Gordon River water is blocked by the tide, water from the King River, and the sides Liberty Pt. This eddy recirculates the polluted King River water flowing south along the eastern side of the harbour, over to the western side of the harbour.

The polluted King River water circulates in the northern third of the harbour on the tide, and is directed down the eastern side of the harbour by the strong northerly flow of the Gordon River water. The Gordon River, having the largest flow rate, is responsible for flushing in the harbour. It controls the pollution in the harbour by blocking the southerly flow of the King River water and flushing the pollution out to the open ocean.

Due to the shallow nature of the harbour, the wind has a significant effect on its circulation. Although the wind predominantly effects the top 20m, its effects are noticeable throughout the entire water column. As the harbour is sensitive to the wind, future research could involve more detailed wind measurements and better wind-water interaction modelling. The simple linear wind stress development model used in this thesis, is comparable in sophistication to the constant friction coefficient assumption used in the wind stress expression. If the expression for this friction coefficient is improved to include wave height development, then air modelling may need to be handled with a primitive equation model that can better predict water stresses.

8.3 Model accuracy and limitations

Creating a numerical model is both art and science. Due to the complexity of both the theory and implementation of the model, the approach taken in developing the model must endeavour to minimise human error. It is pointless implementing a sophisticated model if its complexity introduces errors. The process of developing a numerical model from scratch involves making many mistakes, as does any creative process. Leendertse (1981) said "modeling is certainly not a scientific endeavour, even though it is customary to report is as such", and while "modeling goes hand-in-hand with progress in science and technology" it is "an intuitive art". In the same discussion, Abraham (1981) said there must be a balance between factual knowledge (accumulated in engineering experience), scientific knowledge, and creativity.

The assumptions made in numerical modelling relate to both the details and application of the scheme. Three examples are given to illustrate the effect of such approximations:

1. In creating the river model in this thesis, the Boussinesq approximation was tested. It was shown that when there were large density stratifications, the model with the Boussinesq approximation was not as stable and caused more mixing than the non-Boussinesq model. The choice not to use the Boussinesq approximation gave a small change to the river hydraulics, but no noticeable effect on the harbour in the multi-day time scale used for the comparison. In longer simulations, the effects would become more prominent.
2. The attempt at using zero-dimension equations to model the river boundary conditions on the harbour proved to be unstable and inaccurate. The assumption that the rivers were simple enough to be modelled with a zero-dimension equation was incorrect due to the rivers' complex structure and their interaction with the harbour circulation. To successfully overcome the problem, two-dimensional laterally averaged models were created for the rivers and the sea. These models were shown to be robust and accurate enough to give realistic results.
3. As the two-dimensional laterally averaged model for the sea does not contain any lateral flow, it will not model the along-shore currents in the ocean outside the harbour. Although this will only give a partial representation of the Southern Ocean around the harbour, the sea model still gives a good representation of the tides within the harbour.

As a verification of the assumptions made in creating the model, the model output gave good correlation to the limited field data from the BB-ACDP (Lawson and Treloar, 1994) given the uncertainty in the wind conditions, and also to salinity data from the Gordon River (HEC, 1979). This correlation only verifies the model in general and future research should look at including seasonal variation in a more rigorous verification of the model. The model output indicates the harbour circulation is complex and more velocity measurements are required. The problem is that obtaining field data is expensive and time consuming, especially in the hostile environment of the west coast of Tasmania. While there is an ongoing water quality measuring program, which arose from the MLRRDP, it does not include measurement of harbour circulation.

The measured salinity stratification was used as an initial condition for model. The temperature variation used as an initial condition was arbitrary - with the hope the model would predict a variation similar to the measured one. Unfortunately this did not happen on the week to month time scales used for the modelling. This means a time scale of years would be required to obtain the temperature variations, as they are seasonally based, which would require months or years (of real time) in computer modelling and seasonal modelling is left to future research efforts.

8.4 Model Speed

The model speed is important in practical terms, as all modelling projects are restricted by time. The model speed is the ratio of simulated time in a model run, to the real time it took for the simulation. This will depend on the model's solving algorithms, the computer the model is run on, and model's spatial and temporal resolution. The model in this thesis uses 62 by 148 horizontal grids in Macquarie Harbour, 160 horizontal grids in the Gordon River, 80 horizontal grids in the sea, and 40 horizontal grids in the King River. On the computers that ran the model, this uses 22Mb of RAM for 13 vertical levels and 39Mb of RAM for 23 vertical levels. The RAM usage is primarily from the program's variable allocation, with the executable part of the program only requiring approximately 1Mb. The code for POM is around 3000 lines of FORTRAN program. When the river models are added, the code with comments for the Macquarie Harbour system is around 14500 lines.

The model speed on a SGI Origin 200 is compared for different numbers of vertical levels (7, 13, 23, and 33) in Figure 8.1 using an external time step of 3.0s, with the exception of the 33 level case in which a 2.0s time step was used for numerical stability. The comparison is done over a ten day simulation, where the computer's central processing unit (CPU) is on average

99% dedicated to running the model. A Pentium – 166MHz PC runs the same model 4.8 times slower than the SGI.

The relationship between model resolution and speed seems to be exponential,

$$speed = 30.081e^{-0.0687KB} \tag{8.1}$$

In (8.1) KB is the number of vertical levels. The R^2 statistical correlation factor between (8.1) and the original data is 0.9928, where a R^2 correlation of 1.0000 is a perfect fit.

8.5 Current and future use of the model

The model developed in this thesis has already been used to aid the management of the Macquarie Harbour system, with scope for several future applications (Koehnken, 1998). The model has improved the understanding of harbour dynamics, including the importance of the King River and Gordon River flow rates in the general circulation, and has been used for the assessment of new fish farm lease sites. In the future, the model could be used to assess the impact on the Macquarie Harbour system by the HEC changing it power station usage and for determining the effect of various Mt. Lyell/King River rehabilitation schemes.

8.5.1 Aquaculture

The Tasmanian State Government is pushing an increase in the aquaculture industry's use of Macquarie Harbour. There is an interest in opening more fish farm lease sites in the northern harbour, due to the cost of moving fish farms long distances within the harbour and the need to have the fish farms protected from the weather. The northern waters are closer to the port at Strahan, but are also closer to the polluted water from the King River. As a result of this, the waters north of a line from Yellow Bluff to Sophia Pt have been declared a no fish farm area.

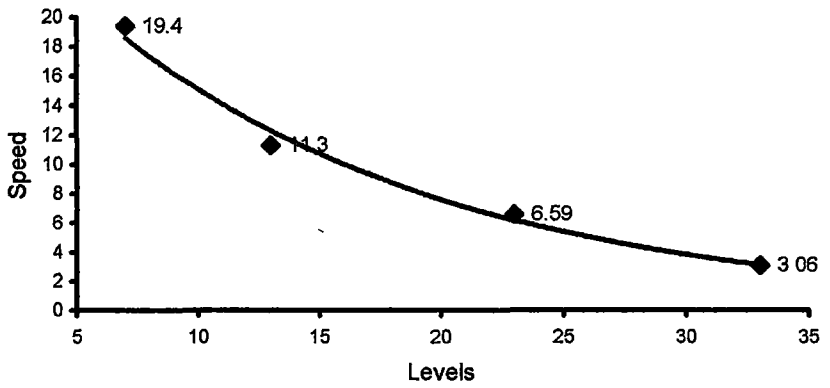

Figure 8.1 Model Speed (simulated time/real time) versus number of vertical levels

There have been four new sites proposed south of Yellow Bluff, but still closer to the King River than the currently used sites, which are in the bays north of Liberty Pt and just south of Liberty Pt. The model output shows there is a danger of having fish kills from the polluted King River water in these proposed farms, especially in the site closest to Yellow Bluff.

The output from the model in combination with water chemistry from the DELM long term monitoring program, are being used to refine the positioning of the proposed and existing farms, and develop appropriate terms and conditions for their future occupation. The State Government is well aware of the possibility of fish kills, as mentioned in Chapter One, with the 1990 fish kills that occurred off Yellow Bluff and further north in Smith Cove (DELM, 1990).

From the State Government's perspective, it has to balance financial gain from increased lease sites against the risk of fish kills or contamination. Fish kills would damage the aquaculture industry as well as the government's credibility. Such an occurrence could also leave the government open to legal action by fish farmers trying to recoup loses, on the grounds the government knew there was a reasonable risk of fish kills in the new sites and still opened the sites for leasing.

Based on the model output, the safest approach would be to only allow fish farming in the harbour south of a line from Liberty Pt to Sophia Pt, but this is not an attractive option to the fish farmers because of the increase to their short term costs. In the long term, the farmers may be better off persisting to farm the cleaner waters and develop techniques to overcome the problems associated with distance and exposure. Maintaining an uncontaminated product is a marketing edge Tasmanian farmers can not afford to relinquish for short term gain.

8.5.2 Different HEC power scheme usage

The HEC has two issues in the near future that will change the way they operate their power stations and so effect the flow regime in the King and Gordon rivers. One is to ensure that they maintain environmental flows in the rivers under new Council of Australia Government (COAG) water reforms. The second is the possibility of the proposed Bass Link scheme going ahead. This scheme proposes to link the state power grid with the mainland grid though undersea cabling across Bass Strait. The different flow regimes created in the King River and Gordon River by either of these two issues will change the circulation and water quality in the rivers and harbour.

The COAG water reforms will change the way that water is used in the state, with the aim of making users pay for the worth of the water and moving to having one water manager. This role would fall to the state's Department of Primary Industries and Fisheries (DPIF).

Currently, large water users like the HEC have licences to control how they release water from their hydro-electric power schemes, but the system does not consider downstream ecological health. Under the new system, the HEC will be just one of many water users under the control of the DPIF and responsible for maintaining an environmental flow through their hydro-electric schemes. An environmental flow should maintain the downstream ecosystem.

Bass Link will mean the state's largest water storages in Lake Gordon, Lake Pedder and Great Lake, which are currently maintained at minimum water levels as reserves for use in power generation in times of drought, could be run much lower because the national grid could provide alternative drought insurance. Currently the smaller run-of-the-river power schemes like the Pieman and Anthony are used more during the wetter winter months and less during summer because their small water storages rely on the winter rains. If Bass Link becomes a reality, it will mean compared to now, there will be higher Gordon River flows in the winter and lower in the summer. This is will accentuate the current seasonal trend, that is higher winter flows and lower summer flows in the Gordon River, and will lead to seasonal polarisation of the water quality structure. Under Bass Link, the Gordon River flows would be closer to the previous natural flow regime, which would lead to a decreased harbour flushing in the summer resulting in an increased chance of fish kills. Although this will also depend on how the King River power scheme is operated and the flows in the Queen River.

The model has shown the importance of the King River and Gordon River flow on the harbour's circulation and water quality. Although the Gordon power scheme only controls 20% of the Gordon River flow, because of the importance of the river to the harbour, it is vital that the HEC is able to predict the effect of its operational variation on the rivers and harbour. In future work it would be possible to use the model to make these predictions.

8.5.3 King River rehabilitation

The ultimate aim for management of the Macquarie Harbour system would be to clean up the King River and the damage caused by the mining operations of the Mt. Lyell Mining and Railway Co. The outcomes of the MLRRDP were acted on in May 1998, with over one million dollars of Federal Government money being used to trial a rehabilitation scheme using sulphate reducing bacteria. This will allow acidic polluted water (pH 2.8 to 3.2) to be processed to a more neutral pH 5.5 with lower metal concentrations.

It is important to be able to predict pollution transport in the King River under different flow regimes or chemical compositions that might result from mine site rehabilitation. The model could be used to make these predictions, including the impact on the harbour water quality.

Already the model is able to give a good representation of the King River plume, but future work with field calibration could further investigate the interaction between the plume and the harbour waters.

8.6 Closure

With a greater understanding of our environment, there is more scope for maintaining and improving our quality of life. The working model created of the Macquarie Harbour system is a useful environmental management tool. The model has already been used to improve the understanding of the harbour and to influence decisions about the harbour's aquaculture industry. While a significant step in understanding the harbour, in reality the model is in its infancy and requires several seasons of field calibration to improve its forecasting ability to the point where it can give more than general information.

References

ABBOTT, M. B., HAVNO, K., AND LINDBERG, S. (1991): The Fourth Generation of Numerical Modelling in Hydraulics, *Journal of Hydraulic Research*, **29**(5), 581-600

ABRAHAM, G. (1981): *Reply to discussion on* "Mathematical Modeling of Flows and Transport of Conservative Substances: Requirements for Predictive Ability" by ABRAHAM, G., VAN OS, A. G., AND VERBOOM, G. (1981), In *Transport Models for Inland and Coastal Waters*, FISCHER, H. B. (Ed), Academic Press, New York, 36-38

ABRAHAM, G., VAN OS, A. G., AND VERBOOM, G. K. (1981): Mathematical Modelling of Flows and Transport of Conservative Substances: Requirements for Predicative Ability, In *Transport Models for Inland and Coastal Waters*, FISCHER, H. B. (Ed), Academic Press, New York, 1-38

BATTEEN, M. L., AND HAN, Y.-J. (1981): On the Computational Noise of Finite-Difference Schemes Used in Ocean Models, *Tellus Series A*, **33**, 387-396

BELL, C. N. (1899): Macquarie Harbour: Its Physical Aspect and Future Prospects, *Papers and Proceedings of Royal Society, Tasmania*, XXVIII - XXXIII

BLUMBERG, A. F. (1977a): Numerical Tidal Model of Chesapeake Bay, *Journal of the Hydraulics Division, ASCE*, **103**(HY1), 1-10

BLUMBERG, A. F. (1977b): Numerical Model of Estuarine Circulation, *Journal of the Hydraulics Division, ASCE*, **103**(HY3), 295-310

BLUMBERG, A. F., AND KANTHA, L. H. (1985): Open Boundary Condition For Circulation Models, *Journal of the Hydraulics Division, ASCE*, **111**(HY2), 237-255

BLUMBERG, A. F., AND MELLOR, G. L. (1987): A Description of a Three-Dimensional Coastal Ocean Circulation Model, In *Three-Dimensional Coastal Ocean Models*, HEAPS, N. S. (Ed), American Geophysical Union, Washington DC, 1-16

BOERICKE, M. R., AND HOGAN, J. M. (1977): An X-Z Hydraulic/Thermal Model for Estuaries, *Journal of the Hydraulics Division, ASCE*, **103**(HY1), 19-37

CAMERLENGO, A. L., AND O'BRIEN, J. J. (1980): Open Boundary Conditions in Rotating Fluids, *Journal of Computational Physics*, **35**, 12-35

CARPENTER, K. M. (1982): *Note on* "Radiation Conditions for the Lateral Boundaries of Limited-Area Numerical Models" by MILLER, M. J., AND THORPE (1981), A. J., *Quarterly Journal of the Royal Meteorological Society*, **108**, 717-719

CARPENTER, P. D., BUTLER, E. C. V., HIGGINS, H. W., MACKEY, D. J., AND NICHOLS, P. D. (1991): Chemistry of Trace Elements, Humic Substances and Sedimentary Organic Matter in Macquarie Harbour, Tasmania, *Australian Journal of Marine Freshwater Research*, **42**, 625-654

CFMI (1995a): Compendium Physical and Chemical Data for Macquarie Harbour for Department of Environment and Land Management, *unpublished report*, Computational Fluid Mechanics International, Adelaide, Australia

CFMI (1995b): Physical and Chemical Model of Macquarie Harbour for Department of Environment and Land Management, *unpublished interim report MH-1-9/95*, Computational Fluid Mechanics International, Adelaide, Australia

CHARNOCK, H. (1967): Flux-Gradient Relations Near the Ground in Unstable Conditions, *Quarterly Journal of the Royal Meteorological Society*, **93**, 97-100

CHAUDHRY, M. H. (1993): *Open Channel Flow*, Prentice-Hall Englewood Cliffs, N. J., 483 pages

CRESSWELL, G. R., EDWARDS, R. J., AND BARKER, B. A. (1989): Macquarie Harbour, Tasmania - Seasonal Oceanographic Surveys in 1985, *Papers and Proceedings of the Royal Society of Tasmania*, **123**, 63-66

CUNGE, J. A., HOLLY, F. M. JR, AND VERWEY, A. (1980): *Practical Aspects of Computational River Hydraulics*, Pitman Advanced Publishing Program, London, 420 pages

DAVIES, A. M. (1987): Spectral Models in Continental Shelf Sea Oceanography, In *Three-Dimensional Coastal Ocean Models*, HEAPS, N. S. (Ed), American Geophysical Union, Washington DC, 71-106

DAVIES, A. M., GRZONKA, R. B., AND STEPHENS, C. V. (1992): Implementation of a Three-Dimensional Hydrodynamic Numerical Sea Model Using Parallel Processing on Cray X-MP Series Computer, *Advances in Parallel Computing*, **2**, 145-185

DAVIES, A. M., AND JONES, J. E. (1992): A Three Dimensional Model of the M2, S2, N2, K1 and O1 Tides in the Celtic and Irish Seas, *Progress in Oceanography*, **29**, 197-234

DAVIES, A. M., AND ALDRIDGE, J. N. (1993): A Numerical Model Study of Parameters Influencing Tidal Currents in the Irish Sea, *Journal of Geophysical Research C Oceans*, **98**(4), 7049-7067

DAVIES, A. M., AND GERRITSEN, H. (1994): An Intercomparison of Three-Dimensional Tidal Hydrodynamic Models of the Irish Sea, *Tellus Series A*, **46**(2), 200-221

DAVIES, H. C. (1983): Limitations of Some Common Lateral Boundary Schemes used in Regional NWP Models, *Monthly Weather Review*, **111**, 1002-1012

DELM (1989): Tasmania 1 : 25 000 series (Sarah, Birchs, McCall, Limekiln, and D'Aguilar), 1st Edition, Land Information Services, Department of Environment and Land Management, 134 Macquarie St, Hobart 7000, Australia

DELM (1990): Fish Kill Report, Macquarie Harbour 11 July 1990, Department of Environment and Land Management, 134 Macquarie St, Hobart 7000, Australia

DELM (1994): South West Tasmania 1 : 250 000 scale map, 2nd Edition, Land Information Services, Department of Environment and Land Management, 134 Macquarie St, Hobart 7000, Australia

EASTON, A. K. (1970): The Tides of the Continent of Australia, Horace Lamb Centre, Flinders University, South Australia

ENGEDAHL, H. (1995): Use of the Flow Relaxation Scheme in a Three-Dimensional Baroclinic Ocean Model with Realistic Topography, *Tellus Series A*, **47A**(3), 365-382

FALCONER, R. A. (1991): Flow and Water Quality Modelling in Coastal and Inland Water, *Journal of Hydraulic Research*, **30**(4), 437-452

FALCONER, R. A., GEORGE, D. G., AND HALL, P. (1991): Three-Dimensional Numerical Modelling of Wind-Driven Circulation in a Shallow Homogeneous Lake, *Journal of Hydrology*, **124**, 59-79

FISCHER, H. B. (1967): The Mechanics of Dispersion in Natural Streams, *Journal of the Hydraulics Division, ASCE*, **93**(HY6), 187-216

FLETCHER, C. A. J. (1988): *Computational Techniques for Fluid Dynamics, Volumes 1 and 2*, Springer-Verlag, 409 pages and 484 pages

FREEMAN, N. G., HALE, A. M., AND DANARD, M. B. (1972): A Modified Sigma Equations' Approach to the Numerical Modeling of Great Lakes Hydrodynamics, *Journal of Geophysical Research*, 77(6), 1050-1060

GALPERIN, B., AND MELLOR, G. L. (1990): A Time-Dependent, Three-Dimensional Model of the Delaware Bay and River System. Part 1: Description of the Model and Tidal Analysis, *Estuarine, Coastal and Shelf Science*, **31**, 231-253

GERDES, R. (1993): A Primative Equation Ocean Circulation Model Using a General Vertical Coorinate Transformation 1. Description and Testing of the Model, *Journal of Geophysical Research C Oceans*, **98**(C8), 14683-14726

GRUNDY, B. (1983): Depth Soundings of Macquarie Harbour at Mouth of Gordon River on 1 March 1983 - as a Hand Drawn 1 : 5000 map, *personal communications 16-1-1998*, Hobart Ports Corporation, 1 Franklin Wharf, Hobart 7000, Australia

HEC (1979): Lower Gordon River Scientific Survey, *unpublished report*, Hydro-Electric Corporation, 4 Elizabeth St, GPO Box 355D, Hobart 7001, Australia

HEC (1993a): Depth Soundings of Macquarie Harbour North of Liberty Point in March 1993 - as XYZ Data File, *personal communications 5-9-1994*, Hydro-Electric Corporation - Surveys, 4 Elizabeth St, GPO Box 355D, Hobart 7001, Australia

HEC (1993b): Depth Soundings of King River in March 1993 - as XYZ Data File and Printed River Sections, *personal communications 16-1-1998*, Hydro-Electric Corporation - Surveys, 4 Elizabeth St, GPO Box 355D, Hobart 7001, Australia

HIRSCH, C. (1988): *Numerical Computation of Internal and External Flows, Volumes 1 and 2*, Wiley-Interscience, John Wiley and Sons, 515 pages and 691 pages

HOLLOWAY, P. E. (1996): A Numerical Model of Internal Tides with Application to the Australian North West Shelf, *Journal of Physical Oceanography*, **26**(1), 21-37

ISRAELI, M., AND ORSZAG, S. A. (1981): Approximation of Radiation Boundary Conditions, *Journal of Computational Physics*, **41**, 115-135

JAMES, W., AND HORNE, C. W. D. (1969): Numerical Computations for Tidal Propagation in the St. Lucia Estuary, *Die Siviele Ingenieur in Suid-Afrika*, Dec, 323-326

JIRKA, G. H. (1989): In Support of Experimental Hydraulics: Three Examples from Environmental Fluid Mechanics, *Journal of Hydraulics Research*, **30**(3), 293-301

KANTHA, L. H., BLUMBERG, A. F., AND MELLOR, G. L. (1990): Computing Phase Speeds at Open Boundary, *Journal of the Hydraulics Division, ASCE*, **116**(4), 592-597

KIM, K. S., AND CHAPRA, S. C. (1997): Temperature Model for Highly Transient Shallow Streams, *Journal of the Hydraulics Division, ASCE*, **123**(1), 30-40

KNAUSS, J. A. (1978): *Introduction to Physical Oceanography*, Prentice-Hill, Englewood Cliffs, N. J. 07632, 338 pages

KOEHNKEN, L. (1996): *Macquarie Harbour – King River Study*, Department of Environment and Land Management, 134 Macquarie St, Hobart 7000, Australia, 236 pages

KOEHNKEN, L. (1998): *personal communications during March and May 1998 about Macquarie Harbour and its Fish Farms*, Department of Environment and Land Management, 134 Macquarie St, Hobart 7000, Australia

KOLMOGOROFF, A. N. (1942): The Equations of Turbulent Motion in an Incompressible Fluid, *Izv Akad Nauk SSSR, Ser Fiz*, **6**(1,2), 56-58

KOUTITAS, C. G. (1987): Three-Dimensional Models of Coastal Circulation: An Engineering Viewpoint, In *Three-Dimensional Coastal Ocean Models*, HEAPS, N. S. (Ed), American Geophysical Union, Washington DC, 107-123

KOUTITAS, C. G. (1988): *Mathematical Models in Coastal Engineering*, Pentech Press, London, 156 pages

KUNDU, P. K. (1990): *Fluid Mechanics*, Academic Press, San Diego and London, 638 pages

LAWSON AND TRELOAR (1994): Macquarie Harbour BB-ADCP Data Report for Department of Environment and Land Management, *unpublished report #1498/J1130*, Lawson and Treloar Pty Ltd, Norberry Tce, 24/177-199 Pacific Hwy, North Sydney 2060, Australia

LEENDERSTE, J. J. (1981): *Discussion on* "Mathematical Modeling of Flows and Transport of Conservative Substances: Requirements for Predictive Ability" by ABRAHAM, G., VAN OS, A. G., AND VERBOOM, G. (1981), In *Transport Models for Inland and Coastal Waters*, FISCHER, H. B. (Ed), Academic Press, New York, 31-35

LEONARD (1977): Discussion on "An X-Z Hydraulic/Thermal Model for Estuaries, Hogran and Boericke (1977)", *Journal of the Hydraulics Division, ASCE*, **103**(HY12), 1494-1496

MADALA, R. V., AND PIACSEK, S. A. (1977): A Semi-Implicit Numerical Model for Baroclinic Oceans, *Journal of Computational Physics*, **23**, 167-178

MARTIN, J. (1988): Application of Two-Dimensional Water Quality Model, *Journal of Environmental Engineering, ASCE*, **114**(2), 317-336

MATTHEWS, J. (1978): *The Sea-State of SW Tasmania*, SWTRS Discussion Paper Number 10, Department of Environment and Land Management, 134 Macquarie St, Hobart 7000, Australia, 43 pages

MELLOR, G. L. (1973): Analytic Prediction of the Properties of Stratified Planetary Surface Layers, *Journal of Atmospheric Science*, **30**, 1061-1069

MELLOR, G. L. (1991): An Equation of State for Numerical Models of Oceans and Esturaries, *Journal of Atmospheric Oceanic Technology*, **8**, 609-611

MELLOR, G. L. (1993): *User's Guide for a Three-Dimensional, Primitive Equation, Numerical Ocean Model*, Unpublished report, Princeton University, NJ, USA, 35 pages

MELLOR, G. L. (1996): *User's Guide for a Three-Dimensional, Primitive Equation, Numerical Ocean Model*, Unpublished report, Princeton University, NJ, USA, 40 pages

MELLOR, G. L., AND EZER, T. (1995): Sea Level Variations Induced by Heating and Cooling: An Evaluation of the Boussinesq Approximation in Ocean Models, *Journal of Geophysical Research*, **100** (C10), 20565 – 20577

MELLOR, G. L., AND YAMADA, T. (1974): A Hierarchy of Turbulence Closure Models for Planetary Boundary Layers, *Journal of Atmospheric Science*, **31**, 1791-1806

MELLOR, G. L., AND YAMADA, T. (1982): Development of a Turbulent Closure Model for Geophysical Fluid Dynamics, *Review of Geophysics and Space Physics*, **20**(4), 851-875

MILLER, M. J., AND THORPE, A. J. (1981): Radiation Conditions for the Lateral Boundaries of Limited-area Numerical Models, *Quarterly Journal of Royal Meteorological Society*, **107**, 615-628

MUNK, W. H., AND ANDERSON, E. R. (1948): Notes on a Theory of the Thermocline, *Journal of Marine Research*, **VII**(3), 275-295

NSWC (1993): Library of Mathematics Subroutines (NSWCDD/TR – 92/425), MORRIS, A. H. (Ed), Naval Surface Warfare Center, Dahlgren Division, Dahlgren, Virginia 22448-5000

ODD, N. V. M. (1981): The Predictive Ability of One-Dimensional Estuary Models, In *Transport Models for Inland and Coastal Waters*, FISCHER, H. B. (Ed), Academic Press, New York, 39-62

ORLANSKI, I (1976): A Simple Boundary Condition for Unbounded Hyperbolic Flows, *Journal of Computational Physics*, **21**, 251-269

PERRELS, P. A. J., AND KARELSE, M. (1981): A Two-Dimensional, Laterally Averaged Model for Salt Intrusion in Estuaries, In *Transport Models for Inland and Coastal Waters*, FISCHER, H. B. (Ed), Academic Press, New York, 483-535

PHILLIPS, N. A. (1957): A Co-ordinate System Having Some Special Advantages for Numerical Forecasting, *Journal of Meteorology*, **14**, 184-186

PRITCHARD, D. W. (1969): Dispersion and Flushing of Pollutants in Esturaries, *Journal of the Hydraulics Division, ASCE,* **95**(HY1), 115-124

ROACHE, P. J. (1976): *Computational Fluid Dynamics*, Hermosa Publishers, P.O. Box 8172, Albuquerque, N. M. 87108, 446 pages

ROTTA, J. C. (1951): Statistische Theorie Nichthomogener Turbulenz, *Z Phys,* **129**, 547-572; **131**, 51-77

RAYMOND, W. H., AND KUO, H. L. (1984): A Radiation Boundary Condition for Multi-Dimensional Flows, *Quarterly Journal of Royal Meteorological Society*, **110**, 535-551

RØED, L. P., AND SMEDSTAD, O. M. (1984): Open Boundary Conditions for Forced Waves in a Rotating Fluid, *Society for Industrial and Applied Mathematics Journal of Scientific and Statistical Computing*, **5**(2), 414-426

SHULMAN, I., AND LEWIS, J. K. (1995): Optimization Approach to the Treatment of Open Boundary Conditions, *Journal of Physical Oceanography*, **25**, 1006-1011

SKOGEN, M. D., SVENDSEN, E., BERNTSEN, J., AKSNES, D., AND UVESTAD, K. B. (1995): Modelling the Primary Production in the North Sea using a Coupled Three-Dimensional Physical-Chemical-Biological Ocean Model, *Estuarine, Coastal and Shelf Science*, **41**, 545-565

SOMMERFELD, A. (1964): *Partial Differential Equations in Physics*, Academic Press, Inc., New York and London, 335 pages

STACEY, M. W., POND, S., AND NOWAK, Z. P. (1995): A Numerical Model of the Circulation in Knight Inlet, British Columbia, Canada, *Journal of Physical Oceanography*, **25**, 1037-1062

TANG, Y., AND GRIMSHAW, R. (1995): Radiation Boundary Conditions in Barotropic Coastal Ocean Numerical Models, *Journal of Computational Physics*, **123**, 96-110

TEASDALE, P., APTE, S., BATLEY, G., AND FORD, P. (1996): The Behaviour of Copper in Sediments and Waters of Macquarie Harbour, Western Tasmania, *Mount Lyell Remediation, Research and Demonstration Program,* Supervising Scientist Report 111, Tourism House, Blackall St, Barton 2600, Australia, 118 pages

TERRY, C. T. (1992): *Waves in Open Channels, honours thesis CM/9,* Civil/Mechanical Engineering Dept, University of Tasmania, Sandy Bay 7005, Australia, 168 pages

VERWEY, A. (1994): *Linkage of Physical and Numerical Aspects of Models Applied in Environmental Studies*, Conference on Hydraulics in Civil Engineering, Brisbane, Australia, 12 pages

VERWEY, A., AND ILIC, S. (1993): A Space-Compact High-Order Implicit Scheme for 1-D Advection Simulations, *Proceedings of the 25th IAHR Congress*, Tokyo, Japan, 355-362

WANG, P.-F. (1992): Review of Equations of Conservation in Curvilinear Coordinates, *Journal Engineering Mechanics, ASCE,* **118**(11), 2265-2281

WATERMAN, P., AND MATTHEWS, J. (1979a): *A Review of Information on the Macquarie Harbour Environment,* SWTRS Discussion Paper Number 20, Department of Environment and Land Management, 134 Macquarie St, Hobart 7000, Australia, 74 pages

WATERMAN, P., AND MATTHEWS, J. (1979b): *Data Summaries: Macquarie Harbour 1979,* SWTRS Discussion Paper Number 21, Department of Environment and Land Management, 134 Macquarie St, Hobart 7000, Australia, 61 pages

WOLF, J. (1978): Interaction of Tide and Surge in a Semi-Infinite Uniform Channel, With Application to Surge Propagation Down the East Coast of Britain, *Applied Mathematical Modelling,* **2** (Dec), 245-253

WYLIE, E. B. (1970): Unsteady Free-Surface Flow Computations, *Journal of the Hydraulics Division, ASCE,* **96**(HY11), 2241-2251

ZAVATARELLI, M., AND MELLOR, G. L. (1995): A Numerical Study of the Mediterranean Sea Circulation, *Journal of Physical Oceanography,* **25**, 1384-1414

Appendix A
Derivations

A.1 Quadratic finite difference operator

Using a grid with variable spacing, such as the vertical σ grid, a centred finite difference operator is derived for the first spatial derivative. In this section the expression "quadratic operator" refers to a parabolic function approximation, as opposed to a linear function approximation. The function f is known at discrete grids point f_L, f_0, and f_U. The subscripts L, 0, and U refer to the spatial locations σ_L, σ_0, and σ_U (Figure A.1).

Assuming the function f varies parabolically between the three points, where $\Delta\sigma_U = \sigma_U - \sigma_0$, $\Delta\sigma_L = \sigma_0 - \sigma_L$, and $\Delta\sigma_T = \Delta\sigma_U + \Delta\sigma_L$ then

$$f = a\sigma^2 + b\sigma + c \tag{A.1}$$

The first vertical derivative of (A.1) is

$$\frac{\partial f}{\partial \sigma} = 2a\sigma + b \tag{A.2}$$

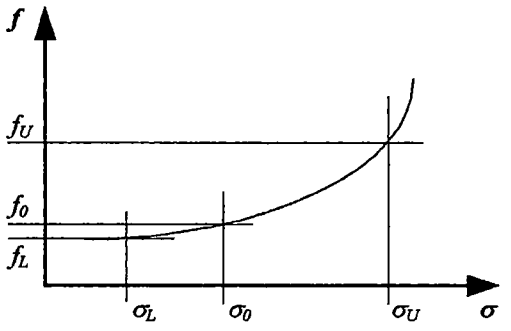

Figure A.1 *f vs.* σ

To solve for the three unknowns in (A.2) (a, b, and c), three equations are made using the known values of the function giving

$$f_U = a(\Delta\sigma_U + \sigma_0)^2 + b(\Delta\sigma_U + \sigma_0) + c \tag{A.3}$$

$$f_0 = a\sigma_0{}^2 + b\sigma_0 + c \tag{A.4}$$

$$f_L = a(\sigma_0 - \Delta\sigma_L)^2 + b(\sigma_0 - \Delta\sigma_L) + c \tag{A.5}$$

Rearranging (A.3), (A.4), and (A.5) gives

$$b = \frac{f_0 - f_L}{\Delta\sigma_L} + a(\Delta\sigma_L - 2\sigma_0) \tag{A.6}$$

$$c = f_0\left(1 - \frac{\sigma_0}{\Delta\sigma_L}\right) + \frac{\sigma_0}{\Delta\sigma_L} f_L + a\left(\sigma_0{}^2 - \sigma_0\Delta\sigma_L\right) \tag{A.7}$$

By combining (A.6) and (A.7),

$$a = \frac{\dfrac{f_U - f_0}{\Delta\sigma_U} + \dfrac{f_L - f_0}{\Delta\sigma_L}}{\Delta\sigma_T} \tag{A.8}$$

Now substituting b from (A.6) back in (A.2) at $\sigma = \sigma_0$ giving

$$\begin{aligned}\frac{\partial f}{\partial \sigma} &= 2a\sigma_0 + \frac{f_0 - f_L}{\Delta\sigma_L} + a(\Delta\sigma_L - 2\sigma_0) \\ &= a\Delta\sigma_L + \frac{f_0 - f_L}{\Delta\sigma_L}\end{aligned} \tag{A.9}$$

Now substitute in a from (A.8) into (A.9), and simplify to give the final expression for the vertical derivative using the quadratic function approximation

$$\frac{\partial f}{\partial \sigma} = \frac{1}{\Delta\sigma_T}\left((f_U - f_0)\frac{\Delta\sigma_L}{\Delta\sigma_U} + (f_0 - f_L)\frac{\Delta\sigma_U}{\Delta\sigma_L}\right) \tag{A.10}$$

For comparison the linear operators for the vertical derivatives are

$$\frac{\partial f}{\partial \sigma} = \frac{1}{\Delta\sigma_T}(f_U - f_L) \text{ or } \frac{\partial f}{\partial \sigma} = \frac{1}{2}\left(\frac{f_U - f_0}{\Delta\sigma_U} + \frac{f_L - f_0}{\Delta\sigma_L}\right) \tag{A.11}$$

Even though both linear operators in (A.11) would be considered second order accurate, the quadratic operator is centred at σ_0 (A.10), while the linear operators are centred at $\sigma_0 + \frac{1}{2}(\Delta\sigma_U - \Delta\sigma_L)$ and $\sigma_0 + \frac{1}{4}(\Delta\sigma_U - \Delta\sigma_L)$ respectively. That is if $\Delta\sigma_U \neq \Delta\sigma_L$ the linear operators are not spatially centred, although the second linear operator above would be closer to being centred than the first. POM uses linear vertical differencing (Mellor, 1996), which could cause inaccuracies when the vertical spacing changes quickly.

A.2 Surface elevation solving terms

A.2.1 Non-Boussinesq

From the non-Boussinesq surface elevation equation with $\rho = \rho'/\kappa_{\rho 1}$ where $\rho' = \rho'_0 + \kappa_{\rho 2}$

$$\frac{\partial \eta}{\partial t} + \frac{\overline{\rho u}}{\overline{\rho}}\frac{\partial D}{\partial x} + \frac{D}{\overline{\rho}}\left(\frac{\partial \overline{\rho}}{\partial t} + \frac{\partial \overline{\rho u}}{\partial x} + \frac{\overline{\rho u}}{B}\frac{\partial B}{\partial x}\right) = 0 \tag{A.12}$$

The difference operators are substituted in to give

$$\eta_i^{\Delta n+1} = \eta_i^{n+1} - \eta_i^n \tag{A.13}$$

$$\eta_i^{\Delta n-1} = \eta_i^{n-1} - \eta_i^n \tag{A.14}$$

$$\frac{\partial \eta}{\partial t} = \frac{\eta_i^{\Delta n+1} - \eta_i^{\Delta n-1}}{2\Delta t} \tag{A.15}$$

$$\frac{\overline{\rho u}}{\overline{\rho}}\frac{\partial D}{\partial x} = \frac{\overline{\rho u}_i^n}{\overline{\rho}_i^n} \times \frac{2\left(D_{i+1}^n - D_{i-1}^n\right) + \theta\left(\eta_{i+1}^{\Delta n+1} - \eta_{i-1}^{\Delta n+1} + \eta_{i+1}^{\Delta n-1} - \eta_{i-1}^{\Delta n-1}\right)}{4\Delta x} \tag{A.16}$$

$$\frac{D}{\overline{\rho}} = \frac{D_i^n + \frac{1}{2}\theta\left(\eta_i^{\Delta n+1} + \eta_i^{\Delta n-1}\right)}{\overline{\rho}_i^n} \tag{A.17}$$

$$\frac{\partial \overline{\rho}}{\partial t} = \frac{\overline{\rho}_i^n - \overline{\rho}_i^{n-1}}{\Delta t} \tag{A.18}$$

$$\frac{\partial \overline{\rho u}}{\partial x} = \frac{\overline{\rho u}_{i+\frac{1}{2}}^n - \overline{\rho u}_{i-\frac{1}{2}}^n}{\Delta x} \tag{A.19}$$

$$\frac{\overline{\rho u}}{B}\frac{\partial B}{\partial x} = \frac{\overline{\rho u}_i^n}{B_i} \times \frac{B_{i+\frac{1}{2}} - B_{i-\frac{1}{2}}}{\Delta x} \tag{A.20}$$

Only the η derivatives contain values at the unknown time step. The unknowns are factored out of (A.12) after terms (A.13)-(A.20) are substituted, to form the equation

$$A_{\eta_{NB}}\eta_{i-1}^{\Delta n+1} + B_{\eta_{NB}}\eta_i^{\Delta n+1} + C_{\eta_{NB}}\eta_{i+1}^{\Delta n+1} = K_{\eta_{NB}} \tag{A.21}$$

Where

$$A_{\eta_{NB}} = -\frac{\overline{\rho' u}_i^n}{\overline{\rho'}_i^n}\frac{\theta}{4\Delta x} \tag{A.22}$$

$$B_{\eta_{NB}} = \frac{1}{2}\left(\frac{1}{\Delta t} + \theta Z_{\eta_{NB}}\right) \tag{A.23}$$

$$C_{\eta_{NB}} = \frac{\overline{\rho' u}_i^n}{\overline{\rho'}_i^n}\frac{\theta}{4\Delta x} \tag{A.24}$$

$$K_{\eta_{NB}} = \frac{\eta^{\Delta n-1}}{2\Delta t} - \frac{\overline{\rho' u}_i^n}{\overline{\rho'}_i^n} \times \frac{2\left(D_{i+1}^n - D_{i-1}^n\right) + \theta\left(\eta_{i+1}^{\Delta n-1} - \eta_{i-1}^{\Delta n-1}\right)}{4\Delta x} - \left(D_i^n + \frac{1}{2}\theta\eta_i^{\Delta n-1}\right)Z_{\eta_{NB}} \tag{A.25}$$

$$Z_{\eta_{NB}} = \frac{1}{\overline{\rho'}_i^n}\left(\frac{\overline{\rho'_{0\,i}}^n - \overline{\rho'_{0\,i}}^{n-1}}{\Delta t} + \frac{\overline{\rho' u}_{i+\frac{1}{2}}^n - \overline{\rho' u}_{i-\frac{1}{2}}^n}{\Delta x} + \frac{\overline{\rho' u}_i^n}{B_i} \times \frac{B_{i+\frac{1}{2}} - B_{i-\frac{1}{2}}}{\Delta x}\right) \tag{A.26}$$

A.2.2 Boussinesq

From the Boussinesq surface elevation equation

$$\frac{\partial \eta}{\partial t} + \bar{u}\frac{\partial D}{\partial x} + D\left(\frac{\partial \bar{u}}{\partial x} + \frac{\bar{u}}{B}\frac{\partial B}{\partial x}\right) = 0 \tag{A.27}$$

The difference operators are substituted in to give

$$\eta_i^{\Delta n+1} = \eta_i^{n+1} - \eta_i^n \tag{A.28}$$

$$\eta_i^{\Delta n-1} = \eta_i^{n-1} - \eta_i^n \tag{A.29}$$

$$\frac{\partial \eta}{\partial t} = \frac{\eta_i^{\Delta n+1} - \eta_i^{\Delta n-1}}{2\Delta t} \tag{A.30}$$

$$\bar{u}\frac{\partial D}{\partial x} = \bar{u}_i^n \times \frac{2\left(D_{i+1}^n - D_{i-1}^n\right) + \theta\left(\eta_{i+1}^{\Delta n+1} - \eta_{i-1}^{\Delta n+1} + \eta_{i+1}^{\Delta n-1} - \eta_{i-1}^{\Delta n-1}\right)}{4\Delta x} \tag{A.31}$$

$$D = D_i^n + \tfrac{1}{2}\theta\left(\eta_i^{\Delta n+1} + \eta_i^{\Delta n-1}\right) \tag{A.32}$$

$$\frac{\partial \bar{u}}{\partial x} = \frac{\bar{u}_{i+\frac{1}{2}}^n - \bar{u}_{i-\frac{1}{2}}^n}{\Delta x} \tag{A.33}$$

$$\frac{\bar{u}}{B}\frac{\partial B}{\partial x} = \frac{\bar{u}_i^n}{B_i} \times \frac{B_{i+\frac{1}{2}} - B_{i-\frac{1}{2}}}{\Delta x} \tag{A.34}$$

Only the η derivatives contain values at the unknown time step. The unknowns are factored out of (A.27) after terms (A.28)-(A.34) are substituted, to form the equation

$$A_{\eta_B}\eta_{i-1}^{\Delta n+1} + B_{\eta_B}\eta_i^{\Delta n+1} + C_{\eta_B}\eta_{i+1}^{\Delta n+1} = K_{\eta_B} \tag{A.35}$$

Where

$$A_{\eta_B} = -\bar{u}_i^n \frac{\theta}{4\Delta x} \tag{A.36}$$

$$B_{\eta_B} = \frac{1}{2}\left(\frac{1}{\Delta t} + \theta Z_{\eta_B}\right) \tag{A.37}$$

$$C_{\eta_B} = \bar{u}_i^n \frac{\theta}{4\Delta x} \tag{A.38}$$

$$K_{\eta_B} = \frac{\eta^{\Delta n-1}}{2\Delta t} - \bar{u}_i^n \times \frac{2\left(D_{i+1}^n - D_{i-1}^n\right) + \theta\left(\eta_{i+1}^{\Delta n-1} - \eta_{i-1}^{\Delta n-1}\right)}{4\Delta x} - \left(D_i^n + \tfrac{1}{2}\theta\eta_i^{\Delta n-1}\right)Z_{\eta_B} \tag{A.39}$$

$$Z_{\eta_B} = \frac{\bar{u}_{i+\frac{1}{2}}^n - \bar{u}_{i-\frac{1}{2}}^n}{\Delta x} + \frac{\bar{u}_i^n}{B_i} \times \frac{B_{i+\frac{1}{2}} - B_{i-\frac{1}{2}}}{\Delta x} \tag{A.40}$$

A.3 Momentum and scalar equations

A.3.1 Non-Boussinesq

A generic non-Boussinesq momentum and scalar conservation equation is used to work out the difference equations. In the equation f could be u, S, T, or C. The terms that are extra to the momentum equation from the scalar conservation equation are multiplied by M, which is one when used in the momentum equation and zero when used for the scalar conservation equation. This is how the computer program is implemented and is designed to minimise coding errors. The generic non-Boussinesq equation is

$$\begin{aligned}\frac{\partial Df}{\partial t}+\frac{\partial Duf}{\partial x}+\frac{\partial \omega f}{\partial \sigma}=&\frac{D}{\rho}\frac{\partial}{\partial x}\left(\rho A_f\frac{\partial f}{\partial x*}\right)+\frac{D}{\rho}\frac{\partial}{\partial \sigma}\left(\rho A_f\frac{\partial f}{\partial x*}\right)\frac{\partial \sigma}{\partial x}\\&+\frac{1}{\rho D}\frac{\partial}{\partial \sigma}\left(\rho K_f\frac{\partial f}{\partial \sigma}\right)+\frac{D}{B}\frac{\partial B}{\partial x}\left(A_f\frac{\partial f}{\partial x*}-uf\right)\\&-M\left(\frac{D^2g}{\rho'+\kappa_{\rho_2}}\int_\sigma^0\left(\frac{\partial \rho'}{\partial x}-\frac{1}{D}\frac{\partial D}{\partial x}\sigma\frac{\partial \rho'}{\partial \sigma}\right)d\sigma+gD\frac{\partial \eta}{\partial x}-\lambda Df|u|\right)\end{aligned}\tag{A.41}$$

Where

$$\frac{\partial f}{\partial x*}=\frac{\partial f}{\partial x}+\frac{\partial f}{\partial \sigma}\frac{\partial \sigma}{\partial x}\tag{A.42}$$

The difference operators are substituted in to give

$$f_{i,k}^{\Delta n+1}=f_{i,k}^{n+1}-f_{i,k}^{n}\tag{A.43}$$

$$f_{i,k}^{\Delta n-1}=f_{i,k}^{n-1}-f_{i,k}^{n}\tag{A.44}$$

$$f=f_{i,k}^{n}+\tfrac{1}{2}\theta\left(f_{i,k}^{\Delta n+1}+f_{i,k}^{\Delta n-1}\right)\tag{A.45}$$

$$A_f=A_{f\,i,k}^{\ n}\tag{A.46}$$

$$\frac{1}{\rho D}=\frac{1}{\rho_i'^n D_i^n}\tag{A.47}$$

$$\frac{D}{\rho}=\frac{D_i^n}{\rho_i'^n}\tag{A.48}$$

$$uf=u_i^n\left(f_{i,k}^{n}+\tfrac{1}{2}\theta\left(f_{i,k}^{\Delta n+1}+f_{i,k}^{\Delta n-1}\right)\right)\tag{A.49}$$

$$\frac{\partial Df}{\partial t}=\frac{\left(D_i^{n+1}-D_i^{n-1}\right)f_{i,k}^{n}+D_i^{n+1}f_{i,k}^{\Delta n+1}-D_i^{n-1}f_{i,k}^{\Delta n-1}}{2\Delta t}\tag{A.50}$$

$$\frac{\partial \eta}{\partial t}=\frac{\eta_i^{n+1}-\eta_i^{n-1}}{2\Delta t}\tag{A.51}$$

$$\frac{\partial f}{\partial x}=\frac{2\left(f_{i+1,k}^{n}-f_{i-1,k}^{n}\right)+\theta\left(f_{i+1,k}^{\Delta n+1}-f_{i-1,k}^{\Delta n+1}+f_{i+1,k}^{\Delta n-1}-f_{i-1,k}^{\Delta n-1}\right)}{4\Delta x}\tag{A.52}$$

$$\frac{\partial B}{\partial x}=\frac{B_{i+1}^{n}-B_{i-1}^{n}}{2\Delta x}\tag{A.53}$$

$$\frac{\partial \rho'}{\partial x}=\frac{\rho_{0\,i+1}'^{n}-\rho_{0\,i-1}'^{n}}{2\Delta x}\tag{A.54}$$

$$\frac{\partial \sigma}{\partial x} = -\frac{1}{D_t^n \Delta x}\left(\sigma_k\left(D_{i+\frac{1}{2}}^n - D_{i-\frac{1}{2}}^n\right) + \eta_{i+\frac{1}{2}}^n - \eta_{i-\frac{1}{2}}^n\right) \tag{A.55}$$

$$\begin{aligned}\frac{\partial Duf}{\partial x} = \frac{1}{4\Delta x}\Big(2\Big(&D_{i+1}^n u_{i+1,k}^n f_{i+1,k}^n - D_{i-1}^n u_{i-1,k}^n f_{i-1,k}^n\Big) \\ &+\theta\Big(u_{i+1,k}^n\left(D_{i+1}^{n+1} f_{i+1,k}^{\Delta n+1} + D_{i+1}^{n-1} f_{i+1,k}^{\Delta n-1}\right) - u_{i-1,k}^n\left(D_{i+1}^{n+1} f_{i-1,k}^{\Delta n+1} + D_{i+1}^{n-1} f_{i-1,k}^{\Delta n-1}\right)\Big)\Big)\end{aligned} \tag{A.56}$$

$$\frac{\partial p'}{\partial \sigma} = \frac{1}{\Delta \sigma_T}\left(\left(\rho_{0i,k+1}'^n - \rho_{0i,k}'^n\right)\frac{\Delta \sigma_L}{\Delta \sigma_U} + \left(\rho_{0i,k}'^n - \rho_{0i,k-1}'^n\right)\frac{\Delta \sigma_U}{\Delta \sigma_L}\right) \tag{A.57}$$

$$\begin{aligned}\frac{\partial \omega f}{\partial \sigma} = \frac{1}{\Delta \sigma_T}\Big(\Big(&\omega_{i,k+1}^n f_{i,k+1}^n - \omega_{i,k}^n f_{i,k}^n + \tfrac{1}{2}\theta\Big(\omega_{i,k+1}^n\left(f_{i,k+1}^{\Delta n+1} + f_{i,k+1}^{\Delta n-1}\right) \\ &- \omega_{i,k}^n\left(f_{i,k}^{\Delta n+1} + f_{i,k}^{\Delta n-1}\right)\Big)\Big)\frac{\Delta \sigma_L}{\Delta \sigma_U} + \Big(\omega_{i,k}^n f_{i,k}^n - \omega_{i,k-1}^n f_{i,k-1}^n \\ &+\tfrac{1}{2}\theta\Big(\omega_{i,k}^n\left(f_{i,k}^{\Delta n+1} + f_{i,k}^{\Delta n-1}\right) - \omega_{i,k-1}^n\left(f_{i,k-1}^{\Delta n+1} + f_{i,k-1}^{\Delta n-1}\right)\Big)\Big)\frac{\Delta \sigma_U}{\Delta \sigma_L}\Big)\end{aligned} \tag{A.58}$$

$$\frac{\partial}{\partial x}\left(\rho A_f \frac{\partial f}{\partial x^*}\right) = \frac{1}{2\Delta x}\left(\rho_{i+1,k}'^n A_{f\,i+1,k} \frac{\partial f}{\partial x^*}^n_{i+1,k} - \rho_{i-1,k}'^n A_{f\,i-1,k} \frac{\partial f}{\partial x^*}^n_{i-1,k}\right) \tag{A.59}$$

$$\begin{aligned}\frac{\partial}{\partial \sigma}\left(\rho A_f \frac{\partial f}{\partial x^*}\right) = \frac{1}{\Delta \sigma_T}\Bigg(&\left(\rho_{i,k+1}'^n A_{f\,i,k+1}^n \frac{\partial f}{\partial x^*}^n_{i,k+1} - \rho_{i,k}'^n A_{f\,i,k}^n \frac{\partial f}{\partial x^*}^n_{i,k}\right)\frac{\Delta \sigma_L}{\Delta \sigma_U} \\ &+\left(\rho_{i,k}'^n A_{f\,i,k}^n \frac{\partial f}{\partial x^*}^n_{i,k} - \rho_{i,k-1}'^n A_{f\,i,k-1}^n \frac{\partial f}{\partial x^*}^n_{i,k-1}\right)\frac{\Delta \sigma_U}{\Delta \sigma_L}\Bigg)\end{aligned} \tag{A.60}$$

$$\frac{\partial f}{\partial x^*}^n_{i,k} = \frac{f_{i+1,k}^n - f_{i-1,k}^n}{2\Delta x} + \frac{1}{\Delta \sigma_T}\left(\left(f_{i,k+1}^n - f_{i,k}^n\right)\frac{\Delta \sigma_L}{\Delta \sigma_U} + \left(f_{i,k}^n - f_{i,k-1}^n\right)\frac{\Delta \sigma_U}{\Delta \sigma_L}\right)\frac{\partial \sigma}{\partial x} \tag{A.61}$$

$$\begin{aligned}&\frac{\partial}{\partial \sigma}\left(\rho K_f \frac{\partial f}{\partial \sigma}\right) \\ &= \frac{2}{\Delta \sigma_T}\Bigg(\rho_{i,k+\frac{1}{2}}'^n \frac{K_{f\,i,k+\frac{1}{2}}}{\Delta \sigma_U}\begin{pmatrix} f_{i,k+1}^n - f_{i,k}^n \\ +\frac{1}{2}\theta\left(f_{i,k+1}^{\Delta n+1} - f_{i,k}^{\Delta n+1} + f_{i,k+1}^{\Delta n-1} - f_{i,k}^{\Delta n-1}\right)\end{pmatrix} \\ &\quad - \rho_{i,k-\frac{1}{2}}'^n \frac{K_{f\,i,k-\frac{1}{2}}}{\Delta \sigma_L}\left(f_{i,k}^n - f_{i,k-1}^n + \tfrac{1}{2}\theta\left(f_{i,k}^{\Delta n+1} - f_{i,k-1}^{\Delta n+1} + f_{i,k}^{\Delta n-1} - f_{i,k-1}^{\Delta n-1}\right)\right)\Bigg)\end{aligned} \tag{A.62}$$

The pressure integral is calculated before the solution elements are put together.

A.3.1.1 Vertical solving

The unknowns are factored out of (A.41) after the substitution of (A.43)-(A.62), to solve in the vertical direction, that is setting $\theta = 0$ for the horizontal derivatives. The final equation is of the form

$$A_{f_k} f_{i,k-1}^{\Delta n+1} + B_{f_k} f_{i,k}^{\Delta n+1} + C_{f_k} f_{i,k+1}^{\Delta n+1} = K_{f\,v,k} \tag{A.63}$$

Where

$$A_{f_k} = \frac{\theta}{\Delta \sigma_T}\left(-\tfrac{1}{2}\omega_{i,k-1}^n \frac{\Delta \sigma_U}{\Delta \sigma_L} - \frac{\rho_{i,k-\frac{1}{2}}'^n}{\rho_{i,k}'^n}\frac{K_{f\,i,k-\frac{1}{2}}}{D_i^n \Delta \sigma_L}\right) \tag{A.64}$$

$$B_{f_k} = \frac{D_i^{n+1}}{2\Delta t} + \frac{\theta D_i^n u_{i,k}^n}{2B_i^n \Delta x}\left(B_{i+\frac{1}{2}}^n - B_{i-\frac{1}{2}}^n\right) + \frac{\theta}{\Delta\sigma_T}\left(\tfrac{1}{2}\omega_{i,k}^n\left(\frac{\Delta\sigma_U}{\Delta\sigma_L} - \frac{\Delta\sigma_L}{\Delta\sigma_U}\right)\right.$$
$$\left. + \frac{1}{D_i^n \rho_{i,k}'^n}\left(\rho_{i,k+\frac{1}{2}}'^n \frac{K_{f_{i,k+\frac{1}{2}}}}{\Delta\sigma_U} + \rho_{i,k-\frac{1}{2}}'^n \frac{K_{f_{i,k-\frac{1}{2}}}}{\Delta\sigma_L}\right)\right) - M\tfrac{1}{2}\theta\lambda_i^n D_i^n \left|u_{i,k}^n\right| \quad \text{(A.65)}$$

$$C_{f_k} = \frac{\theta}{\Delta\sigma_T}\left(\tfrac{1}{2}\omega_{i,k+1}^n \frac{\Delta\sigma_L}{\Delta\sigma_U} - \frac{\rho_{i,k+\frac{1}{2}}'^n}{\rho_{i,k}'^n}\frac{K_{f_{i,k+\frac{1}{2}}}}{D_i^n \Delta\sigma_U}\right) \quad \text{(A.66)}$$

$$K_{f_k} = \sum_{L=1}^{11} K_{f_k}^L \quad \text{(A.67)}$$

$$K_{f_k}^1 = \frac{D_i^{n-1} f_i^{\Delta n-1} - \left(D_i^{n+1} - D_i^{n-1}\right) f_{i,k}^n}{2\Delta t} \quad \text{(A.68)}$$

$$K_{f_k}^2 = -\frac{D_{i+1}^n u_{i+1,k}^n f_{i+1,k}^n - D_{i-1}^n u_{i-1,k}^n f_{i-1,k}^n}{2\Delta x} \quad \text{(A.69)}$$

$$K_{f_k}^3 = -\frac{1}{\Delta\sigma_T}\left(\left(\omega_{i,k+1}^n f_{i,k+1}^n - \omega_{i,k}^n f_{i,k}^n + \tfrac{1}{2}\theta\left(\omega_{i,k+1}^n f_{i,k+1}^{\Delta n-1} - \omega_{i,k}^n f_{i,k}^{\Delta n-1}\right)\right)\frac{\Delta\sigma_L}{\Delta\sigma_U}\right.$$
$$\left. + \left(\omega_{i,k}^n f_{i,k}^n - \omega_{i,k-1}^n f_{i,k-1}^n + \tfrac{1}{2}\theta\left(\omega_{i,k}^n f_{i,k}^{\Delta n-1} - \omega_{i,k-1}^n f_{i,k-1}^{\Delta n-1}\right)\right)\frac{\Delta\sigma_U}{\Delta\sigma_L}\right) \quad \text{(A.70)}$$

$$K_{f_k}^4 = -D_i^n u_{i,k}^n \left(f_{i,k}^n + \tfrac{1}{2}\theta f_{i,k}^{\Delta n-1}\right)\frac{B_{i+\frac{1}{2}}^n - B_{i-\frac{1}{2}}^n}{B_i^n \Delta x} \quad \text{(A.71)}$$

$$K_{f_k}^5 = \frac{D_i^n}{2\rho_{i,k}'^n \Delta x}\left(\rho_{i+1,k}'^n A_{f_{i+1,k}} \frac{\partial f}{\partial x^*}^n_{i+1,k} - \rho_{i-1,k}'^n A_{f_{i-1,k}} \frac{\partial f}{\partial x^*}^n_{i-1,k}\right) \quad \text{(A.72)}$$

$$K_{f_k}^6 = \frac{1}{\rho_{i,k}'^n \Delta\sigma_T}\left(\left(\rho_{i,k+1}'^n A_{f}{}^n_{i,k+1} \frac{\partial f}{\partial x^*}^n_{i,k+1} - \rho_{i,k}'^n A_{f}{}^n_{i,k} \frac{\partial f}{\partial x^*}^n_{i,k}\right)\frac{\Delta\sigma_L}{\Delta\sigma_U}\right.$$
$$+ \left(\rho_{i,k}'^n A_{f}{}^n_{i,k} \frac{\partial f}{\partial x^*}^n_{i,k} - \rho_{i,k-1}'^n A_{f}{}^n_{i,k-1} \frac{\partial f}{\partial x^*}^n_{i,k-1}\right)\frac{\Delta\sigma_U}{\Delta\sigma_L}$$
$$\left. \times\left(\sigma_k\left(D_{i+\frac{1}{2}}^n - D_{i-\frac{1}{2}}^n\right) + \eta_{i+\frac{1}{2}}^n - \eta_{i-\frac{1}{2}}^n\right)\right) \quad \text{(A.73)}$$

$$K_{f_k}^7 = \frac{2}{D_i^n \rho_{i,k}'^n \Delta\sigma_T}\left(\rho_{i,k+\frac{1}{2}}'^n \frac{K_{f_{i,k+\frac{1}{2}}}}{\Delta\sigma_U}\left(f_{i,k+1}^n - f_{i,k}^n + \tfrac{1}{2}\theta\left(f_{i,k+1}^{\Delta n-1} - f_{i,k}^{\Delta n-1}\right)\right)\right.$$
$$\left. - \rho_{i,k-\frac{1}{2}}'^n \frac{K_{f_{i,k-\frac{1}{2}}}}{\Delta\sigma_L}\left(f_{i,k}^n - f_{i,k-1}^n\right) + \tfrac{1}{2}\theta\left(f_{i,k}^{\Delta n-1} - f_{i,k-1}^{\Delta n-1}\right)\right) \quad \text{(A.74)}$$

$$K_{f_k}^8 = \frac{D_i^n A_{f}{}^n_{i,k}}{4B_i \Delta x^2}\left(B_{i+1} - B_{i-1}\right)\left(f_{i+1,k}^n - f_{i-1,k}^n\right) \quad \text{(A.75)}$$

$$K_{f_k}^9 = -M\frac{D_i^{n2} g}{\rho_{i,k}'^n}\sum_{k=1}^{k_{max}}\frac{\Delta\sigma_k}{2\Delta x}\left(\rho_{0i+1,k}'^n - \rho_{0i-1,k}'^n - \frac{D_{i+1}^n - D_{i-1}^n}{D_i^n}\sigma_k \frac{\partial \rho'^n}{\partial\sigma}_{i,k}\right) \quad \text{(A.76)}$$

$$K_{f_k}^{10} = -MgD_i^n \frac{\eta_{i+\frac{1}{2}}^n - \eta_{i-\frac{1}{2}}^n}{\Delta x} \quad \text{(A.77)}$$

$$\overset{11}{K}_{f_k} = M\lambda_i^n D_i^n \left(f_{i,k}^n + \tfrac{1}{2}\theta f_{i,k}^{\Delta n-1}\right)\left|u_{i,k}^n\right| \tag{A.78}$$

$$\frac{\partial \rho'^{\,n}}{\partial \sigma}_{i,k} = \frac{1}{\Delta\sigma_T}\left(\left(\rho'^{\,n}_{0i,k+1} - \rho'^{\,n}_{0i,k}\right)\frac{\Delta\sigma_L}{\Delta\sigma_U} + \left(\rho'^{\,n}_{0i,k} - \rho'^{\,n}_{0i,k-1}\right)\frac{\Delta\sigma_U}{\Delta\sigma_L}\right) \tag{A.79}$$

$$\frac{\partial f}{\partial x^*}^{n}_{i,k} = \frac{f_{i+1,k}^n - f_{i-1,k}^n}{2\Delta x} + \frac{1}{\Delta\sigma_T}\left(\left(f_{i,k+1}^n - f_{i,k}^n\right)\frac{\Delta\sigma_L}{\Delta\sigma_U} + \left(f_{i,k}^n - f_{i,k-1}^n\right)\frac{\Delta\sigma_U}{\Delta\sigma_L}\right)\frac{\partial\sigma}{\partial x} \tag{A.80}$$

$$\lambda_i^n = gn^2\left(\frac{B_i D_i^n}{B_i + 2D_i^n}\right)^{-4/3} \tag{A.81}$$

A.3.1.2 Horizontal solving

For solving in the horizontal direction $\theta = 0$ for the vertical derivatives. The final equation is of the form

$$A_{f_i} f_{i-1,k}^{\Delta n+1} + B_{f_i} f_{i,k}^{\Delta n+1} + C_{f_i} f_{i+1,k}^{\Delta n+1} = K_{f_{h,i}} \tag{A.82}$$

Where

$$A_{f_i} = -\frac{\theta}{4\Delta x} u_{i-1,k}^n D_{i-1}^{n+1} \tag{A.83}$$

$$B_{f_i} = \frac{D_i^{n+1}}{2\Delta t} + \frac{\theta D_i^n u_{i,k}^n}{2B_i^n \Delta x}\left(B_{i+\frac{1}{2}}^n - B_{i-\frac{1}{2}}^n\right) - M\lambda_i^n D_i^n \left|u_{i,k}^n\right| \tag{A.84}$$

$$C_{f_i} = \frac{\theta}{4\Delta x} u_{i+1,k}^n D_{i+1}^{n+1} \tag{A.85}$$

$$K_{f_k} = \sum_{L=1}^{11} \overset{L}{K}_{f_k} \tag{A.86}$$

$$\overset{1}{K}_{f_i} = \frac{D_i^{n-1} f_i^{\Delta n-1} - \left(D_i^{n+1} - D_i^{n-1}\right) f_{i,k}^n}{2\Delta t} \tag{A.87}$$

$$\begin{aligned}\overset{2}{K}_{f_i} = -\frac{1}{2\Delta x}\Big(&D_{i+1}^n u_{i+1,k}^n f_{i+1,k}^n - D_{i-1}^n u_{i-1,k}^n f_{i-1,k}^n \\ &+ \tfrac{1}{2}\theta\left(u_{i+1,k}^n D_{i+1}^{n-1} f_{i+1,k}^{\Delta n-1} - u_{i-1,k}^n D_{i-1}^{n-1} f_{i-1,k}^{\Delta n-1}\right)\Big)\end{aligned} \tag{A.88}$$

$$\overset{3}{K}_{f_i} = -\frac{1}{\Delta\sigma_T}\left(\left(\omega_{i,k+1}^n f_{i,k+1}^n - \omega_{i,k}^n f_{i,k}^n\right)\frac{\Delta\sigma_L}{\Delta\sigma_U} + \left(\omega_{i,k}^n f_{i,k}^n - \omega_{i,k-1}^n f_{i,k-1}^n\right)\frac{\Delta\sigma_U}{\Delta\sigma_L}\right) \tag{A.89}$$

$$\overset{4}{K}_{f_i} = -D_i^n u_{i,k}^n \left(f_{i,k}^n + \tfrac{1}{2}\theta f_{i,k}^{\Delta n-1}\right)\frac{B_{i+\frac{1}{2}}^n - B_{i-\frac{1}{2}}^n}{B_i^n \Delta x} \tag{A.90}$$

$$\overset{5}{K}_{f\,k} = \frac{D_i^n}{2\rho'^{\,n}_{i,k}\Delta x}\left(\rho'^{\,n}_{i+1,k} A_{f\,i+1,k} \frac{\partial f}{\partial x^*}^{n}_{i+1,k} - \rho'^{\,n}_{i-1,k} A_{f\,i-1,k} \frac{\partial f}{\partial x^*}^{n}_{i-1,k}\right) \tag{A.91}$$

$$\begin{aligned}\overset{6}{K}_{f_k} = \frac{1}{\rho'^{\,n}_{i,k}\Delta\sigma_T}\Bigg(&\left(\rho'^{\,n}_{i,k+1} A_{f\,i,k+1}^{\;n} \frac{\partial f}{\partial x^*}^{n}_{i,k+1} - \rho'^{\,n}_{i,k} A_{f\,i,k}^{\;n} \frac{\partial f}{\partial x^*}^{n}_{i,k}\right)\frac{\Delta\sigma_L}{\Delta\sigma_U} \\ &+ \left(\rho'^{\,n}_{i,k} A_{f\,i,k}^{\;n} \frac{\partial f}{\partial x^*}^{n}_{i,k} - \rho'^{\,n}_{i,k-1} A_{f\,i,k-1}^{\;n} \frac{\partial f}{\partial x^*}^{n}_{i,k-1}\right)\frac{\Delta\sigma_U}{\Delta\sigma_L} \\ &\times\left(\sigma_k\left(D_{i+\frac{1}{2}}^n - D_{i-\frac{1}{2}}^n\right) + \eta_{i+\frac{1}{2}}^n - \eta_{i-\frac{1}{2}}^n\right)\end{aligned} \tag{A.92}$$

$$K_{f_k}^{7} = \frac{2}{D_i^n \rho'^n_{i,k} \Delta\sigma_T}\left(\rho'^n_{i,k+\frac{1}{2}} \frac{K_{f\,i,k+\frac{1}{2}}}{\Delta\sigma_U}\left(f^n_{i,k+1} - f^n_{i,k} + \tfrac{1}{2}\theta\left(f^{\Delta n-1}_{i,k+1} - f^{\Delta n-1}_{i,k}\right)\right)\right. \\ \left. - \rho'^n_{i,k-\frac{1}{2}} \frac{K_{f\,i,k-\frac{1}{2}}}{\Delta\sigma_L}\left(f^n_{i,k} - f^n_{i,k-1}\right) + \tfrac{1}{2}\theta\left(f^{\Delta n-1}_{i,k} - f^{\Delta n-1}_{i,k-1}\right)\right) \tag{A.93}$$

$$K_{f_i}^{8} = \frac{D_i^n A^n_{f\,i,k}}{4B_i \Delta x^2}\left(B_{i+1} - B_{i-1}\right)\left(f^n_{i+1,k} - f^n_{i-1,k}\right) \tag{A.94}$$

$$K_{f_k}^{9} = -M \frac{D_i^{n2} g}{\rho'^n_{i,k}} \sum_{k=1}^{k_{\max}} \frac{\Delta\sigma_k}{2\Delta x}\left(\rho'^n_{0i+1,k} - \rho'^n_{0i-1,k} - \frac{D^n_{i+1} - D^n_{i-1}}{D^n_i}\sigma_k \frac{\partial \rho'^n}{\partial \sigma}_{i,k}\right) \tag{A.95}$$

$$K_{f_i}^{10} = -MgD_i^n \frac{\eta^n_{i+\frac{1}{2}} - \eta^n_{i-\frac{1}{2}}}{\Delta x} \tag{A.96}$$

$$K_{f_k}^{11} = M\lambda_i^n D_i^n\left(f^n_{i,k} + \tfrac{1}{2}\theta f^{\Delta n-1}_{i,k}\right)\left|u^n_{i,k}\right| \tag{A.97}$$

$$\frac{\partial \rho'^n}{\partial \sigma}_{i,k} = \frac{1}{\Delta\sigma_T}\left(\left(\rho'^n_{0i,k+1} - \rho'^n_{0i,k}\right)\frac{\Delta\sigma_L}{\Delta\sigma_U} + \left(\rho'^n_{0i,k} - \rho'^n_{0i,k-1}\right)\frac{\Delta\sigma_U}{\Delta\sigma_L}\right) \tag{A.98}$$

$$\frac{\partial f^n}{\partial x^*}_{i,k} = \frac{f^n_{i+1,k} - f^n_{i-1,k}}{2\Delta x} + \frac{1}{\Delta\sigma_T}\left(\left(f^n_{i,k+1} - f^n_{i,k}\right)\frac{\Delta\sigma_L}{\Delta\sigma_U} + \left(f^n_{i,k} - f^n_{i,k-1}\right)\frac{\Delta\sigma_U}{\Delta\sigma_L}\right)\frac{\partial\sigma}{\partial x} \tag{A.99}$$

$$\lambda_i^n = gn^2\left(\frac{B_i D_i^n}{B_i + 2D_i^n}\right)^{-4/3} \tag{A.100}$$

A.3.2 Boussinesq

For coding simplicity the non-Boussinesq equations are used with $\rho'_0 = 0$ except in the pressure terms. A switch variable is multiplied by the ρ'_0 terms that is either zero or one. This reduces human coding errors.

Appendix B
Macquarie Harbour bathymetry data

The next 12 pages contains the bathymetry data for Macquarie Harbour (in metres) for the 250m horizontal grid (references to grid indexes). Any depth less than or equal to 0.1m is defined as land. It has been arranged in regions shown in Table B.1.

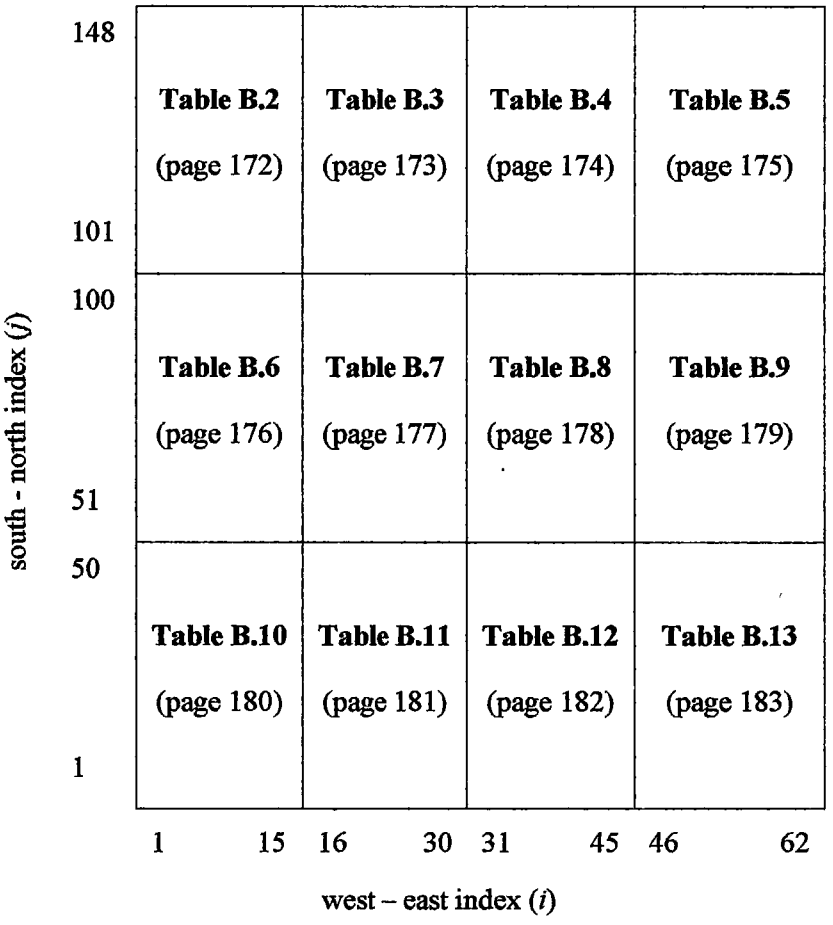

Table B.1 Key for Macquarie Harbour bathymetry regions

148	0.1	0.1	0.1	0.1	0.1	0.1	0.1	0.1	0.1	0.1	0.1	0.1	0.1	0.1	0.1
147	0.1	0.1	0.1	0.1	0.1	0.1	0.1	0.1	0.1	0.1	0.1	0.1	0.1	0.1	0.1
146	0.1	0.1	0.1	0.1	0.1	0.1	0.1	0.1	0.1	0.1	0.1	0.1	0.1	0.1	0.0
145	0.1	0.1	0.1	0.1	0.1	0.1	0.1	0.1	0.1	0.1	0.1	0.1	12.0	0.0	0.0
144	0.1	0.1	0.1	0.1	0.1	0.1	0.1	0.1	0.1	0.1	0.1	0.1	12.0	0.0	0.0
143	0.1	0.1	0.1	0.1	0.1	0.1	0.1	0.1	0.1	0.1	0.1	0.1	14.6	0.1	0.1
142	0.1	0.1	0.1	0.1	0.1	0.1	0.1	0.1	0.1	0.1	0.1	6.4	6.4	1.0	0.1
141	0.1	0.1	0.1	0.1	0.1	0.1	0.1	0.1	0.1	1.0	0.1	5.5	5.0	1.0	1.0
140	0.1	0.1	0.1	0.1	0.1	0.1	0.1	0.1	1.0	1.0	0.1	4.6	1.8	1.0	1.0
139	0.1	0.1	0.1	0.1	0.1	0.1	1.0	1.0	1.0	0.1	0.1	3.8	2.0	1.0	1.0
138	0.1	0.1	0.1	0.1	0.1	1.0	1.0	1.0	1.0	0.1	3.7	3.7	2.5	1.2	1.0
137	0.1	0.1	0.1	0.1	0.1	1.0	1.0	1.0	1.0	0.1	4.6	5.8	3.0	1.5	1.0
136	0.1	0.1	0.1	0.1	0.1	0.1	1.0	1.0	1.0	0.1	5.0	6.4	4.0	1.3	1.0
135	0.1	0.1	0.1	0.1	0.1	0.1	0.1	1.0	1.0	0.1	3.3	7.3	2.6	1.0	1.0
134	0.1	0.1	0.1	0.1	0.1	0.1	0.1	0.1	1.0	0.1	3.9	7.5	1.7	1.0	1.0
133	0.1	0.1	0.1	0.1	0.1	0.1	0.1	0.1	1.0	0.1	3.6	7.0	2.5	1.0	1.0
132	0.1	0.1	0.1	0.1	0.1	0.1	0.1	1.0	1.0	0.1	3.3	7.3	3.9	1.0	1.0
131	0.1	0.1	0.1	0.1	0.1	0.1	1.0	1.0	1.0	0.1	3.5	6.4	4.6	1.0	1.0
130	0.1	0.1	0.1	0.1	0.1	0.1	1.0	1.0	1.0	1.6	3.3	5.7	5.6	1.6	1.0
129	0.1	0.1	0.1	0.1	0.1	1.0	1.0	1.0	1.0	1.4	2.4	4.2	4.9	4.9	1.8
128	0.1	0.1	0.1	0.1	0.1	1.0	1.0	1.0	1.0	1.0	1.3	2.4	4.5	5.1	4.8
127	0.1	0.1	0.1	1.0	1.0	1.0	1.0	1.0	1.0	1.0	1.0	1.0	2.6	5.5	5.5
126	0.1	0.1	0.1	1.0	1.0	1.0	1.0	1.0	1.0	1.0	1.0	1.0	1.4	2.9	5.8
125	0.1	0.1	0.1	0.1	1.0	1.0	1.0	1.0	1.0	1.0	1.0	1.0	1.0	1.8	3.9
124	0.1	0.1	0.1	0.1	0.1	1.0	1.0	1.0	1.0	1.0	1.0	1.0	1.0	1.8	1.8
123	0.1	0.1	0.1	0.1	0.1	1.0	1.0	1.0	1.0	1.0	1.0	1.0	1.0	1.1	1.3
122	0.1	0.1	0.1	0.1	0.1	0.1	1.0	1.3	1.0	1.0	1.0	1.0	1.0	1.3	1.3
121	0.1	0.1	0.1	0.1	0.1	0.1	1.0	1.0	1.0	1.0	1.0	1.0	1.5	1.8	1.4
120	0.1	0.1	0.1	0.1	0.1	1.0	1.0	1.0	1.0	1.0	1.0	1.0	1.9	1.9	1.4
119	0.1	0.1	0.1	0.1	0.1	1.0	1.0	1.2	1.1	1.0	1.0	1.0	1.4	1.9	1.8
118	0.1	0.1	0.1	0.1	1.0	1.1	1.9	2.1	1.4	1.0	1.0	1.0	1.3	1.6	1.5
117	0.1	0.1	1.0	1.0	1.0	1.5	2.2	2.0	1.3	1.0	1.0	1.0	1.8	1.7	1.3
116	0.1	1.0	1.4	1.9	1.8	1.6	1.6	1.3	1.0	1.0	1.0	1.7	1.8	1.5	1.5
115	0.1	1.2	2.5	3.5	3.5	2.1	1.6	0.1	1.0	1.0	1.0	1.9	1.6	1.4	1.4
114	0.1	1.9	3.4	4.6	4.3	2.8	2.2	2.4	2.8	1.5	1.8	1.6	1.4	1.4	1.3
113	0.1	2.3	4.1	4.9	5.1	4.8	4.4	3.3	4.8	4.0	1.7	1.3	1.4	1.3	1.2
112	0.1	1.7	3.3	4.7	5.8	6.9	6.5	4.9	4.8	4.5	1.8	1.1	1.1	1.3	1.3
111	0.1	1.0	1.6	3.0	2.9	1.0	4.5	4.1	7.3	7.8	4.9	1.7	1.1	1.3	2.1
110	0.1	0.1	1.0	1.0	1.0	1.0	1.0	1.0	1.0	6.8	8.5	5.0	2.1	1.2	3.5
109	0.1	0.1	0.1	1.0	1.0	1.0	0.1	0.1	1.0	1.5	8.5	7.3	5.0	2.3	7.7
108	0.1	0.1	0.1	0.1	0.1	0.1	0.1	0.1	0.1	1.0	11.8	11.5	10.6	10.2	16.4
107	0.1	0.1	0.1	0.1	0.1	0.1	0.1	0.1	0.1	0.1	1.0	15.5	14.4	15.1	18.8
106	0.1	0.1	0.1	0.1	0.1	0.1	0.1	0.1	0.1	0.1	3.6	14.4	15.1	16.1	18.2
105	0.1	0.1	0.1	0.1	0.1	0.1	0.1	0.1	0.1	1.0	5.0	12.5	14.3	15.4	17.3
104	0.1	0.1	0.1	0.1	0.1	0.1	0.1	1.0	1.0	1.5	5.2	9.1	11.7	13.2	15.2
103	0.1	0.1	0.1	0.1	0.1	0.1	0.1	1.0	1.0	2.4	4.6	6.9	8.8	10.5	12.1
102	0.1	0.1	0.1	0.1	0.1	0.1	0.1	1.0	1.0	2.1	3.5	4.9	7.0	7.9	9.9
101	0.1	0.1	0.1	0.1	0.1	0.1	0.1	0.5	1.0	1.1	2.2	3.0	4.3	5.1	6.4
	1	**2**	**3**	**4**	**5**	**6**	**7**	**8**	**9**	**10**	**11**	**12**	**13**	**14**	**15**

Table B.2 Bathymetry of Macquarie Harbour – region 1

148	0.1	0.1	0.1	0.1	0.1	0.1	0.1	0.1	0.1	0.1	0.1	0.1	0.1	0.1	0.1
147	0.1	0.1	0.1	0.1	0.1	0.1	0.1	0.1	0.1	0.1	0.1	0.1	0.1	0.1	0.1
146	0.0	0.0	0.1	0.1	0.1	0.1	0.1	0.1	0.1	0.1	0.1	0.1	0.1	0.1	0.1
145	0.0	0.1	0.1	0.1	0.1	0.1	0.1	0.1	0.1	0.1	0.1	0.1	0.1	0.1	0.1
144	0.1	0.1	0.1	0.1	0.1	0.1	0.1	0.1	0.1	0.1	0.1	0.1	0.1	0.1	0.1
143	0.1	0.1	0.1	0.1	0.1	0.1	0.1	0.1	0.1	0.1	0.1	0.1	0.1	0.1	0.1
142	0.1	0.1	0.1	0.1	0.1	0.1	0.1	0.1	0.1	0.1	0.1	0.1	0.1	0.1	0.1
141	0.1	0.1	0.1	0.1	0.1	0.1	0.1	0.1	0.1	0.1	0.1	0.1	0.1	0.1	0.1
140	1.0	1.0	0.1	0.1	0.1	0.1	0.1	0.1	0.1	0.1	0.1	0.1	0.1	0.1	0.1
139	1.0	1.0	1.0	0.1	0.1	0.1	0.1	0.1	0.1	0.1	0.1	0.1	0.1	1.0	1.0
138	1.0	1.0	1.0	1.0	0.1	0.1	0.1	0.1	0.1	0.1	0.1	0.1	0.1	1.0	1.0
137	1.0	1.0	1.0	1.0	0.1	0.1	0.1	0.1	0.1	0.1	0.1	0.1	0.1	1.0	2.0
136	1.0	1.0	1.0	1.0	0.1	0.1	0.1	0.1	0.1	0.1	0.1	0.1	0.1	1.0	2.0
135	1.0	1.0	1.0	1.0	1.0	0.1	0.1	0.1	0.1	0.1	0.1	0.1	0.1	1.0	2.0
134	1.0	1.0	1.0	1.0	1.0	0.1	0.1	0.1	0.1	0.1	0.1	0.1	0.1	1.0	1.0
133	1.0	1.0	1.0	1.0	1.0	0.1	0.1	0.1	0.1	0.1	0.1	0.1	0.1	0.1	1.0
132	1.0	1.0	1.0	1.0	1.0	0.1	0.1	0.1	0.1	0.1	0.1	0.1	0.1	0.1	0.1
131	1.0	1.0	1.0	1.0	1.0	0.1	0.1	0.1	0.1	0.1	0.1	0.1	0.1	0.1	0.1
130	1.0	1.0	1.0	1.0	1.0	1.0	0.1	0.1	0.1	0.1	0.1	0.1	0.1	0.1	0.1
129	1.0	1.0	1.0	1.0	1.0	1.0	0.1	0.1	0.1	0.1	0.1	0.1	0.1	0.1	1.0
128	1.0	1.0	1.0	1.0	1.0	1.0	0.1	0.1	0.1	0.1	0.1	0.1	1.0	1.0	1.0
127	2.1	1.0	1.0	1.0	1.0	1.0	1.0	0.1	0.1	0.1	0.1	1.0	1.0	1.0	1.0
126	4.8	1.9	1.0	1.0	1.0	1.0	1.0	1.0	0.1	0.1	0.1	1.0	1.0	1.0	1.0
125	4.7	4.9	2.1	1.0	1.0	1.0	1.0	1.0	1.0	1.0	1.0	1.0	1.0	1.0	1.0
124	6.1	7.6	6.2	2.1	1.0	1.0	1.0	1.0	1.0	1.0	1.0	1.0	1.0	1.0	1.1
123	1.5	6.3	8.4	4.6	1.6	1.0	1.0	1.0	1.0	1.0	1.0	1.0	1.0	1.5	1.5
122	1.8	2.4	5.4	7.7	5.9	3.7	4.2	3.1	1.0	2.2	1.1	1.4	3.5	2.8	1.1
121	1.7	2.0	2.7	4.7	7.6	7.3	5.3	7.0	7.1	6.2	4.0	4.9	8.5	4.8	1.5
120	1.5	1.7	1.8	3.5	6.5	7.7	7.8	5.5	6.9	7.6	6.4	9.3	8.5	6.4	3.5
119	1.5	1.9	2.6	3.8	5.8	7.1	7.6	7.5	6.1	6.7	5.8	7.7	9.3	9.5	8.0
118	1.2	1.5	2.4	3.2	3.3	3.2	7.1	7.4	7.3	8.1	7.7	8.7	11.0	11.8	12.2
117	1.1	1.4	2.0	2.6	2.8	4.2	6.1	7.9	8.8	9.1	8.9	10.3	12.1	12.3	14.4
116	1.3	1.6	2.0	2.9	4.6	5.9	6.3	8.0	9.8	10.2	10.3	11.2	13.0	12.7	14.9
115	1.4	1.6	2.2	4.2	7.6	7.6	6.7	8.0	10.1	11.3	11.6	13.2	16.3	16.3	17.0
114	1.4	1.5	3.6	8.7	11.7	10.3	8.9	9.4	10.8	12.5	12.5	13.4	17.0	20.6	22.3
113	1.1	2.4	7.9	15.3	17.2	15.2	10.8	12.2	14.5	16.8	15.2	13.0	16.2	23.3	29.7
112	2.5	6.5	16.1	24.1	25.9	21.9	16.0	19.5	23.7	24.9	22.1	15.2	14.9	23.8	34.3
111	4.7	14.9	24.6	30.2	33.5	31.7	28.4	31.1	32.7	33.8	33.8	20.8	21.1	26.8	34.1
110	10.8	23.1	30.1	33.6	33.7	34.7	33.7	30.3	32.1	37.5	39.6	37.1	35.9	40.2	41.9
109	15.7	27.4	33.5	35.5	28.9	29.2	35.2	30.5	27.4	35.4	39.4	41.1	43.0	45.7	46.2
108	19.8	25.5	31.2	34.4	36.8	34.6	35.3	36.1	31.5	33.4	37.2	38.6	41.7	44.8	46.6
107	21.8	24.7	28.4	30.9	31.2	32.3	32.4	33.1	32.7	31.2	31.8	31.9	38.0	42.1	46.2
106	19.9	22.3	25.8	28.6	27.2	25.9	26.2	26.9	27.7	26.7	26.8	30.8	51.4	47.4	51.6
105	18.4	20.0	22.0	26.0	25.9	21.8	22.3	23.3	24.0	23.7	23.8	38.3	46.0	46.2	49.1
104	16.6	17.6	18.7	19.1	20.2	20.2	20.1	20.4	21.9	24.6	33.4	45.3	45.8	47.0	49.3
103	14.0	15.3	16.6	17.3	17.6	19.5	22.0	18.8	21.1	25.4	38.6	44.3	45.8	47.6	49.9
102	11.8	13.2	14.0	15.1	16.2	17.8	23.4	22.0	21.6	28.8	38.7	44.9	47.1	48.4	50.0
101	8.6	11.5	13.3	13.6	15.6	16.5	17.9	19.9	20.8	28.3	37.6	43.5	47.7	49.4	50.9
	16	**17**	**18**	**19**	**20**	**21**	**22**	**23**	**24**	**25**	**26**	**27**	**28**	**29**	**30**

Table B.3 Bathymetry of Macquarie Harbour – region 2

148	0.1	0.1	0.1	0.1	0.1	0.1	0.1	0.1	0.1	0.1	0.1	0.1	0.1	0.1	0.1
147	0.1	0.1	0.1	0.1	0.1	0.1	0.1	0.1	0.1	0.1	0.1	0.1	0.1	0.1	0.1
146	0.1	0.1	0.1	0.1	0.1	0.1	0.1	0.1	0.1	0.1	0.1	0.1	0.1	0.1	0.1
145	0.1	0.1	0.1	0.1	0.1	0.1	0.1	0.1	0.1	0.1	0.1	0.1	0.1	0.1	0.1
144	0.1	0.1	0.1	0.1	0.1	0.1	0.1	0.1	0.1	0.1	0.1	0.1	0.1	0.1	0.1
143	0.1	0.1	0.1	0.1	0.1	0.1	0.1	0.1	0.1	0.1	0.1	0.1	0.1	0.1	0.1
142	0.1	0.1	0.1	0.1	0.1	0.1	0.1	0.1	0.1	0.1	0.1	0.1	0.1	0.1	0.1
141	0.1	0.1	0.1	0.1	1.0	1.0	1.0	1.0	1.0	0.1	0.1	0.1	0.1	0.1	0.1
140	0.1	0.1	0.1	1.0	1.0	1.0	2.5	2.5	1.0	1.0	1.0	1.0	1.0	0.1	0.1
139	1.0	1.0	1.0	1.0	2.0	2.5	5.0	5.0	5.0	2.0	1.0	1.0	1.0	1.0	0.1
138	1.0	2.0	2.0	2.0	2.0	2.5	5.0	2.5	2.5	5.0	1.0	1.0	1.0	2.0	1.0
137	2.0	2.0	1.0	1.0	1.0	1.0	2.5	0.1	0.1	0.5	1.0	1.0	2.0	9.8	13.7
136	2.0	2.0	1.0	1.0	0.1	1.0	1.0	0.1	0.1	2.4	1.0	1.0	7.7	18.6	22.4
135	2.0	1.0	0.1	0.1	0.1	1.0	4.8	3.0	5.0	5.2	3.8	1.9	13.5	18.6	27.9
134	1.0	1.0	0.1	0.1	2.5	4.6	7.9	14.1	19.8	21.8	12.0	8.4	15.9	21.7	31.5
133	1.0	0.1	0.1	1.0	7.7	10.1	10.2	12.1	26.9	25.8	14.3	17.2	15.8	25.7	31.7
132	0.1	1.0	1.0	2.4	11.2	15.1	13.1	15.6	17.7	31.7	24.2	16.0	25.7	32.7	31.3
131	1.0	1.0	1.0	1.9	10.8	19.0	15.0	22.2	32.4	32.0	32.6	26.6	31.8	39.9	34.5
130	1.0	1.0	1.5	3.4	7.9	21.8	21.5	25.8	30.9	31.7	34.4	38.6	32.5	42.0	36.4
129	1.0	1.3	1.9	13.0	20.6	25.5	27.7	28.2	30.0	32.0	34.0	37.4	38.7	36.9	34.6
128	1.5	2.8	7.0	16.2	23.1	27.9	28.7	29.5	31.3	32.7	33.6	34.8	35.9	35.2	33.7
127	1.2	2.8	12.8	18.5	22.0	30.3	30.6	32.7	33.8	33.6	33.9	34.4	34.7	34.3	32.6
126	1.3	5.2	12.3	17.1	22.3	31.4	32.9	34.2	34.6	34.8	34.5	34.3	34.0	33.4	32.2
125	1.4	4.6	10.2	14.9	22.2	32.0	33.9	34.3	34.9	35.4	35.1	34.6	33.8	32.9	31.3
124	2.2	4.8	8.5	13.8	25.3	35.8	37.0	35.1	35.1	35.5	35.7	35.1	34.2	32.5	30.9
123	2.2	4.0	6.7	15.3	26.4	35.3	37.2	36.5	35.8	35.7	36.1	35.6	34.2	32.4	29.8
122	1.7	3.2	13.2	20.3	34.8	35.8	38.1	37.2	37.5	36.3	37.1	35.7	34.8	32.3	28.9
121	2.4	11.1	22.2	29.8	34.3	34.1	37.7	39.0	38.3	37.4	38.6	35.8	34.4	31.9	27.7
120	2.1	15.5	24.5	30.5	37.0	37.9	35.2	37.8	38.7	38.7	37.3	35.9	34.5	26.8	14.5
119	5.7	10.3	20.0	27.6	33.9	40.3	40.3	39.4	39.5	39.6	37.7	35.1	30.1	14.3	7.0
118	12.1	12.5	15.7	20.3	29.3	38.9	41.1	40.6	39.8	40.1	39.5	31.7	24.9	12.3	6.2
117	18.2	18.2	16.4	19.6	31.2	38.6	41.4	41.1	39.2	37.2	38.1	27.5	17.3	11.3	2.7
116	21.2	21.8	23.1	26.9	33.2	37.9	40.8	41.6	39.4	35.9	31.3	28.5	18.2	10.2	4.8
115	23.5	29.2	28.9	33.0	36.9	39.5	40.9	39.7	36.4	34.9	30.3	27.4	18.5	13.7	22.2
114	24.0	37.9	36.1	39.7	41.1	42.6	43.7	37.9	32.7	28.8	27.0	26.4	24.2	18.9	12.1
113	35.3	40.8	42.2	43.5	45.9	45.9	42.0	34.4	30.7	26.6	23.2	21.9	18.5	14.7	10.9
112	40.4	43.6	46.1	47.4	48.8	47.2	42.2	36.4	30.8	26.5	22.5	18.6	19.1	14.1	9.4
111	41.1	45.5	48.4	50.3	49.9	47.0	44.7	34.8	30.6	25.4	21.0	16.3	12.5	12.7	9.8
110	41.1	44.8	50.5	50.8	49.2	47.3	39.5	27.8	21.6	17.3	17.0	12.9	9.0	7.4	6.9
109	45.5	46.8	50.4	50.8	46.8	37.9	29.9	23.3	13.7	7.8	9.3	7.8	5.9	5.4	5.4
108	48.4	49.1	50.4	49.6	40.2	26.1	16.5	15.3	17.4	9.6	5.7	4.6	3.5	3.1	3.6
107	52.5	51.4	51.1	47.5	36.2	20.7	11.5	9.0	10.4	8.5	5.0	3.2	1.1	1.0	1.0
106	52.8	52.4	50.1	45.8	41.5	29.6	12.3	9.2	8.2	7.2	4.3	1.8	1.0	1.0	1.0
105	50.8	51.8	46.6	37.0	29.2	26.9	18.2	12.2	9.2	6.8	4.1	1.7	1.0	0.1	0.1
104	51.1	50.4	45.7	35.5	24.3	19.2	15.3	11.4	8.1	5.2	3.3	1.5	1.0	0.1	0.1
103	51.6	49.7	45.6	32.4	20.8	16.5	12.3	8.1	5.6	2.1	1.5	1.0	1.0	0.1	0.1
102	50.7	49.2	44.9	35.9	18.4	9.9	7.5	3.5	3.1	1.0	1.0	1.0	0.1	0.1	0.1
101	50.9	49.9	44.2	36.6	29.4	5.2	4.2	2.7	1.0	1.0	1.0	1.0	0.1	0.1	0.1
	31	**32**	**33**	**34**	**35**	**36**	**37**	**38**	**39**	**40**	**41**	**42**	**43**	**44**	**45**

Table B.4 Bathymetry of Macquarie Harbour – region 3

148	0.1	0.1	0.1	0.1	0.1	0.1	0.1	0.1	0.1	0.1	0.1	0.1	0.1	0.1	0.1	0.1	0.1
147	0.1	0.1	0.1	0.1	0.1	0.1	0.1	1.0	1.0	1.0	0.1	0.1	0.1	0.1	0.1	0.1	0.1
146	0.1	0.1	0.1	0.1	0.1	0.1	0.1	0.1	1.0	1.0	1.0	0.1	0.1	0.1	0.1	0.1	0.1
145	0.1	0.1	0.1	0.1	0.1	0.1	0.1	0.1	0.1	1.0	1.0	0.1	0.1	0.1	0.1	0.1	0.1
144	0.1	0.1	0.1	0.1	0.1	0.1	0.1	0.1	1.0	1.0	1.8	0.1	0.1	0.1	0.1	0.1	0.1
143	0.1	0.1	0.1	0.1	0.1	0.1	0.1	0.1	1.0	5.2	13.7	1.7	0.1	0.1	0.1	0.1	0.1
142	0.1	0.1	0.1	0.1	0.1	0.1	1.0	0.1	5.8	12.7	20.2	2.4	1.0	0.1	0.1	0.1	0.1
141	0.1	0.1	0.1	0.1	0.1	0.1	1.0	7.5	19.0	23.7	23.8	18.9	4.4	1.0	0.1	0.1	0.1
140	0.1	0.1	0.1	0.1	0.1	0.1	1.0	9.8	18.7	23.6	22.0	11.9	4.3	1.0	1.0	1.0	0.1
139	0.1	0.1	0.1	0.1	0.1	1.0	4.0	13.4	21.6	24.0	10.9	1.0	1.0	1.0	1.0	1.0	0.1
138	4.6	7.5	2.1	0.1	0.1	1.0	7.4	20.3	27.6	24.2	1.0	1.0	0.1	0.1	0.1	0.1	0.1
137	16.7	20.3	14.4	6.0	1.0	5.8	17.7	26.8	29.6	15.9	1.0	0.1	0.1	0.1	0.1	0.1	0.1
136	13.0	23.3	26.9	15.4	4.7	6.1	27.1	36.3	24.8	1.0	1.0	0.1	0.1	0.1	0.1	0.1	0.1
135	28.8	26.7	30.3	22.8	16.7	10.4	33.2	29.6	10.0	1.0	0.1	0.1	0.1	0.1	0.1	0.1	0.1
134	31.6	28.9	29.9	30.3	20.6	15.2	38.0	22.6	5.0	0.1	0.1	1.5	0.1	0.1	0.1	0.1	0.1
133	30.6	30.5	33.2	34.9	31.4	33.6	35.6	20.1	4.4	13.6	9.5	5.8	2.8	0.1	0.1	0.1	0.1
132	30.9	30.9	34.9	41.1	33.7	39.6	35.2	20.5	14.7	19.9	16.1	10.8	5.2	1.0	0.1	0.1	0.1
131	32.7	31.9	32.8	40.2	40.0	37.8	31.5	25.3	19.2	18.1	14.3	11.9	7.3	2.7	0.1	0.1	0.1
130	34.3	33.8	33.7	36.3	36.6	30.7	26.4	24.3	22.0	18.1	15.8	12.8	8.0	3.0	1.0	0.1	0.1
129	33.6	33.1	32.8	32.2	30.0	17.6	14.8	12.2	20.4	17.9	15.8	12.1	7.2	1.5	1.0	0.1	0.1
128	32.7	31.5	30.9	29.4	26.9	3.0	2.5	3.0	10.0	17.7	14.7	11.1	5.3	1.0	1.0	0.1	0.1
127	31.1	30.2	28.2	26.8	24.2	1.9	1.5	1.9	5.0	5.0	13.3	9.4	3.9	1.0	0.1	0.1	0.1
126	30.2	28.2	25.0	21.8	17.0	0.1	1.2	0.1	0.1	5.0	5.0	5.3	1.0	1.0	0.1	0.1	0.1
125	29.6	26.5	20.4	14.8	8.0	0.1	1.2	0.1	0.1	0.1	0.1	0.1	0.1	1.0	0.1	0.1	0.1
124	27.9	24.5	16.8	5.5	6.0	0.1	1.2	0.1	0.1	0.1	0.1	0.1	0.1	0.1	0.1	0.1	0.1
123	27.0	20.5	7.5	2.5	0.1	0.1	0.1	0.1	0.1	0.0	0.1	0.1	0.1	0.1	0.1	0.1	0.1
122	23.1	15.5	1.0	0.1	0.1	0.1	0.1	0.1	0.1	0.0	0.1	0.1	0.1	0.1	0.1	0.1	0.1
121	15.4	1.2	0.1	0.1	0.1	0.1	0.1	0.1	0.1	0.0	0.1	0.1	0.1	0.1	0.1	0.1	0.1
120	6.3	1.0	0.1	0.1	0.1	0.1	0.1	0.1	0.1	0.0	0.1	0.1	0.1	0.1	0.1	0.1	0.1
119	3.8	1.0	0.1	0.1	0.1	0.1	0.1	0.1	0.1	0.0	0.1	0.1	0.1	0.1	0.1	0.1	0.1
118	3.6	1.0	0.1	0.1	0.1	0.1	0.1	0.1	0.1	0.0	0.1	0.1	0.1	0.1	0.1	0.1	0.1
117	1.7	1.0	0.1	0.1	0.1	0.1	0.1	0.1	0.1	0.1	0.1	0.1	0.1	0.1	0.1	0.1	0.1
116	1.0	1.2	0.1	0.1	0.1	1.0	1.0	0.1	0.1	0.1	0.1	0.1	0.1	0.1	0.1	0.1	0.1
115	13.2	16.1	5.8	1.2	1.0	1.0	1.0	0.1	0.1	0.1	0.1	0.1	0.1	0.1	0.1	0.1	0.1
114	9.1	6.7	3.1	1.7	1.0	1.0	1.0	1.0	1.0	0.1	0.1	0.1	0.1	0.1	0.1	0.1	0.1
113	5.5	2.2	3.8	1.5	1.2	1.0	1.0	1.0	1.0	1.0	0.1	0.1	0.1	0.1	0.1	0.1	0.1
112	6.5	5.5	4.2	2.8	1.0	1.0	1.0	1.0	0.1	0.1	0.1	0.1	0.1	0.1	0.1	0.1	0.1
111	6.6	5.2	4.0	2.6	1.1	1.0	0.1	0.1	0.1	0.1	0.1	0.1	0.1	0.1	0.1	0.1	0.1
110	5.4	4.3	3.4	2.1	1.0	1.0	0.1	0.1	0.1	0.1	0.1	0.1	0.1	0.1	0.1	0.1	0.1
109	4.7	3.8	2.5	1.1	1.0	0.1	0.1	0.1	0.1	0.1	0.1	0.1	0.1	0.1	0.1	0.1	0.1
108	4.0	2.8	1.6	1.0	1.0	0.1	0.1	0.1	0.1	0.1	0.1	0.1	0.1	0.1	0.1	0.1	0.1
107	1.6	1.3	1.0	1.0	1.0	0.1	0.1	0.1	0.1	0.1	0.1	0.1	0.1	0.1	0.1	0.1	0.1
106	1.0	1.0	1.0	0.1	0.1	0.1	0.1	0.1	0.1	0.1	0.1	0.1	0.1	0.1	0.1	0.1	0.1
105	1.0	1.0	1.0	0.1	0.1	0.1	0.1	0.1	0.1	0.1	0.1	0.1	0.1	0.1	0.1	0.1	0.1
104	0.1	0.1	0.1	0.1	0.1	0.1	0.1	0.1	0.1	0.1	0.1	0.1	0.1	0.1	0.1	0.1	0.1
103	0.1	0.1	0.1	0.1	0.1	0.1	0.1	0.1	0.1	0.1	0.1	0.1	0.1	0.1	0.1	0.1	0.1
102	0.1	0.1	0.1	0.1	0.1	0.1	0.1	0.1	0.1	0.1	0.1	0.1	0.1	0.1	0.1	0.1	0.1
101	0.1	0.1	0.1	0.1	0.1	0.1	0.1	0.1	0.1	0.1	0.1	0.1	0.1	0.1	0.1	0.1	0.1
	46	**47**	**48**	**49**	**50**	**51**	**52**	**53**	**54**	**55**	**56**	**57**	**58**	**59**	**60**	**61**	**62**

Table B.5 Bathymetry of Macquarie Harbour – region 4

100	0.1	0.1	0.1	0.1	0.1	0.1	0.1	0.1	1.0	1.0	1.0	1.4	2.0	2.3	2.5
99	0.1	0.1	0.1	0.1	0.1	0.1	0.1	0.1	0.1	0.1	0.1	1.1	1.0	1.0	1.0
98	0.1	0.1	0.1	0.1	0.1	0.1	0.1	0.1	0.1	0.1	0.1	0.1	0.1	0.1	0.1
97	0.1	0.1	0.1	0.1	0.1	0.1	0.1	0.1	0.1	0.1	0.1	0.1	0.1	0.1	0.1
96	0.1	0.1	0.1	0.1	0.1	0.1	0.1	0.1	0.1	0.1	0.1	0.1	2.9	4.1	5.6
95	0.1	0.1	0.1	0.1	0.1	0.1	0.1	0.1	0.1	1.0	2.4	5.2	7.1	8.4	9.6
94	0.1	0.1	0.1	0.1	0.1	0.1	0.1	0.1	1.0	3.3	6.7	9.9	12.0	13.3	13.8
93	0.1	0.1	0.1	0.1	0.1	0.1	0.1	1.0	2.8	7.1	11.7	15.3	16.8	18.0	17.7
92	0.1	0.1	0.1	0.1	0.1	0.1	1.0	2.6	5.8	10.5	16.0	20.2	19.8	20.5	20.1
91	0.1	0.1	0.1	0.1	0.1	1.0	2.1	4.7	8.0	12.3	16.9	19.8	20.0	20.7	20.6
90	0.1	0.1	0.1	1.0	1.0	1.3	3.2	6.1	9.2	12.9	16.6	19.2	20.3	20.7	20.7
89	0.1	0.1	0.1	1.0	1.0	1.6	3.5	6.7	9.6	13.0	16.1	18.8	20.3	20.5	20.5
88	0.1	0.1	0.1	1.0	1.0	1.5	3.5	7.0	9.6	12.8	15.6	17.9	19.4	20.0	20.3
87	0.1	0.1	0.1	0.1	1.0	1.3	3.3	6.9	9.5	12.5	15.1	17.0	18.1	19.6	20.0
86	0.1	0.1	0.1	0.1	1.0	1.4	3.0	6.4	9.4	12.3	14.3	15.8	18.0	18.9	19.8
85	0.1	0.1	0.1	1.0	1.0	1.2	2.7	6.3	9.4	11.7	13.4	15.9	17.7	19.1	19.6
84	0.1	0.1	0.1	0.1	1.0	1.0	2.4	5.6	9.5	11.2	13.5	16.4	18.1	18.8	19.5
83	0.1	0.1	0.1	0.1	0.1	1.0	2.2	5.6	9.0	11.7	15.6	17.1	18.4	19.2	19.4
82	0.1	0.1	0.1	0.1	0.1	1.0	3.5	8.9	12.0	15.3	16.8	18.3	19.4	20.3	20.2
81	0.1	0.1	0.1	0.1	0.1	1.0	7.0	12.2	14.9	16.1	17.3	18.3	19.9	21.5	20.3
80	0.1	0.1	0.1	0.1	0.1	1.0	14.3	14.4	14.3	15.4	16.5	17.8	19.5	21.4	20.0
79	0.1	0.1	0.1	0.1	0.1	4.9	9.2	11.8	13.3	13.6	15.1	16.5	18.1	19.2	19.4
78	0.1	0.1	0.1	0.1	1.0	1.2	5.0	6.1	8.5	12.3	13.1	14.8	16.4	17.8	17.8
77	0.1	0.1	0.1	1.0	1.0	1.0	2.5	4.2	6.5	8.7	12.0	12.9	14.3	15.4	16.1
76	0.1	0.1	0.1	1.0	1.0	1.0	1.0	2.9	5.2	6.9	8.7	12.0	12.4	13.5	15.0
75	0.1	0.1	0.1	1.0	1.0	1.0	1.0	2.2	3.9	5.8	7.3	9.3	10.6	12.4	14.1
74	0.1	0.1	0.1	1.0	0.1	1.0	1.0	1.5	2.9	4.6	6.6	7.9	9.6	12.0	13.2
73	0.1	0.1	0.1	0.1	0.1	1.0	1.0	1.0	2.2	3.9	5.6	7.7	9.5	11.1	12.3
72	0.1	0.1	0.1	0.1	0.1	1.0	1.0	1.0	1.6	3.1	5.0	7.4	9.0	10.0	12.0
71	0.1	0.1	0.1	0.1	0.1	0.1	1.0	1.0	1.2	2.8	5.0	6.8	8.6	10.2	12.0
70	0.1	0.1	0.1	0.1	0.1	0.1	1.0	1.0	1.2	3.0	4.8	6.6	8.5	10.3	12.2
69	0.1	0.1	0.1	0.1	0.1	0.1	0.1	1.0	1.2	2.8	5.0	7.1	9.0	10.6	12.6
68	0.1	0.1	0.1	0.1	0.1	0.1	1.0	1.0	1.3	2.9	5.4	7.8	9.7	11.4	13.1
67	0.1	0.1	0.1	0.1	0.1	0.1	1.0	1.0	1.7	3.2	6.1	9.0	10.9	13.0	14.4
66	0.1	0.1	0.1	0.1	0.1	0.1	1.0	1.0	2.4	3.9	7.2	10.4	13.2	14.2	16.3
65	0.1	0.1	0.1	0.1	0.1	0.1	1.0	1.0	2.9	5.4	8.9	13.2	14.3	16.7	17.9
64	0.1	0.1	0.1	0.1	0.1	0.1	1.0	1.0	2.5	8.6	13.4	16.0	19.2	19.7	20.5
63	0.1	0.1	0.1	0.1	0.1	0.1	1.0	1.0	6.1	13.7	16.3	19.8	22.5	24.4	25.3
62	0.1	0.1	0.1	0.1	0.1	0.1	0.1	1.0	2.8	14.1	17.6	20.4	23.3	26.8	28.4
61	0.1	0.1	0.1	0.1	0.1	0.1	0.1	1.0	3.1	8.0	14.7	17.8	19.8	24.3	27.6
60	0.1	0.1	0.1	0.1	0.1	0.1	1.0	1.0	2.7	5.9	11.6	14.8	18.7	22.2	26.1
59	0.1	0.1	0.1	0.1	0.1	0.1	0.1	1.0	1.4	4.8	10.1	14.4	17.8	21.6	24.4
58	0.1	0.1	0.1	0.1	0.1	0.1	0.1	1.0	1.2	4.7	9.6	14.0	18.0	21.1	24.1
57	0.1	0.1	0.1	0.1	0.1	0.1	0.1	1.0	1.4	4.8	9.4	14.1	18.3	21.6	24.0
56	0.1	0.1	0.1	0.1	0.1	0.1	0.1	1.0	1.0	4.6	9.4	14.4	19.1	22.2	24.4
55	0.1	0.1	0.1	0.1	0.1	0.1	0.1	1.0	1.0	4.4	9.5	14.6	19.3	22.4	24.7
54	0.1	0.1	0.1	0.1	0.1	0.1	0.1	0.1	1.0	4.2	9.5	14.7	19.2	22.4	24.6
53	0.1	0.1	0.1	0.1	0.1	0.1	0.1	0.1	1.0	4.6	9.6	14.8	19.6	22.3	24.2
52	0.1	0.1	0.1	0.1	0.1	0.1	0.1	0.1	1.6	4.8	9.1	14.2	19.7	21.4	23.2
51	0.1	0.1	0.1	0.1	0.1	0.1	0.1	1.0	1.3	4.1	7.5	11.6	15.6	18.6	21.0
	1	**2**	**3**	**4**	**5**	**6**	**7**	**8**	**9**	**10**	**11**	**12**	**13**	**14**	**15**

Table B.6 Bathymetry of Macquarie Harbour – region 5

100	2.7	7.2	13.2	14.4	15.6	16.6	17.2	18.2	21.5	30.3	41.7	44.0	47.7	49.5	50.5
99	1.0	1.0	0.1	14.7	16.4	16.8	17.0	18.0	20.2	31.1	44.0	46.8	47.9	49.3	49.6
98	0.1	0.1	0.1	15.6	16.7	16.9	17.0	18.2	20.9	28.3	45.2	47.0	47.9	48.8	49.5
97	0.1	0.1	10.8	14.9	16.0	16.7	17.0	18.1	22.4	30.3	41.0	45.7	47.5	48.1	48.3
96	7.5	9.5	11.9	15.1	16.1	16.9	17.2	18.4	24.0	32.5	40.3	44.6	46.4	46.9	47.0
95	10.6	11.7	12.9	14.8	16.5	17.5	18.3	21.8	29.0	35.6	41.0	44.3	45.5	46.4	46.1
94	13.7	14.0	14.6	15.5	16.8	18.7	22.9	32.1	37.3	39.8	42.4	44.5	45.9	46.6	45.7
93	16.9	16.5	16.6	17.4	18.3	20.3	26.3	33.8	38.9	42.0	43.7	44.5	45.0	45.4	45.1
92	19.1	18.4	18.2	18.8	20.0	22.5	26.9	33.0	37.7	41.6	44.2	45.6	45.1	45.2	44.6
91	20.0	19.4	19.2	19.9	21.4	23.7	27.1	31.2	36.5	40.7	43.8	45.5	46.1	45.5	44.9
90	20.4	19.9	19.7	20.6	22.4	24.6	27.6	31.3	35.9	40.0	43.1	45.1	46.0	45.8	45.0
89	20.4	20.3	20.3	21.3	23.0	25.3	28.3	32.0	35.9	39.8	42.9	45.1	46.3	46.3	44.3
88	20.5	20.6	21.0	22.1	23.7	26.0	29.0	32.5	36.2	39.9	43.1	45.6	46.8	46.6	43.2
87	20.5	20.8	21.4	22.5	24.3	26.5	29.3	32.8	36.4	40.3	43.9	46.6	47.8	46.2	41.8
86	20.3	20.8	21.8	22.7	24.4	26.6	29.2	32.9	37.1	41.0	44.8	47.7	49.2	47.5	42.9
85	20.1	20.8	22.0	23.0	24.5	26.7	29.0	32.5	37.2	42.3	45.8	48.8	50.1	48.3	43.8
84	20.0	20.5	21.9	23.4	25.1	27.1	28.8	32.5	38.4	43.4	46.9	49.5	50.4	48.1	43.3
83	19.8	20.6	21.8	23.7	26.0	28.6	30.9	35.8	40.8	45.6	48.1	50.0	50.5	48.0	43.0
82	20.1	20.8	22.6	25.3	27.8	30.5	34.7	40.2	44.8	47.7	49.5	50.0	50.0	46.8	40.6
81	19.7	20.5	22.1	25.8	29.4	29.6	37.0	43.6	48.0	49.6	49.6	48.2	48.4	43.2	36.5
80	19.3	19.6	20.6	24.6	29.5	29.7	36.6	42.0	43.4	49.4	50.3	48.6	46.9	37.8	32.0
79	18.7	18.7	19.4	22.2	27.4	30.9	35.6	39.8	43.3	47.3	49.6	50.3	46.3	38.9	32.5
78	17.8	18.6	19.7	22.5	26.6	30.6	34.8	38.9	42.4	45.9	48.7	47.8	44.6	39.3	33.9
77	17.0	18.3	20.0	23.0	26.9	31.3	34.9	38.6	42.0	44.3	46.7	45.6	42.7	38.8	34.5
76	16.7	17.8	19.8	23.0	26.6	30.6	34.4	38.2	41.4	43.4	44.4	43.7	41.4	37.9	34.4
75	15.9	17.1	19.1	22.3	25.8	29.5	33.7	37.9	41.0	42.5	43.0	42.0	40.2	37.3	34.0
74	14.7	16.5	18.5	21.5	24.8	28.3	32.7	38.0	41.0	41.9	41.9	41.0	39.2	36.7	33.6
73	14.2	16.0	17.9	20.7	24.1	27.8	32.2	37.2	40.1	41.0	41.1	40.2	38.6	36.2	33.2
72	14.0	15.8	17.8	20.4	24.1	28.1	32.2	36.2	38.9	40.2	40.4	39.6	38.1	35.8	33.0
71	13.9	15.9	18.2	21.0	24.6	28.4	32.3	35.8	38.4	39.7	39.9	39.2	37.8	35.6	32.7
70	14.2	16.2	18.6	21.6	25.0	28.7	32.6	36.1	38.6	39.7	39.8	39.0	37.6	35.4	32.6
69	14.5	16.7	19.1	21.9	25.3	29.0	33.0	36.8	39.3	40.0	39.8	38.8	37.4	35.3	32.8
68	15.4	17.5	19.5	22.4	25.7	29.1	33.3	37.6	40.2	40.3	39.7	38.6	37.0	35.0	32.5
67	16.6	18.6	20.9	23.5	26.3	29.0	33.4	37.9	39.9	40.1	39.5	38.3	36.5	34.4	31.6
66	17.9	20.1	22.4	25.1	27.8	30.6	35.0	39.5	40.3	40.0	39.1	37.8	36.0	33.7	30.7
65	19.4	21.7	24.2	26.9	30.0	33.3	36.9	39.8	40.3	39.6	38.3	36.9	35.3	33.0	29.9
64	21.6	24.1	26.3	28.8	32.0	35.4	38.1	39.8	39.8	38.7	37.0	35.6	34.1	32.2	29.1
63	25.8	27.1	28.8	31.1	34.1	37.3	39.5	40.0	39.0	37.2	35.4	33.7	32.5	31.2	28.1
62	29.1	29.2	29.9	31.7	34.8	38.5	40.5	40.0	38.1	34.5	31.8	29.8	28.2	27.0	24.2
61	29.2	29.9	30.2	31.5	34.7	38.9	41.2	39.7	38.0	32.0	29.4	27.1	24.8	22.0	19.3
60	27.5	29.2	29.7	30.2	33.7	37.1	38.7	38.1	35.9	32.5	30.0	27.9	24.8	20.9	18.3
59	26.4	27.8	29.1	30.8	33.2	35.5	36.8	36.6	35.9	33.8	31.4	30.3	27.1	23.1	20.5
58	26.1	27.7	29.2	30.8	32.7	34.2	35.0	35.5	34.7	33.6	31.9	30.1	27.5	24.4	21.0
57	26.2	28.2	29.3	30.6	32.2	33.3	34.2	34.3	33.7	32.5	31.2	29.2	27.0	24.1	20.8
56	26.3	28.0	29.5	30.5	31.7	32.7	33.4	33.3	32.6	31.5	30.0	28.5	26.3	23.4	20.1
55	26.5	28.1	29.4	30.4	31.4	32.2	32.5	32.4	31.7	30.6	29.4	27.9	25.6	22.7	19.3
54	26.4	28.0	29.1	30.2	31.2	31.8	31.9	31.7	31.3	30.1	29.0	27.4	25.1	22.2	18.8
53	25.9	27.3	28.6	29.8	30.7	31.2	31.4	31.2	30.9	30.0	28.9	27.2	25.0	22.1	18.5
52	24.8	26.4	27.8	29.0	30.1	30.5	30.8	30.9	30.7	30.1	29.1	27.4	25.0	22.0	18.0
51	23.1	25.0	26.6	27.8	28.8	29.6	30.1	30.5	30.6	30.3	29.5	27.9	25.4	22.0	17.7
	16	**17**	**18**	**19**	**20**	**21**	**22**	**23**	**24**	**25**	**26**	**27**	**28**	**29**	**30**

Table B.7 Bathymetry of Macquarie Harbour – region 6

100	50.5	49.5	41.1	20.2	14.5	6.7	4.5	1.7	1.0	1.0	1.0	1.0	0.1	0.1	0.1
99	49.9	48.6	43.3	22.6	9.1	4.0	2.6	1.7	1.0	1.0	1.0	0.1	0.1	0.1	0.1
98	48.8	46.7	40.9	28.5	17.7	10.5	5.0	5.9	3.1	1.1	0.1	0.1	0.1	0.1	0.1
97	46.8	44.7	39.8	30.8	21.5	16.5	16.2	11.5	6.0	2.7	1.0	0.1	0.1	0.1	0.1
96	45.4	42.8	37.9	29.5	21.6	17.9	16.4	11.3	6.9	3.6	1.4	0.1	0.1	0.1	0.1
95	43.9	40.9	35.6	27.9	19.9	17.7	14.6	10.9	7.8	4.1	1.6	1.0	0.1	0.1	0.1
94	43.1	40.2	35.5	29.0	23.0	18.4	14.5	10.7	7.2	4.6	1.6	1.0	0.1	0.1	0.1
93	43.2	40.4	36.6	31.4	25.8	19.9	15.2	11.1	7.1	3.8	1.3	1.0	0.1	0.1	0.1
92	43.2	41.4	38.4	34.1	29.4	22.5	17.1	12.2	7.3	3.2	1.0	1.0	0.1	0.1	0.1
91	43.6	41.9	39.3	36.3	33.0	28.1	20.2	13.5	7.4	2.5	1.0	0.1	0.1	0.1	0.1
90	43.5	41.7	39.4	37.2	34.3	29.8	22.4	14.4	7.5	1.6	1.0	0.1	0.1	0.1	0.1
89	41.9	40.4	38.5	37.1	34.9	31.7	23.5	14.7	7.7	2.1	1.0	0.1	0.1	0.1	0.1
88	39.5	37.0	36.6	35.9	34.4	31.6	24.2	15.3	7.7	1.3	1.0	0.1	0.1	0.1	0.1
87	37.3	34.0	33.4	33.7	32.6	29.8	23.1	15.0	7.6	1.9	1.0	0.1	0.1	0.1	0.1
86	37.0	30.5	28.6	29.8	30.1	26.2	20.5	13.7	7.0	1.7	1.0	0.1	0.1	0.1	0.1
85	37.7	30.6	25.1	25.0	25.9	22.9	18.1	12.3	5.8	1.0	1.0	0.1	0.1	0.1	0.1
84	38.4	32.6	29.4	21.1	20.9	19.4	16.0	10.3	4.8	1.0	0.1	0.1	0.1	0.1	0.1
83	38.0	33.5	28.2	22.2	18.7	18.8	13.3	8.7	3.5	1.0	0.1	0.1	0.1	0.1	0.1
82	35.6	31.7	27.3	22.1	18.1	16.2	9.5	5.9	2.4	1.0	0.1	0.1	0.1	0.1	0.1
81	31.9	28.3	24.5	21.0	18.2	14.7	3.8	3.6	1.3	1.0	0.1	0.1	0.1	0.1	0.1
80	28.1	25.3	22.4	20.1	18.6	17.4	11.8	4.5	1.1	1.0	0.1	0.1	0.1	0.1	0.1
79	28.1	24.6	22.0	20.2	19.5	16.5	11.7	5.3	1.8	1.0	0.1	0.1	0.1	0.1	0.1
78	29.7	26.0	22.7	20.2	18.0	14.8	10.4	6.0	2.1	1.0	0.1	0.1	0.1	0.1	0.1
77	30.2	26.2	22.9	19.6	16.9	13.4	9.5	5.8	2.1	1.0	0.1	0.1	0.1	0.1	0.1
76	30.3	26.3	22.5	19.0	15.7	12.4	8.7	5.1	1.9	1.0	0.1	0.1	0.1	0.1	0.1
75	30.2	26.2	22.2	18.4	14.8	11.6	8.1	5.0	1.8	1.0	0.1	0.1	0.1	0.1	0.1
74	29.9	25.8	21.6	17.7	14.2	10.9	7.7	4.8	2.1	1.0	0.1	0.1	0.1	0.1	0.1
73	29.6	25.4	21.0	17.2	13.7	10.4	7.3	4.8	2.3	1.0	0.1	0.1	0.1	0.1	0.1
72	29.4	25.1	20.8	16.8	13.2	10.0	7.0	4.6	2.5	1.0	1.0	0.1	0.1	0.1	0.1
71	29.0	24.7	20.3	16.4	12.7	9.5	6.6	4.3	2.3	1.0	1.0	0.1	0.1	0.1	0.1
70	29.0	24.3	19.6	15.8	12.2	8.9	6.1	3.8	1.8	1.0	1.0	0.1	0.1	0.1	0.1
69	29.4	24.3	19.1	15.2	11.6	8.3	5.4	3.1	1.2	1.0	0.1	0.1	0.1	0.1	0.1
68	29.4	24.2	19.1	14.8	10.9	7.5	4.6	2.2	1.0	1.0	0.1	0.1	0.1	0.1	0.1
67	28.0	23.3	18.5	14.1	10.1	6.7	3.7	1.2	1.0	0.1	0.1	0.1	0.1	0.1	0.1
66	26.9	22.2	17.5	13.1	9.0	5.5	2.8	1.0	1.0	0.1	0.1	0.1	0.1	0.1	0.1
65	26.0	21.3	16.5	11.9	7.7	4.1	1.6	1.0	0.1	0.1	0.1	0.1	0.1	0.1	0.1
64	25.1	20.3	15.3	10.4	6.0	2.4	1.0	1.0	0.1	0.1	0.1	0.1	0.1	0.1	0.1
63	23.8	19.0	13.4	8.4	4.6	1.1	1.0	0.1	0.1	0.1	0.1	0.1	0.1	0.1	0.1
62	20.4	15.7	10.3	6.5	3.0	1.0	1.0	0.1	0.1	0.1	0.1	0.1	0.1	0.1	0.1
61	16.4	11.6	6.7	4.1	2.2	1.0	0.1	0.1	0.1	0.1	0.1	0.1	0.1	0.1	0.1
60	15.6	8.8	3.6	3.3	2.5	1.9	0.1	0.1	0.1	0.1	0.1	0.1	0.1	0.1	0.1
59	16.4	9.9	5.3	3.8	3.2	2.7	1.0	0.1	0.1	0.1	0.1	0.1	0.1	0.1	0.1
58	16.8	12.0	8.2	5.7	3.9	2.9	1.5	0.1	0.1	0.1	0.1	0.1	0.1	0.1	0.1
57	16.7	12.3	8.6	6.0	3.9	2.6	1.5	1.0	0.1	0.1	0.1	0.1	0.1	0.1	0.1
56	16.2	12.3	8.6	5.7	3.9	2.7	1.3	1.0	0.1	0.1	0.1	0.1	0.1	0.1	0.1
55	15.5	11.7	8.1	5.4	3.3	2.3	1.1	1.0	1.0	0.1	0.1	0.1	0.1	0.1	0.1
54	14.8	10.9	7.3	4.6	2.6	1.5	1.0	1.0	1.0	0.1	0.1	0.1	0.1	0.1	0.1
53	14.1	9.8	6.1	3.4	1.6	1.0	1.0	2.0	1.0	0.1	0.1	0.1	0.1	0.1	0.1
52	13.3	8.6	4.4	1.8	1.0	1.0	2.0	2.0	1.0	0.1	0.1	0.1	0.1	0.1	0.1
51	12.8	7.5	2.5	2.5	0.1	2.5	2.5	2.5	1.0	0.1	0.1	0.1	0.1	0.1	0.1
	31	**32**	**33**	**34**	**35**	**36**	**37**	**38**	**39**	**40**	**41**	**42**	**43**	**44**	**45**

Table B.8 Bathymetry of Macquarie Harbour – region 7

100	0.1	0.1	0.1	0.1	0.1	0.1	0.1	0.1	0.1	0.1	0.1	0.1	0 1	0.1	0.1	0.1	0.1
99	0.1	0.1	0.1	0.1	0.1	0.1	0.1	0.1	0.1	0.1	0.1	0.1	0.1	0.1	0.1	0.1	0.1
98	0.1	0.1	0.1	0.1	0.1	0.1	0.1	0.1	0.1	0.1	0.1	0.1	0.1	0.1	0.1	0.1	0.1
97	0.1	0.1	0.1	0.1	0.1	0.1	0.1	0.1	0.1	0.1	0.1	0.1	0.1	0.1	0.1	0.1	0.1
96	0.1	0.1	0.1	0.1	0.1	0.1	0.1	0.1	0.1	0.1	0.1	0.1	0.1	0.1	0.1	0.1	0.1
95	0.1	0.1	0.1	0.1	0.1	0.1	0.1	0.1	0.1	0.1	0.1	0.1	0.1	0.1	0.1	0.1	0.1
94	0.1	0.1	0.1	0.1	0.1	0.1	0.1	0.1	0.1	0.1	0.1	0.1	0.1	0.1	0.1	0.1	0.1
93	0.1	0.1	0.1	0.1	0.1	0.1	0.1	0.1	0.1	0.1	0.1	0.1	0.1	0.1	0.1	0.1	0.1
92	0.1	0.1	0.1	0.1	0.1	0.1	0.1	0.1	0.1	0.1	0.1	0.1	0.1	0.1	0.1	0.1	0.1
91	0.1	0.1	0.1	0.1	0.1	0.1	0.1	0.1	0.1	0.1	0.1	0.1	0.1	0.1	0.1	0.1	0.1
90	0.1	0.1	0.1	0.1	0.1	0.1	0.1	0.1	0.1	0.1	0.1	0.1	0.1	0.1	0.1	0.1	0.1
89	0.1	0.1	0.1	0.1	0.1	0.1	0.1	0.1	0.1	0.1	0.1	0.1	0.1	0.1	0.1	0.1	0.1
88	0.1	0.1	0.1	0.1	0.1	0.1	0.1	0.1	0.1	0.1	0.1	0.1	0.1	0.1	0.1	0.1	0.1
87	0.1	0.1	0.1	0.1	0.1	0.1	0.1	0.1	0.1	0.1	0.1	0.1	0.1	0.1	0.1	0.1	0.1
86	0.1	0.1	0.1	0.1	0.1	0.1	0.1	0.1	0.1	0.1	0.1	0.1	0.1	0.1	0.1	0.1	0.1
85	0.1	0.1	0.1	0.1	0.1	0.1	0.1	0.1	0.1	0.1	0.1	0.1	0.1	0.1	0.1	0.1	0.1
84	0.1	0.1	0.1	0.1	0.1	0.1	0.1	0.1	0.1	0.1	0.1	0.1	0.1	0.1	0.1	0.1	0.1
83	0.1	0.1	0.1	0.1	0.1	0.1	0.1	0.1	0.1	0.1	0.1	0.1	0.1	0.1	0.1	0.1	0.1
82	0.1	0.1	0.1	0.1	0.1	0.1	0.1	0.1	0.1	0.1	0.1	0.1	0.1	0.1	0.1	0.1	0.1
81	0.1	0.1	0.1	0.1	0.1	0.1	0.1	0.1	0.1	0.1	0.1	0.1	0.1	0.1	0.1	0.1	0.1
80	0.1	0.1	0.1	0.1	0.1	0.1	0.1	0.1	0.1	0.1	0.1	0.1	0.1	0.1	0.1	0.1	0.1
79	0.1	0.1	0.1	0.1	0.1	0.1	0.1	0.1	0.1	0.1	0.1	0.1	0.1	0.1	0.1	0.1	0.1
78	0.1	0.1	0.1	0.1	0.1	0.1	0.1	0.1	0.1	0.1	0.1	0.1	0.1	0.1	0.1	0.1	0.1
77	0.1	0.1	0.1	0.1	0.1	0.1	0.1	0.1	0.1	0.1	0.1	0.1	0.1	0.1	0.1	0.1	0.1
76	0.1	0.1	0.1	0.1	0.1	0.1	0.1	0.1	0.1	0.1	0.1	0.1	0.1	0.1	0.1	0.1	0.1
75	0.1	0.1	0.1	0.1	0.1	0.1	0.1	0.1	0.1	0.1	0.1	0.1	0.1	0.1	0.1	0.1	0.1
74	0.1	0.1	0.1	0.1	0.1	0.1	0.1	0.1	0.1	0.1	0.1	0.1	0.1	0.1	0.1	0.1	0.1
73	0.1	0.1	0.1	0.1	0.1	0.1	0.1	0.1	0.1	0.1	0.1	0.1	0.1	0.1	0.1	0.1	0.1
72	0.1	0.1	0.1	0.1	0.1	0.1	0.1	0.1	0.1	0.1	0.1	0.1	0.1	0.1	0.1	0.1	0.1
71	0.1	0.1	0.1	0.1	0.1	0.1	0.1	0.1	0.1	0.1	0.1	0.1	0.1	0.1	0.1	0.1	0.1
70	0.1	0.1	0.1	0.1	0.1	0.1	0.1	0.1	0.1	0.1	0.1	0.1	0.1	0.1	0.1	0.1	0.1
69	0.1	0.1	0.1	0.1	0.1	0.1	0.1	0.1	0.1	0.1	0.1	0.1	0.1	0.1	0.1	0.1	0.1
68	0.1	0.1	0.1	0.1	0.1	0.1	0.1	0.1	0.1	0.1	0.1	0.1	0.1	0.1	0.1	0.1	0.1
67	0.1	0.1	0.1	0.1	0.1	0.1	0.1	0.1	0.1	0.1	0.1	0.1	0.1	0.1	0.1	0.1	0.1
66	0.1	0.1	0.1	0.1	0.1	0.1	0.1	0.1	0.1	0.1	0.1	0.1	0.1	0.1	0.1	0.1	0.1
65	0.1	0.1	0.1	0.1	0.1	0.1	0.1	0.1	0.1	0.1	0.1	0.1	0.1	0.1	0.1	0.1	0.1
64	0.1	0.1	0.1	0.1	0.1	0.1	0.1	0.1	0.1	0.1	0.1	0.1	0.1	0.1	0.1	0.1	0.1
63	0.1	0.1	0.1	0.1	0.1	0.1	0.1	0.1	0.1	0.1	0.1	0.1	0.1	0.1	0.1	0.1	0.1
62	0.1	0.1	0.1	0.1	0.1	0.1	0.1	0.1	0.1	0.1	0.1	0.1	0.1	0.1	0.1	0.1	0.1
61	0.1	0.1	0.1	0.1	0.1	0.1	0.1	0.1	0.1	0.1	0.1	0.1	0.1	0.1	0.1	0.1	0.1
60	0.1	0.1	0.1	0.1	0.1	0.1	0.1	0.1	0.1	0.1	0.1	0.1	0.1	0.1	0.1	0.1	0.1
59	0.1	0.1	0.1	0.1	0.1	0.1	0.1	0.1	0.1	0.1	0.1	0.1	0.1	0.1	0.1	0.1	0.1
58	0.1	0.1	0.1	0.1	0.1	0.1	0.1	0.1	0.1	0.1	0.1	0.1	0.1	0.1	0.1	0.1	0.1
57	0.1	0.1	0.1	0.1	0.1	0.1	0.1	0.1	0.1	0.1	0.1	0.1	0.1	0.1	0.1	0.1	0.1
56	0.1	0.1	0.1	0.1	0.1	0.1	0.1	0.1	0.1	0.1	0.1	0.1	0.1	0.1	0.1	0.1	0.1
55	0.1	0.1	0.1	0.1	0.1	0.1	0.1	0.1	0.1	0.1	0.1	0.1	0.1	0.1	0.1	0.1	0.1
54	0.1	0.1	0.1	0.1	0.1	0.1	0.1	0.1	0.1	0.1	0.1	0.1	0.1	0.1	0.1	0.1	0.1
53	0.1	0.1	0.1	0.1	0.1	0.1	0.1	0.1	0.1	0.1	0.1	0.1	0.1	0.1	0.1	0.1	0.1
52	0.1	0.1	0.1	0.1	0.1	0.1	0.1	0.1	0.1	0.1	0.1	0.1	0.1	0.1	0.1	0.1	0.1
51	0.1	0.1	0.1	0.1	0.1	0.1	0.1	0.1	0.1	0.1	0.1	0.1	0.1	0.1	0.1	0.1	0.1
	46	**47**	**48**	**49**	**50**	**51**	**52**	**53**	**54**	**55**	**56**	**57**	**58**	**59**	**60**	**61**	**62**

Table B.9 Bathymetry of Macquarie Harbour – region 8

50	0.1	0.1	0.1	0.1	0.1	0.1	0.1	1.0	1.0	2.5	5.2	8.1	11.2	14.3	17.7
49	0.1	0.1	0.1	0.1	0.1	0.1	0.1	0.1	1.0	1.0	2.5	4.4	6.4	9.3	13.7
48	0.1	0.1	0.1	0.1	0.1	0.1	0.1	0.1	0.1	1.0	1.0	1.1	1.7	3.5	9.3
47	0.1	0.1	0.1	0.1	0.1	0.1	0.1	0.1	0.1	0.1	1.0	1.0	1.0	1.0	5.7
46	0.1	0.1	0.1	0.1	0.1	0.1	0.1	0.1	0.1	0.1	0.1	0.1	1.0	1.0	3.6
45	0.1	0.1	0.1	0.1	0.1	0.1	0.1	0.1	0.1	0.1	0.1	0.1	1.0	1.0	2.9
44	0.1	0.1	0.1	0.1	0.1	0.1	0.1	0.1	0.1	0.1	0.1	0.1	0.1	1.0	2.5
43	0.1	0.1	0.1	0.1	0.1	0.1	0.1	0.1	0.1	0.1	0.1	0.1	1.0	1.0	1.9
42	0.1	0.1	0.1	0.1	0.1	0.1	0.1	0.1	0.1	0.1	0.1	0.1	0.1	1.0	1.1
41	0.1	0.1	0.1	0.1	0.1	0.1	0.1	0.1	0.1	0.1	0.1	0.1	0.1	1.0	1.2
40	0.1	0.1	0.1	0.1	0.1	0.1	0.1	0.1	0.1	0.1	0.1	0.1	1.0	1.0	1.0
39	0.1	0.1	0.1	0.1	0.1	0.1	0.1	0.1	0.1	0.1	0.1	0.1	0.1	1.0	1.0
38	0.1	0.1	0.1	0.1	0.1	0.1	0.1	0.1	0.1	0.1	0.1	0.1	0.1	1.0	1.0
37	0.1	0.1	0.1	0.1	0.1	0.1	0.1	0.1	0.1	0.1	0.1	0.1	0.1	1.0	1.0
36	0.1	0.1	0.1	0.1	0.1	0.1	0.1	0.1	0.1	0.1	0.1	0.1	0.1	1.0	1.0
35	0.1	0.1	0.1	0.1	0.1	0.1	0.1	0.1	0.1	0.1	0.1	0.1	0.1	1.0	1.0
34	0.1	0.1	0.1	0.1	0.1	0.1	0.1	0.1	0.1	0.1	0.1	0.1	0.1	1.0	1.0
33	0.1	0.1	0.1	0.1	0.1	0.1	0.1	0.1	0.1	0.1	0.1	0.1	1.0	1.0	1.0
32	0.1	0.1	0.1	0.1	0.1	0.1	0.1	0.1	0.1	0.1	0.1	0.1	1.0	1.0	1.0
31	0.1	0.1	0.1	0.1	0.1	0.1	0.1	0.1	0.1	0.1	0.1	1.0	1.0	1.0	1.0
30	0.1	0.1	0.1	0.1	0.1	0.1	0.1	0.1	0.1	0.1	0.1	0.1	1.0	1.0	1.0
29	0.1	0.1	0.1	0.1	0.1	0.1	0.1	0.1	0.1	0.1	0.1	1.0	1.0	1.0	0.1
28	0.1	0.1	0.1	0.1	0.1	0.1	0.1	0.1	0.1	0.1	0.1	0.1	1.0	1.0	1.7
27	0.1	0.1	0.1	0.1	0.1	0.1	0.1	0.1	0.1	0.1	0.1	1.0	1.0	1.0	2.1
26	0.1	0.1	0.1	0.1	0.1	0.1	0.1	0.1	0.1	0.1	0.1	0.1	1.0	1.0	2.2
25	0.1	0.1	0.1	0.1	0.1	0.1	0.1	0.1	0.1	0.1	1.0	1.0	1.0	1.3	2.5
24	0.1	0.1	0.1	0.1	0.1	0.1	0.1	0.1	0.1	1.0	1.0	1.0	1.0	1.7	2.7
23	0.1	0.1	0.1	0.1	0.1	0.1	0.1	0.1	1.0	1.0	1.5	1.5	1.5	2.0	2.8
22	0.1	0.1	0.1	0.1	0.1	0.1	0.1	1.0	1.0	1.5	2.0	2.0	2.0	2.0	2.9
21	0.1	0.1	0.1	0.1	0.1	1.0	1.0	1.0	1.5	2.0	2.0	2.0	2.0	2.0	2.8
20	0.1	0.1	0.1	0.1	0.1	1.0	1.0	1.5	2.0	2.0	2.0	2.0	2.5	2.5	2.6
19	0.1	0.1	0.1	1.0	1.0	1.5	1.5	2.0	2.0	2.0	2.0	2.0	2.5	2.5	2.5
18	0.1	0.1	0.1	1.0	1.0	1.5	2.0	2.0	2.0	2.0	2.0	2.0	2.5	2.5	2.5
17	0.1	0.1	1.0	1.5	1.5	2.0	2.0	2.0	2.0	2.0	2.0	2.0	2.5	2.5	2.5
16	0.1	0.1	1.0	1.5	2.0	2.0	2.0	2.0	2.0	2.0	2.0	2.0	2.0	2.0	2.5
15	0.1	0.1	1.0	1.5	1.5	1.5	1.5	1.5	2.0	2.0	2.0	2.0	2.0	2.0	2.5
14	0.1	1.0	1.0	1.0	1.0	1.0	1.0	1.0	1.5	1.5	2.0	2.0	2.0	2.0	2.0
13	0.1	1.0	1.0	1.0	0.1	0.1	0.1	1.0	1.0	1.0	1.5	2.0	2.0	2.0	2.0
12	0.1	1.0	0.1	0.1	0.1	0.1	0.1	0.1	1.0	1.0	1.0	1.5	1.5	1.5	1.5
11	0.1	0.1	0.1	0.1	0.1	0.1	0.1	0.1	0.1	0.1	1.0	1.0	1.0	1.0	1.0
10	0.1	0.1	0.1	0.1	0.1	0.1	0.1	0.1	0.1	0.1	0.1	1.0	1.0	1.0	1.0
9	0.1	0.1	0.1	0.1	0.1	0.1	0.1	0.1	0.1	0.1	0.1	0.1	0.1	0.1	0.1
8	0.1	0.1	0.1	0.1	0.1	0.1	0.1	0.1	0.1	0.1	0.1	0.1	0.1	0.1	0.1
7	0.1	0.1	0.1	0.1	0.1	0.1	0.1	0.1	0.1	0.1	0.1	0 1	0.1	0.1	0.1
6	0.1	0.1	0.1	0.1	0.1	0.1	0.1	0.1	0.1	0.1	0.1	0.1	0.1	0.1	0.1
5	0.1	0.1	0.1	0.1	0.1	0.1	0.1	0.1	0.1	0.1	0.1	0.1	0.1	0.1	0.1
4	0.1	0.1	0.1	0.1	0.1	0.1	0.1	0.1	0.1	0.1	0.1	0.1	0.1	0.1	0.1
3	0.1	0.1	0.1	0.1	0.1	0.1	0.1	0.1	0.1	0.1	0.1	0.1	0.1	0.1	0.1
2	0.1	0.1	0.1	0.1	0.1	0.1	0.1	0.1	0.1	0.1	0.1	0.1	0.1	0.1	0.1
1	0.1	0.1	0.1	0.1	0.1	0.1	0.1	0.1	0.1	0.1	0.1	0.1	0.1	0.1	0.1
	1	**2**	**3**	**4**	**5**	**6**	**7**	**8**	**9**	**10**	**11**	**12**	**13**	**14**	**15**

Table B.10 Bathymetry of Macquarie Harbour – region 9

50	20.9	23.4	25.1	26.3	27.3	28.3	29.2	30.1	30.5	30.6	30.1	28.9	26.3	22.6	18.0
49	18.6	21.9	23.4	24.4	25.5	26.7	28.1	29.5	30.5	30.8	30.7	30.0	27.5	23.8	18.9
48	15.7	19.8	21.2	22.3	23.3	24.7	26.7	28.9	30.4	30.7	30.8	30.5	29.1	25.7	20.6
47	11.7	16.3	18.8	20.3	21.2	22.4	25.1	27.9	29.8	30.2	30.6	31.0	30.7	27.9	22.9
46	9.1	13.9	17.5	19.6	20.0	20.8	23.9	26.6	28.6	29.6	30.4	31.2	31.2	29.4	24.6
45	7.6	12.4	16.9	20.2	20.6	21.5	23.6	25.8	27.7	29.2	30.3	31.1	31.2	30.0	25.0
44	6.5	11.1	15.6	19.2	20.9	21.8	23.3	25.2	27.1	28.8	30.0	30.9	30.7	28.4	23.8
43	5.5	9.7	14.0	17.8	20.0	21.2	22.7	24.5	26.5	28.4	29.9	30.9	30.6	27.8	22.4
42	4.6	8.3	12.1	15.5	18.0	19.7	21.4	23.4	25.7	28.0	29.9	31.0	30.8	27.8	22.2
41	3.9	7.1	10.4	13.5	16.1	18.1	19.9	22.1	24.9	27.6	29.8	31.1	31.0	28.2	22.4
40	3.2	6.0	9.0	11.9	14.5	16.7	18.6	21.0	24.3	27.3	29.6	31.1	31.2	28.0	21.9
39	2.4	5.1	7.9	10.7	13.4	15.9	18.2	20.8	24.1	27.1	29.5	31.0	30.8	26.5	20.0
38	1.9	4.2	6.9	9.7	12.7	15.5	18.1	20.8	24.2	27.2	29.5	30.8	30.1	24.1	18.6
37	1.6	3.6	6.0	9.0	12.2	15.5	18.7	21.7	24.8	27.5	29.6	30.8	31.0	27.7	20.4
36	1.2	2.8	5.1	8.1	11.9	15.9	19.6	22.8	25.5	27.8	29.4	30.3	30.3	26.9	20.6
35	1.0	1.8	3.8	6.9	11.4	16.4	20.7	23.8	26.3	28.1	29.1	29.2	28.1	24.8	19.5
34	1.0	1.0	2.0	5.0	10.4	16.9	21.7	24.8	27.0	28.4	28.8	28.4	26.5	23.1	18.1
33	1.0	1.0	1.0	2.2	9.3	16.2	21.7	25.5	27.9	28.9	28.8	27.7	25.4	22.1	17.3
32	1.0	1.0	1.0	3.1	9.6	16.2	22.1	26.6	29.1	29.5	28.7	27.1	24.8	21.7	17.0
31	1.0	1.0	2.5	6.0	11.4	17.1	23.0	28.6	30.5	30.0	28.6	26.5	24.0	20.8	16.5
30	1.4	2.5	4.7	8.3	13.4	19.3	24.5	29.6	31.4	30.4	28.2	25.6	22.9	20.0	16.3
29	0.1	3.8	6.1	9.5	14.1	19.1	24.1	29.6	31.5	30.3	26.8	23.8	21.6	19.4	16.4
28	3.2	4.7	6.9	9.9	13.5	17.3	20.9	25.7	29.4	24.3	23.3	21.3	19.7	18.5	16.3
27	3.6	5.1	7.1	9.7	12.5	15.2	17.5	20.0	20.2	19.4	19.9	19.4	18.6	17.7	16.5
26	3.8	5.2	7.1	9.2	11.4	14.0	15.6	17.0	17.5	17.7	18.1	18.2	17.8	17.4	16.6
25	3.8	5.3	7.2	8.7	11.1	12.9	14.2	15.5	15.9	16.5	17.0	17.4	17.5	17.3	16.9
24	4.0	5.4	6.9	8.8	10.5	12.0	13.4	14.3	14.8	15.4	16.1	16.7	17.1	17.4	17.4
23	4.0	5.2	6.8	8.4	9.2	11.5	12.5	13.3	14.1	14.5	15.3	16.0	16.7	17.5	18.0
22	3.9	5.0	6.5	8.1	8.8	10.8	11.9	12.8	13.3	13.8	14.6	15.4	16.3	17.5	18.1
21	3.7	4.6	7.0	8.0	8.4	10.2	11.1	12.1	12.5	13.0	13.9	14.7	15.6	16.9	17.7
20	3.4	4.6	5.0	7.0	8.0	9.0	10.2	10.9	11.7	12.3	13.2	14.0	14.9	16.2	17.3
19	3.1	3.8	5.0	6.0	6.6	7.0	8.9	9.8	10.8	11.3	12.3	13.1	14.1	15.3	16.3
18	2.8	3.3	5.5	5.0	5.5	6.0	8.1	9.0	9.9	10.4	11.3	12.2	13.4	14.2	15.0
17	2.5	3.2	5.0	4.0	4.2	5.0	7.2	8.1	8.9	9.5	10.3	11.1	12.2	12.9	13.7
16	2.5	3.2	4.0	3.5	3.5	4.0	6.4	7.2	8.0	8.4	9.3	10.3	11.0	11.6	12.1
15	3.6	3.2	3.1	3.2	3.4	3.6	5.6	6.3	7.0	7.5	8.5	9.2	9.8	10.1	10.5
14	3.5	2.8	2.5	2.4	2.5	3.2	4.8	5.5	6.1	6.8	7.4	8.0	8.3	8.5	8.5
13	3.5	2.7	2.8	2.4	2.0	3.0	4.0	4.5	5.1	5.6	6.4	6.7	6.8	7.0	7.1
12	1.5	2.8	3.1	2.8	2.0	2.8	3.2	3.8	4.0	4.7	5.4	5.4	5.5	5.6	5.7
11	1.0	2.5	2.7	4.2	3.5	2.5	3.2	3.3	3.9	4.3	4.3	4.4	4.5	4.5	4.3
10	1.0	1.0	3.0	4.8	4.5	3.0	2.1	2.4	2.6	3.0	3.2	3.5	3.5	3.5	3.4
9	0.1	1.0	4.0	4.6	3.0	3.0	1.5	1.8	2.0	2.2	2.5	2.7	2.6	2.6	2.5
8	1.0	1.0	5.5	5.0	4.0	3.0	1.0	1.4	1.5	1.6	1.8	1.9	1.9	1.9	1.8
7	1.0	1.0	6.2	4.0	3.0	3.0	1.0	1.0	1.0	1.1	1.2	1.3	1.3	1.3	1.2
6	0.1	1.0	8.0	3.0	2.0	2.0	1.0	1.0	1.0	1.0	1.0	1.0	1.0	1.0	1.0
5	0.1	1.0	9.0	1.0	1.0	1.0	1.0	1.0	1.0	1.0	1.0	1.0	1.0	1.0	1.0
4	0.1	0.1	10.0	0.1	0.1	1.0	1.0	1.0	1.0	1.0	0.1	1.0	1.0	1.0	1.0
3	0.1	0.1	10.5	0.1	0.1	0.1	0.1	0.1	0.1	0.1	0.1	0.1	0.1	0.1	0.1
2	0.1	0.1	11.0	0.1	0.1	0.1	0.1	0.1	0.1	0.1	0.1	0.1	0.1	0.1	0.1
1	0.1	0.1	0.1	0.1	0.1	0.1	0.1	0.1	0.1	0.1	0.1	0.1	0.1	0.1	0.1
	16	**17**	**18**	**19**	**20**	**21**	**22**	**23**	**24**	**25**	**26**	**27**	**28**	**29**	**30**

Table B.11 Bathymetry of Macquarie Harbour – region 10

50	12.9	7.4	2.0	2.5	2.5	2.5	2.5	2.5	1.0	0.1	0.1	0.1	0.1	0.1	0.1
49	13.8	8.6	3.7	2.5	2.5	2.5	2.5	2.5	1.0	0.1	0.1	0.1	0.1	0.1	0.1
48	15.4	10.3	5.7	2.5	2.5	2.5	2.5	2.5	1.0	0.1	0.1	0.1	0.1	0.1	0.1
47	17.3	11.9	7.3	3.8	1.7	1.0	1.0	1.0	1.0	0.1	0.1	0.1	0.1	0.1	0.1
46	18.6	13.0	8.1	4.4	1.9	1.0	1.0	1.0	0.1	0.1	0.1	0.1	0.1	0.1	0.1
45	18.9	13.2	8.2	4.2	1.5	1.0	1.0	0.1	0.1	0.1	0.1	0.1	0.1	0.1	0.1
44	18.2	12.6	7.6	3.4	1.0	1.0	0.1	0.1	0.1	0.1	0.1	0.1	0.1	0.1	0.1
43	17.0	11.8	6.7	2.5	1.0	1.0	0.1	0.1	0.1	0.1	0.1	0.1	0.1	0.1	0.1
42	16.5	11.3	6.1	1.2	1.0	0.1	0.1	0.1	0.1	0.1	0.1	0.1	0.1	0.1	0.1
41	16.6	11.1	6.2	2.1	1.0	0.1	0.1	0.1	0.1	0.1	0.1	0.1	0.1	0.1	0.1
40	16.1	11.0	6.6	3.1	1.0	0.1	0.1	0.1	0.1	0.1	0.1	0.1	1.0	1.0	1.0
39	15.3	10.8	6.7	3.5	1.3	1.0	0.1	0.1	0.1	0.1	0.1	0.1	0.1	1.0	1.0
38	14.7	10.4	6.5	3.4	1.3	1.0	0.1	0.1	0.1	0.1	0.1	0.1	0.1	0.1	1.0
37	14.8	10.1	6.0	2.9	1.0	1.0	0.1	0.1	1.0	1.0	1.0	0.1	0.1	0.1	1.0
36	14.6	9.4	5.0	2.0	1.0	1.0	0.1	0.1	1.0	1.0	1.0	1.0	1.0	1.0	1.0
35	13.6	8.1	3.6	1.0	1.0	0.1	0.1	0.1	1.0	2.0	2.0	1.0	1.0	1.0	2.0
34	12.3	6.4	1.8	1.0	0.1	0.1	0.1	1.0	1.0	2.0	2.0	1.0	1.0	1.0	2.0
33	11.2	4.9	1.0	1.0	0.1	0.1	0.1	1.0	1.0	2.0	2.0	2.0	2.0	2.0	2.0
32	10.9	4.5	1.0	0.1	1.0	1.0	1.0	1.0	2.5	2.5	2.5	2.5	2.5	2.5	0.1
31	11.3	6.2	2.5	1.0	1.0	1.0	1.0	1.0	2.5	2.5	2.5	2.5	2.5	2.5	2.5
30	12.2	8.1	4.9	2.8	1.5	1.0	1.0	1.0	2.5	2.5	2.5	2.5	2.5	2.5	2.5
29	13.0	9.8	7.0	4.8	3.0	2.5	2.5	2.5	2.5	3.0	3.0	3.0	3.0	2.5	2.5
28	13.9	11.4	8.9	6.7	5.0	5.0	5.0	5.0	5.0	5.0	5.0	5.0	5.0	5.0	5.0
27	14.8	12.9	10.9	8.7	6.5	5.0	5.0	5.0	5.0	5.0	5.0	5.0	5.0	5.0	5.0
26	15.6	14.5	12.9	11.1	8.8	5.9	5.0	5.0	5.0	5.0	5.0	5.0	5.0	5.0	5.0
25	16.5	15.9	15.1	13.8	11.5	8.1	5.0	5.0	5.0	5.0	5.0	5.0	5.0	5.0	5.0
24	17.3	17.4	17.2	16.8	15.0	10.6	5.0	2.5	2.5	2.5	2.5	2.5	2.5	2.5	2.5
23	18.0	18.3	18.9	19.4	19.3	13.8	4.7	1.0	1.0	1.0	2.5	2.5	2.5	2.5	1.0
22	18.7	19.0	19.7	20.4	21.0	19.3	3.6	1.0	0.1	1.0	1.0	1.0	1.0	1.0	1.0
21	18.5	19.2	19.6	20.1	20.6	20.7	9.9	1.7	0.1	0.1	0.1	0.1	1.0	1.0	1.0
20	17.9	18.6	19.2	19.6	20.1	20.5	15.4	6.2	1.0	0.1	0.1	0.1	0.1	0.1	0.1
19	17.0	17.6	18.1	18.5	18.7	18.4	14.7	7.7	1.7	0.1	0.1	0.1	0.1	0.1	0.1
18	15.8	16.1	16.5	16.7	16.4	15.2	12.0	7.3	2.7	1.0	0.1	0.1	0.1	0.1	0.1
17	14.1	14.4	14.6	14.5	14.0	12.5	9.9	6.5	3.4	1.4	1.0	1.0	1.0	1.0	1.0
16	12.4	12.2	12.6	12.2	11.6	10.3	8.1	5.7	3.4	2.5	2.5	2.5	2.5	2.5	2.5
15	10.3	10.4	10.6	10.1	9.4	8.3	6.5	5.0	5.0	5.0	5.0	5.0	5.0	2.5	2.5
14	8.6	8.6	8.7	8.1	7.5	6.5	5.0	5.0	5.0	5.0	5.0	5.0	2.5	1.0	1.0
13	7.1	6.9	6.9	6.3	5.6	5.0	5.0	5.0	5.0	5.0	5.0	5.0	2.5	1.0	0.1
12	5.6	5.4	5.3	5.0	5.0	5.0	5.0	5.0	2.5	2.5	2.5	2.5	1.0	1.0	0.1
11	4.1	3.7	3.3	2.6	2.5	2.5	2.5	2.5	2.5	2.5	1.0	1.0	0.1	0.1	0.1
10	3.3	3.0	2.5	2.2	1.5	1.0	1.0	1.0	1.0	1.0	1.0	1.0	0.1	0.1	0.1
9	2.4	2.1	1.7	1.2	1.0	1.0	1.0	1.0	1.0	1.0	1.0	0.1	0.1	0.1	0.1
8	1.6	1.4	1.0	1.0	1.0	1.0	1.0	0.1	0.1	1.0	1.0	0.1	0.1	0.1	0.1
7	1.0	1.0	1.0	1.0	1.0	0.1	0.1	0.1	0.1	1.0	1.0	0.1	0.1	0.1	0.1
6	1.0	1.0	1.0	1.0	1.0	0.1	0.1	0.1	0.1	0.1	0.1	0 1	0.1	0.1	0.1
5	1.0	1.0	1.0	1.0	1.0	0.1	0.1	0.1	0.1	0.1	0.1	0.1	0.1	0.1	0.1
4	1.0	1.0	0.1	0.1	0.1	0.1	0.1	0.1	0.1	0.1	0.1	0.1	0.1	0.1	0.1
3	0.1	0.1	0.1	0.1	0.1	0.1	0.1	0.1	0.1	0.1	0.1	0.1	0.1	0.1	0.1
2	0.1	0.1	0.1	0.1	0.1	0.1	0.1	0.1	0.1	0.1	0.1	0.1	0.1	0.1	0.1
1	0.1	0.1	0.1	0.1	0.1	0.1	0.1	0.1	0.1	0.1	0.1	0.1	0.1	0.1	0.1
	31	**32**	**33**	**34**	**35**	**36**	**37**	**38**	**39**	**40**	**41**	**42**	**43**	**44**	**45**

Table B.12 Bathymetry of Macquarie Harbour – region 11

50	0.1	0.1	0.1	0.1	0.1	0.1	0.1	0.1	0.1	0.1	0.1	0.1	0.1	0.1	0.1	0.1	0.1
49	0.1	0.1	0.1	0.1	0.1	0.1	0.1	0.1	0.1	0.1	0.1	0.1	0.1	0.1	0.1	0.1	0.1
48	0.1	0.1	0.1	0.1	0.1	0.1	0.1	0.1	0.1	0.1	0.1	0.1	0.1	0.1	0.1	0.1	0.1
47	0.1	0.1	0.1	0.1	0.1	0.1	0.1	0.1	0.1	0.1	0.1	0.1	0.1	0.1	0.1	0.1	0.1
46	0.1	0.1	0.1	0.1	0.1	0.1	0.1	0.1	0.1	0.1	0.1	0.1	0.1	0.1	0.1	0.1	0.1
45	0.1	0.1	0.1	0.1	0.1	0.1	0.1	0.1	0.1	0.1	0.1	0.1	0.1	0.1	0.1	0.1	0.1
44	0.1	0.1	0.1	0.1	0.1	0.1	0.1	0.1	0.1	0.1	0.1	0.1	0.1	0.1	0.1	0.1	0.1
43	0.1	1.0	1.0	0.1	0.1	0.1	0.1	0.1	0.1	0.1	0.1	0.1	0.1	0.1	0.1	0.1	0.1
42	0.1	1.0	1.0	0.1	0.1	0.1	0.1	0.1	0.1	0.1	0.1	0.1	0.1	0.1	0.1	0.1	0.1
41	1.0	1.0	1.0	0.1	0.1	0.1	0.1	0.1	0.1	0.1	0.1	0.1	0.1	0.1	0.1	0.1	0.1
40	1.0	1.0	0.1	0.1	0.1	0.1	0.1	0.1	0.1	0.1	0.1	0.1	0.1	0.1	0.1	0.1	0.1
39	1.0	1.0	1.0	1.0	0.1	0.1	0.1	0.1	0.1	0.1	0.1	0.1	0.1	0.1	0.1	0.1	0.1
38	2.0	2.0	1.0	1.0	0.1	0.1	0.1	0.1	0.1	0.1	0.1	0.1	0.1	0.1	0.1	0.1	0.1
37	2.0	2.0	1.0	1.0	0.1	0.1	0.1	0.1	0.1	0.1	0.1	0.1	0.1	0.1	0.1	0.1	0.1
36	2.0	2.0	1.0	1.0	1.0	0.1	0.1	0.1	0.1	0.1	0.1	0.1	0.1	0.1	0.1	0.1	0.1
35	2.0	2.0	1.0	1.0	1.0	0.1	0.1	0.1	0.1	0.1	0.1	0.1	0.1	0.1	0.1	0.1	0.1
34	2.0	2.0	1.0	1.0	0.1	0.1	0.1	0.1	0.1	0.1	0.1	0.1	0.1	0.1	0.1	0.1	0.1
33	2.0	2.0	1.0	1.0	0.1	0.1	0.1	0.1	0.1	0.1	0.1	0.1	0.1	0.1	0.1	0.1	0.1
32	0.1	2.5	1.0	1.0	0.1	0.1	0.1	0.1	0.1	0.1	0.1	0.1	0.1	0.1	0.1	0.1	0.1
31	2.5	2.5	1.0	1.0	0.1	0.1	0.1	0.1	0.1	0.1	0.1	0.1	0.1	0.1	0.1	0.1	0.1
30	2.5	2.5	1.0	1.0	0.1	0.1	0.1	0.1	0.1	0.1	0.1	0.1	0.1	0.1	0.1	0.1	0.1
29	2.5	2.5	1.0	0.1	0.1	0.1	0.1	0.1	0.1	0.1	0.1	0.1	0.1	0.1	0.1	0.1	0.1
28	2.5	2.5	1.0	0.1	0.1	0.1	0.1	0.1	0.1	0.1	0.1	0.1	0.1	0.1	0.1	0.1	0.1
27	2.5	1.0	1.0	0.1	0.1	0.1	0.1	0.1	0.1	0.1	0.1	0.1	0.1	0.1	0.1	0.1	0.1
26	2.5	1.0	0.1	0.1	0.1	0.1	0.1	0.1	0.1	0.1	0.1	0.1	0.1	0.1	0.1	0.1	0.1
25	2.5	1.0	0.1	0.1	0.1	0.1	0.1	0.1	0.1	0.1	0.1	0.1	0.1	0.1	0.1	0.1	0.1
24	1.0	1.0	0.1	0.1	0.1	0.1	0.1	0.1	0.1	0.1	0.1	0.1	0.1	0.1	0.1	0.1	0.1
23	1.0	0.1	0.1	0.1	0.1	0.1	0.1	0.1	0.1	0.1	0.1	0.1	0.1	0.1	0.1	0.1	0.1
22	0.1	0.1	0.1	0.1	0.1	0.1	0.1	0.1	0.1	0.1	0.1	0.1	0.1	0.1	0.1	0.1	0.1
21	0.1	0.1	0.1	0.1	0.1	0.1	0.1	0.1	0.1	0.1	0.1	0.1	0.1	0.1	0.1	0.1	0.1
20	0.1	0.1	0.1	0.1	0.1	0.1	0.1	0.1	0.1	0.1	0.1	0.1	0.1	0.1	0.1	0.1	0.1
19	0.1	1.0	0.1	0.1	0.1	1.0	1.0	0.1	0.1	0.1	0.1	0.1	0.1	0.1	0.1	0.1	0.1
18	1.0	1.0	1.0	1.0	1.0	1.0	1.0	0.1	0.1	0.1	0.1	0.1	0.1	0.1	0.1	0.1	0.1
17	1.0	1.0	2.5	2.5	2.5	2.5	1.0	0.1	0.1	0.1	0.1	0.1	0.1	0.1	0.1	0.1	0.1
16	2.5	2.5	2.5	2.5	2.5	2.5	1.0	1.0	0.1	0.1	0.1	0.1	0.1	0.1	0.1	0.1	0.1
15	2.5	2.5	2.5	2.5	2.5	1.0	0.1	0.1	0.1	0.1	0.1	0.1	0.1	0.1	0.1	0.1	0.1
14	1.0	1.0	1.0	1.0	1.0	1.0	0.1	0.1	0.1	0.1	0.1	0.1	0.1	0.1	0.1	0.1	0.1
13	1.0	0.1	0.1	0.1	0.1	0.1	0.1	0.1	0.1	0.1	0.1	0.1	0.1	0.1	0.1	0.1	0.1
12	0.1	0.1	0.1	0.1	0.1	0.1	0.1	0.1	0.1	0.1	0.1	0.1	0.1	0.1	0.1	0.1	0.1
11	0.1	0.1	0.1	0.1	0.1	0.1	0.1	0.1	0.1	0.1	0.1	0.1	0.1	0.1	0.1	0.1	0.1
10	0.1	0.1	0.1	0.1	0.1	0.1	0.1	0.1	0.1	0.1	0.1	0.1	0.1	0.1	0.1	0.1	0.1
9	0.1	0.1	0.1	0.1	0.1	0.1	0.1	0.1	0.1	0.1	0.1	0.1	0.1	0.1	0.1	0.1	0.1
8	0.1	0.1	0.1	0.1	0.1	0.1	0.1	0.1	0.1	0.1	0.1	0.1	0.1	0.1	0.1	0.1	0.1
7	0.1	0.1	0.1	0.1	0.1	0.1	0.1	0.1	0.1	0.1	0.1	0.1	0.1	0.1	0.1	0.1	0.1
6	0.1	0.1	0.1	0.1	0.1	0.1	0.1	0.1	0.1	0.1	0.1	0.1	0.1	0.1	0.1	0.1	0.1
5	0.1	0.1	0.1	0.1	0.1	0.1	0.1	0.1	0.1	0.1	0.1	0.1	0.1	0.1	0.1	0.1	0.1
4	0.1	0.1	0.1	0.1	0.1	0.1	0.1	0.1	0.1	0.1	0.1	0.1	0.1	0.1	0.1	0.1	0.1
3	0.1	0.1	0.1	0.1	0.1	0.1	0.1	0.1	0.1	0.1	0.1	0.1	0.1	0.1	0.1	0.1	0.1
2	0.1	0.1	0.1	0.1	0.1	0.1	0.1	0.1	0.1	0.1	0.1	0.1	0.1	0.1	0.1	0.1	0.1
1	0.1	0.1	0.1	0.1	0.1	0.1	0.1	0.1	0.1	0.1	0.1	0.1	0.1	0.1	0.1	0.1	0.1
	46	**47**	**48**	**49**	**50**	**51**	**52**	**53**	**54**	**55**	**56**	**57**	**58**	**59**	**60**	**61**	**62**

Table B.13 Bathymetry of Macquarie Harbour – region 12

Appendix C
River bathymetry data

The bathymetry data for three river models is presented on the next two pages (Table C.1). Values are given as a function of the horizontal grid index, using a 250m grid. When a depth or width is not given for a horizontal grid, the model uses linear interpolation for intermediate values. For the Gordon River and sea, the original data has been smoothed because the features are poorly resolved with a 250m grid in the model and cause numerical instability.

Table C.1 Location of river bathymetry tables

Horizontal grid index	Original Depth (m)	Smoothed Depth (m)	Width (m)
1	5.0	5.0	70.00
6	8.0	8.0	76.75
12	13.0	13.0	83.50
16	14.5	14.5	88.00
20	20.5	14.6	92.50
22	20.0	14.8	94.75
23	15.0	15.0	95.88
24	10.0	15.5	97.00
28	23.0	16.0	101.50
29	15.0	15.0	102.63
32	8.0	14.7	106.00
40	14.5	14.5	115.00
44	11.5	13.5	119.50
46	12.5	12.5	121.75
48	7.0	12.3	124.00
51	12.0	12.2	127.38
55	9.0	11.7	131.88
56	20.0	11.5	133.00
58	10.0	11.0	135.25
62	13.0	12.0	139.75
64	18.5	12.5	142.00
65	13.0	13.0	143.13
67	15.0	14.0	145.38
72	11.0	13.0	151.00
73	19.0	12.0	152.13
74	12.5	12.5	153.25
76	10.5	12.7	155.50
80	14.0	13.0	160.00
84	12.0	12.0	164.50
86	23.0	13.0	166.75
88	12.0	12.0	169.00
92	17.0	13.5	173.50
94	13.0	13.0	175.75
96	13.5	13.5	178.00
98	12.0	14.2	180.25
100	15.0	15.0	182.50
102	21.5	21.5	184.75
104	16.5	23.5	187.00
106	27.5	24.5	189.25
108	26.5	25.0	191.50
112	22.5	22.5	196.00
116	12.0	18.0	200.50
118	18.0	20.0	202.75
121	21.5	21.5	206.13
123	27.5	26.0	208.38
129	24.5	24.5	215.13
134	11.0	15.0	220.75
136	10.5	13.5	223.00
142	7.5	10.0	229.75
144	16.0	13.0	232.00
148	17.0	15.0	236.50
159	11.0	11.0	250.00
160	10.5	10.5	250.00

Table C.2 Gordon River bathymetry, with original depth from HEC (1979) and smoothed depth used in the model; the width is unchanged in the smoothing process

Horizontal grid index	Depth (m)	Width (m)
1	0.50	30.00
7	0.60	40.00
13	0.65	57.00
17	0.70	58.90
22	0.80	82.96
27	0.90	80.18
29	0.95	88.82
31	1.00	80.18
32	1.05	93.85
33	1.10	104.12
34	1.10	114.98
35	1.10	124.94
36	1.15	145.91
38	1.20	250.00
40	1.20	250.00

Table C.3 King River bathymetry, from HEC (1993b)

Horizontal grid index	Original depth (m)	Smoothed depth (m)	Original width (m)	Smoothed width (m)
1	90.00	90.00	1000	1000
24	73.15	73.15	760	760
44	51.21	51.21	560	560
57	27.43	27.43	430	430
67	12.80	12.80	330	330
68	10.97	10.97	320	320
69	9.51	9.51	310	310
70	8.23	8.23	300	300
71	7.32	7.50	280	280
72	7.32	9.38	250	250
73	5.49	11.25	220	220
74	10.97	13.50	150	183
75	18.00	15.00	75	150
76	16.00	14.50	170	183
77	14.63	13.00	210	216
78	12.00	12.00	250	250
80	12.00	12.00	250	250

Table C.4 Sea bathymetry, with original depth and width from Admiralty map 3531, 1980 Edition, and Admiralty map 353, 1967 Edition

Appendix D
Typical model parameters

This appendix gives typical model parameters for the numerical model of the Macquarie Harbour system, used by both the river models and POM, along with the typical vertical grid spacing used. Variables in non-italic capital letters are FORTRAN variable names (from the model).

COMMON

Horizontal grid spacing	DX = DY = 250m
Number of vertical grids (σ levels)	KB = 23
External time step	DTE = 3.0s
Minimum (midnight) heat flux	0.0
Minimum (midnight) temperature	11°C
Maximum (midday) heat flux	-1.2×10^{-4}Km/s = -502W/m^2 (the negative sign means the water column is warming)
Surface cooling coefficient	10^{-5}
Maximum (midday) temperature	18°C
Temperature bias	TBIAS = 15°C
Salinity bias	SBIAS = 20‰
Wind friction coefficient	10^{-6}
Surface cooling coefficient	10^{-5}

POM

Split between internal and external solving mode	ISPLIT = 20
Horizontal diffusion constant for the Smagorinsky diffusivity	HORCON = 0.08 *see note below
Bottom friction height	Z0B = 5mm *see note below
Minimum bottom friction coefficient	CBMIN = 0.001
Calculation mode	MODE = 3 (three dimensional)
Temperature top surface boundary condition	NBC = 1

Note:
Values of HORCON = 0.04, 0.08 and 0.12 and values of Z0B = 4mm, 5mm and 6mm where tested and the model was found to not be sensitive to these values (due to the momentum dominated flow from the rivers and tide). These 20% variations at the end of a 10 days simulation caused variations in the Table D.1.

HORCON =	**0.04**	**0.08**	**0.12**	% difference	
	A	**B**	**C**	**B to A**	**B to C**
Vel. mag. **top** (m/s)	4.02E-02	3.95E-02	3.99E-02	1.7%	1.0%
Vel. mag. **all** (m/s)	2.22E-02	2.18E-02	2.09E-02	2.0%	-3.9%
U **top** (m/s)	3.85E-03	3.95E-03	4.09E-03	-2.4%	3.8%
U **all** (m/s)	2.49E-03	2.55E-03	2.39E-03	-2.3%	-6.1%
V **top** (m/s)	6.60E-03	6.20E-03	6.36E-03	6.3%	2.6%
V **all** (m/s)	-5.06E-03	-5.04E-03	-5.01E-03	0.5%	-0.6%
S **top** (‰)	1.46E+01	1.46E+01	1.45E+01	0.0%	-0.3%
S **all** (‰)	1.69E+01	1.69E+01	1.69E+01	0.0%	-0.1%
T **top** (°C)	1.50E+01	1.50E+01	1.50E+01	0.0%	-0.2%
T **all** (°C)	1.47E+01	1.47E+01	1.47E+01	0 0%	0.0%
C **top** (kg/m^3)	9.72E-05	9.90E-05	1.01E-04	-1.9%	1.8%
C **all** (kg/m^3)	4.00E-05	4.07E-05	3.74E-05	-1.9%	-8.2%

Z0B =	**4mm**	**5mm**	**6mm**	% difference	
	A	**B**	**C**	**B to A**	**B to C**
Vel. mag. **top** (m/s)	4.02E-02	3.95E-02	3.92E-02	1.7%	-0 9%
Vel. mag. **all** (m/s)	2.22E-02	2.18E-02	2.12E-02	2.0%	-2.6%
U **top** (m/s)	3.85E-03	3.95E-03	3.89E-03	-2.4%	-1.5%
U **all** (m/s)	2.49E-03	2.55E-03	2.38E-03	-2.3%	-6.5%
V **top** (m/s)	6.60E-03	6.20E-03	5.57E-03	6.3%	-10.2%
V **all** (m/s)	-5.06E-03	-5.04E-03	-5.03E-03	0.5%	-0.1%
S **top** (‰)	1.46E+01	1.46E+01	1.46E+01	0.0%	0.0%
S **all** (‰)	1.69E+01	1.69E+01	1.69E+01	0.0%	0.0%
T **top** (°C)	1.50E+01	1.50E+01	1.51E+01	0.0%	0.1%
T **all** (°C)	1.47E+01	1.47E+01	1.47E+01	0.0%	0.1%
C **top** (kg/m^3)	9.72E-05	9.90E-05	1.04E-04	-1.9%	5.3%
C **all** (kg/m^3)	4.00E-05	4.07E-05	4.24E-05	-1.9%	4.1%

Table D.1 Average harbour properties for different values of HORCON and Z0B. ("top" and "all" refer to the levels within the harbour model that were averaged)

RIVER

Temporal forward weighting	$\theta = 0.62$
Horizontal mixing length factor of river width	0.8
Maximum horizontal mixing length	200m
Maximum horizontal diffusion	$250 m^2/s$
Minimum horizontal diffusion	$5 m^2/s$
Maximum vertical mixing length	1m
Maximum vertical diffusion	$5 \times 10^{-3} m^2/s$
Minimum vertical diffusion	$10^{-5} m^2/s$

VERTICAL GRID SPACING, for *KB = 23*

Vertical grid index (k)	σ value
(top) 1	0.000
2	-0.025
3	-0.050
4	-0.100
5	-0.150
6	-0.200
7	-0.250
8	-0.300
9	-0.350
10	-0.400
11	-0.450
12	-0.500
13	-0.550
14	-0.600
15	-0.650
16	-0.700
17	-0.750
18	-0.800
19	-0.850
20	-0.900
21	-0.950
22	-0.975
(bottom) 23	-1.000

Appendix E
Model output for tide cycle

This appendix gives detailed circulation and pollution concentrations in Macquarie Harbour during its tide cycle. Horizontal sections through the harbour are given at various depths. Table E.1 gives the list of the figures in the appendix.

Table E.1 List of figures

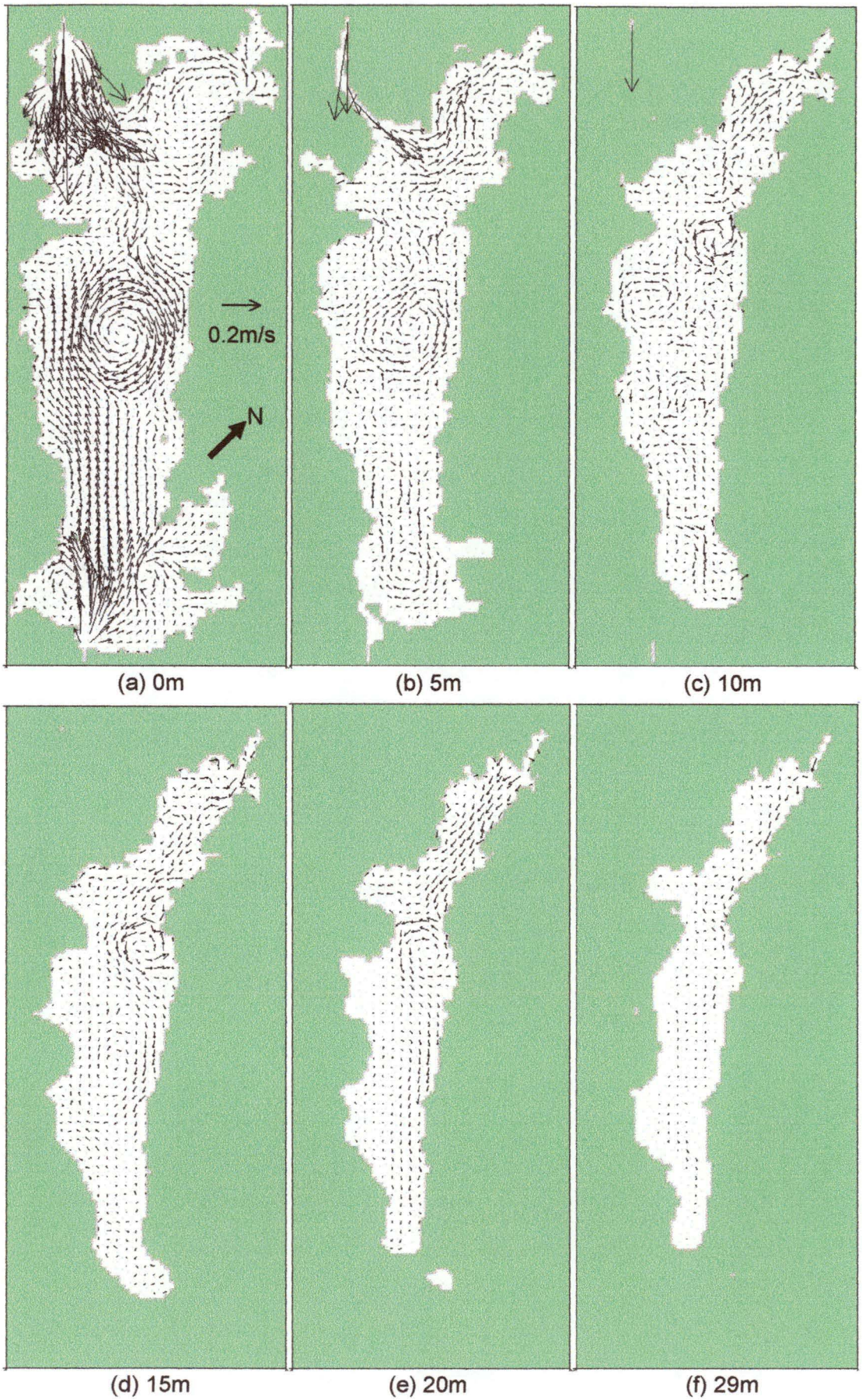

Figure E.1 Horizontal velocity, flood tide

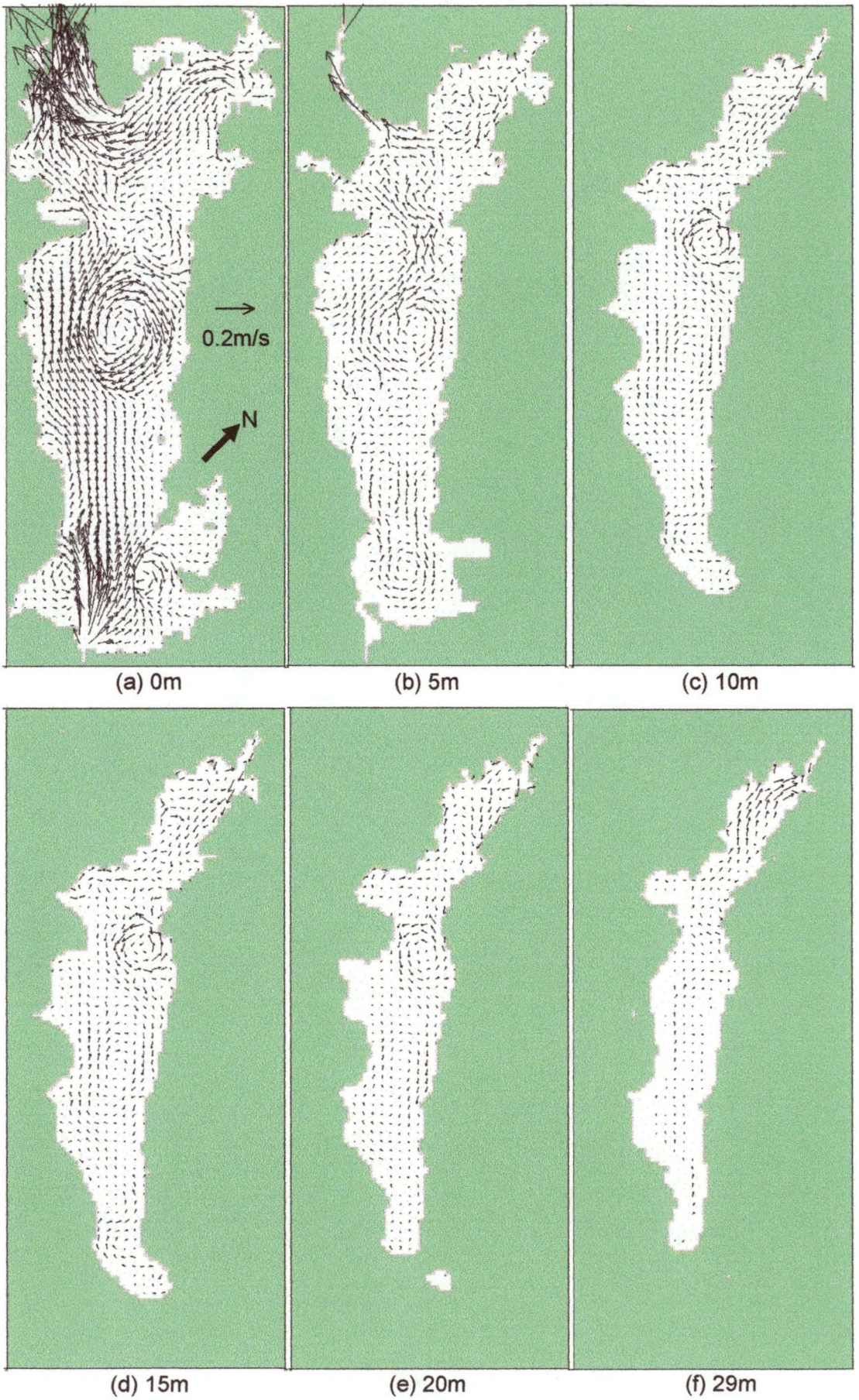

Figure E.2 Horizontal velocity, ebb tide

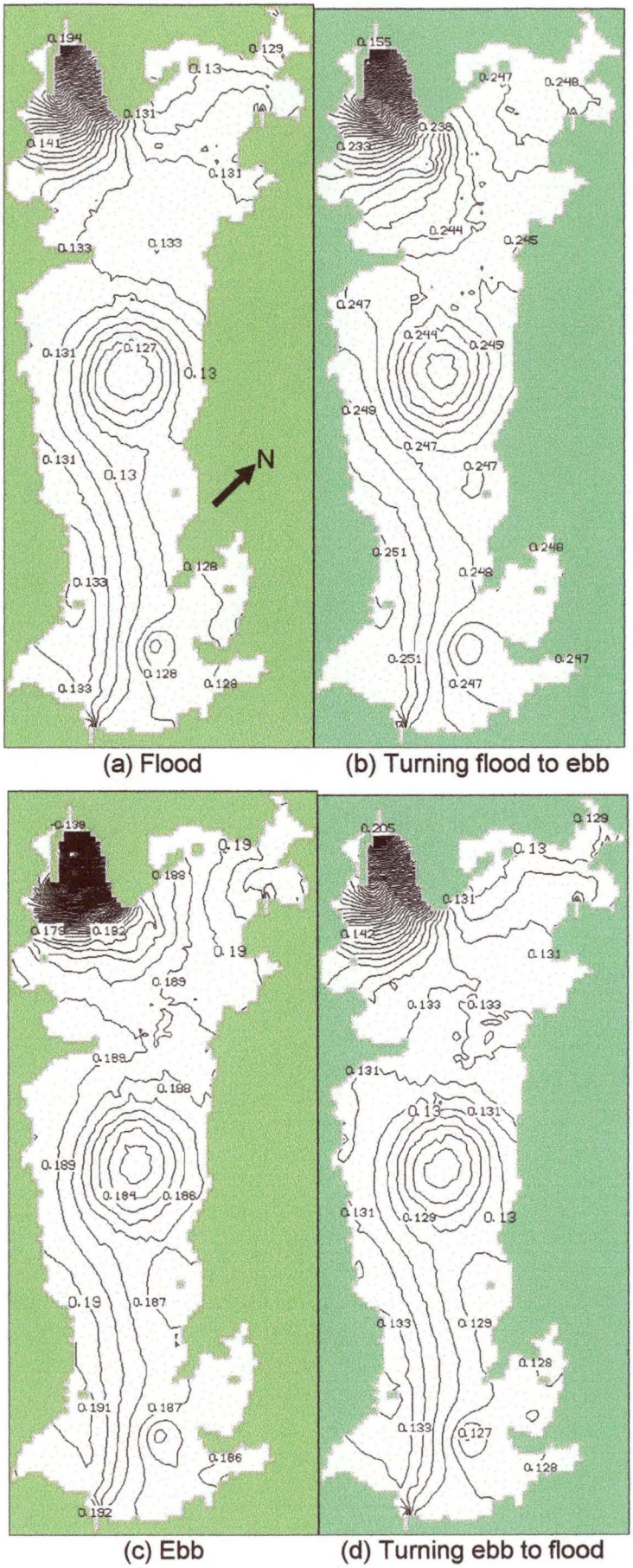

Figure E.3 Surface elevation, 0.001m contours

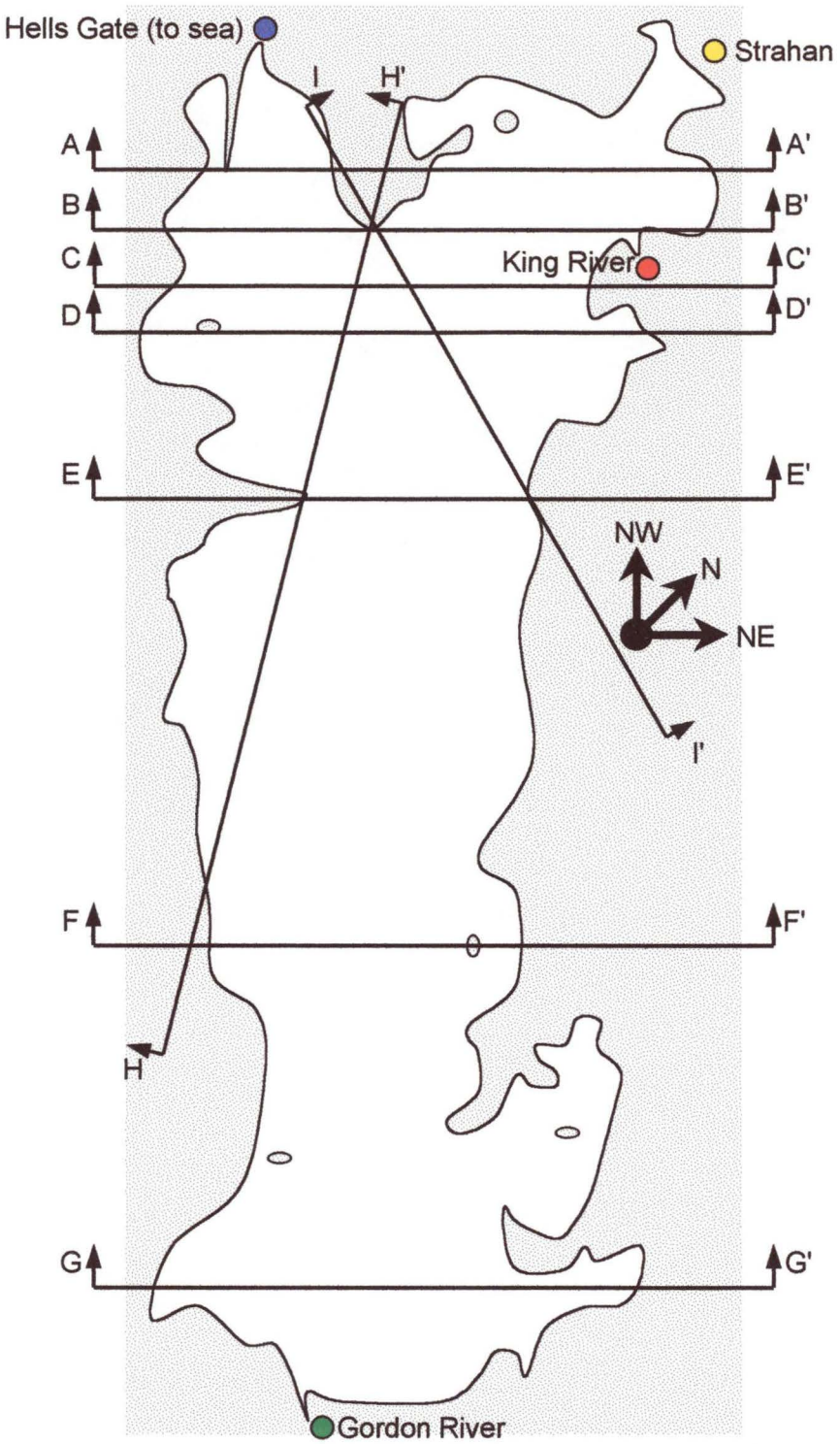

Figure E.4 Definitions of vertical sections in Macquarie Harbour

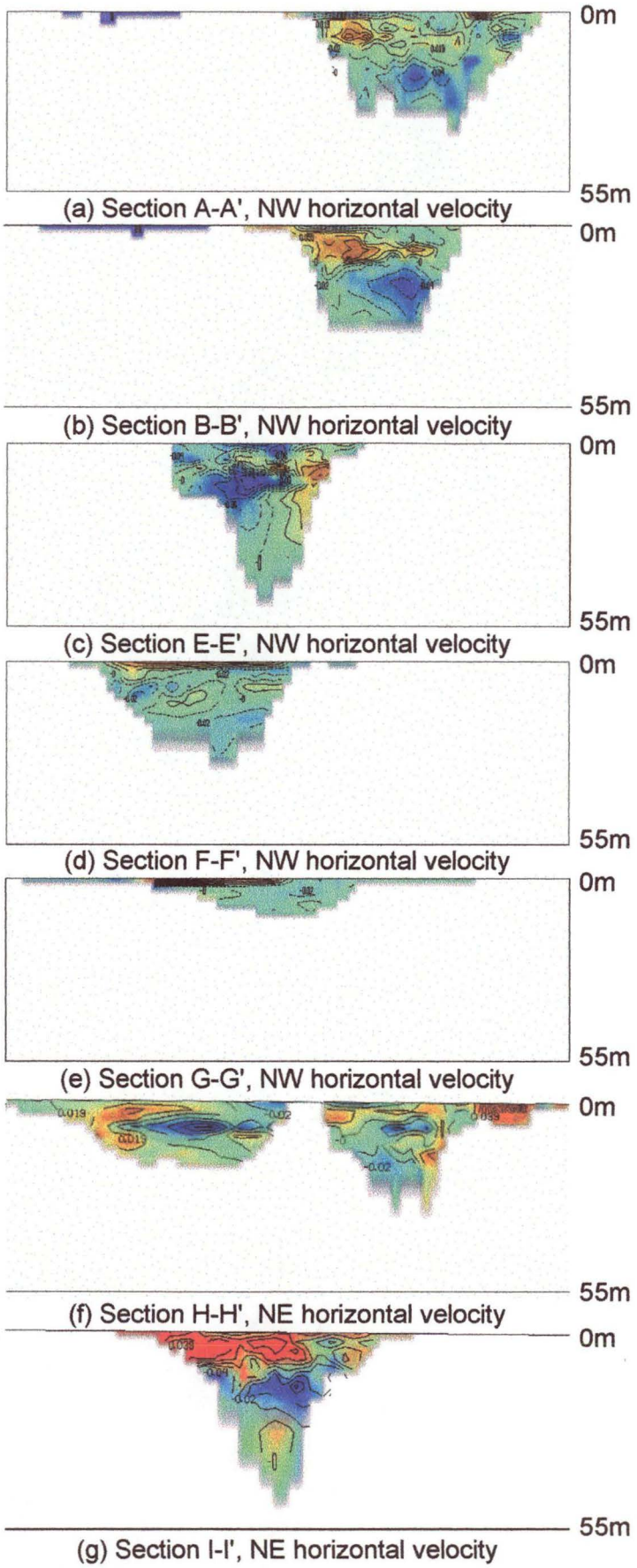

Figure E.5 Velocity during **flood** tide, 0.02m/s contours, red is positive (away), blue is negative (towards)

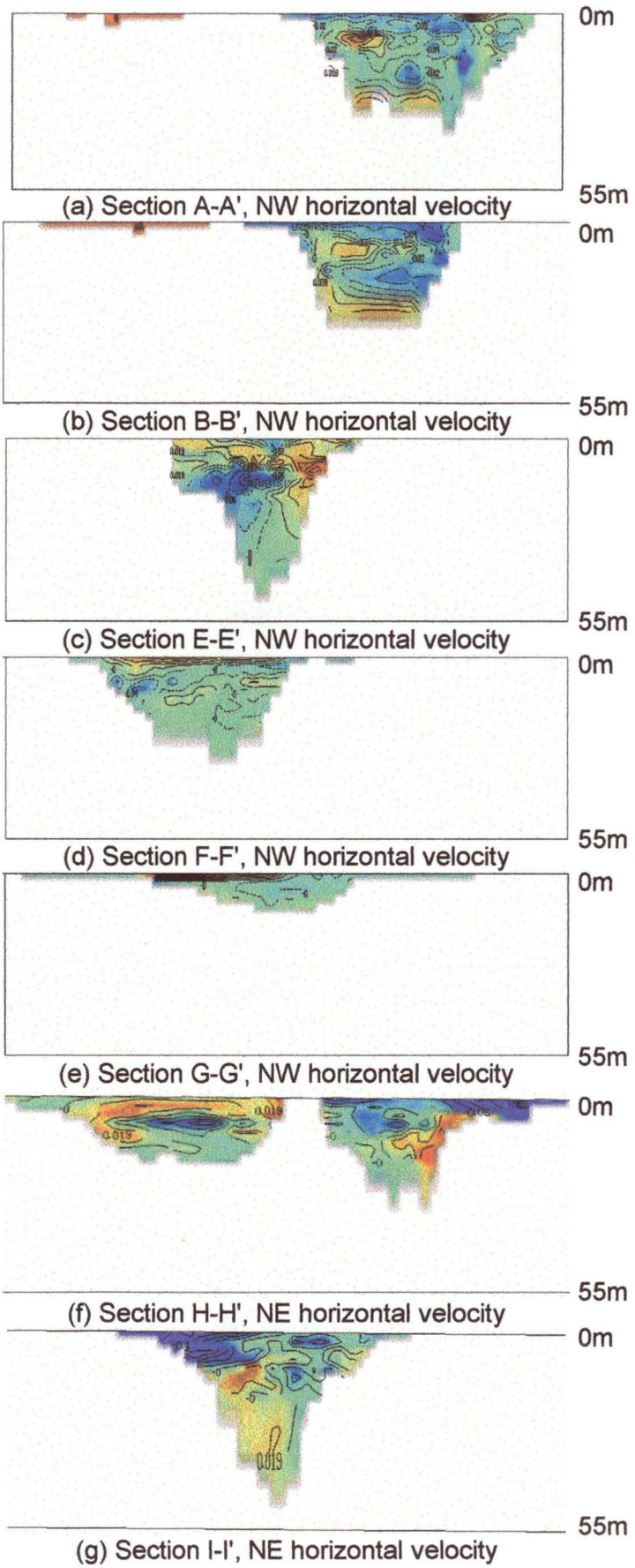

Figure E.6 Velocity during **ebb** tide, 0.02m/s contours, red is positive (away), blue is negative (towards)

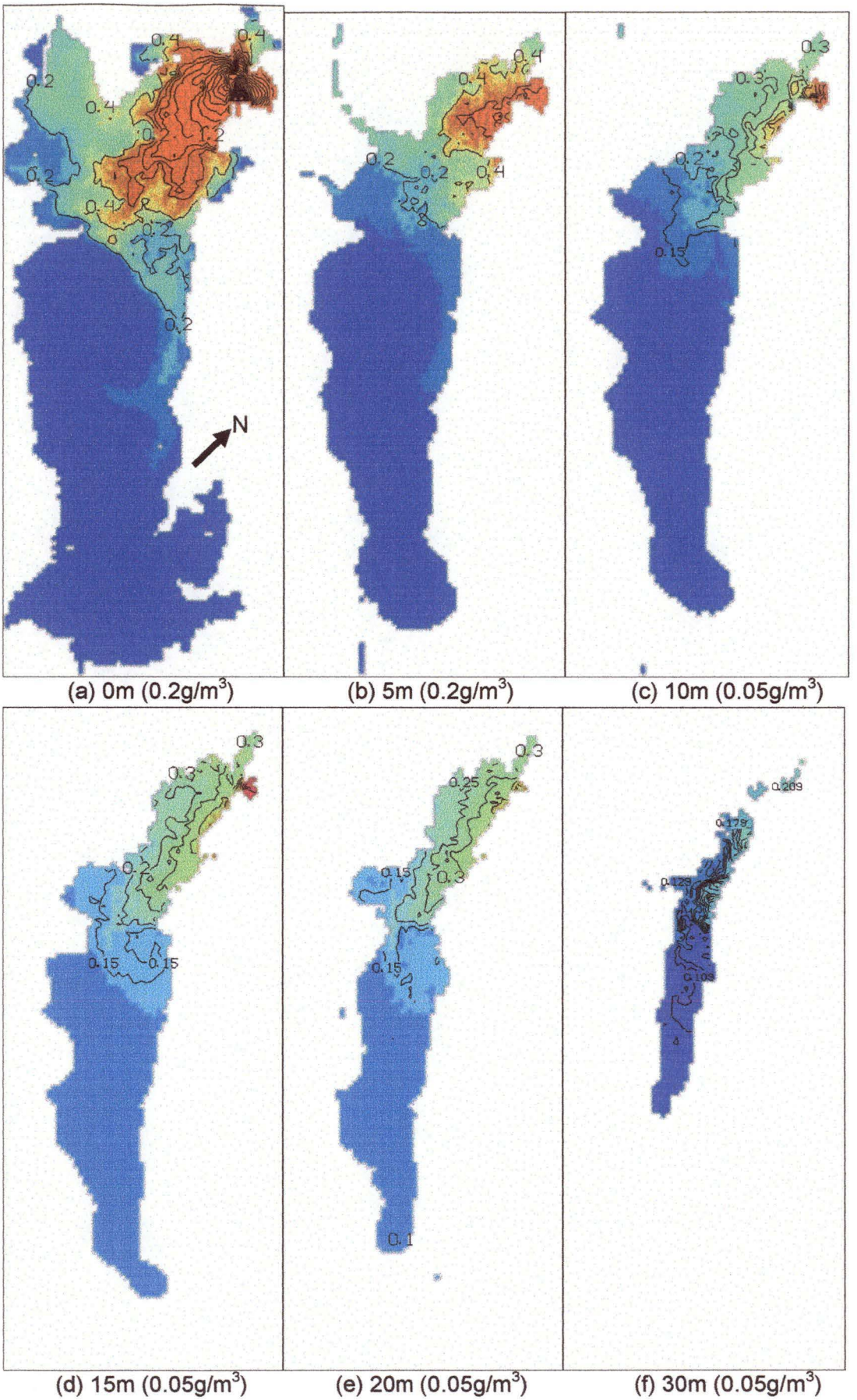

Figure E.7 Pollution concentration (g/m^3), contours after depths, tide flood to ebb

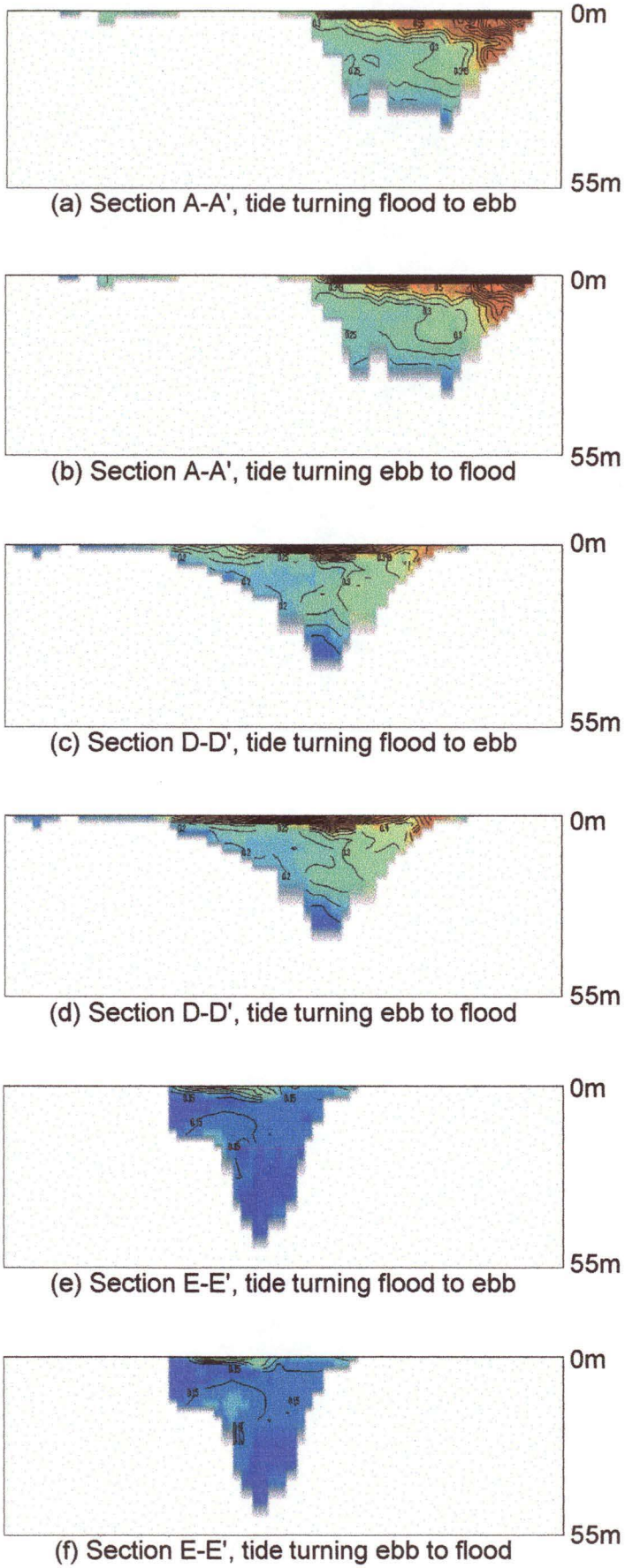

Figure E.8 Pollution concentration (g/m^3), $0.2g/m^3$ contours

Appendix F
Model output for wind response

This appendix gives the circulation and water quality of Macquarie Harbour under a wind forcing similar to a weather front passing the harbour. In previous cases there has been no wind stress applied to the harbour. The wind in this case was applied for 2 days at 2.5m/s from the SE; this is then ramped over one hour up to 10m/s from the SE. After two further days at the 10m/s, the wind is swung clockwise to the NE over four days, still at 10m/s.

Model output is given at ebb tides. This corresponds to when the wind is blowing from the SE at the end of the first two days, at the end of second two days, and thereafter at tidal periods as the wind rotates from blowing SE around to the wind blowing from the NE. Table F.1 gives the list of the figures in the appendix.

Table F.1 List of figures

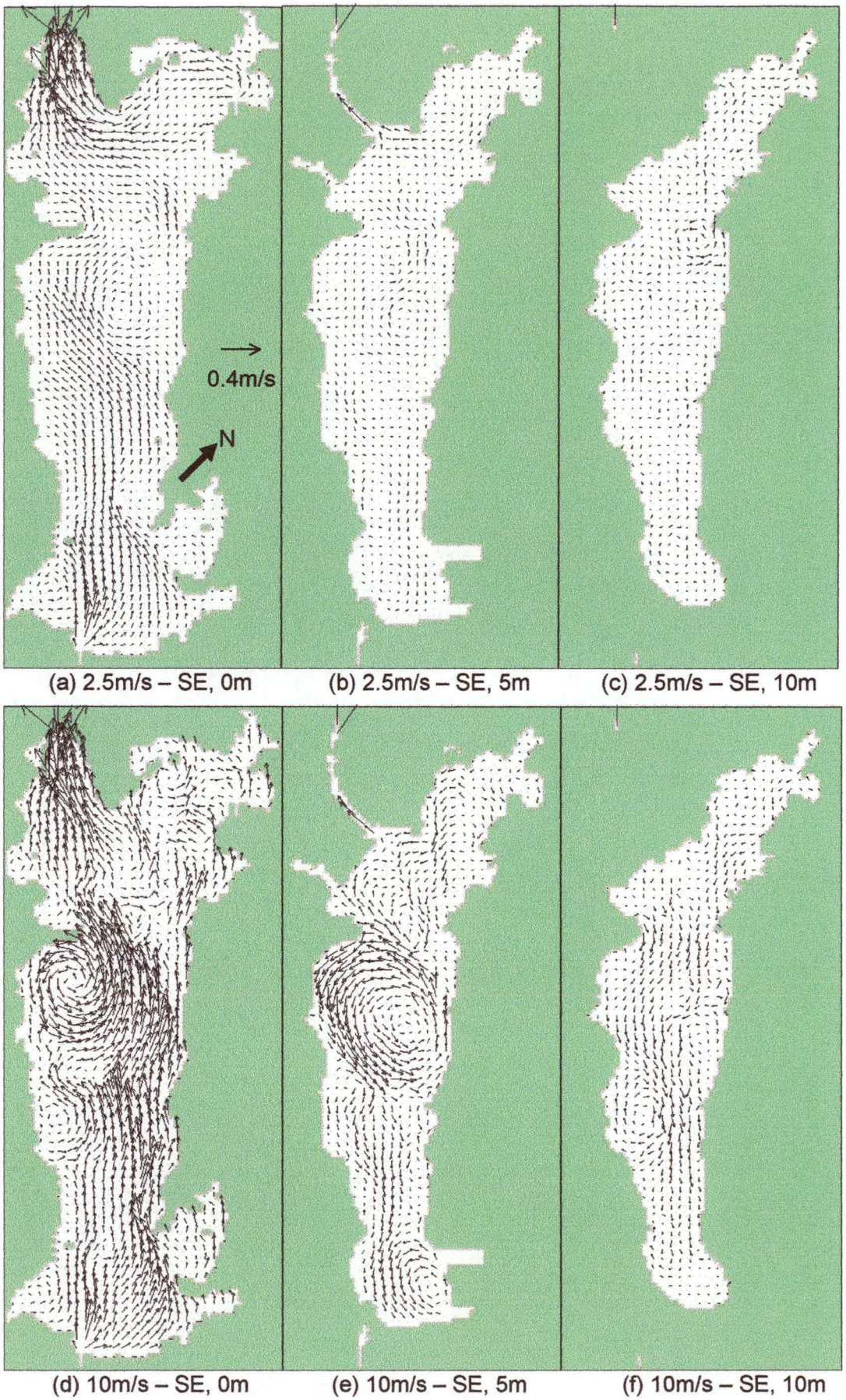

Figure F.1 Horizontal velocity with wind from SE at 2.5m/s and 10m/s

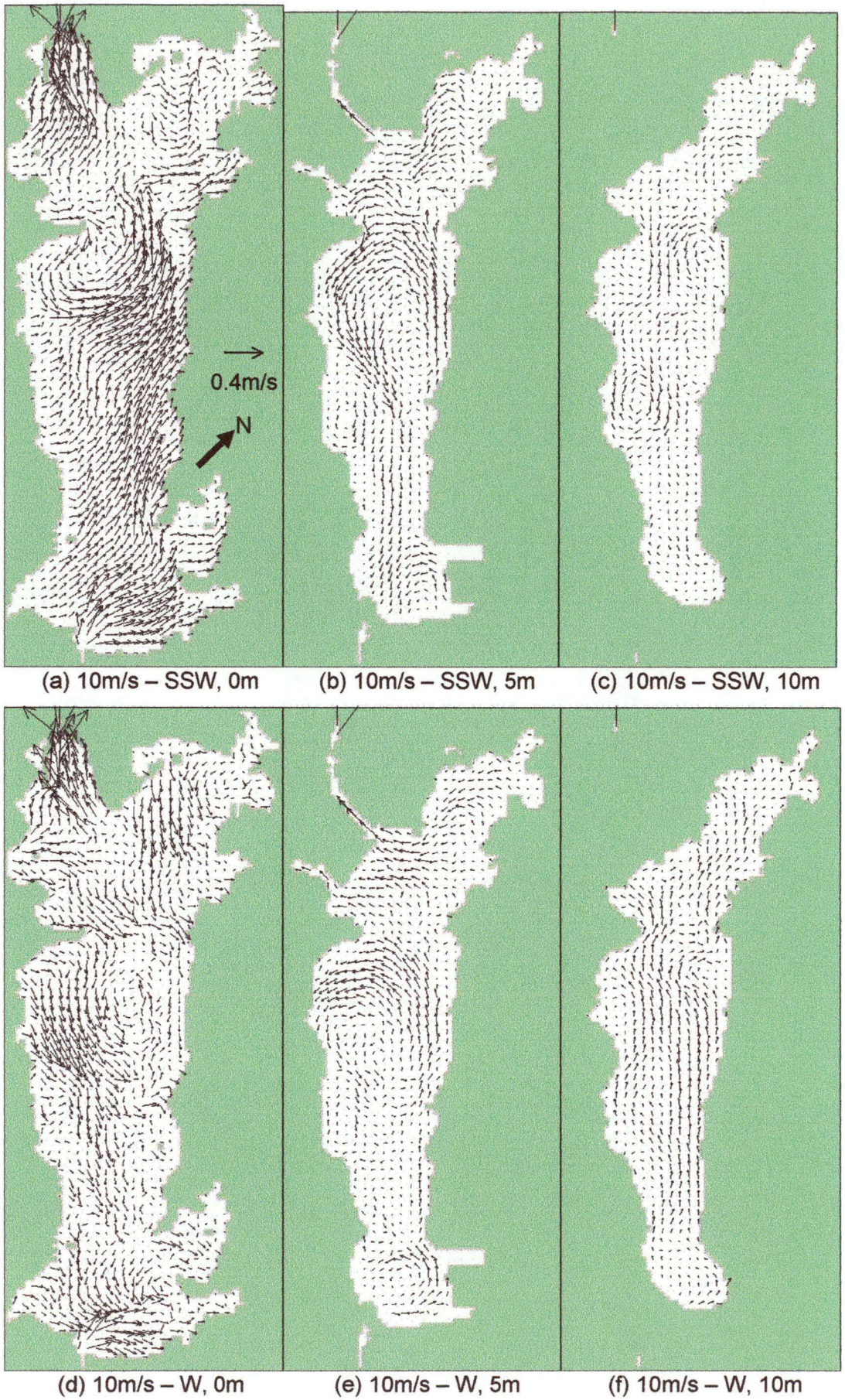

Figure F.2 Horizontal velocity with wind from SSW and W at 10m/s

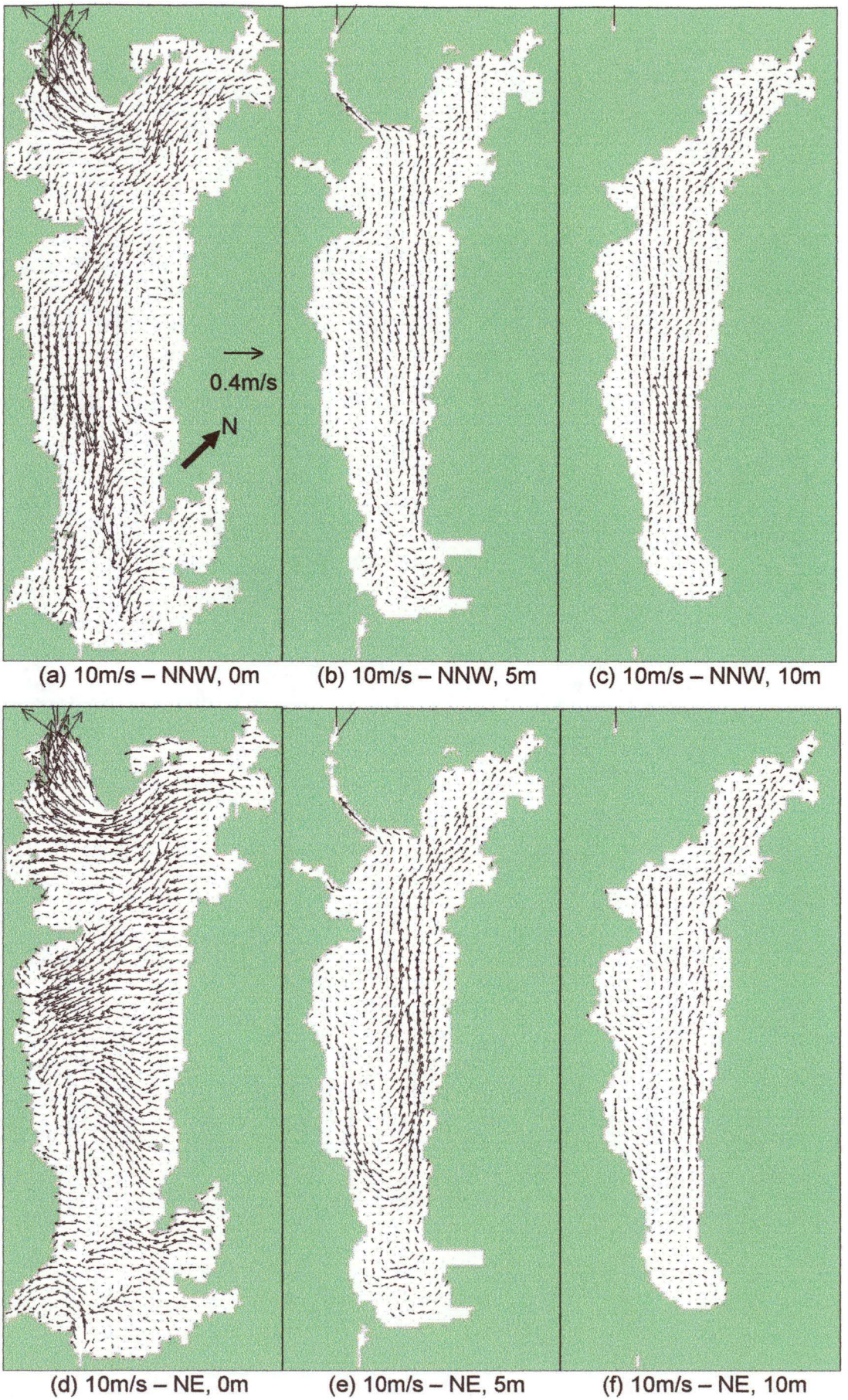

Figure F.3 Horizontal velocity with wind from NNW and NE at 10m/s

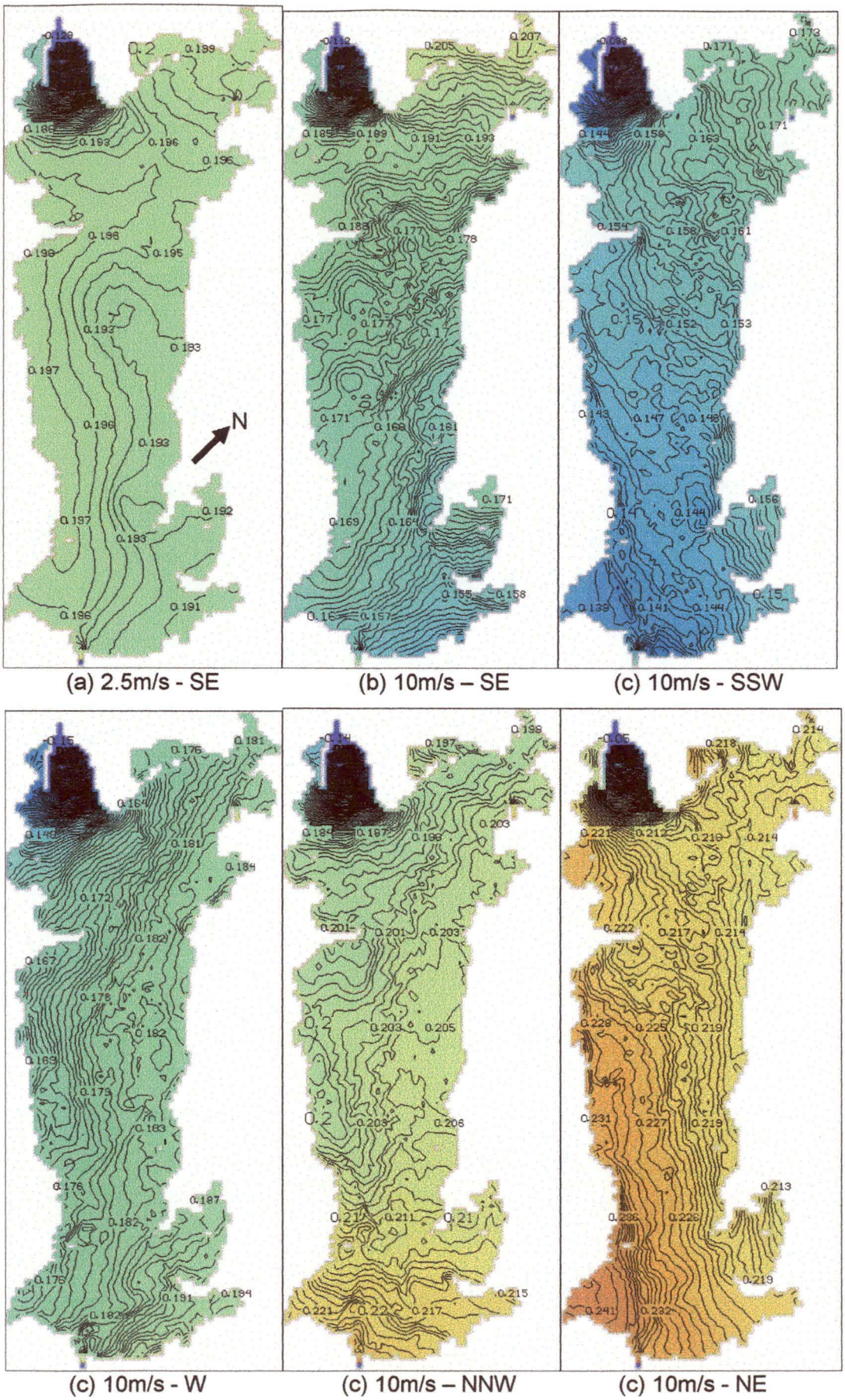

Figure F.4 Surface elevation, 0.001m contours

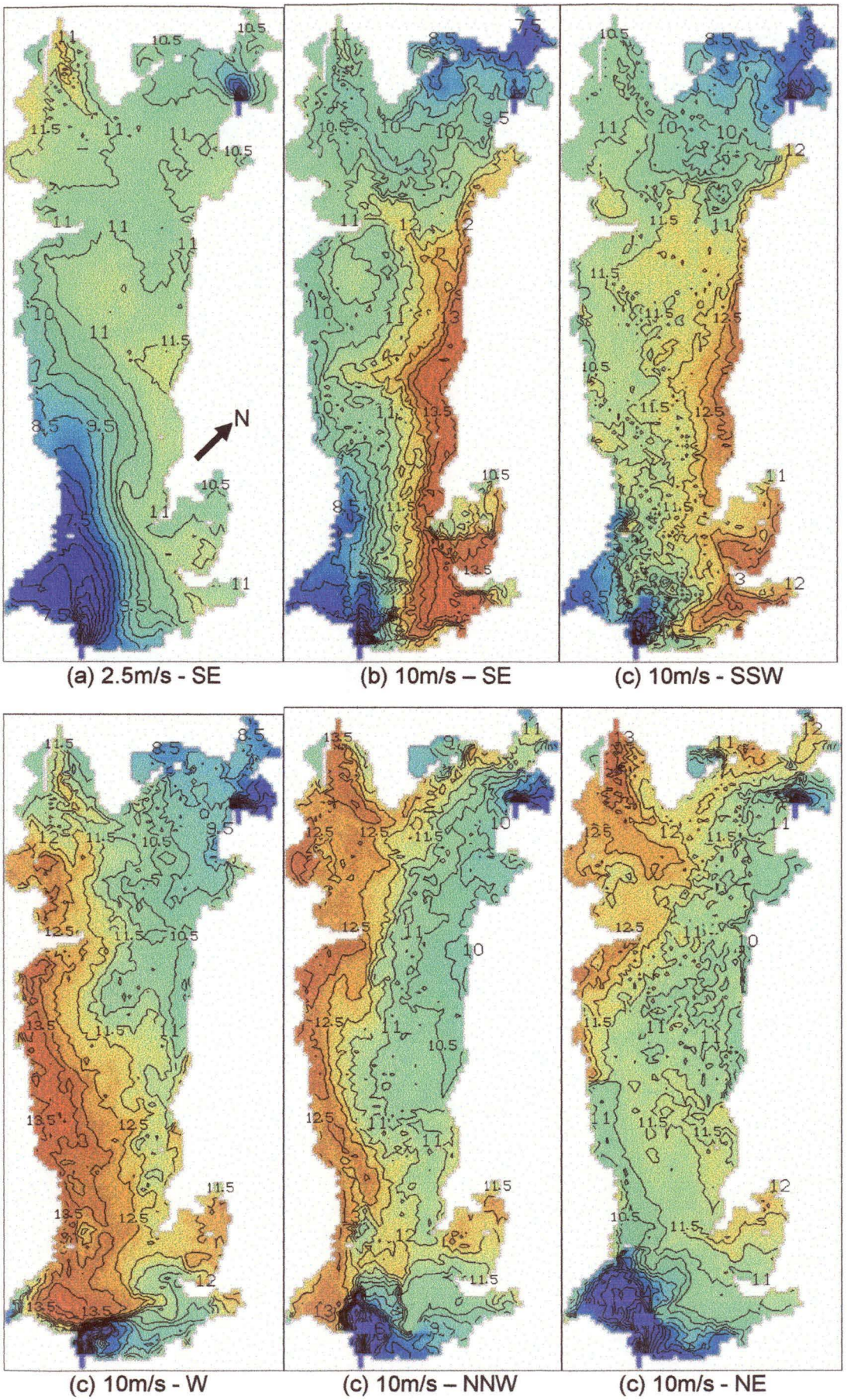

Figure F.5 Surface salinity (‰), 0.5‰ contours

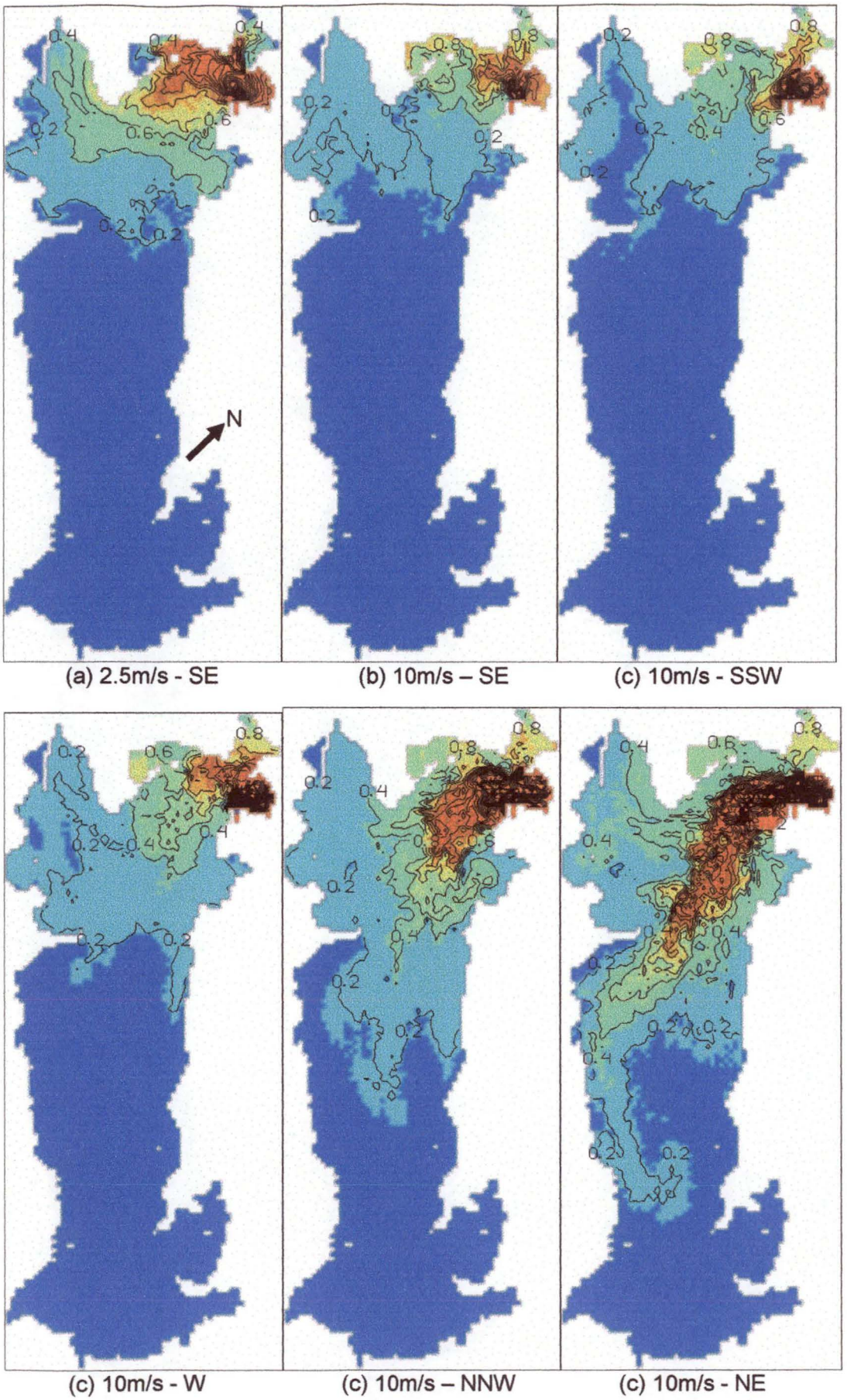

Figure F.6 Surface pollution concentration (g/m^3), 0.2g/m^3 contours